UNIVERSITY OF SOUTHAMPTON

Small scale physical processes and phytoplankton growth in shelf seas

Christopher Mark Moore

This thesis is submitted for
Doctor of Philosophy

Faculty of Science
School of Ocean and Earth Science

January 2002

UNIVERSITY OF SOUTHAMPTON

ABSTRACT

FACULTY OF SCIENCE

SCHOOL OF OCEAN AND EARTH SCIENCE

Doctor of Philosophy

Small scale physical processes and phytoplankton growth in shelf seas

by

Christopher Mark Moore

Detailed physical and biological observations collected in shelf sea regions, dominated by tidal mixing fronts or internal tides, were analysed in terms of the effect of physical forcing on phytoplankton growth. Microstructure measurements were used to quantify differences in vertical mixing and hence nutrient and light supply across regimes. The Fast Repetition Rate Fluorometer (FRRF) was used to obtain high-resolution data on the physiological state of the associated phytoplankton communities, with the aim of testing hypotheses relating growth to changing environmental conditions. Observations were made during three research cruises, RRS *Challenger*, in the Western English Channel, 1999 and RV *Kaharoa*, off the North East New Zealand coast, 1998 and 2000. The work represents one of the first attempts to collect and interpret FRRF data in a defined physical context within natural ecosystems.

Results from the 1999 cruise indicate that physical forcing in the region of a tidal mixing front has a pronounced influence on the physiology of the associated phytoplankton communities. FRRF based observations were consistent with nutrient limitation towards the stratified side of tidal mixing fronts, while deep vertical mixing caused light limitation within the mixed region. The observed enhancement of chlorophyll in the region of tidal mixing fronts therefore results, at least partly, from *in situ* growth.

Results from the 1998 and 2000 cruises demonstrate that internal tide dissipation can be responsible for high vertical nitrate fluxes and pronounced variations in phytoplankton light climate. Interpretation of physiological data from the 2000 cruise was difficult due to the complexity of the physical processes observed. However, physiological variability due to vertical motions and upwelling in the region is demonstrated.

Changes in FRRF derived photophysiology, as described by the photosynthetic efficiency (F_v/F_m) and the functional absorption cross section (σ_{PSII}), are shown to be related to photosynthetic parameters measured by ^{14}C derived carbon fixation. In particular a striking inverse correlation between FRRF derived σ_{PSII} and ^{14}C P^* vs. E derived maximal photosynthetic rates (P^*_{max}) was observed. FRRF derived photosynthetic rates are shown to compare favourably with ^{14}C derived rates, given the limitations of both techniques.

The magnitude and form of tidal dissipation is shown to have a pronounced effect on the ecology of shelf seas. It is suggested that regions dominated by internal tides are likely to be sites of higher new-production than tidal mixing fronts and highly stratified regions. The degree to which phytoplankton physiology and species specific adaptations may regulate the fluxes of energy and chemical constituents through shelf sea ecosystems is also discussed.

Graduate School of the Southampton Oceanography Centre

This PhD dissertation by

Christopher Mark Moore

has been produced under the supervision of the following persons

Supervisors:

Prof. P.M. Holligan, Dr. J. Sharples

Chair of Advisory Panel:

Prof. W.J. Jenkins

Member of Advisory Panel:

Dr. D.J. Hydes

Contents

1. Introduction 1

1.1 General background 1
1.1.1 Introduction to physical – biological coupling 1
1.1.2 Photosynthesis and growth 1
1.1.3 Light 5
1.1.4 Nutrients 7
1.1.5 Scaling in the oceans 10
1.2 Tidal mixing fronts and internal waves as two case studies in physical – biological interactions in shelf seas 11
1.2.1 Shelf sea tidal mixing fronts as a biological-physical system 11
1.2.2 Internal waves as a biological-physical system 17
1.3 Fast Repetition Rate Fluorometry (FRRF): a method for overcoming the biological sampling problem? 21
1.3.1 The sampling problem 21
1.3.2 Active fluorescence techniques: Background to use of the FRRF 22
1.3.3 Acclimation of the photosynthetic apparatus to changes in irradiance 28
1.4 Principal objectives 29

2. Methods 31

2.1 Background to sampling strategy 31
2.2 FRRF data collection and processing 31
2.2.1 Instrument description and deployment strategies 31
2.2.2 Initial data analysis 33
2.3 Microstructure measurements 34
2.3.1 Instrument description 34
2.3.2 Principals of measurement and data analysis 35
2.3.3 Vertical nutrient fluxes 37
2.4 Additional observations 37
2.4.1 Hydrographic data 38
2.4.2 Biological data 39
2.4.3 Satellite and *in situ* spectral data 41

3. Biological - physical interactions 1: A field study of a tidal mixing front 43

3.1 Introduction, study region and sampling strategy 43
3.2 Results 1: Physical controls on nutrient and light availability 44
3.2.1 General hydrography, chlorophyll distribution and mixing regime 44
3.2.2 Nutrient distributions 48
3.2.3 Physical controls on nutrient fluxes 50
3.2.4 Controls on light availability 52
3.2.5 Summary and inferences for growth limiting factors 54
3.3 Results 2: Impact of physical forcing on phytoplankton physiology 54
3.3.1 Frontal scale variations in physiology 54
3.3.2 Relationship of physiological variations to nutrient availability 57
3.3.3 Relationship of physiological variations to light 1: Diel variability 58
3.3.4 Relationship of physiological variations to light 2: σ_{PSII} photoacclimation and mixing 59
3.4 Discussion 62

4. Biological - physical interactions 2: Field studies of internal tides 67

4.1 Introduction, study region and sampling strategy 67
4.2 1998 study: Internal tide dissipation and nitrate flux 70
4.2.1 Moorings 70
4.2.2 Microstructure observations and nutrient fluxes 77
4.2.3 Possible consequences for phytoplankton nutrient and light climate 80
4.3 2000 study: Internal bores and physiological response 81
4.3.1 Mooring data and internal dynamics 81
4.3.2 Microstructure, mixing and nutrient fluxes 86
4.3.3 Phytoplankton distribution 90
4.3.4 Physiological variability 94
4.4 Discussion 100

5. Comparisons between FRRF and ^{14}C P* vs. E derived physiological parameters and productivity estimates 112

5.1 Introduction and description of P* vs. E data sets 112
5.1.1 ^{14}C P* vs. E determinations 112
5.1.1.1 Spectral dependencies of σ_{PSII}, α^* and E_K 114
5.2 Comparisons for 1999 data set 117
5.2.1 Relationships between FRRF and ^{14}C physiological parameters 117
5.2.2 Estimation of n_{PSII} 119
5.2.3 Comparisons of α^* estimates by FRRF and ^{14}C 120
5.2.4 Calculation of E_K and sensitivity of FRRF productivity to E_K 122
5.2.5 FRRF vs. ^{14}C derived P*, models used and comparisons 126
5.3 Comparisons for 2000 data set 129
5.3.1 Relationships between FRRF and ^{14}C physiological parameters 129
5.3.2 Comparisons of α^* estimates by FRRF and ^{14}C and E_K calculations 130
5.3.3 FRRF vs. ^{14}C derived P* 132
5.4 Discussion 134

6. Synthesis of productivity estimates 146

6.1 Introduction 146
6.2 ^{14}C and FRRF *in situ* productivity estimates from 1999 cruise 146
6.2.1 ^{14}C derived in situ productivity 146
6.2.2 FRRF derived in situ productivity 147
6.2.3 Overall comparisons between in situ productivity estimates 148
6.2.4 Integrated daily productivity 148
6.3 FRRF derived *in situ* productivity from the 2000 cruise: possible magnitudes of spectral effects 150
6.4 Synthesis of productivity estimates, Nitrate fluxes and physiological indices 152
6.4.1 General inter site characteristics 152
6.4.2 Biomass-specific integrated production rates and 'new production' 154
6.5 Estimated growth rates 158
6.5.1 Problems of calculating growth: the requirement for C:Chl estimates 158
6.5.2 Vertical partitioning of growth at U2: maintenance of the DCM 159
6.5.3 Estimated site specific growth rates and controls 161
6.6 Physically driven export 164
6.7 Discussion 166

7. Summary and Conclusions 172

7.1 Evaluation of the FRRF technique 172
7.1.1 Scales of physiological variability 172
7.1.2 Relationship of FRRF derived productivity to phytoplankton photosynthesis and carbon fixation 173
7.1.3 Extending the range of productivity estimates: what are the important parameters? 174
7.2 Physical controls on shelf sea productivity 178
7.2.1 Tidal mixing fronts 178
7.2.2 Regions of high seasonal stratification 178
7.2.3 Internal tide dominated regions 180
7.2.4 Auxiliary energy and Ergoclines 181
7.3 Conclusions and further work 182

8. References 185

Appendices 201

A1 Scaling arguments and mixing in stratified fluids 201
A2 Checks on FRRF data quality and analysis 203
A3 Persons responsible for data collection 209
A4 Fluorescence – chlorophyll calibrations for 1999 cruise 210
A5 Relationships between nutrients during 1999 cruise 211
A6 Detailed temperature and velocity structure during 2000 cruise 212
A7 Fluorescence and transmittance-chlorophyll calibrations for 1999 cruise 217
A8 A model of phytoplankton photoacclimation within a photosynthetron 219

List of figures

Fig. 1.1	Arrangement of photosynthetic apparatus and 'Z-scheme'	3
Fig. 1.2	Schematic of light penetration and the concept of critical depth	6
Fig. 1.3	Schematic showing sources and sinks of nutrients within a water column and vertical nutrient profiles	9
Fig. 1.4	Schematic of physiological and physical time-scales	11
Fig. 1.5	Schematic cross-section of a tidal mixing front in a shelf sea	13
Fig. 1.6	Examples of shelf sea tidal mixing fronts as observed in satellite data	14
Fig. 1.7	Schematic of internal tide and soliton packet generation at the shelf edge	18
Fig. 1.8	Shelf break cooling as observed in satellite data	20
Fig. 1.9	Schematic of de-activation pathways for excitation energy	22
Fig. 1.10	Example of *in situ* fluorescence induction curve	26
Fig. 2.1	Picture of the FRRF instrument showing the optical head	32
Fig. 2.2	FRRF instruments as deployed *in situ*	33
Fig. 2.3	Example fit of observed spectrum of vertical temperature gradient microstructure to the Batchelor form	36
Fig. 3.1	Stations occupied during cruise CH145 during August 1999 and satellite data from from 9th July 1999	43
Fig. 3.2	Frontal cross sections of temperature and chlorophyll from 1999 cruise	45
Fig. 3.3	Physical variability for three fixed stations during 1999 cruise	48
Fig. 3.4	Frontal distribution of temperature and nitrate during 1999 cruise	49
Fig. 3.5	Physical forcing, chlorophyll and nutrient distributions at fixed station U2 occupied during 1999 cruise	51
Fig. 3.6	Vertical light attenuation and chlorophyll distribution at fixed station U2 occupied during 1999 cruise	53
Fig. 3.7	Contoured cross frontal CTD/FRRF data from 1999 cruise	55
Fig. 3.8	Cross frontal temperature and physiological variability from SeaSoar runs during 1999 cruise	56
Fig. 3.9	Nitrate concentration and F_v/F_m vs. temperature for frontal region during 1999 cruise	57
Fig. 3.10	Diel variability of $\Delta F'/F_M'$ and σ_{PSII}' during all four 25hr stations Occupied during 1999 cruise	58
Fig. 3.11	Relationship of phytoplankton physiology to instantaneous irradiance during 1999 cruise	59
Fig. 3.12	Photoacclimation and mixing as controls on σ_{PSII}' for 1999 cruise	61
Fig. 4.1	Study region and positions of moorings deployed during 1998 and 2000 cruises	68
Fig. 4.2	SAR image of internal wave packets propagating on-shelf off North East New Zealand	70
Fig. 4.3	Set-up and instrumentation used on mooring transect during 1998 experiment	71
Fig. 4.4	Time series of surface wind speed and water column vertical thermal structure at the two principal moorings during 1998 experiment	72
Fig. 4.5	Temperature and current variance spectra from moorings during 1998	73
Fig. 4.6	Example temperature structure, shear and Richardson number, 1998	74
Fig. 4.7	Temperature density relationship for 1998 experiment	75
Fig. 4.8	Mean vertical profiles of internal wave energies during 1998	76
Fig, 4.9	Tidally averaged diffusivity profiles for 1998 experiment	78
Fig. 4.10	Vertical distributions of nitrate, chlorophyll and nitrate gradients, during 1998 experiment	79
Fig. 4.11	Light depth and nitrate variability driven by internal tidal motions	80
Fig. 4.12	Set-up and instrumentation used on two principal moorings during 2000 experiment	82
Fig. 4.13	Time series of thermal structure during 2000 experiment	83
Fig. 4.14	Detailed structure of a soliton packet from 2000 cruise	85
Fig. 4.15	Example temperature structure, shear and Richardson number, 2000	86
Fig. 4.16	Observations of mixing parameters during 2000 experiment	87

Fig. 4.17	Nitrate temperature relationship for 2000 cruise	88
Fig. 4.18	Example time series of calculated nitrate distributions and fluxes from 2000 experiment	89
Fig. 4.19	Data from initial CTD survey during 2000 cruise	91
Fig. 4.20	Time series of phytoplankton distribution and physiology at station PK occupied during 2000 cruise	92
Fig. 4.21	Sea surface chlorophyll concentration derived from SeaWifs data for 2000 experiment	93
Fig. 4.22	Chlorophyll temperature relationship at station PK during 2000 cruise	94
Fig. 4.23	Cross shelf physiological variability during 2000 cruise	95
Fig. 4.24	Data from final CTD survey during 2000 cruise	98
Fig. 4.25	Detailed time series observations from 30th November 2000	99
Fig. 4.26	Example of results of an irradiance shift experiment	100
Fig. 4.27	AVHRR derived sea surface temperature data for 2000 experiment	102
Fig. 4.28	Results from simple model for quantifying increase in irradiance due to internal motions	106
Fig. 4.29	Observed relationship between $\Delta F'/F_M'$ and irradiance during second CTD transect on 3rd December 2000	109
Fig. 5.1	Examples of P vs. E data and fits for the 1999 and 2000 cruises	114
Fig. 5.2	Normalised excitation and absorption spectra	116
Fig. 5.3	Relationships between FRRF and ^{14}C (P* vs. E) physiological parameters from the 1999 cruise	118
Fig. 5.4	Mean values of a* (475) vs. $\sigma_{PSII}/(F_v/F_m)$ for 1999 cruise	120
Fig. 5.5	Relationship between ^{14}C and FRRF derived estimates of α* from the 1999 cruise	121
Fig. 5.6	Example of relationship between $\Delta F'/F_M'$ and irradiance	124
Fig. 5.7	Variability in FRRF derived E_K estimates at site U2 during 1999 cruise	125
Fig. 5.8	Results of P* calculations based on FRRF data for the U2 site	127
Fig. 5.9	Relationships between ^{14}C and FRRF derived P* and irradiance for 1999 cruise	128
Fig. 5.10	Relationships between FRRF and ^{14}C (P* vs. E) physiological parameters from the 2000 cruise	130
Fig. 5.11	Relationship between ^{14}C and FRRF derived estimates of α* from the 2000 cruise	131
Fig. 5.12	Variability in FRRF derived E_K estimates at site PK during 2000 cruise	132
Fig. 5.13	Relationships between ^{14}C and FRRF derived P* and irradiance for 2000 cruise	133
Fig. 5.14	Relationships between E_K, P^*_{max} and the reciprocal of σ_{PSII}' for both the 1999 and 2000 data sets	136
Fig. 5.15	Results from a simple model of photo-acclimation within a Photosynthetron	141
Fig. 5.16	Final comparisons between FRRF and ^{14}C derived productivity rates for the 1999 and 2000 ^{14}C P* vs. E experiments	143
Fig 6.1	Vertical profiles of chlorophyll specific and volume specific productivity from stations occupied during the 1999 cruise	147
Fig. 6.2	Comparisons of FRRF and ^{14}C *in situ* productivity rates during 1999	149
Fig. 6.3	Influence of differences between *in situ* and FRRF excitation spectra	152
Fig. 6.4	Synthesis of key biological characteristics of all the sites studied	155
Fig. 6.5	Biomass (chlorophyll) specific productivity from all sites studied	156
Fig. 6.6	Vertical profiles of production and estimated community growth at station U2 during 1999 cruise	160
Fig. 6.7	Relationships between estimated gross site growth rate and environmental and physiological factors	163
Fig. 6.8	Observations of physically driven export of phytoplankton at site U2 during 1999 cruise	164
Fig. 7.1	Result of simple productivity model applied to cross frontal FRRF data obtained using the SeaSoar undulator during 1999 cruise	177

List of tables

Table 1.1	Notation for fluorescence derived physiological parameters	25
Table 2.1	Summary of cruises and data acquired and analysed in thesis	42
Table 3.1	Sampling performed during CH145, 1999 cruise	44
Table 4.1	Sampling performed during internal wave cruises, 1998 and 2000	69
Table 5.1	Locations, sampling times and depths for discrete samples incubated for ^{14}C P* vs. E determinations	113
Table 6.1	Estimated productivity at the four sites studied during the 1999 cruise	150
Table 6.2	Estimated productivity at site PK during the 2000 cruise	151
Table 6.3	Synthesis of nitrate fluxes and new and total productivity estimates	158
Table 7.1	Sensitivity analysis and results of simple FRRF productivity model	176

Acknowledgements

I would like to thank the following for all their assistance, advice and support throughout the period over which this work was undertaken and during the preparation of the thesis:
Firstly I am very grateful to Patrick Holligan and Jonathan Sharples, not only for all their supervision and encouragement, but also for setting me off in a very interesting field of research.
Numerous people gave insightful advice into the scientific aspects of this work. I'd particularly like to thank Ed Abraham, Phil Boyd, Mike Lucas, Craig Stevens and Dave Suggett for stimulating discussions on phytoplankton physiology/ecology and shelf sea physical processes.
The fieldwork would not have been possible without the help of a large number of people, in addition to those mentioned above I am particularly thankful to: Sarah Bury, Neil Fisher, Mark Gall, Peter Hill, David Hydes, Tom Rippeth, John Simpson and Ray Wilton. I am also grateful to the officers and crew of the RRS *Challenger* (August 1999) and the RV *Kaharoa* (November – December 1998 & 2000).
Mike Head always provided prompt and good advice on the operation of SCAMP, while Justin Dunning and John Atkins from Chelsea instruments provided support for the FRRF.
The work was funded by the Natural Environment Research Council (studentship GT04/98/267/MS and grant GR3/11829).
Thanks to all at the National Institute for Water and Atmosphere Research for hosting me during the field trips to New Zealand. Thanks also to all the friends, family, officemates and housemates who have put up with me over the past three years (particularly Clare, who is sitting next to me as I write this and wanted a mention).

Finally, a very special thank-you to Vicky for all her care and support.

Abbreviations

The following is a list of abbreviations used in this thesis

Term	Definition	Units	Page
Photosynthetic parameters			
P	Volume specific photosynthetic rate	mg C m^{-3} hr^{-1}	4
P*	Chlorophyll specific photosynthetic rate	mg C (mg Chl *a*)$^{-1}$ hr^{-1}	4
E	Irradiance	μ E $m^{-2}s^{-1}$	5
a*	Chlorophyll *a* specific absorption	m^2 (mg Chl *a*)$^{-1}$	39
ETR	Linear photosynthetic electron transport rate	electrons RC^{-1} s^{-1}	27
n_{PSII}	number of PSII reaction centres	mol RCII (mol Chl *a*)$^{-1}$	27
PQ	Photosynthetic quotient	mol O_2 (mol CO_2)$^{-1}$	27
P vs E parameters*			
P^*_{max}	Maximal photosynthetic rate	mg C (mg chl a)$^{-1}$ hr^{-1}	41
α*	Maximum light utilisation coefficient	mg C (mg chl a)$^{-1}$ hr^{-1} (μ E m^{-2} s^{-1})$^{-1}$	41
E_k	Light saturation parameter (= P^*_{max} /α*)	μ E m^{-2} s^{-1}	41

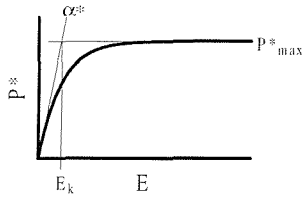

Schematic of P vs. E curve, indicating parameters*

Fluorescence parameters			
F_0,F_M	Minimal and maximal fluorescence yields measured in dark adapted state	a.u.	22
F_0',F',F_M'	Minimal, steady state and maximal fluorescence yields measured under ambient irradiance	a.u.	24, 25
F_V	Variable fluorescence (=F_M-F_0)	a.u.	25
ΔF'	Change in fluorescence yield measured under ambient light (=F'$_M$-F')	a.u.	25
F_V'	Variable fluorescence measured under ambient light (=F_M'-F_0')	a.u.	25
F_V/F_M	Maximum quantum efficiency of photochemistry	D	23
$\Delta F'/F_M'$	Quantum yield of photochemistry measured under ambient light	D	25
σ_{PSII}	Functional absorption cross section of PSII in the dark	Å^2 quanta^{-1}	23, 24
σ_{PSII}'	Functional absorption cross section of PSII under ambient light	Å^2 quanta^{-1}	23, 24
τ_{PSII}	Minimum PSII turnover time	s	122

Abbreviations used: cont.

Physical parameters

k_d	Vertical diffuse attenuation coefficient	m^{-1}	5
Q	Rate of surface heat input	$W\ m^{-2}$	12
ρ	Density	$kg\ m^{-3}$	36
N^2	Buoyancy frequency	s^{-1}	36
K_T, K_ρ	Eddy diffusivity of heat (K_T) or mass (K_ρ)	$m^2\ s^{-1}$	35, 37
χ	Rate of dissipation of thermal variance	$°C^2\ s^{-1}$	35
ε	Rate of dissipation of turbulent kinetic energy	$m^2\ s^{-3}$	36
R_f	Flux Richardson number	D	37
R_i	Gradient Richardson number	D	74
f	Coriolis parameter	s^{-1}	76

Notes: For units, a.u. indicates arbitrary units, D indicates a dimensionless quantity. Page indicates page number where definition or derivation can be found.

1. Introduction

1.1 General background

1.1.1 Introduction to physical – biological coupling

Phytoplankton require two basic resources, nutrients and light, in order for them to be able to photosynthesise and grow. It has long been recognised that the supply of both of these resources within the oceans is controlled by the physical nature of the fluid environment in which these organisms live (Gran and Braarud, 1935; Riley, 1942; Sverdrup, 1953). However, quantification of the effect of physical variability on phytoplankton dynamics has been limited by an inability to resolve the relevant scales of the physical and, more severely, the biological components of the system.

Within the majority of marine systems the sources of nutrients and light to the water column are from different directions. Light intensity increases towards the surface, whereas inorganic nutrient concentrations increase with depth. This simple vertical separation imposes the fundamental bottom up constraint on primary production within the oceans; population growth may be limited by low nutrients in the surface regions, or low light in deeper regions. Physical processes which cause transport between these regions of high light and high nutrients can therefore cause enhancement of photosynthesis and hence production and growth.

1.1.2 Photosynthesis and growth

Photosynthesis is the process by which phytoplankton utilise light energy in order to produce the chemical energy required for the reduction of inorganic carbon and growth (Falkowski and Raven, 1997). The photosynthetic mechanism is principally a two-stage process consisting of the 'light' and 'dark' reactions. The first step is light dependent and consists of the photochemical oxidation of water using light captured in a pigment (chlorophyll) complex. The reduction of nicotine adenine dinucleotide phosphate ($NADP^+$) to NADPH and the conversion of adenosine diphosphate (ADP) and inorganic phosphate (Pi) to adenosine triphosphate (ATP) also result from the light reactions:

$$2H_2O + 2NADP^+ + 3ADP + 3Pi + 8photons \xrightarrow{chl} O_2 + 2NADPH + 2H^+ + 3ATP \quad (1.1)$$

The second series of light independent ('dark') reactions are catalysed by enzymes and utilise the NADPH and ATP to reduce CO_2:

$$CO_2 + 2NADPH + 2H^+ + 3ATP \xrightarrow{enzmes} CH_2O + H_2O + 2NADP^+ + 3ADP + 3Pi \quad (1.2)$$

Thus the overall photosynthetic reaction can be written:

$$2H_2O + CO_2 + 8photons \rightarrow CH_2O + H_2O + O_2 \quad (1.3)$$

and results in carbon dioxide fixation as well as the evolution of oxygen.

The basis of the photosynthetic reactions

The photosynthetic apparatus required for the light reactions is organised on and around membranes known as thylakoids in order that a physical separation between reduced and oxidised chemical species can be maintained (*Fig. 1.1a*). Within eukaryotic algae these membranes separate the lumen, where the water is split, from the stroma where ATP and NADPH production occurs. The whole apparatus is located in organelles called chloroplasts. The initial step in the light reactions is the absorption of light by a complex of pigments, the light-harvesting antenna. Excitation energy in the antenna is then transferred to specific sites, reaction centres, where the photochemical reaction occurs. The reaction centres are of two types, photosystem 1 (PSI) and photosystem 2 (PSII) (*Fig. 1.1*).

Understanding of the light dependent reactions is based on the conceptual 'Z –scheme' (*Fig. 1.1b*). Excitation energy is received from the antenna pigments in the reaction centres, PSII receiving a photon first. Electrons are then moved through a transport chain of redox reactions between the two reaction centres until PSI is excited (see *Fig. 1.1b*). The rates of these reactions are highly variable, with the re-oxidation of plastoquinol (PQH_2) to plastoquinone (PQ) typically being the slowest and taking around 1-15ms (Hansson and Wydrzynski, 1990; Krause and Weis, 1991; Kolber and Falkowski, 1993; Falkowski and Raven, 1997).

The light independent ('dark') reactions occur within the chloroplast stroma (*Fig 1.1a*). Carbon dioxide is reduced in a series of reactions known as the photosynthetic carbon reduction cycle or Calvin – Benson cycle (Falkowski and Raven, 1997). These reactions are catalysed by a number of enzymes, principal amongst which is ribulose-1,5-bisphosphate carboxylase/oxygenase (Rubisco).

(a)

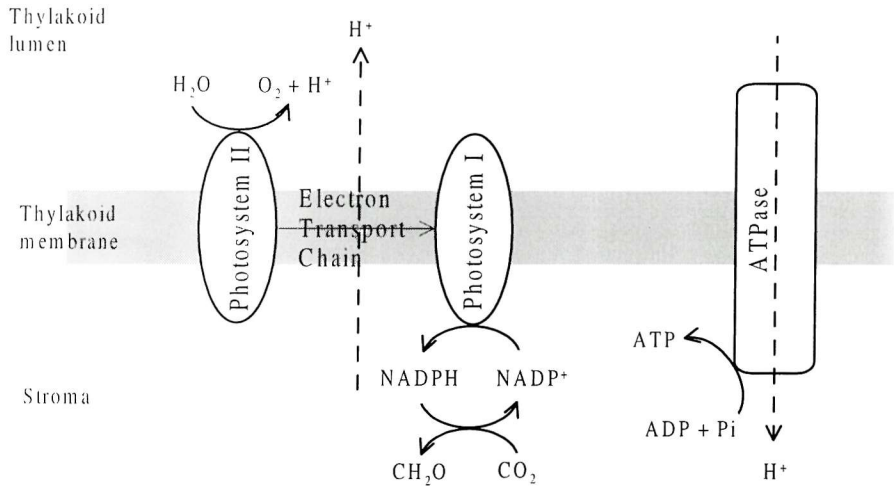

(b)

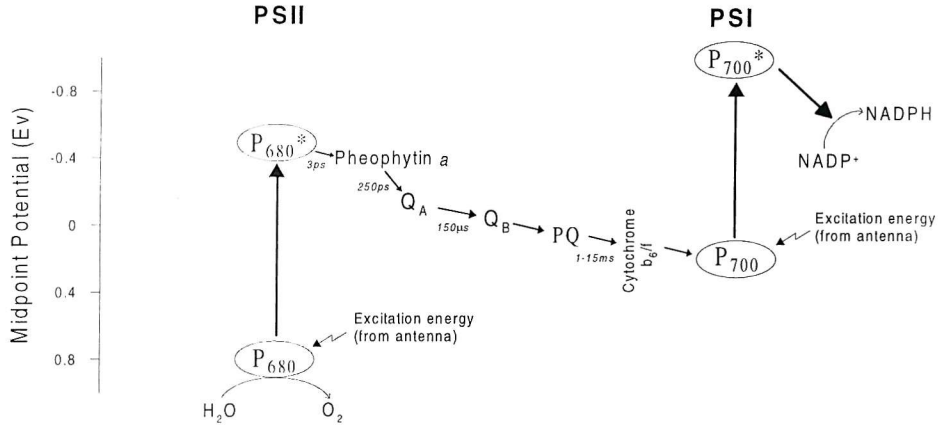

Fig. 1.1 (a) Arrangement of photosynthetic apparatus for eukaryotic algae. Water is split in the thylakoid lumen generating protons. Protons are pumped across the thylakoid membrane by the electron transport chain. The proton gradient is dissipated through the ATPase producing ATP within the stroma. The production of NADPH also occurs in the stroma which is the site of the Calvin-Benson cycle of carbon fixation. (b) Simplified schematic of the Z-scheme showing the pathways of electron transport during the light dependent stage of photosynthesis. Light energy absorbed by the antenna is transferred to P_{680} (the chlorophyll-a molecule of RCII) causing the molecule to be raised to an excited state (P_{680}^{*}). A charge separation then occurs, P_{680}^{*} is oxidised to P_{680}^{+} and a primary acceptor (pheophytin *a*) is reduced. P_{680}^{+} is reduced by the oxidation of a water molecule. Pheophytin a^{-} is rapidly re-oxidised by the secondary acceptor (Q_A). The electron is then transferred through a series of further redox reactions ($Q_B \rightarrow Q_B^{-}$, PQ$\rightarrow$ PQH_2, etc.) until it arrives at P_{700} (the chlorophyll-a molecule of RCI). Here energy is again received from the antenna and causes the molecule to be raised to an excited state (P_{700}^{*}). A second charge separation then occurs with a further electron transport pathway which eventually results in the reduction of $NADP^{+}$ to NADPH. Turnover times for electron transfer are from Krause and Weis, (1991) and Raven and Falkowski, (1997 and are shown in italics.

The overall photosynthetic rate

The combination of the light and dark reactions determine the overall photosynthetic or production rate (P) which can be defined in terms of the rate of oxygen evolution or carbon fixation (c.f. Eq. 1.3) (e.g. Sakshaug et al. 1997; Falkowski and Raven, 1997). Since carbon is one of the basic units of 'currency' within all ecosystems, the production rate will be reported in terms of carbon fixation unless otherwise stated. Further, productivity can be defined as a biomass specific rate (P^B), where the superscript indicates normalisation to an index of biomass.

Typically within the oceanographic literature productivity is normalised to chlorophyll (P^*), as the chlorophyll concentration is routinely and easily measured (Sakshaug et al., 1997). The measurement of phytoplankton carbon (C), a truer index of biomass, is difficult in the marine environment (Eppley, 1980). The ratio of carbon to chlorophyll (C:Chl) is therefore also difficult to obtain.

Population growth

Ultimately the carbon fixed by the photosynthetic process is used for growth. The population growth rate (μ) is defined as the rate of increase of biomass normalised to the population size at that time $1/C(\partial C/\partial t)$ (Eppley, 1980). The relationship between the chlorophyll specific net photosynthetic rate (P^*) and the specific growth rate is therefore:

$$\mu = \frac{\partial C/\partial t}{C} = \frac{P^*}{C:Chl} \tag{1.4}$$

Values of C:Chl can vary greatly under different environmental conditions hence the chlorophyll-specific photosynthetic rate can often not be directly related to population growth (Eppley, 1972; Geider, 1987; Cullen and Lewis, 1988; Cullen *et al.*, 1992; Cloern *et al.*, 1995; Sakshaug *et al.*, 1997).

Acclimation and adaptation to environmental conditions

Phytoplankton have the ability to alter their cellular machinery in response to differing environmental conditions. In keeping with Falkowski and LaRoche, (1991), such adjustment cell physiology will be termed acclimation. Additionally different taxonomic groups of phytoplankton may have specific traits which make them suited to certain environments. Adaptation will refer to this genetic pre-disposition of a species to a particular ecological niche. Both adaptation and acclimation will affect the productivity

and growth rates of a population, as differences in cellular machinery, which result from varying levels of light and nutrients, will alter the ability of cells to utilise these resources. The relationship between production and specific growth rate (Eq. 1.4) is thus one manifestation of the importance of adaptation and acclimation.

1.1.3 Light

The wavelengths of light utilised by phytoplankton for photosynthesis lie within a band from 400 – 700nm, light within this range being referred to as photosynthetically available radiation (PAR). Hereafter PAR will be referred to as irradiance (E). As already stated, light in aquatic ecosystems is supplied from above, as sunlight. The amount of light (E(0)) arriving just below the sea-surface is controlled by many factors including time of year, time of day, latitude, cloudiness and wave state (Kirk, 1994). After penetrating the sea surface, light levels decrease exponentially with depth, i.e. $E(z) = E(0)e^{-k_d z}$, where k_d is the vertical attenuation coefficient of downward irradiance (*Fig 1.2a*). The rate of attenuation is controlled by absorption within the water itself and the amount of absorbing and scattering material in the water, including suspended sediments and phytoplankton (Kirk, 1994). The well-lit upper area of the water column is referred to as the euphotic zone and is often taken to be that region above which either 0.1 or 1% of surface light is experienced.

The amount of light experienced by any single phytoplankton cell over a day will be critically dependent on the depth of the cell. Vertical movements of phytoplankton by physical processes within the upper ocean can therefore alter the total amount of light received, and hence the ability to photosynthesise (Lewis et al. 1984a, Kirk 1994). The upper region of the water column is often found to be homogenous with respect to density (un-stratified). This upper 'mixed layer' is often taken to be the depth below which surface mixing does not penetrate. Phytoplankton below this region, within the pycnocline (thermocline)[1], are assumed to be relatively static in vertical position, while cells within the mixed layer depth are assumed to be circulated throughout the mixed layer (*Fig 1.2a*). However, it is worth noting that rates of turbulent mixing within the upper ocean are highly variable and the interaction of mixing with the depth of the mixed layer and the vertical movements of particles is complex (e.g. Shay and Gregg, 1986; Agrawal et al. 1992; D'Asaro and Dairiki, 1997).

[1] For the majority of shelf sea cases, the term pycnocline can be replaced with thermocline

Critical depths

The concept of critical depth has proved to be a useful paradigm describing the utilisation of light by phytoplankton (Gran and Braarud, 1935; Sverdrup, 1953; Smetacek and Passow, 1990; Obata et al, 1996). The underlying concept of the critical depth is simply a balance between the production (P) and respiration (R) occurring within a water column (*Fig 1.2b*). Two points within the water column determine this balance, the compensation depth, where respiration balances production, and the critical depth (Z_{cr}), the point above which the vertically integrated production balances the vertically integrated respiration. Thus for the water column above Z_{cr} the net production is positive and positive growth can occur. It is therefore generally assumed that if the depth of the mixed layer (as indicated by the thermocline) is shallower than Z_{cr} net primary production occurs within the water column.

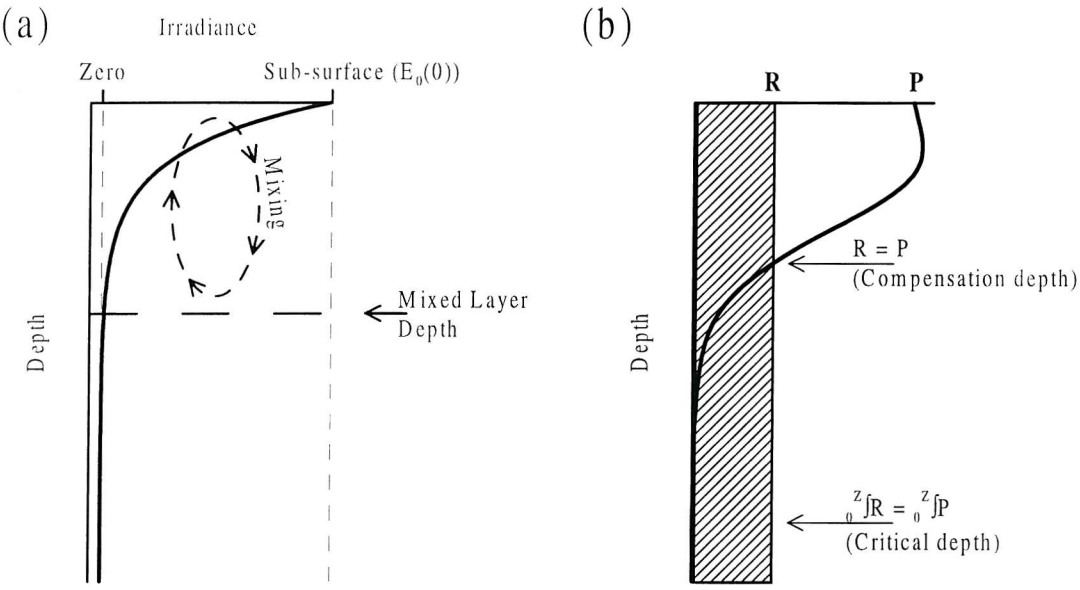

Fig. 1.2 Light penetration and the concept of critical depth. (a) Schematic showing exponential decrease of irradiance within a water column. The mixed layer depth, as governed by the penetration of near surface wind driven mixing, is usually taken to be the depth at which the thermocline commences. Cells in the upper mixed layer are subject to vertical motions driven by turbulent mixing. (b) The concept of critical depth. The volume specific respiration rate (R) is assumed to be constant within the water column while production decreases with depth as a consequence of decreasing irradiance. The points where respiration balances production and integrated respiration balances integrated production are the compensation and critical depths respectively.

Although conceptually useful, certain problems remain with critical depth theory including confusion over whether respiration terms apply to net community or just phytoplankton (Smetacek and Passow, 1990) and the oversimplification inherent in the concept of a mixed

layer (Smetacek and Passow, 1990; Huisman et al. 1999). Additionally the measurement of community or phytoplankton respiration within the environment is difficult, creating problems in verifying the model. Observations which appear to contradict the theory (Townsend et al. 1992) have been criticised as it is often unclear whether the critical depth was estimated correctly (Mann and Lazier, 1996). The extension of the theory to allow for variable rates of vertical mixing demonstrates that under conditions of low turbulence phytoplankton cells can be maintained close enough to the surface over the diel period for growth to occur irrespective of the 'mixed layer' depth (Huismann et al., 1999). Such a mechanism was recognised by earlier authors and effectively constitutes an extension of the concept of critical depth to a 'critical integrated daily irradiance' as defined by the degree of vertical mixing, the surface light level and the loss (respiratory) terms (Sverdrup, 1953; Smetacek and Passow, 1990).

Spectral effects

Due to the nature of the absorption spectrum of both the water and the phytoplankton, shorter wavelengths within the PAR band are attenuated more strongly than longer wavelengths. This causes the spectral quality of the irradiance field changes with depth (Kirk, 1994; Falkowski and Raven, 1997). The depth of phytoplankton within the water column will therefore effect the spectral nature of the light field, as well as the total irradiance experienced.

1.1.4 Nutrients

Nutrient species and Redfield ratios

The principal nutrients necessary for phytoplankton growth are inorganic forms of nitrogen, phosphorus and (for diatoms) silicate (Falkowski and Raven, 1997). However the importance of micro-nutrients, such as iron, in certain regions is becoming increasingly clear (e.g. Behrenfeld et al. 1996; Boyd et al. 2000). Nitrate typically becomes the limiting nutrient first in shelf seas, while the depletion of silicate triggers the transition away from diatom-dominated populations.

The Redfield ratio (Redfield, 1958) is a fundamental paradigm in biological oceanography and concerns the ratio of the key chemical species (C:N:P) in both particulate material and in inorganic dissolved form. This ratio appears to be highly conserved and conforms to around 106:16:1 (e.g. Redfield, 1934, 1958, Copin-Montegut and Copin-Montegut, 1983, Falkowski, 2000). The existence of such a ratio is extremely convenient. For example,

estimates of nitrogen, phosphorus and carbon uptake rates and fluxes are thus freely inter-changeable and modelling of ocean biogeochemical processes is considerably simplified (e.g. Broecker and Peng, 1982; Fasham et al. 1990). However, the C:N:P ratio for uptake by phytoplankton as well as the intra-cellular ratio is variable and dependent on growth conditions (e.g. Falkowksi and Raven, 1997; Geider et al., 1998; Falkowski, 2000). Additionally, various observations have pointed to a decoupling between nitrogen and carbon uptake, particularly over short time-scales O(days) and within shelf-seas (Sambrotto et al. 1993; Sambrotto and Langdon, 1994; Bury *et al.* 2001). The Redfield ratio therefore remains a very useful description of some average condition, but one which should be treated with caution in certain situations.

General distribution, sources and sinks

The distribution of nutrients within the water column is principally determined by the balance between rates of uptake by phytoplankton and inputs, including horizontal and vertical advection, atmospheric deposition, diffusion, nitrogen fixation and regeneration (*Fig. 1.3*). Within temperate shelf seas, deep vertical mixing during winter brings relatively high concentrations of inorganic nutrients to the surface. As light levels and stratification increase in spring, the lower rate of vertical mixing (or shallower mixing depth) causes the amount of light received by phytoplankton to exceed a critical value (see above) and a bloom develops (Sverdrup, 1953; Pingree et al., 1978; Mann and Lazier, 1996).

The high levels of production during this spring bloom, which is typically dominated by diatoms, rapidly uses up the inorganic nutrients in the surface layer (*Fig. 1.3b*). Hence by the summer months the nutrient supply to the upper water column is dominated by vertical mixing across the thermocline and regeneration within the surface. At the same time a proportion of the particulate material generated by phytoplankton growth and by higher trophic processes within the upper water column sinks and is remineralised at depth (*Fig. 1.3*).

Once surface nutrients have been depleted, the thermocline region represents the boundary between the high nutrient and high light portions of the water column (*Fig. 1.3*). Thus the possibility of nutrient supply to this region via turbulent mixing from below, combined with an adequate light supply from above, has often been invoked to explain the frequent observation of enhanced chlorophyll (the deep chlorophyll maximum, DCM) within the thermocline (e.g. Anderson, 1969; Cullen and Eppley, 1981; Holligan et al. 1984b; Sharples et al. 2001a).

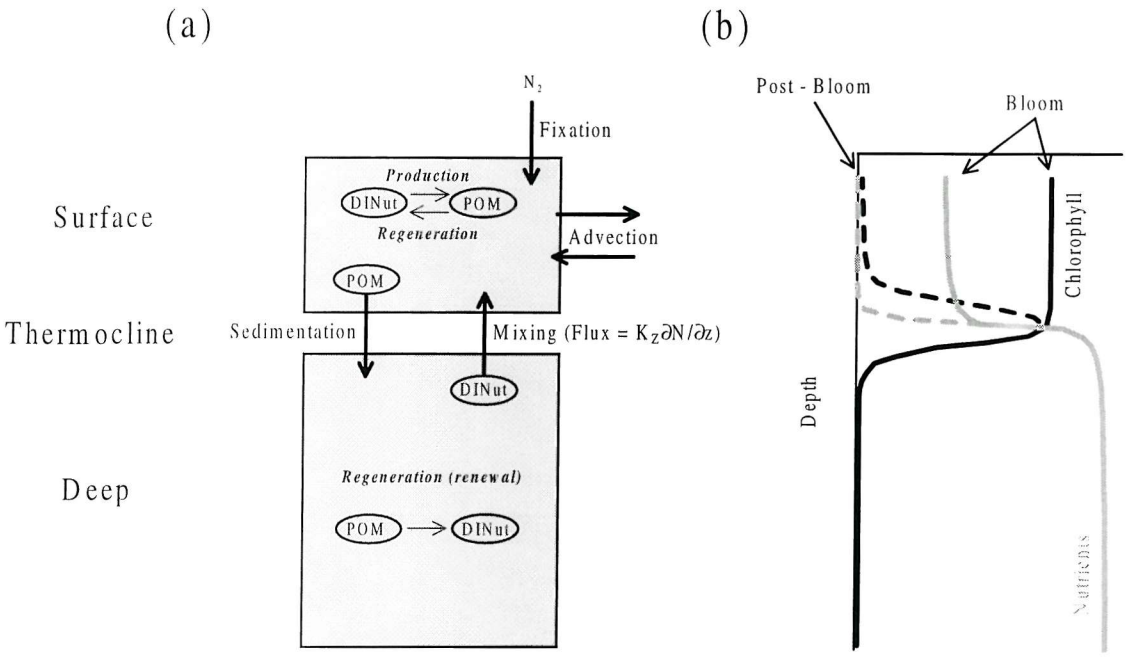

Fig. 1.3 Schematic showing sources and sinks of nutrients within the water column and typical vertical profiles of nutrients. (a) Nutrient sources and sinks and the principal fluxes within a stratified water column. POM – Particulate organic matter, DINut – dissolved inorganic nutrients. In this simplified diagram POM indicates all particulate material including live phytoplankton, detritus and higher trophic levels (zooplankton etc.). Regenerative processes are also simplified. For example, the transfer of POM to dissolved organic material both directly and via the microbial loop before being transformed to DINut is not illustrated. DINut could be replaced by DIN (dissolved inorganic nitrogen) in the majority of shelf seas. (b) Typical vertical profiles of nutrient (grey) and chlorophyll (black) during bloom (solid) and post bloom (dotted) conditions. Diagram is simply representative of the likely distribution of chlorophyll and nutrients under conditions of adequate light prior to and following the depletion of surface nutrients. The relative magnitudes are not meant to represent every situation as, for example, thermocline concentrations of chlorophyll may exceed bloom values in the same location (e.g. Holligan, 1984b; Sharples et al. 2001a)

New and regenerated production

The sources of nutrients can be divided into those supporting 'new' and 'regenerated' production (Dugdale and Goering, 1967). New production refers to those nutrients brought into a region from outside. In terms of nitrogen new production is usually based on nitrate. Regenerated production is that which is supported by nutrients returned to the dissolved pool following the breakdown of particulate material. Again in terms of nitrogen, the important regenerated species are ammonium and to a lesser extent urea. The general pattern of nitrate supply within a stratified water column is thus based on a combination of new production supported by nitrate mixed across the thermocline, and regenerated production based on ammonium, with ammonium preferentially taken up over nitrate (e.g.

Eppley and Peterson, 1979; Lewis et al. 1986; Harrison et al. 1987; Harrison et al. 1996; Planas et al. 1999). The ratio of new to total production is termed the f-ratio (Harrison et al. 1987).

The distinction between new and regenerated production is important, as over sufficiently large scales, the mixing of new nitrate across the thermocline should balance the export of nitrogen in the form of particulate and dissolved organic forms (see *Fig. 1.3*), (Eppley and Peterson, 1979). Hence ultimately the Redfield ratio and f-ratio link the supply of inorganic nitrogen to the biologically driven export of carbon from the surface ocean (Eppley and Peterson, 1979).

1.1.5 Scaling in the oceans

Physical forcing within the marine environment spans a large range of time and space scales, from thousands of kilometres and multiples of years, through to the small scale variations which result from turbulent mixing. As mentioned above, the largest signal of mixing/stratification in temperate shelf seas is typically the seasonal cycle. However smaller scale events, such as transient storms, also alter stratification and mixing. Variability caused by tidal processes working on semi-diurnal or fortnightly (spring – neap) periods is also of potential importance in shelf seas.

Similarly the range of time-scales over which phytoplankton can alter their photosynthetic apparatus in order to cope with changes in the physical environment is also large. Specifically the time-scales of adjustment to changes in irradiance can range from a few minutes for individual cells, through to a few weeks as the phytoplankton community changes (Falkowski, 1984). Variations in phytoplankton physiological parameters related to changes in the nutrient regime are measured in tens of hours (e.g. Behrenfeld *et al* 1996). It is therefore apparent that in order to understand the system in an ecological context, identification of the important scales and the processes which operate at these scales is essential.

By comparing some of the scales of phytoplankton acclimation to scales of physical variability and the specific growth rate (*Fig 1.4*), it is possible to gain an appreciation of the scales of overlap between physical forcing and the biological response.

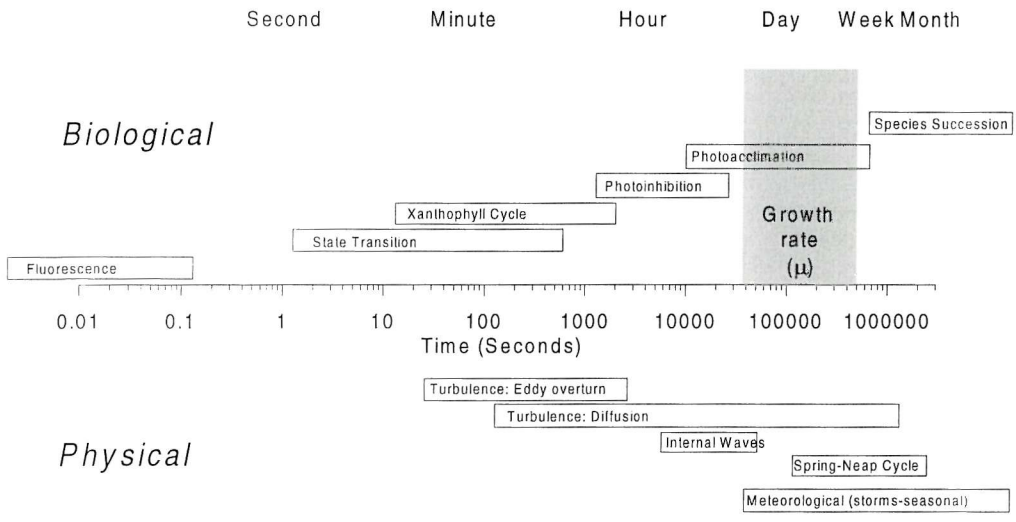

Fig. 1.4 Schematic showing some approximate time-scales of physiological and physical variability associated with phytoplankton ecology. Time-scales associated with turbulent mixing represent the range that could be expected using simple scaling arguments (see Denman and Gargett, 1983 and *Appendix 1*). Some of the physical and physiological processes are further addressed in the following sections.

1.2 Tidal mixing fronts and internal waves as two case studies in physical – biological interactions in shelf seas

1.2.1 Shelf sea tidal mixing fronts as a biological-physical system

The physical mechanism of tidal front generation

Within shelf seas, the competition between mixing due to tidally generated turbulence at the seabed, and buoyancy input due to surface heating, has a fundamental effect on the physical regime (Simpson and Hunter, 1974; Simpson, 1981). Over much of the continental shelf, increasing surface heating during spring inputs sufficient buoyancy into the water column to cause stratification to develop. However in certain regions, characterised by strong mean tidal currents and/or shallow water depths, the water column remains mixed throughout the year, as the average tidally generated mixing is sufficient to overcome the tendency of surface heating to generate stratification (Simpson and Hunter,

1974; Pingree and Griffiths, 1978; Simpson, 1981). The boundaries between the mixed and stratified regions are areas of high horizontal gradients known as shelf sea tidal mixing fronts (e.g. Simpson, 1981, *Figs.1.5 & 1.6*). In these frontal areas, the buoyancy input acting to stratify the water column balances the mixing effect of the tide.

The energetic balance and h/U^3

Simpson and Hunter, (1974) derived terms for the contribution of buoyancy input due to surface heating and mixing due to tides, on the rate of change of potential energy (P.E.) within a water column. In simplified form, the rate of change of the potential energy anomaly (the increase in P.E. in a mixed water column as compared to a stratified water column) was shown to be:

$$\frac{\partial(P.E.(mixed) - P.E.(stratified))}{\partial t} = C_1 Q - C_2 \frac{U^3}{h} \tag{1.5}$$

Where Q is the net rate of surface heat input, U is the depth mean tidal current speed, h is the water depth, C_1 and C_2 are constants and t is time. Thus for a constant heat input, the influence of tidal mixing on water column stratification can be evaluated in terms of the ratio h/U^3 (Simpson and Hunter, 1974; Pingree and Griffiths 1978). The frontal position, where the surface heat input and tidal mixing balance, should therefore correspond to a critical value of h/U^3.

Such simple energetic arguments appear to predict the positions of shelf sea tidal mixing fronts reasonably well (Simpson and Hunter, 1974; Pingree and Griffiths 1978; Loder and Greenberg, 1986). However it has since been shown that the physical structure and position of tidal fronts will be altered by variations in mixing efficiency, wind mixing and cross-frontal circulation (Simpson and Bowers, 1981; Bowers and Simpson, 1987; Pederson, 1994; Simpson and Sharples, 1994).

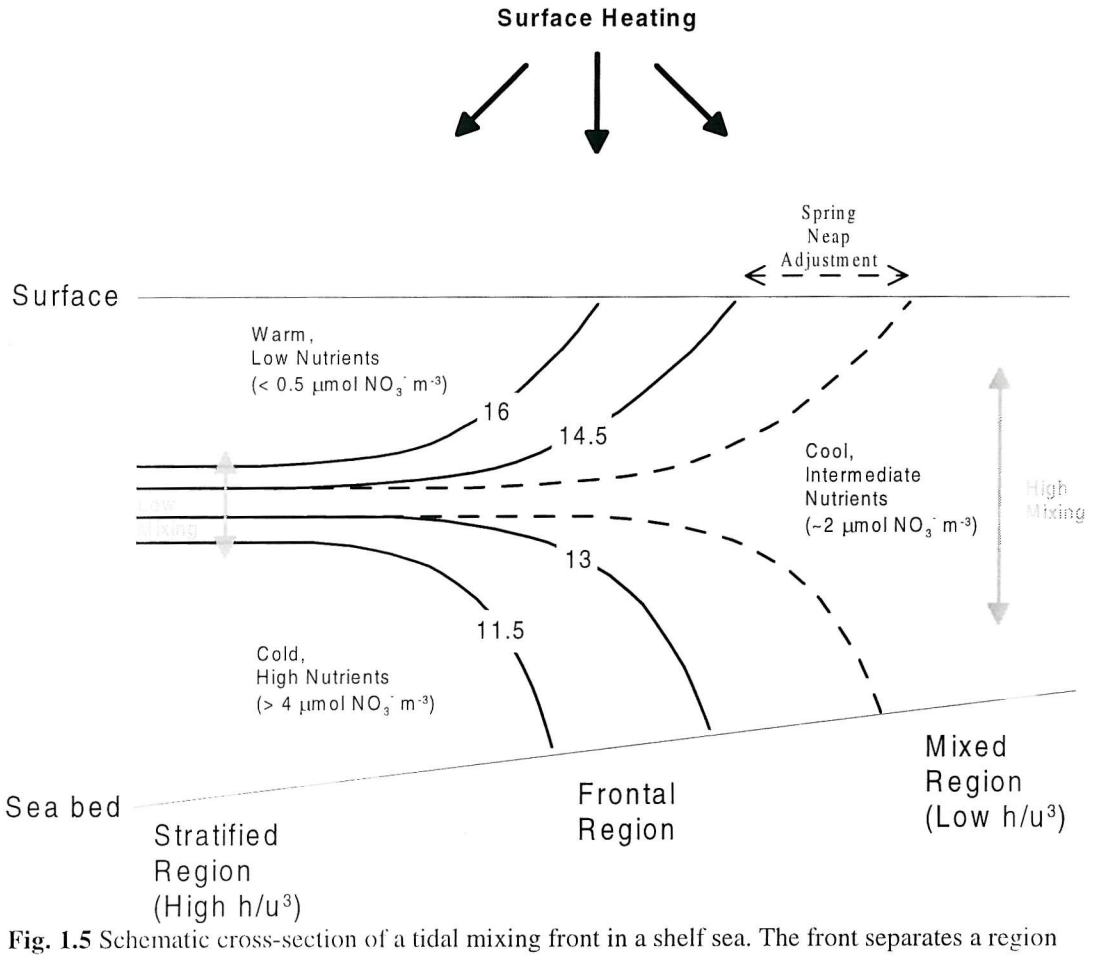

Fig. 1.5 Schematic cross-section of a tidal mixing front in a shelf sea. The front separates a region that is kept well mixed by tidally generated turbulence (right hand side of diagram) from a region that is stratified by the input of buoyancy due to surface heating (left hand side). Black lines are temperature contours, the dotted line indicating the extension of the front into shallower and/or higher mean tidal current regions during neap tides. Temperature and nitrate levels are representative of the Ushant tidal mixing front in August (Holligan, 1981).

Spring-neap adjustment

As frontal position is dependent on the ratio h/U^3, changes in U due to the spring-neap cycle of tidal currents would be expected to drive corresponding changes in frontal position. For example during neap tides, the stratified region could be expected to extend in towards shallower water due to the decreasing tidal currents (*Fig. 1.5*).

Such movement is observed, although the adjustment is typically around 4 km, compared to the 20 – 30 km predicted using the h/U^3 criterion (Simpson and Bowers, 1981; Bisagni and Sano, 1993). During the increase in tidal currents towards spring tides, the tidal mixing must act to break down buoyancy stored during neap tides in addition to the instantaneous input of surface heating (Simpson, 1981; Simpson and Bowers, 1981). The increased stratification also lowers the efficiency of tidal mixing and the combination of these two

effects is likely to cause the smaller observed spring – neap adjustments (Simpson, 1981; Simpson and Bowers, 1981).

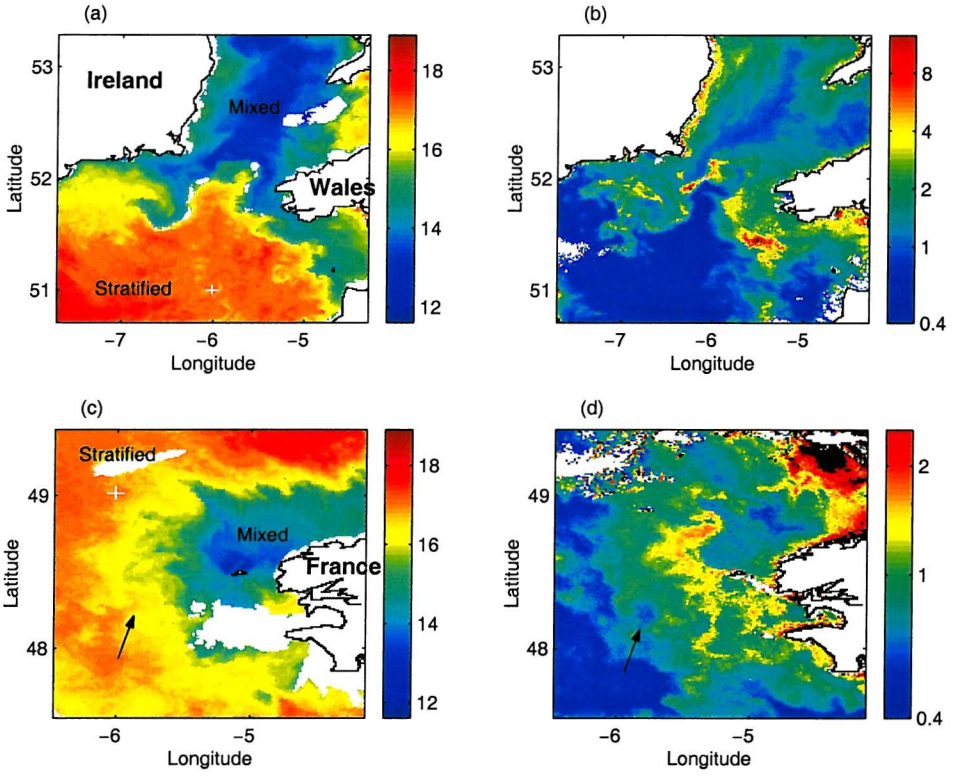

Fig. 1.6 Examples of shelf sea tidal mixing fronts as observed in satellite data. (a & c) Advanced High Resolution Radiometer (AVHRR) derived sea surface temperature (SST, °C) for the Celtic Sea front (a) and the Ushant front (c). (b & d) SeaWiFS (Sea-viewing Wide Field-of-view Sensor) derived surface chlorophyll distribution (mg m^{-3}) for the same regions. The boundaries between the mixed (cooler) and stratified (warmer) waters are marked by strong thermal gradients and enhanced chlorophyll levels. Eddy activity at a number of scales is apparent in the region of the fronts, see arrows in (c & d). All data were collected on 21st July 2000 by the NERC Dundee Satellite Receiving Station and processed by the Remote Sensing Data Analysis Service (Plymouth Marine Laboratory)

Biological consequences of tidal mixing fronts

Increased biological activity in the region of tidal mixing fronts has been observed for some time, with strong relationships existing between both vertical and horizontal temperature gradient regions and increased levels of chlorophyll *a* (e.g. Pingree *et al.* 1975; Savidge, 1976, Pingree *et al.*, 1977, 1978). At a species level, it has often been observed that different functional groups of phytoplankton will tend to dominate in certain regions of the front and at different times (Pingree *et al.* 1978; Simpson, *et al.* 1979; Holligan, 1981; Holligan *et al.* 1980, 1984b; Videau, 1987). Dinoflagellates are often found in frontal

regions and within the thermocline, whereas diatoms and small flagellates are usually more abundant in the mixed and surface stratified areas respectively.

Causes of increased biomass

Various hypotheses for increased phytoplankton biomass around fronts have been proposed. Most of these centre on enhanced production occurring in these regions although convergence in frontal areas should not be neglected (LeFevre 1986; Franks, 1992). Both horizontal and vertical gradient regions (e.g. shelf sea fronts and thermoclines) constitute boundaries between water masses with different biogeochemical and physical characteristics. Three such water masses meet in the vicinity of a tidal mixing front (*Fig. 1.5*).

In accordance with the principles introduced earlier, on the stratified side of the front a high light nutrient depleted top layer is separated from a nutrient rich bottom layer by the thermocline. The thermocline represents the boundary between these two regions and *in situ* growth can be supported here by a vertical flux of nitrate from below and an adequate level of irradiance from above (Jamart *et al.* 1977, 1979; Varela *et al.* 1992; Sharples and Tett, 1994; Sharples *et al.* 2001a). The vertical flux of nitrate through the thermocline also exerts an upper limit on the level of new production which can occur in the surface layers (Dugdale and Goering, 1969; Eppley and Peterson, 1979).

On the mixed side of the front nutrients are not generally fully depleted. This suggests that phytoplankton are light limited in this region (Holligan, 1981). However, the amount of light received by phytoplankton cells on the mixed side of the front will be governed by the water column depth and mixing rate. Thus for tidal mixing fronts where the mixed side is in deep water (e.g. 100m for the Ushant front off north-west France), light limitation and relatively low biomass may occur within the mixed water column (Pingree *et al.* 1977; Holligan, 1981). Conversely if the mixed side is in shallower water (e.g. <60m for the Georges Bank system in the Gulf of Maine), the average light levels encountered by phytoplankton will be higher, allowing increased levels of production on the mixed side (Loder and Platt, 1985; Horne *et al.* 1989).

Nutrient supply to frontal phytoplankton populations

Within the transitional region of the front, consistently high biomass and sustained growth requires that there is a supply of nutrients to the system (Pingree *et al.* 1975; Loder and Platt, 1985). Three principal routes for the supply of nitrate necessary for sustained new production have been identified. The first of these mechanisms is the variation in stratified

area brought about by the springs-neaps frontal adjustment (Pingree *et al.* 1975). As the tidal currents reduce towards neap tides, the stratified area increases. A region of relatively high nutrient water is thus trapped near the surface under high light conditions. Conversely as the tidal currents increase again towards spring tides, this region will be re-mixed and the nutrients replenished. Thus the fortnightly spring-neap cycle drives a stratification-mixing cycle in the frontal region and supplies nutrients for growth (Pingree et al. 1975; Bisagni and Sano, 1993; Morin et al. 1993).

The second suggested mechanism is cross frontal nutrient exchange by baroclinic eddies (Pingree, 1978, 1979). The difference in density between the mixed and stratified surface regions of the front cause the formation of an along front current. This 'frontal jet' will cause instabilities in the front to grow and form eddies on both the mixed and stratified side which can transport nutrients across the boundary. These eddy structures have characteristic time scales of a few days and spatial scales of 20-40km (Pingree, 1978, see also *Fig. 1.6*).

The final mechanism proposed to generate significant nitrate flux is vertical diffusion. As previously discussed when considering the thermocline region on the stratified side, turbulent mixing of a nitrate gradient can cause a vertical nitrate flux. Moving from the stratified to the mixed side of the front, it seems likely that the amount of turbulent mixing occurring at the region of the nitrate gradient may increase (*see Fig 1.5*). It has therefore been proposed that the supply of nutrients from vertical diffusion is increased in the frontal region, while water column stability is still sufficient for a high light levels to be experienced by the phytoplankton (Pingree *et al.* 1975 Tett, 1981). Estimates of the importance of this process for primary production in frontal regions vary greatly (Holligan *et al.* 1984b; Loder and Platt, 1985; Horne *et al.* 1989; Horne *et al.* 1996). This is likely to be due to the problems with developing robust estimates of mixing (diffusivity) over the appropriate time-scales, caused by the large degree of spatial and temporal variability of diffusivity in such regimes (Loder *et al.* 1993).

Loder and Platt, (1985) proposed that vertical turbulent supply is likely to be the most important nutrient supply mechanism, with spring-neap adjustment and eddy transfer following in that order. Additionally, they estimated that the combination of spring-neap adjustment and vertical mixing were capable of supporting 80% of the nitrate requirement for frontal populations. However, many simplifications were necessary in order to derive the estimated fluxes, in particular the unrealistic assumption of a constant value for diffusivity.

1.2.2 Internal waves as a biological-physical system

Internal waves and tides are often generated within stratified water columns by the action of currents over changes of bathymetry (e.g. Sandstrom and Elliot, 1984; Lueck and Mudge, 1997). The passage of such vertical perturbations of the density field will directly effect the light climate of phytoplankton populations (Kamykowski, 1974; Cullen *et al.* 1983; Lande and Yentsch, 1988). The breaking of internal waves can also enhance mixing and the diapycnal nutrient flux (Sandstrom and Elliot, 1984; Holligan *et al.* 1985; Pingree *et al.* 1986; Brickman and Loder, 1993; Sharples *et al.* 2001b).

Generation and on shelf propagation of internal waves

One of the principal generation sites of internal waves in shelf-sea waters is the shelf break (Huthnance, 1989). Here the interaction of tidal currents with the continental shelf can generate large amplitude internal waves, often referred to as the internal or baroclinic tide. Although much work is still focused on the exact mechanisms of internal wave generation and propagation away from the shelf edge, the basic process is well established (Baines, 1982; Holloway, 1994; Gerkema, 1996; Xing and Davies, 1998; Guizien et al. 1999; New and Pingree, 2000). The internal tide is generated over the continental slope when the ebbing tidal flow causes a downward deflection of the thermocline (Baines, 1982; Gerkema, 1996). As the tidal currents slacken this depression separates into an on-shelf and an off-shelf part (*Fig 1.7*). These vertical perturbations of the thermocline then propagate both on-shelf and off-shelf as internal waves (Pingree *et al.* 1986; Holloway et al. 1999).

The propagation of the internal tide onto the shelf is a complex process. The long wavelength perturbation generated at the shelf edge often evolves into a series (packet) of higher frequency internal waves referred to as solitons (Sandstrom and Elliot, 1984; Pingree *et al.* 1986, Holloway, 1987, 1991; Holloway et al. 1999; *Fig 1.7b*). Additionally, as the internal waves propagate into shallow water, hydraulic jumps or internal bore like structures can develop (e.g. Shea and Broenkow, 1982; Pineda, 1991, 1994, 1999, Leichter *et al.* 1996).

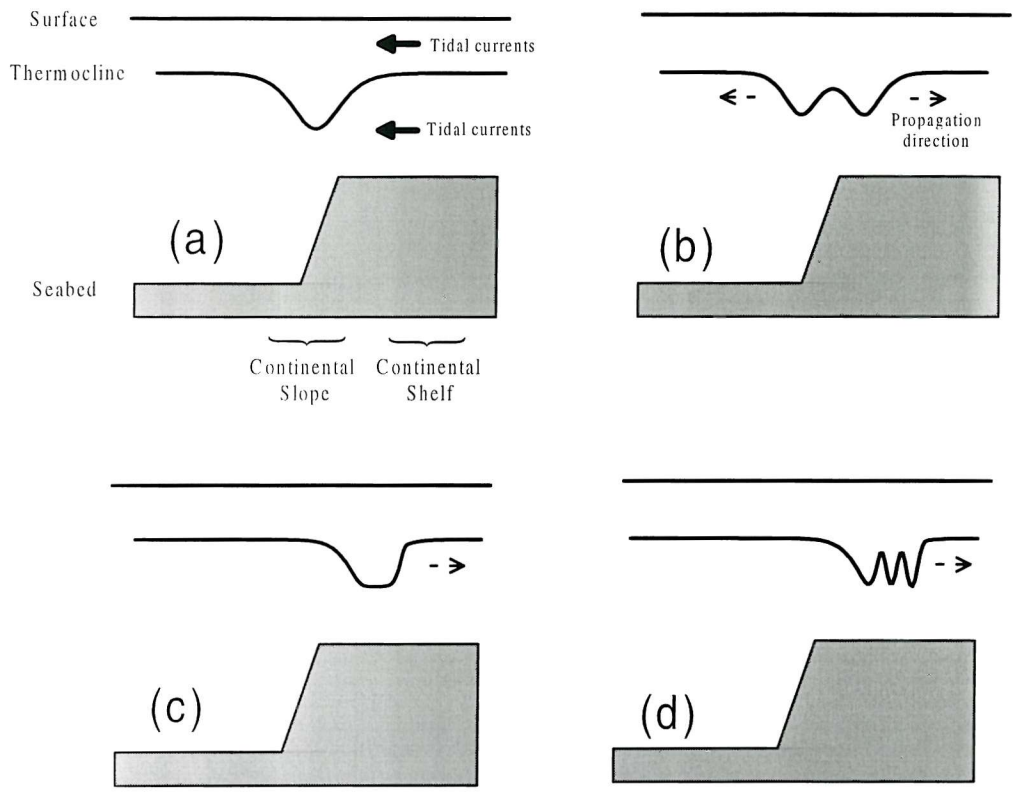

Fig. 1.7 Schematic of internal tide and soliton packet generation at the shelf edge. (a) Offshore tidal streaming generates a depression in the thermocline at the shelf edge. (b) As the tidal currents slacken this disturbance splits and begins to propagate both on- and off- shelf (c) On-shelf propagating wave steepens as it moves in to shallower water. (d) A series of solitons form in the trough of the internal tide as it propagates further on-shelf. Note this schematic is highly simplified and illustrates the process in a simple two layer ocean. In reality the continuous stratification results in waves following characteristic paths or rays (e.g. Holloway, 1996). Off-shelf propagating wave is not illustrated in (c & d).

Possible influences of internal waves on phytoplankton light climate

The movement of the thermocline, caused by the passage of the internal tide, will cause movement of phytoplankton populations within the vertical light gradient. The effect such variations in light intensity may have on the production rate will be dependent on many processes, including the degree of linearity of the wave. The frequency of the variations in light intensity in relation to the rate at which phytoplankton acclimate to this changing light may also be important (Kamykowski, 1974; Lewis *et al.* 1984a; Lande and Yentsch, 1988; see below).

Lande and Yentsch (1988) point out that, due to the exponential nature of the underwater light field, any linear vertical perturbation of phytoplankton about a mean depth will generally cause an increase in the total irradiance the cells are exposed to during the day. However, as recognised by these authors, in near surface waters the photoacclimation of phytoplankton may de-couple the total irradiance experienced by individual cells from the growth rate (Kahru, 1983). Additionally, large amplitude non-linear motions may cause vertical movements which are not symmetrical with respect to a mean depth. Frequently the internal tide is better described as a propagating depression of the thermocline, rather than a linear oscillation about a fixed depth. The timing of the internal tide or higher frequency solitons with respect to the diurnally varying light field will also affect the integrated daily irradiance (Kamykowski, 1974).

Internal waves as 'nutrient pumps'

The idea that internal waves can provide a vertical transport of nutrients has been investigated by many authors since first suggested by Cooper (1947). As the internal tide propagates both on- and off-shelf, the energy in the large amplitude waves is transferred to smaller scales through the internal solitons and bore like structures. Shear is generated within the thermocline by the passage of these non-linear waves. This shear can in turn cause instabilities and breaking to arise. The internal wave energy thus passes to the smallest (turbulent) scales and is dissipated, contributing to increased vertical mixing (e.g. Sandstrom and Elliot, 1984; Bogucki and Garrett, 1993; Sandstrom and Oakey, 1995; Inall *et al.* 2000; Sharples *et al.* 2001b; Jeans and Sherwin, 2001; Lien and Gregg, 2001).

Enhanced mixing can in turn contribute to an increased vertical flux of nutrients in such regions and therefore to a higher rate of (new) production (Holligan *et al.* 1985; Pingree *et al.* 1986; Sharples *et al.* 2001b). Quantifying the magnitude of this effect can be approached in two ways, the vertical flux of nutrients can either be estimated, or the phytoplankton nutrient uptake rates can be estimated and assumed to equal the vertical flux. Little work using the latter method has been performed in regions dominated by large internal motions and the former technique remains problematic due to the highly intermittent nature of the breaking/dissipative processes. Long time scale averages based on the loss of energy in the observed internal wave field as it propagates on shelf can be used to calculate an average diffusivity and hence nutrient flux (Holloway, 1984; Largier, 1994). Such estimates have been observed to compare favourably with more direct methods and the majority of studies conclude that internal wave breaking contributes significantly to enhanced mixing and nutrient flux (Sandstrom and Oakey, 1995; Sharples *et al.* 2001b).

Shelf edge cooling and nutrient fluxes

Regions of cooler water have often been observed at the shelf edge (Dickson et al. 1980, *Fig. 1.8*). It is thought that this band of cooler water is caused by increased mixing generated by the internal tide, possibly via interaction with the wind driven mixed layer (New and Pingree, 1990; Mazé and Tareau, 1990). Nutrients brought to the surface by the increased mixing have the potential to increase phytoplankton growth. The frequent observation of enhanced chlorophyll associated with the band of cooler water at the shelf edge is consistent with such a mechanism (Pingree and Mardell, 1981; Pingree *et al.*, 1986, *Fig. 1.8*). Observations at the shelf edge therefore provide strong, although somewhat indirect, evidence of the importance of internal waves for biological systems.

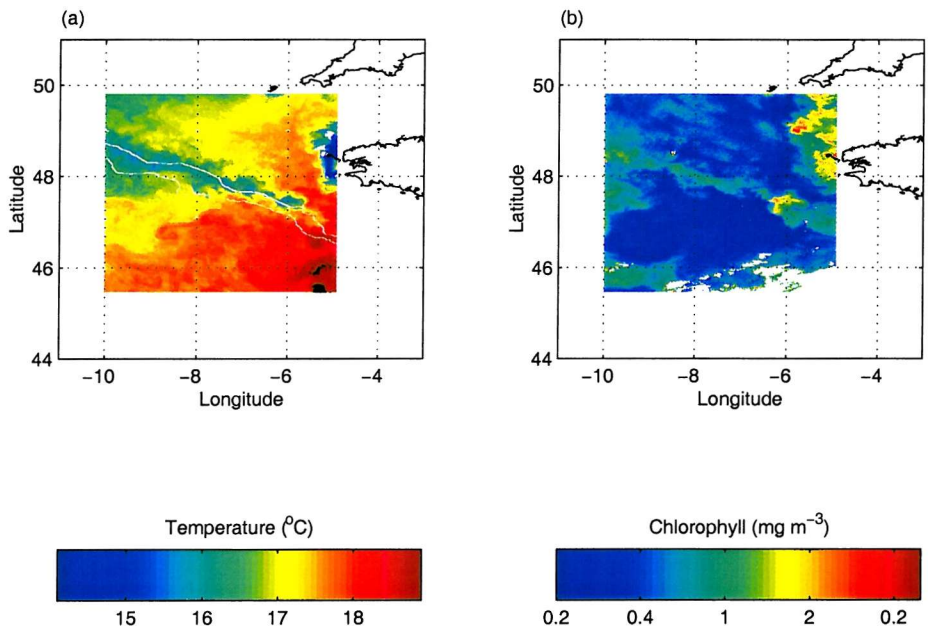

Fig. 1.8 Shelf break cooling as observed in satellite data. (a) Advanced Very High Resolution Radiometer (AVHRR) derived sea surface temperature (SST, °C) for a section of the North West European continental shelf break. (b) SeaWiFS (Sea-viewing Wide Field-of-view Sensor) derived surface chlorophyll distribution (mg m^{-3}) for the same regions. Data collected on 9th July 1999. The 200 and 2000m depth contours are marked in (a). A band of cooler water associated with higher chlorophyll concentrations is clearly aligned with the 200m contour.

1.3 Fast Repetition Rate Fluorometry (FRRF): a method for overcoming the biological sampling problem?

1.3.1 The sampling problem

From the discussion above, it is apparent that shelf sea regions are highly dynamic and are characterised by complex physical-biological interactions. Quantification of the effects of physical forcing on phytoplankton growth rates has remained difficult, as the scales at which phytoplankton physiology and hence growth can be measured in the marine environment are poorly matched to the scales of physical observations and variability. As an example, the physiological state of phytoplankton populations around a front is often inferred from three to five profiles of relatively coarse vertical resolution, see Pingree *et al.* (1975), Holligan *et al.* (1984), Videau, (1987).

An inability to sample variations in phytoplankton physiology at the relevant scales often results in the biological response to physical forcing being inferred from observations of biomass (or species), rather than changes in the productivity or growth rate of the population. This distinction is important, as different ecological processes determine standing stock and growth rate. The productivity and growth of a phytoplankton community is controlled by the response of the community to environmental conditions. However, the accumulation of phytoplankton biomass is not just a function of growth, as many other factors including rates of grazing and sedimentation may also control standing stock (e.g. Banse, 1992; De Baar, 1994).

An increased understanding of how specific processes affect the availability of nutrients and light is therefore not the only requirement in the study of physical-biological interactions. A technique for extending the scales at which physiology and growth can be observed *in situ* is also required in order to test hypotheses concerning the response of phytoplankton to environmental variability. Active fluorescence techniques are one possible way of bridging the gap between the scales at which the physical and biological aspects of such complex systems are observed.

1.3.2 Active fluorescence techniques: Background to use of the FRRF

Excitation and active fluorescence

Excitation energy that is absorbed within the antenna pigments of a phytoplankton cell can only be de-activated via a limited number of pathways. The energy can either be transferred to a reaction centre and used to drive the photochemical reactions described above (§ 1.1.2), be dissipated as heat, or be re-emitted as fluorescence. The de-activation pathways compete for the excitation energy, enabling active fluorescence techniques to be used as a tool for investigating the physiological state of the photosynthetic apparatus.

At room temperature, the majority of the fluorescence emitted by chlorophyll *a* is derived from PSII (Krause and Weis, 1991; Falkowski and Raven, 1997). Under conditions of low light the primary acceptor molecule of PSII (Q_A) is oxidized (*Fig. 1.9*). The majority of excitation energy can therefore be used to drive photochemistry and fluorescence is at a minimum (F_0, Table 1.1); the reaction centre is open. If the amount of light increases so that the rate of excitation transfer to PSII (and hence electron transfer to Q_A) exceeds the rate at which electrons are removed from the acceptor molecule, additional energy arriving at the PSII reaction centre cannot be used to drive photochemistry. The acceptor becomes reduced and fluorescence rises to a maximum level (F_m); the reaction centre is now closed (*Fig. 1.9*).

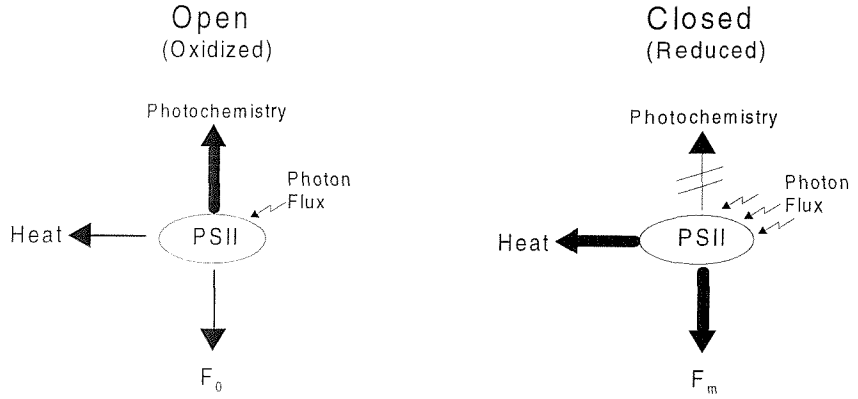

Fig. 1.9 Schematic of de-activation pathways for excitation energy. When excitation is low, the reaction centre is open and fluorescence is low. An increase in excitation energy causes the acceptor side of PSII to become reduced. Photochemistry is blocked and fluorescence increases.

Physiological interpretation of the fluorescence signal: F_v/F_m and σ_{PSII}

Using the relationship between fluorescence yield and the redox state of PSII, the increase in chlorophyll *a* fluorescence caused by the closure of PSII reaction centres under

increasing irradiance can be used to infer some physiological parameters. The fluorescence yield (ΦF) can now be expressed as (Kraus and Weis, 1991):

$$\Phi F = k_f/(k_f + k_d + k_p) \tag{1.6}$$

where k_f, k_d and k_p are the rate constants for de-activation by fluorescence, as heat and by photochemistry respectively. When phytoplankton are dark-adapted, i.e. all the PSII reaction centres are open, using (Eq. 1.6) the fluorescence yield will be at a minimal level:

$$\Phi F_0 = k_f/(k_f + k_d + k_p) \tag{1.7}$$

However, under conditions of saturating irradiance when all the reaction centres are closed, excitation of PSII cannot cause a charge separation, thus $k_p = 0$. The maximum fluorescence yield is therefore:

$$\Phi F_m = k_f/(k_f + k_d) \tag{1.8}$$

Using similar arguments, and (Eqs. 1.7 & 1.8), it is possible to obtain an expression for the quantum efficiency of photochemistry:

$$\Phi_p = k_p/(k_f + k_d + k_p) = (\Phi F_m - \Phi F_0)/ \Phi F_m = F_v/F_m \tag{1.9}$$

where $F_v = F_m - F_0$ (e.g. Krause and Weis, 1991; Olson *et al.* 1996; Falkowski and Raven, 1997). This ratio of the variable fluorescence yield to the maximum fluorescence yield (F_v/F_m) has become an increasingly widely measured parameter in phytoplankton ecology (e.g. Falkowski *et al.* 1991; Geider *et al.* 1993; Greene *et al.* 1994; Olaizola *et al.* 1996; Graziano *et al.* 1996; Strutton *et al.* 1997; Behrenfeld and Kolber, 1999; Boyd *et al.* 1999) and is believed to be related to the availability of nutrients (Kolber *et al.* 1988; Kolber *et al.* 1990; Berges *et al.* 1996). F_v/F_m approaches a species independent maximal value of 0.65 in nutrient replete cultures if measured with a single turnover fluorescence technique (Kolber *et al.* 1988; Kolber *et al.* 1998). Although recent work suggests that high F_v/F_m can be maintained under conditions of balanced nutrient limited growth (Parkhill *et al.* 2001), lower F_v/F_m is generally indicative of nutrient stress (Kolber *et al.* 1988).

A second physiological parameter which can be measured using variable fluorescence is the effective absorption cross section of PSII (σ_{PSII}). This parameter describes the probability of a photon striking a photosynthetically capable target (Falkowski and Raven, 1997). The use of short flashes of light to excite PSII results in the emission of pulses of fluorescence. Increasing the intensity of the excitation flashes results in an increasing

fluorescence yield. The shape of fluorescence/intensity curve can be fit by a Poisson function to derive the effective absorption cross section (σ_{PSII}):

$$\frac{F(E)-F_0}{F_V}=1-e^{-\sigma_{PSII}E} \tag{1.10}$$

where F is the fluorescence yield at flash intensity E (Ley and Mauzerall, 1982; Falkowski *et al.* 1986). If the flash intensity E is known in absolute units, σ_{PSII} can be calculated (m^2 $quanta^{-1}$ or $Å^2$ $quanta^{-1}$).

The value of σ_{PSII} indicates the efficiency with which light is intercepted by the phytoplankton. Higher values of σ_{PSII} will tend to be associated with cultures or populations which have been growing at low light intensities, as the phytoplankton increase their photochemical 'target size' to maximize light absorption (Kolber *et al.* 1988; Vassiliev *et al.* 1994). σ_{PSII} has also been shown to increase under both nitrogen starvation (Kolber *et al.* 1988; Herzig and Falkowski, 1989; Berges *et al*; 1996) and iron starvation (Greene *et al.* 1991; Timmermans *et al.* 2001). Under conditions of nutrient limitation the number of functional reaction centres declines, the antenna complex therefore provides light to fewer reaction centres and hence saturates these faster (Falkowski, 1992). Unlike F_V/F_m, taxonomic variability is apparent in σ_{PSII}, (Kolber *et al.* 1988).

Differences between fluorescence parameters measured in ambient light and dark conditions

Fluorescence yields under ambient and dark conditions vary due to a number of complex processes including the reduction of the various members of the electron transport chain and non-photochemical quenching processes (see below). In keeping with van Kooten and Snel (1990), as well as the majority of recent literature (e.g. Gorbunov *et al.* 2001), the following terminology will be adopted. The minimal and maximal fluorescence yield measured under a dark acclimated state (e.g. at night or after 10-15 minutes relaxation in the dark) are denoted F_0 and F_M. The steady state, minimal and maximal fluorescence yields measured under ambient light are denoted F', F_0' and F_M', and the functional absorption cross section measured under ambient light is denoted σ_{PSII}' (Table 1.1).

Term	Definition	Units
F_0,F_M	Minimal and maximal fluorescence yields measured in dark adapted state	a.u.
F_0',F',F_M'	Minimal, steady state and maximal fluorescence yields measured under ambient irradiance	a.u.
F_V	Variable fluorescence (=F_M-F_0)	a.u.
$\Delta F'$	Change in fluorescence yield measured under ambient light (=F'_M-F')	a.u.
F_V'	Variable fluorescence measured under ambient light (=F_M'-F_0')	a.u.
F_V/F_M	Maximum quantum efficiency of photochemistry	D
$\Delta F'/F_M'$	Quantum yield of photochemistry measured under ambient light	D
σ_{PSII}	Functional absorption cross section of PSII in the dark	$Å^2$ $quanta^{-1}$
σ_{PSII}'	Functional absorption cross section of PSII under ambient light	$Å^2$ $quanta^{-1}$

Table 1.1 Notation for fluorescence derived physiological parameters. For units, a.u. is arbitrary units and D signifies a dimensionless quantity

The Fast-Repetition Rate Fluorometer (FRRF)

Various techniques have been used to study active fluorescence, including pump and probe (Falkowski *et al.* 1986; Kolber and Falkowski, 1993) and pulse amplitude modulation (PAM) fluorometry (Hofstraat *et al.* 1994). The FRRF technique uses a rapid series of individually sub-saturating light pulses which cumulatively saturate the reaction centres (*Fig 1.10*). The duration and interval between pulses (around 1μs) is such that a whole flash sequence of around 50-100 pulses occurs within a single turnover of the PSII reaction centres (Kolber *et al.* 1998). This means that only the primary stable electron acceptor (Q_A) undergoes large changes in redox state during the saturation process, as the time constant for the reduction of Q_B (Q_A^-,Q_B → Q_A,Q_B^-) is around 100-200μs (Krause and Weis, 1991; Kolber *et al.* 1998, see also *Fig. 1.1*). Estimates of F_v/F_m and σ_{PSII} can therefore be made very rapidly and the use of the instrument in a submersible form allows *in situ* measurement of these physiological parameters of a phytoplankton population.

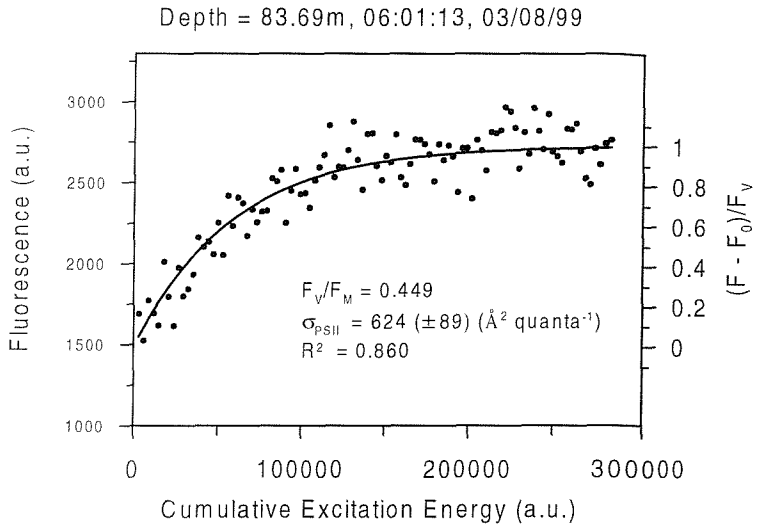

Fig. 1.10 An *in situ* fluorescence induction curve measured at a depth of 87m at a mixed site on the NW European shelf using a submersible FRRF. The increase in fluorescence from F_0 to F_m can be fitted to (Eq. 1.10) using a least squares technique (black line), to give the value of σ_{PSII}. In order to use (Eq. 1.10) in the case of cumulative saturation, it must be assumed that the amount of Q_A^- re-oxidation occurring during the flash protocol can be neglected. It is also necessary to assume that there is no transfer of excitation energy between PSII reaction centres, as this would alter the shape of the saturation curve (Ley and Mauzerall, 1986; Berges *et al.* 1996; Kolber *et al.* 1998). These assumptions do not necessarily hold and a more robust biophysical model can be developed for general case (Kolber, 1997; Kolber *et al.* 1998 see also *Appendix 2*)

The use of active fluorescence for the calculation of photosynthetic rates

Fluorescence derived parameters can be used to calculate rates of photosynthetic electron transport (Genty *et al.* 1989; Kolber and Falkowski, 1993), and thus estimate primary production. A biophysical model can be developed which relates the rate of photosynthesis as measured by gross oxygen evolution (P^*_{O2}) to fluorescence measurable parameters because PSII is responsible for both oxygen evolution and variable fluorescence (Falkowski and Raven, 1997). Further, by assuming a balance between oxygen evolution and carbon fixation, the rate of biomass specific carbon fixation (P^*) can also be estimated.

The photosynthetic electron transport rate (ETR) can be estimated using the following photosynthetic model (e.g. Genty *et al.* 1989; Kolber and Falkowski, 1993; Flameling and Kromkamp, 1998; Kolber et al. 2000):

$$ETR = \Delta F'/F_M' \; \sigma_{PSII}' \; E \qquad \text{for } E < E_k \tag{1.11a}$$

$$ETR = \Delta F'/F_M' \; \sigma_{PSII}' \; E_k \qquad \text{for } E \geq E_k \tag{1.11b}$$

Where E is the irradiance and E_k is the saturation light intensity. Kolber and Falkowski (1993) and Suggett *et al.* (2001) use more complex forms of (Eq. 1.11), however the added complexity does not greatly alter the derived rates. The simplest equation for the calculation of ETR (Eq. 1.11) is thus adopted here (Flameling and Kromkamp, 1998; Kolber et al. 2000).

In order to convert the ETR to an equivalent carbon fixation rate (P*), the number of PSII reaction centres (n_{PSII}), the photosynthetic quotient (PQ, the ratio of moles O_2 evolved:per mole carbon fixed) and the quantum efficiency of electron transport through PSII are required (Kolber and Falkowski, 1993). It will be assumed that the latter term is constant (=0.25) i.e. 4 photons are required for the generation of 1 molecule of O_2 within PSII, noting that this may be invalid especially at high irradiances (Flameling and Kromkamp 1998). Thus the FRRF derived chlorophyll specific rate of carbon fixation (P^*_{FRRF}) expressed in units of [mg C (mg chl *a*)$^{-1}$ hr^{-1}] can be calculated as:

$$P^*_{FRRF} = A\frac{n_{PSII}\,ETR}{PQ} \tag{1.12}$$

where the ETR is expressed in units of electrons per PSII reaction centre per second (e RC^{-1} s^{-1}), n_{PSII} is the number of reaction centres per chl *a* molecule (mol RCII/mol chl *a*). The factor A is assumed to be constant (=18.6) and includes a factor of 1/0.65 to convert F_v/F_m to a measure of the proportion of functional reaction centres (Geider et al. 1993; Kolber and Falkowski, 1993), as well as the previous factor of 0.25 and the conversion of, moles of carbon and chlorophyll *a* to mg, and s^{-1} to hr^{-1}.

The number of reaction centres per chlorophyll *a* molecule (n_{PSII}) must typically be assumed (≈1/500), although this may be variable and is a source of some uncertainty in the use of (Eq. 1.12) (Kolber and Falkowski, 1993). A method for the estimation of this parameter was proposed by Suggett *et al.* (2001).

1.3.3 Acclimation of the photosynthetic apparatus to changes in irradiance

State transitions

As electron transport requires PSI and PSII to work in series, any imbalance in the distribution of light energy between these two photosystems will result in a reduction of efficiency within the photosynthetic apparatus. The state transition is a mechanism which allows for the re-distribution of energy between the two photosystems (Ley, 1980; Allen, 1992; Falkowski and Raven, 1997). This process is relatively rapid, occurring on time-scales of seconds to minutes (Ley, 1980) and is thought to involve the de-coupling of part of the light harvesting complex from one of the photosystems, followed by migration to the other photosystem (Allen, 1992, Falkowski and Raven 1997).

Non-photochemical quenching

Over slightly longer time-scales, phytoplankton can reduce the amount of excitation energy utilised for photochemistry by increasing the amount of energy dissipated as heat within the antenna. Increased heat dissipation leads to a decrease in both F_0 and F_m which is independent of the redox state of Q_A (Falkowski and Raven, 1997). This process is known as non-photochemical quenching and can be associated with decreases in σ_{PSII} on the order of 50% (Falkowski *et al.* 1994; Olaizola *et al.* 1994). These changes occur on time-scales measured in 10s of minutes and (at least in diatoms) are thought to be associated with a reversible reaction between two xanthopyll pigments (Olaizola and Yamamoto, 1994).

Photoacclimation

Over time periods of a few hours to a few days, phytoplankton will acclimate to the mean long term irradiance they encounter (e.g. Falkowski, 1980; Falkowski, 1984; Post *et al.* 1984; Cullen and Lewis, 1988). A variety of parameters can be altered on these time-scales. In particular as irradiance increases, a reduction in chlorophyll *a* per cell as well as a decrease in the ratio of photosynthetic to non-photosynthetic pigments occurs (e.g. Berner *et al.* 1989). Variations in pigmentation have a large effect on the absorption properties of phytoplankton, both the functional and optical absorption cross sections decreasing at higher growth irradiance (Ley and Mauzerall, 1982; Falkowski *et al.* 1985; Kolber *et al.*, 1988; Berner *et al.*, 1989). This reduction is due to an increase in the proportion of pigments that absorb light but do not transfer excitation energy to PSII. The increased self-shading of chlorophyll molecules as their density increases within the cell, termed the 'package effect', also contributes to lower optical absorption cross sections in

low light acclimated cells (Dubinsky *et al.* 1986; Berner *et al.* 1989; Falkowski and Raven, 1997).

The kinetics of photoacclimation have been widely studied, with half times ranging from fractions to tens of hours (e.g. Falkowski, 1980; Lewis *et al.*, 1984a; Cullen and Lewis,, 1988; Sukenik *et al.*, 1990; Dusenberry *et al.* 2001). In the natural environment acclimation time scales may be greater than the photoperiod, however it appears that phytoplankton acclimate to the mean daily irradiance rather than shade acclimating at night (Post *et al.*, 1984).

Species succession

Over time-scales of days to weeks, changes in the light environment may occur which cause different species to become more suited to a location due to their specific adaptive traits (Falkowski, 1984). Thus changes in the degree of stratification in a region or time of year can cause changes in the community structure.

1.4 Principal objectives

The main objective of this thesis is to demonstrate how physical processes in shelf seas affect the growth and distribution of phytoplankton. This will be achieved by attempting to quantify the contribution of physical forcing to variations in light and nutrient flux using a variety of techniques, principal amongst which are estimates of turbulent mixing rates derived from microstructure measurements. Further, the physiological and hence growth response of phytoplankton to such changes in physical forcing will be investigated using biological data including FRRF-based observations. The work thus represents some of the first attempts to collect and interpret FRRF data in well defined physical contexts.

A description of the general methods used in this study is provided in *Chapter 2*, with particular attention to the FRRF technique and microstructure measurements for estimating turbulence dissipation and mixing rates. The scientific objectives addressed in the subsequent four chapters are:

Chapter 3 *An evaluation of the effects of physical forcing on phytoplankton physiology in the vicinity of a tidal mixing front.* FRRF based physiological observations are interpreted in terms of differentials in light availability and nutrient fluxes, driven by

the gradient of vertical mixing from highly stratified to fully mixed waters. Physiological data are used to asses whether the high chlorophyll concentrations in the vicinity of frontal regions results from active growth.

Chapter 4 *An evaluation of the influence of large amplitude internal waves on phytoplankton.* Detailed physical observations enable the flux of nutrients generated by internal wave breaking to be quantified. An attempt is made to quantify the direct result of vertical motions on the light climate experienced by phytoplankton. FRRF derived physiological data are interpreted in relation to both vertical motions through the light gradient and the general physical oceanography of the study region.

Chapter 5 *An evaluation of productivity estimated using the application of photosynthetic models to FRRF data.* Relationships between environmentally driven changes in FRRF derived photophysiology and ^{14}C derived carbon fixation are investigated. FRRF and ^{14}C P^* vs. E derived photosynthetic rates and physiological parameters are compared. Discrepancies between the methods, which may result from the inherently different nature of the two measures of photosynthesis, or from the limitations involved in applying current photosynthetic models to field FRRF data, are discussed.

Chapter 6 *A synthesis of estimated productivity rates and inferred new production rates from the shelf sea sites investigated during the previous chapters.* The ability of the FRRF technique to estimate mean daily *in situ* productivity rates is assessed. Physical and biological data from the preceding chapters is utilised to evaluate the factors limiting production and growth. Ecological differences between the study sites are interpreted in terms of both the magnitude of tidal dissipation and the form this dissipation takes.

2. Methods

2.1 Background to sampling strategy

Data collected during three cruises will be presented in this thesis, one on the North West European continental shelf and two on the New Zealand continental shelf (*Table 2.1*). Common methods of FRRF data acquisition and analysis will be discussed in this chapter. The less traditional physical measurements will be discussed, specifically microstructure estimates of turbulent mixing rates. A brief description of the methods used for additional data collection including chlorophyll, nutrients, pigments and ^{14}C uptake experiments is also included. Cruise specific methods and sampling strategies are discussed further in the relevant chapters.

2.2 FRRF data collection and processing

2.2.1 Instrument description and deployment strategies

Instrument description

The FRRF instruments used were manufactured by Chelsea Instruments (CI Fastracka™). The optical head of the instrument consists of two separate excitation sources consisting of banks of blue light LED's with a peak emission spectrum of 478nm and approximately a 30nm half-bandwidth, (*Fig 2.1*). Some of the light from the excitation source is absorbed by the *in situ* phytoplankton population, a proportion being re-emitted as fluorescence at a wavelength of around 680nm. The fluorescence signal emitted by the sample is then measured by a single shared photo-multiplier tube (PMT). This set-up allows measurement of initial and saturated fluorescence under conditions of ambient light and following rapid removal into the dark. Parameters measured in the 'light chamber' thus correspond to F', F_M' and $\Delta F'/F_M'$ under daylight conditions, with parameters measured in the 'dark chamber' corresponding to F_0', F_M' and F_V'/F_M' (c.f. *Table 1.1*).

Saturation flash protocol

During all deployments, variable chlorophyll fluorescence was stimulated using a saturating sequence of 100 1.1μs duration flashes, at 1.7μs intervals, the entire

fluorescence saturation protocol therefore lasting around 280µs. This whole sequence was performed 16 times and the fluorescence transients averaged internally to form one measurement. For *in situ* operations and most on-deck work, data were stored internally for download at a later time, although data were acquired in real – time during some deck-board operations during the final cruise.

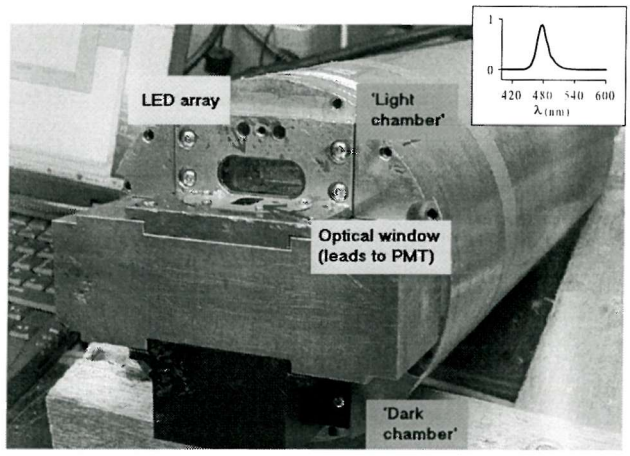

Fig. 2.1 Picture of the FRRF instrument showing the optical head. The set-up of the sampling areas exposed and shaded from ambient light (the 'light' and 'dark' chambers respectively), is identical, the dark chamber having a simple cover to remove phytoplankton from ambient irradiance. Inset: FRRF emission spectrum

Deployment modes

The FRRF was interfaced to a CI PAR sensor and pressure sensor during all *in situ* deployments and power was provided by the manufacturers purpose built battery packs. Two principal *in situ* modes of deployment were undertaken. During all cruises the FRRF instrument was attached to the CTD frame to obtain vertical profiles of phytoplankton physiological parameters (*Fig 2.2a,b*). Unfortunately, due to instrument failure, only limited data was collected during the 1998 cruise. Profiles with the CTD frame were performed as slowly as possible (~1ms^{-1}) in order that high vertical resolution and some averaging could be accomplished. During the Nov-Dec 2000 cruise the CTD was Yo-Yo'd around six times during each cast in order to improve the vertical sampling resolution.

Additionally the FRRF was attached to the underside of a towed undulator (SeaSoar) during the August 1999 cruise (*Fig 2.2c*).

Bench-top operation

FRRF instruments were also employed for sampling the underway non-toxic supply during the August 1999 cruise, as well as being employed in a bench-top mode for sampling a series of laboratory studies throughout the last cruise. For underway sampling the ships non-toxic supply was plumbed straight into the 'dark chamber' of the FRRF. During the 2000 cruise, discrete samples collected from a variety of depths within the water column

were placed into acid rinsed opaque bottles. These bottles were then placed in a water bath cooled to sea surface temperature for > 15 minutes to allow relaxation of both photochemical and non-photochemical quenching. A sub-sample was then transferred to the 'dark chamber' of the FRRF instrument for analysis.

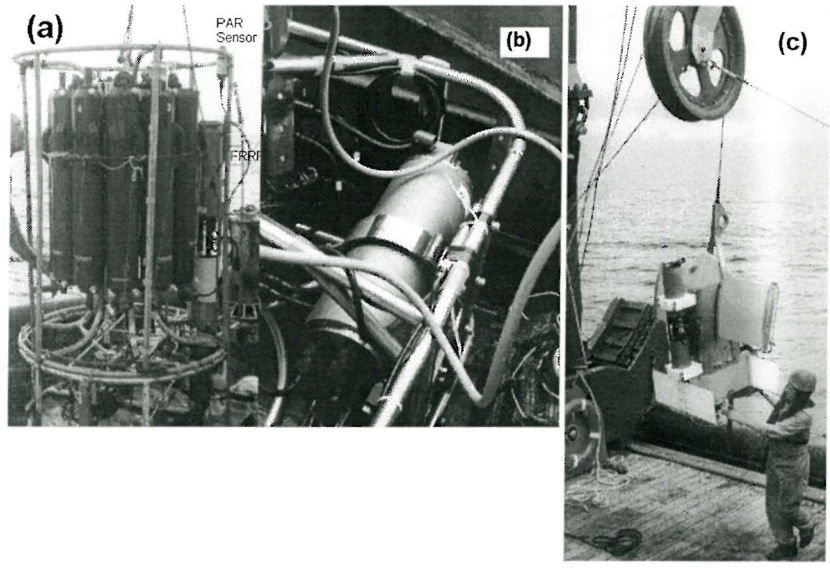

Fig. 2.2 FRRF instruments as deployed *in situ*. (a,b) FRRF's attached to CTD frames, (a), Nov-Dec 2001, (b) August 1999. (c) FRRF attached to SeaSoar undulator

A series of light manipulation experiments were also performed during the final cruise. Samples were incubated in acid washed 20 l polycarbonate carboys placed inside a purpose built incubator cooled to sea surface temperature. The light level was controlled by placing a variety of neutral density filters in front of a bank of 6 halogen spot lights. Samples were agitated by continuously bubbling filtered air through the incubation chamber. Physiological measurements were performed by pumping the samples through the 'dark chamber' of a deck board FRRF, the output from the instrument being recorded directly onto a PC. A single peristaltic pump and series of switchable valves allowed samples to be pumped to waste or re-circulated after passing through the FRRF instrument. The switching system also allowed rinsing of the FRRF 'dark chamber' between analyses of different samples.

2.2.2 Initial data analysis

Analysis of fluorescence signals and retrieval of physiological measurements

Data from *in situ* deployments were downloaded to PC's. The fluorescence transients were then fitted to the model of Kolber *et al.* (1998), in order to retrieve F_0, F_M and σ_{PSII}. This fitting procedure was performed in two ways, the first utilising the custom software provided by the instrument manufacturers and originated by Z.S. Kolber. The second

method used custom software written in MATLAB™ by the author and based on original codes provided by S.Laney.

In order to assess the sensitivity of physiological parameter estimation to variations between instruments and raw data analysis, a series of tests were carried out using both field and simulated data sets. Details of these tests on data quality are presented in *Appendix 2*. In summary, comparisons between different instruments were good, while errors in F_v/F_m and σ_{PSII} were estimated to be below 10% in the majority of cases, rising to around 20% in low chlorophyll regions. No major differences could be detected between the two methods for curve fitting and blank correction was thought to be of minor importance in the majority of cases (see *Appendix 2*). *In situ* FRRF data was typically binned into 5m intervals for each vertical profile. Values for which the estimated uncertainty in the measured parameter (e.g. σ_{PSII}) was greater than 20% were rejected. Standard deviations of the 5m depth binned data for the 2000 cruise were generally lower than for the 1999 cruise. This resulted from the increased number of samples in individual depth bins as a result of the Yo-Yo nature of the CTD profiles. Increased accuracy of the mean values for 5m depth binned data was thus likely for the 2000 cruise.

2.3 Microstructure measurements

2.3.1 Instrument description

Two different microstructure instruments were employed for the estimation of turbulent dissipation and mixing rates. During the Nov-Dec 1998 & 2000 cruises on the New Zealand shelf, the Self-Contained Autonomous Microstructure Profiler (SCAMP, e.g. Ruddick *et al.* 2000) was used to measure the vertical temperature gradient microstructure. The SCAMP instrument free-falls through the water column at around 10cm s^{-1}, sampling a pair of fast thermistors (Thermometrics FP07's) at 100Hz. The instrument thus resolves the temperature gradient microstructure at scales O(mm). During the August 1999 cruise, vertical profiles of velocity gradient microstructure were obtained using the Free-fall Light Yo-Yo (FLY) shear profiler (Dewey *et al.* 1987). FLY free-falls through the water at a rate of around 80cm s^{-1} and resolves horizontal velocity shear at a scale of around 1cm by way of an airfoil probe (Dewey *et al.* 1987). Both instruments were also used to measure vertical profiles of salinity and temperature. SCAMP is fitted with a combined temperature

and conductivity cell and additional fast conductivity sensor, whilst FLY employs a separate conductivity cell and fast temperature sensor.

2.3.2 Principals of measurement and data analysis

Temperature gradient microstructure

Resolution of the smallest scales of temperature gradient allows both the vertical diffusivity of heat (K_T) and the turbulent dissipation rate (ε) to be estimated. Under the assumptions that the vertical flux of thermal variance dominates lateral fluxes and that the turbulent field is isotropic, the vertical heat diffusivity can be written, (Osborn and Cox, 1972):

$$K_T = \frac{\chi}{2}\left(\frac{\partial \overline{T}}{\partial z}\right)^{-2} \tag{2.1}$$

where $\partial \overline{T}/\partial z$ is the mean vertical temperature gradient and χ is the rate of dissipation of thermal variance estimated as:

$$\chi = 6D_t\overline{\left(\frac{\partial T}{\partial z}\right)^2} \tag{2.2}$$

with D_t the molecular heat diffusivity ($= 1.4 \times 10^{-7}$ m^2s^{-1}).

The rate of dissipation of turbulent kinetic energy (ε) can be estimated by fitting the observed temperature gradient spectrum to the Batchelor spectrum, (Batchelor, 1959; Gibson and Schwarz, 1963; Dillon and Caldwell, 1980; Oakey, 1982). This was performed on SCAMP data in 1m segments using the method of Ruddick *et al.* (2000), (*Fig 2.3*).

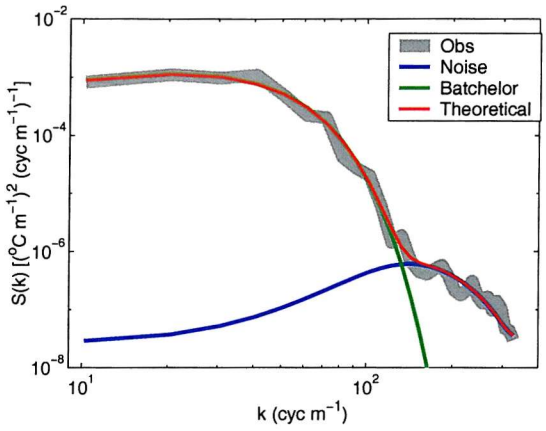

Fig. 2.3. Fitting of observed spectrum of vertical temperature gradient microstructure to the Batchelor form. Observed spectra are generated on 1m segments of the vertical profile. The theoretical spectrum is then calculated as the sum of the Batchelor spectrum and the modelled noise spectrum for the SCAMP thermistors and electronics. The observed spectrum is then fitted to the theoretical spectrum using a maximum likelihood technique (Ruddick *et al.* 2000, Sharples *et al.* 2001b). For the shown fit the Batchelor wave number is 89 m^{-1} and $\varepsilon = 2.7 \times 10^{-9}$ $m^2 s^{-3}$.

Velocity gradient microstructure

Resolution of velocity shear at the scales measured by FLY enables direct estimation of the dissipation rate, provided the turbulence field is again assumed to be isotropic, using (e.g. Osborn, 1974; Osborn, 1980):

$$\varepsilon = 7.5\mu\overline{\left(\frac{\partial u}{\partial z}\right)^2} \tag{2.3}$$

where μ is the kinematic viscosity of seawater ($=1.0 \times 10^{-6}$ $m^2 s^{-1}$). The mean square shear ($\overline{(\partial u/\partial z)^2}$) was calculated from vertical FLY profiles using the observed spectrum of vertical velocity gradient microstructure within 1.5m segments following Simpson *et al.* (1996). The initial analysis of FLY data for the 1999 cruise was performed by N. Fisher, T. Rippeth and J. Simpson (see *Appendix 3*).

Knowledge of the background gradient against which this turbulent dissipation is working, as signified by the buoyancy frequency:

$$N^2 = \frac{-g}{\rho}\frac{\partial \rho}{\partial z} \tag{2.4}$$

(where g and ρ are the acceleration due to gravity and the density respectively), then allows estimation of the eddy diffusivity of density according to Osborn (1980):

$$K_\rho = \frac{R_f}{1 - R_f} \frac{\varepsilon}{N^2} \tag{2.5}$$

where R_f is the flux Richardson number and is taken to be 0.17 (e.g. Osborn, 1980; Moum, 1996).

Relative quality of retrieved mixing information

Turbulence in marine environments is by nature patchy in both time and space. The slower fall speed of the SCAMP instrument necessarily results in a lower sampling resolution. Additionally the degree of relative drift between the instrument and the ship during a profile is increased. This often resulted in SCAMP profiles not being performed to the full water depth, while a greater number of FLY profiles could be performed in the same period and would all impact the bottom. The relative quality of the turbulence parameters and mean mixing rates etc. retrieved from the FLY data sets was therefore generally superior to those estimated using SCAMP data.

2.3.3 Vertical nutrient fluxes

The principal reason for the collection of microstructure data was to estimate the vertical nutrient flux under a variety of conditions. For any given nutrient of concentration A, the vertical nutrient flux can be calculated once the vertical nutrient gradient and the vertical diffusivity (K_Z) are known, according to:

$$\text{nutrient flux} = -K_Z \left(\frac{\partial A}{\partial z} \right) \tag{2.6}$$

In order to implement this model it was assumed that the vertical diffusivity of all properties was equal (i.e. $K_T = K_\rho = K_Z$). Calculations of vertical nutrient fluxes using methods similar to the one described have been performed in both open ocean and shelf sea regions by Lewis *et al.* (1986) and Horne *et al.* (1996) amongst others.

2.4 Additional observations

In order to provide information on the physical and ecological context in which FRRF and microstructure measurements were obtained, a suite of additional observations were collected on all cruises. Due to the time constraints imposed by FRRF and microstructure

observations, much of this additional data collection was not performed by the author (*Appendix 3*).

2.4.1 Hydrographic data

Temperature, salinity and currents

Profiles of temperature and conductivity (and hence salinity) against depth (CTD profiles) were obtained during all cruises. Two types of CTD (see *Table 2.1*) were deployed using standard protocols and were calibrated against reversing thermometers and discrete water samples analysed on a Guildline Autosal salinometer. Salinity calibrations of CTD's were better than ±0.005 (PSS78) for all cruises and temperature calibrations better than ±0.004°C. Standard chlorophyll fluorometers were also attached to the CTD frame during all cruises and a Chelsea instruments transmissometer was attached to the frame during the Nov-Dec 2000 cruise (*Table 2.1*).

A vessel-mounted RDI narrowband Acoustic Doppler Current Profiler (ADCP) was operated on the RRS *Challenger* throughout the August 1999 cruise, providing vertical profiles of current velocity.

Mooring arrays, principally consisting of self logging thermistors and upward facing SonTek ADCP's, were also deployed during the two cruises on the New Zealand shelf (Nov – Dec 1998 & 2000). The precise set-up of the mooring arrays during these two experiments will be described in more detail in Chapter 4.

Nutrients

Water samples were collected for nutrient analysis during all three cruises in Niskin bottles using the CTD sampling rosette. During the August 1999 cruise, samples were analysed for nitrate, silicate and phosphate on board using a Burkard segmented flow AA-II type autoanalyzer. Nitrate plus nitrite was evaluated following the standard sulphanilamide and napthyl-ethylene diamine dihydrochloride method (Grasshoff *et al.*, 1983). Dissolved silicon analysis followed the standard AAII molybdate-ascorbic acid method with the addition of a 37 °C heating bath (Hydes, 1984). Phosphate analysis also followed the standard AAII method of Hydes, (1984). All samples were run in duplicate. The calibration ranges used were 0 -2.5 mmol m^{-3} for phosphate and 0-10 mmol m^{-3} for nitrate and silicate. Detection limits were (1% of full scale) 0.025 mmol m^{-3} for phosphate and 0.1 mmol m^{-3} for nitrate and silicate. The mean differences between duplicates were, in terms of

concentration, 0.05 mmol m^{-3}, 0.04 mmol m^{-3}, and 0.015 mmol m^{-3} for nitrate, silicate and phosphate respectively.

During the Nov – Dec 1998 & 2000 cruises samples were frozen immediately after collection then returned to the laboratory and again analysed using the standard sulphanilimide and napthyl-ethylene diamine dihydrochloride method (Grasshoff et al. 1983) The detection limit for nitrate for the Nov – Dec 1998 & 2000 cruises was 0.07 mmol m^{-3}.

A Valeport SUV-6 *in situ* spectrophotometer (see Finch *et al.* 1998) was interfaced with the CTD during the 1999 cruise, as an attempt to provide vertically well-resolved nitrate profiles. A WS Ocean Systems NAS2 nitrate auto-analyser was deployed on one of the moorings during the 1998 cruise.

2.4.2 Biological data

Chlorophyll and HPLC

Chlorophyll *a* concentrations were measured by filtering water through Whatman GF/F filters. Analyses were performed on-board using the Welschmeyer (1994) technique on a Turner Designs digital Fluorometer during the 1999 cruise. Samples were frozen for return to the lab and analysed using the acidification technique in 1998 and 2000.

A further sub-set of water samples were filtered and frozen for analysis of pigments, determined by HPLC, on return to shore during the 1999 cruises (*Table 2.1*). Pigments were analysed according to the methods of Barlow et al. (1997) on a Thermo Separation products HPLC. Additionally water samples were collected and fixed with Lugol's iodine for microscope identification of phytoplankton.

Absorption measurements

Phytoplankton absorption spectra were measured on filtered samples following Tassan and Ferrari (1995), using a Hitachi U-3000 spectrophotometer fitted with a φ60 integrating sphere, for the 1999 cruise. Absorption spectra were corrected for scattering using a wavelength dependent path-length amplification factor typical for eukaryotic phytoplankton, (β-correction, Kirk, 1994). The absorption was then normalised to chlorophyll *a* in order to generate the wavelength dependant chlorophyll specific absorption ($a^*(\lambda)$).

^{14}C uptake experiments: simulated in situ

Further data on the physiological state and productivity of the phytoplankton populations was obtained by the use of standard ^{14}C uptake experiments. During the August 1999 cruise on deck simulated *in-situ* ^{14}C incubations were performed at each station, following protocols previously adopted for this region (Holligan et al. 1984b). Samples were collected at 6 depths corresponding to 95, 55, 30, 14, 4.5 and 1% of surface irradiance. For each depth three 80ml polycarbonate light bottles and 1 dark bottle were filled with seawater and inoculated with 100µl of 100 µCi ml^{-1} buffered $NaH^{14}CO_3$ working stock. The bottles were incubated on deck for 6-8hrs at sea surface temperature in an incubator shaded with neutral density filters to simulate the irradiance at the sampling depth. After incubation samples were filtered onto 25mm Whatman GF/F filters. These filters were then fumed over 10% HCl for 20mins to remove unfixed inorganic ^{14}C prior to being placed in 7ml plastic Pony vials to which 5mls Packard Hisafe 3 scintillation cocktail had been added. Samples were counted (DPM) on a Wallac 1414 WinSpectral DSA-based liquid scintillation counter.

The precise activity of the ^{14}C spikes was determined from standards. Exactly 100µl of the working stock was added to 10ml Carbasorb. From this, 5 replicates of 100µl were placed in 7 ml Pony vials to which 5mls Packard Supermix scintillation cocktail was added. The samples were counted on the scintillation counter together with the experimental samples.

^{14}C uptake experiments: P vs. E*

Additionally a number of short term (1-2 hr) P* vs. E incubations were performed in a photosynthetron (Lewis and Smith. 1983) cooled to sea surface temperature during both the 1999 and 2000 cruises. For the 1999 cruises sub-samples were incubated at a range of 14 irradiances from 2 – 2500 µE m^{-2} s^{-1} in 80ml incubation bottles. Each bottle was inoculated with 100µl of 100 µCi ml^{-1} buffered $NaH^{14}CO_3$ working stock, resulting in a final activity of around 0.125 µCi ml^{-1} as above. Samples were incubated for between 1 and 3 hrs (typically 2) then treated as described above for the 1999 simulated *in situ* experiments. Irradiance was measured at all positions within the photosynthetron using a Biospherical instruments QSL-100 4π quantum sensor.

For the 2000 cruise a similar method to Hawes *et al.* (1997) was employed. Sub-samples (60ml) were dispensed into 65ml polycarbonate bottles with 35µl of ~350 µCi ml^{-1} buffered $NaH^{14}CO_3$ working stock added, resulting in a final activity of around 0.2 µCi ml^{-1}. Bottles were incubated at 10 irradiances from 8 – 1074 µE m^{-2} s^{-1} in a radial photosynthetron similar to that described by Babin *et al.* (1994). Irradiance was measured at all positions

within the photosynthetron on return to the laboratory. After 1hr incubation time samples were filtered onto 25mm Whatman GF/F filters. Filters were then fumed over 10% HCL and the radioactivity determined on a Wallac scintillation counter using Hisafe scintillation cocktail.

Data from all the P* vs. E experiments were fitted to the model of Platt et al. (1980) in order to calculate the chlorophyll specific maximum carbon uptake rate (P^*_{max}), the maximum light utilisation coefficient (α^*) and the light saturation parameter E_k ($=P^*_{max}/\alpha^*$) (e.g. Sakshaug et al. 1997). For the 1999 data, values of α^* were corrected to correspond to a 'white' spectrum using the measured chlorophyll specific absorption and lamp spectra as described by various authors (see Chapter 5 & e.g. Dubinsky et al. 1986; Cleveland et al. 1989).

Chlorophyll *a* values derived using HPLC will tend to be lower than those derived using a fluorometric technique. For the 1999 cruise values of chlorophyll specific productivity (P*) and hence P^*_{max} and α^* were calculated using HPLC data or fluorometric (Welshmeyer, 1994) data scaled to HPLC levels using the observed relationship between the two techniques (HPLC chl *a* = 0.63 fluorometric chl *a*, $r^2 = 0.985$, n=49). However only fluorometric (acidification technique) chlorophyll *a* data was available for the 2000 cruise. This may have introduced some systematic differences between the two P* vs. E data sets.

2.4.3 Satellite and *in situ* spectral data

Satellite data was available for both the 1999 and 2000 cruises. Data on sea-surface temperature were available from the Advanced High Resolution Radiometer (AVHRR), while data from the NASA Sea-viewing Wide Field-of-view Sensor (SeaWiFS) was used to estimate sea-surface chlorophyll *a* concentrations. For the 1999 cruise satellite data was received by the NERC Dundee Satellite Receiving Station and processed by the Remote Sensing Data Analysis Service (Plymouth Marine Laboratory). For the 2000 cruise satellite data was processed at the National Institute for Water & Atmospheric Research (NIWA). SeaWiFS processing for the latter cruise was courtesy of M. Pinkerton.

In situ spectral data was also collected during the 2000 cruise. A Satlantic Profiling Multichannel Radiometer (SPMR) was used to obtain vertical profiles of upwelling and downwelling irradiance at the 7 wavelength bands corresponding to the SeaWiFS spectral bands. A second radiometer was used to obtain the above-surface incident irradiance for

normalisation. SPMR data were collected and analysed using the methods of Murphy *et al.* (2001).

Regime	**INTERNAL WAVES**		**TIDAL MIXING FRONT**
Location	**NE New Zealand Shelf**		**Western English Channel**
Ship	**RV Kaharoa (KAH98/08)**	**RV Kaharoa (KAH00/13)**	**RRS Challenger (CH145)**
Dates	**25th Nov – 8th Dec 1998***	**21st Nov - 3rd Dec 2000***	**31st Jul – 14th Aug 1999****
CTD package	Seabird 911 + Wetlabs fluorometer	Seabird 911 + Wetlabs fluorometer + CI transmissometer	Neil Brown MKII + CI aquatracka fluorometer
FRRF Deployment	--------	CTD + incubators	CTD + SeaSoar + underway
Microstructure	SCAMP	SCAMP	FLY
Moorings	4 (see Chapter 4)	3 (see Chapter 4)	--------
Nutrients	Nitrate (frozen) + WS-Ocean Systems NAS2 nitrate analyser (on mooring)	Nitrate (frozen)	Nitrate, Silicate and Phosphate (analysed on-board) + SUV-6
Chlorophyll	Frozen, acidification	Frozen, acidification	On-board, Welshmeyer
HPLC Pigments	--------	--------	Frozen
Absorption	--------	--------	Frozen
^{14}C –expts	--------	P vs. E	P vs. E, & simulated *In Situ*

Table 2.1 Summary of cruises and data acquired and analysed in this thesis. Regime indicates principal physical process of interest. Locations are rough guides only, see appropriate chapters for detailed maps, *Chapter 3*-1999 cruise, *Chapter 4*-1998 & 2000 cruises. Dates are an indication of experimental periods. *Moorings deployed at commencement of cruise, due to other commitments on station ship work with CTD/FRRF and SCAMP commenced on 2nd December and 26th November for the 1998 and 2000 cruises respectively. ** Failure of CTD winch during 1999 cruise resulted in no CTD operations being possible until 6th August. Blanks indicate no useful data acquired. Persons primarily responsible for analysis are indicated in *Appendix 3*.

3. Biological - physical interactions 1: A field study of a tidal mixing front

3.1 Introduction, study region and sampling strategy

In August 1999 a field study of the Ushant tidal mixing front in the Western approaches to the English Channel was carried out on-board the RRS *Challenger,* cruise CH145 (*Fig 2.1*). The principal observational strategy was based around a series of fixed stations (U2, M and E, see *Fig 3.1* & *Table 3.1*) each occupied for 25hrs whilst alternate CTD and FLY profiles were carried out. During these 25hr stations one complete set of observations consisted of five consecutive FLY profiles (an ensemble), followed by a CTD/FRRF cast. The time between FLY-CTD pairs was thus around 70 minutes once any re-positioning of the ship was performed. FLY profiles were not obtained at station E.

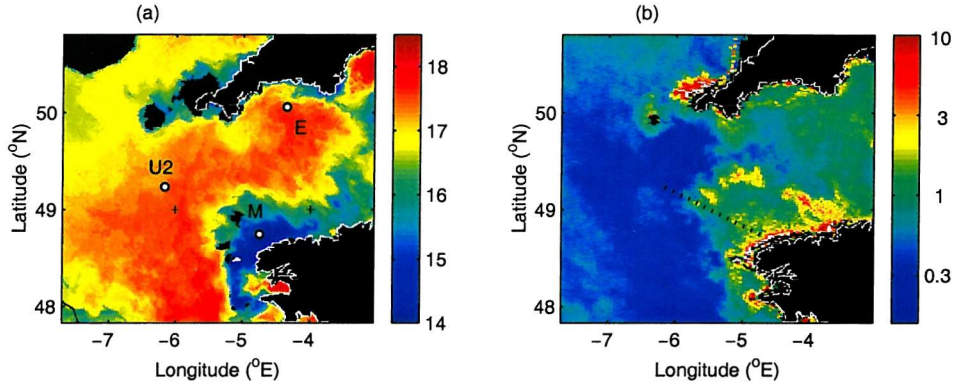

Fig. 3.1 Stations occupied during cruise CH145 during August 1999 and satellite data from from 9th July 1999.

(a) Sites occupied for 25hr surveys superimposed on advanced high resolution radiometer (AVHRR) derived sea-surface temperature (SST). The three sites chosen clearly span a large range of physical conditions from mixed inshore waters (M) to highly stratified offshore waters (U2).

(b) SeaWiFS (Sea-viewing Wide Field-of-view Sensor) derived surface chlorophyll distribution, with SeaSoar track superimposed (dotted line). Enhancement of chlorophyll in the frontal region is observed.

Satellite data received by the NERC Dundee Satellite Receiving Station and processed by the Remote Sensing Data Analysis Service (Plymouth Marine Laboratory)

A number of cross frontal transects (*Fig 3.1*) were also performed using the SeaSoar towed undulator with an FRRF attached. A transect was also performed with the standard CTD/FRRF package. Dates of fixed stations and details of the sampling performed are presented in *Table 3.1*.

25 hr Time Series			
Location	**Time/Date**	**No/Type of obs.**	**Additional Info.**
M (M2) (water depth, 104m)	6th – 7th August 1999 218.36 – 219.45 JD	21 FLY ensembles 20 CTD casts	44 chl a, 19 lug, 12 HPLC, 12 nuts, 17 abs, 4 PE, 1 SIS
M (M3)	12th – 13th August 1999 224.31 – 225.37 JD	21 FLY ensembles 21 CTD casts	66 chl a, 12 lug, 9 HPLC, 66 nuts, 12 abs, 5 PE, 1 SIS
U2 (water depth, 118m)	8th – 9th August 1999 220.54 – 221.63 JD	19 FLY ensembles 20 CTD casts	52 chl a, 20 lug, 17 HPLC, 55 nuts, 14 abs, 4 PE, 1 SIS
E	10th – 11th August 1999 222.74 – 223.87 JD	25 CTD casts	40 chl a, 6 lug, 4 HPLC, 16 nuts, 4 PE, 1 SIS
SeaSoar runs			
U2 – M	2nd – 3rd August 1999 214.53 – 215.06 JD	SeaSoar run + FRRF	6 chl a (from non-toxic)
M – U2	8th August 1999 220.02 – 220.49 JD	SeaSoar run + FRRF + Fluor.	19 chl a (from non-toxic)
CTD Transect			
U2 – M (L1 – L6)	9th – 10th August 1999 221.84 – 222.38 JD	7 CTD casts	21 chl a, 21 lug, 21 nuts, 2 PE

Table 3.1 Sampling performed during CH145. *Notes:* chl a – chlorophyll a sample, lug – lugols preserved phytoplankton sample, HPLC – filter taken for subsequent pigment analysis, nuts – nutrient sample, abs – filter collected for subsequent chlorophyll specific absorption, PE – ^{14}C P vs. E curve, SIS – ^{14}C simulated *In Situ* incubation. Fluor. – indicates standard chlorophyll fluorometer present. A chlorophyll fluorometer was also present on CTD package. Positions of stations and transects are marked in *Figs 3.1 & 3.2*.

3.2 Results 1: Physical controls on nutrient and light availability

3.2.1 General hydrography, chlorophyll distribution and mixing regime

Frontal temperature structure

The frontal position could be observed clearly in the SST distribution on 9th July 1999 (*Fig. 3.1*). On the mixed side of the front (e.g. around station M) surface temperatures were around 14°C, increasing to over 18°C in the surface waters on the stratified side.

Vertical temperature structure through the frontal region (M-U2) was typical of a tidal mixing front, progressing from highly stratified conditions at U2, to fully mixed during spring tides at M (*Fig. 3.2*).

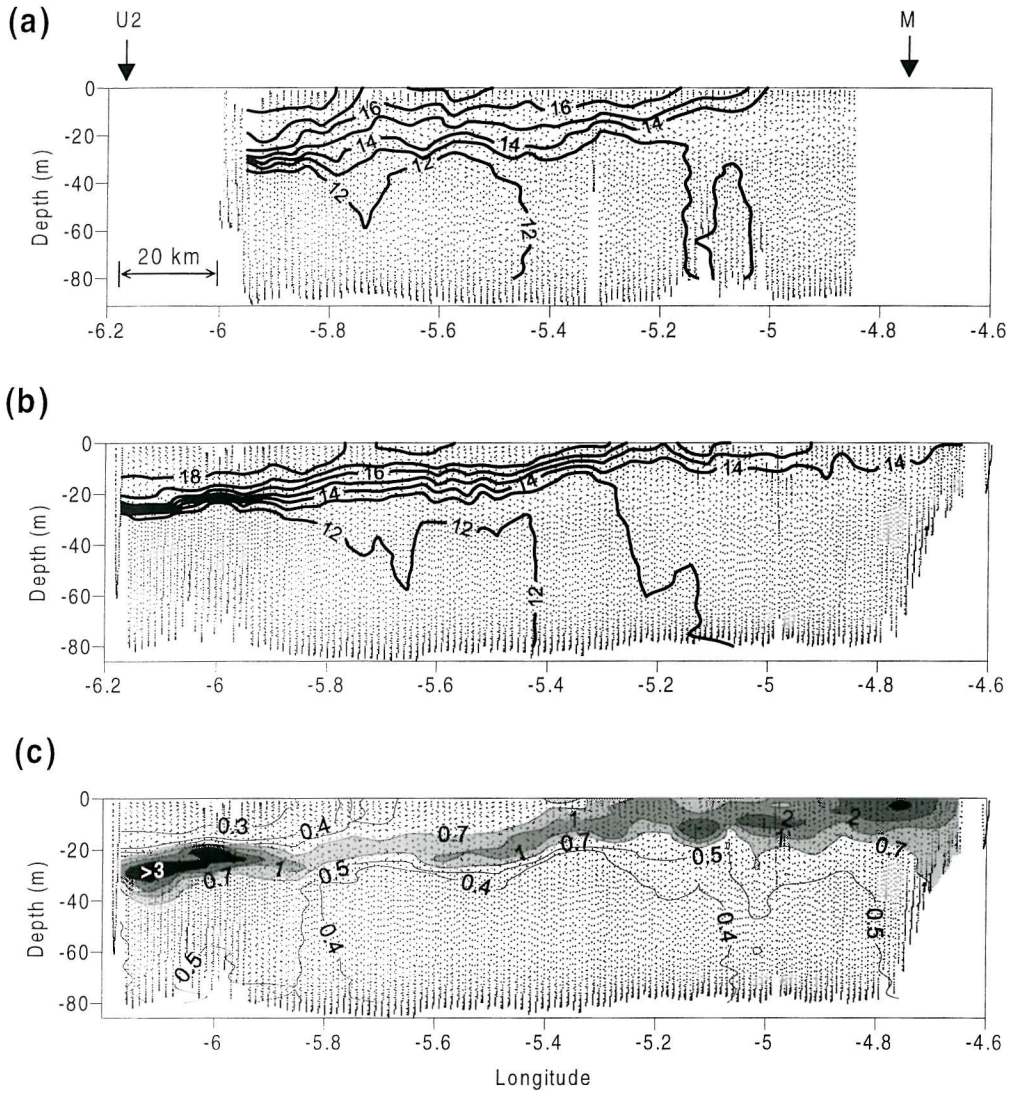

Fig. 3.2 Frontal cross sections of temperature and chlorophyll. (a) temperature structure during spring tides (2nd August 1999), (b) temperature structure during neap tides (8th August 1999), (c) chlorophyll distribution (mg m^{-3}) during neap tides (8th August 1999). Data was collected using the SeaSoar undulator, sample points used for contouring shown. Temperature is contoured every 1°C from 12-18°C. Chlorophyll is from standard fluorometer flown on SeaSoar during second run calibrated against discrete surface values (see *Appendix 4*). The positions of stations U2 and M are also indicated.

A marked spring-neap adjustment of the frontal position was apparent, the frontal region extending shoreward of station M during neap tides. The displacements between the points at which the 13°C and 14°C isotherms outcropped at the surface were around 12 and 32km respectively between spring and neap tides. This represents a large frontal excursion, greater than the ~4km typical of tidal mixing fronts, although roughly equivalent to the ~20km equilibrium adjustment estimated by simple energetic arguments (Simpson, 1981; Simpson and Bowers, 1981). Such a large excursion was consistent with earlier observations from the Ushant region (Pingree *et al.* 1977; Morin *et al*; 1993).

Chlorophyll distribution and taxonomic variability

The distribution of chlorophyll fluorescence was closely associated with the physical structure of the front (*Fig. 3.2c*). There was a strong correspondence between the regions of maximum phytoplankton biomass and the regions of maximum thermal gradient (*Fig. 3.2b & c*). The highest observed chlorophyll *a* levels were associated with the thermocline region on the stratified side of the front, reaching >50 mg m^{-3} at U2 on 8th August 1999. High levels (>2 mg m^{-3}) were also associated with the region in which the thermocline outcropped at the surface. Intermediate levels of chlorophyll, around 1 mg m^{-3}, were observed within fully mixed water columns, whilst the lowest values of <0.3 mg m^{-3} were measured in the surface stratified waters around U2.

Microscope observations showed that the phytoplankton populations were dominated by a mixed diatom and dinoflagellate assemblage at site M. Small eukaryotic flagellates and a coccolithophore (*Calyptrosphaera oblonga*) dominated in the surface water and thermocline respectively at U2. In the region of site E, a bloom of the coccolithophore *Emiliania huxleyi* was observed by satellite during the preceding 2-3 weeks, but had declined by the time of our observations. The distribution of different taxonomic groups was confirmed by the HPLC data. A high 19 hexanoyloxyfucoxanthin (Hex) to chlorophyll *a* ratio was evident at U2 particularly within the thermocline region, indicating a prymnesiophyte population (e.g. Millie *et al.* 1993; Claustre, 1994; Jeffrey, 1997 Jeffrey and Vesk, 1997). In contrast, relatively high fucoxanthin to chlorophyll *a* ratios and low concentrations of peridinin, indicated the presence of diatoms and some dinoflagellates within the community at M during both neap and spring tides (Jeffrey, 1997). A high chlorophyll *b*:chlorophyll *a* ratio observed at this site may have been caused by the presence of dinoflagellates containing chlorophyll *b*, as has previously been reported for the region (Sournia *et al.*, 1992).

Variations in stratification and mixing rates

25hr time-series of dissipation rates were obtained using the FLY profiler during three of the four occupations of fixed stations. The sites corresponded to the two ends of the cross frontal transects, U2 and M, with M being occupied twice, M2 (neap tides) and M3 (spring tides). Distinctly different physical conditions were observed during all three surveys (*Fig. 3.3*). The U2 site was highly stratified throughout the time series. The mean temperature in the tidally mixed bottom layer was 11.137°C (s.d. = 0.003°C) and was separated from the warmer surface waters (18.7 ± 0.1°C for depths <5m) by a sharp thermocline (*Fig. 3.3a*). The lower portion of the water column was mixed during the first 25 hr period at M (M2, $6^{th} - 7^{th}$ August 1999, neap tides) and a weak thermocline (13.74 – 14.50°C) extended from around 20m to the surface (*Fig. 3.3c*). During the second 25 hr time series at the inshore station (M3) the tidal currents had increased to near the maximum of the springs-neaps cycle and the water column was typically fully mixed (*Fig. 3.3e*). A small degree of near surface stratification still existed, however this was intermittent and was likely to have been caused by tidal advection of semi-persistent stratified patches of water.

Variability in dissipation rates (ε) at all three stations displayed similar patterns (*Fig. 3.3b,d & f*). Dissipation increased towards the bottom of the water column and showed a quarter-diurnal signal driven by the tidal currents. Higher up in the water column, the period of maximum dissipation lagged behind the maximum tidal current, this being driven by the vertical movement of the region of highest shear (Simpson *et al.* 2000). At U2 a marked minimum in the dissipation rate was associated with the thermocline region (*Fig. 3.3b*), ε being as low as $10^{-8} - 10^{-9}$ m^2 s^{-3} (*Fig. 3.5b*). Dissipation rates were higher at M than U2 and increased between the two 25 hr periods at M in accordance with the increasing tidal currents (*Fig. 3.3d & f*). Tidal mixing was apparent at the surface during M3, the dissipation rate at around 10 m being an order of magnitude greater than during M2. The site E was stratified, the thermocline being more diffuse than at U2.

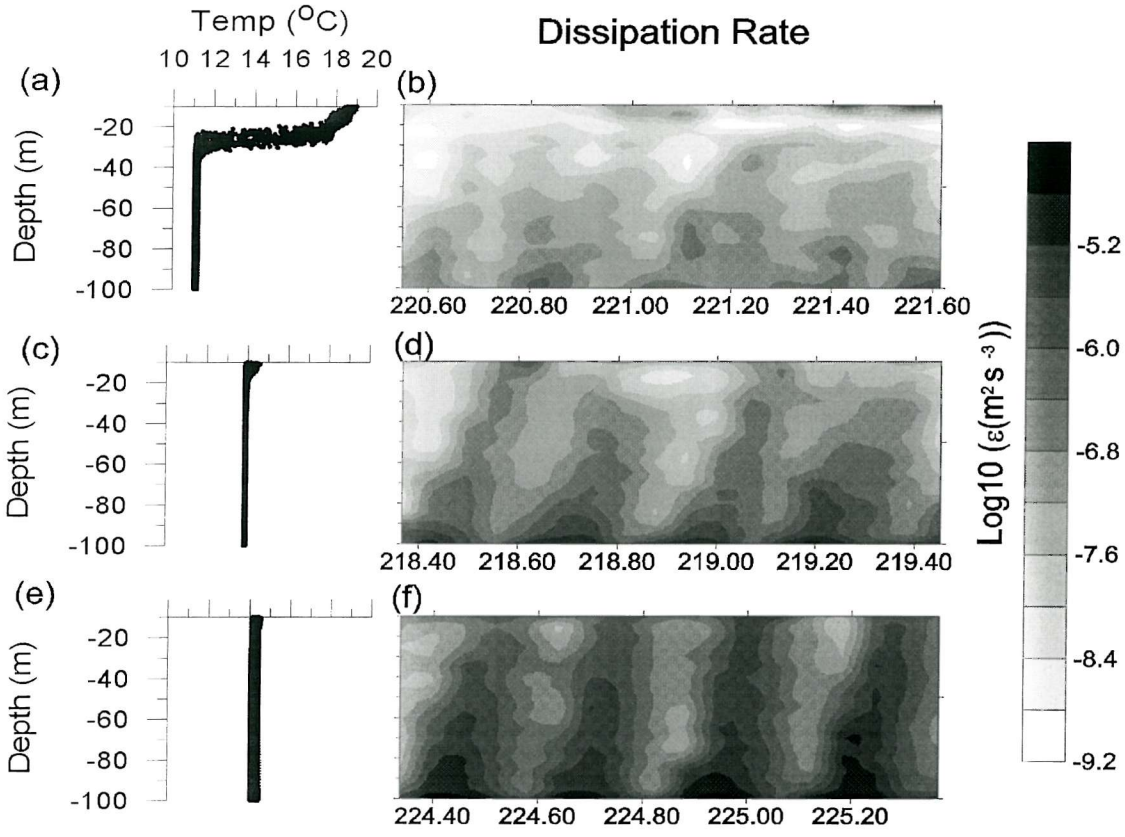

Fig. 3.3 Physical variability between the three fixed stations for which FLY profiles were obtained (a) & (b) U2 (8^{th} – 9^{th} August 1999), (c) & (d) M2 (6^{th} – 7^{th} August 1999), (e) & (f) M3 (12^{th} – 13^{th} August 1999).

(a,c & e) Temperature against depth for all the CTD casts at the three sites.

(e,d & f) Rate of dissipation of turbulent kinetic energy. Contour plots of dissipation against time (Day of year 1999) and depth were produced using the mean dissipation value from each of the profile bursts averaged into 5m depth bins. Plots are thus composed of between 19 and 21 approximately evenly spaced depth profiles of dissipation (see *Table 2.1*)

3.2.2 Nutrient distributions

General nutrient distribution

Concentrations of nitrate, phosphate and silicate were highly correlated throughout the frontal region ($R^2 = 0.95$ for nitrate vs. phosphate and $R^2 = 0.68$ for nitrate vs. silicate, see *Appendix 5*). A model II regression of the nitrate and phosphate data indicated an inorganic dissolved N:P ratio of around 14 and some residual phosphate at zero nitrate. Nitrate concentrations could therefore be considered indicative of both nitrate and phosphate availability.

As expected (e.g. Holligan, 1981), nitrate concentrations decreased from undetectable in surface waters on the stratified side of the front, through medium values (around 2.4 mmol N m^{-3}) on the mixed side, to the highest values (around 5.7 mmol N m^{-3}), observed in the bottom mixed layer on the stratified side (*Fig. 3.4*). A sharp nitracline was thus apparent during the U2 station, while much lower vertical nutrient gradients were observed during the two stations at M. Deep water nutrient concentrations at site E were lower than those on the main transect line and reduced towards the surface.

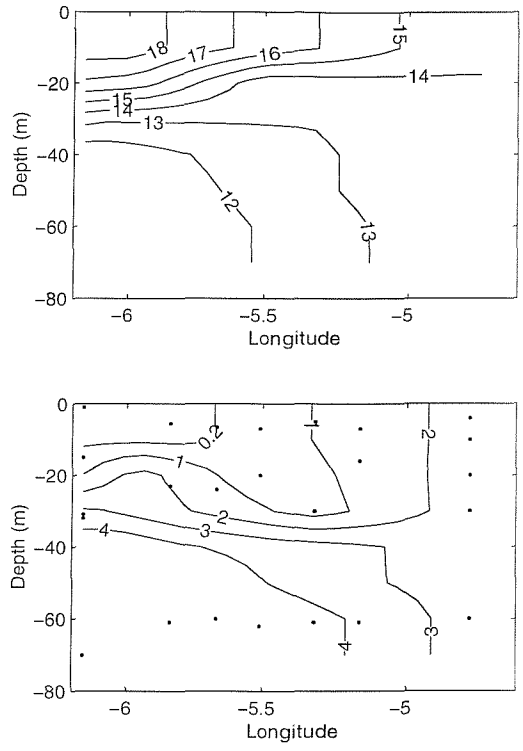

Fig. 3.4 Cross frontal distribution of temperature (top) and nitrate (bottom) from CTD survey on 9th-10th August 1999, stations U2, L1-L6, M. Positions of discrete water samples collected for nitrate analysis are indicated on lower plot

Nutrient availability for phytoplankton

Nitrate concentrations within the mixed regions were generally maintained above 1 mmol N m^{-3} (*Fig. 3.4*). Thus phytoplankton photosynthesis and growth were unlikely to have been nutrient limited in such areas. Conversely very low nutrient concentrations (<0.1 mmol N m^{-3}) were associated with the surface stratified waters, such conditions being likely to produce nutrient stress. The possible mechanisms driving vertical nutrient supply in the stratified frontal regions are now discussed. An attempt to quantify the vertical nitrate flux is also made.

3.2.3 Physical controls on nutrient fluxes

Rates of nutrient supply to near surface and thermocline populations are controlled by physical processes, including cross frontal transfer by eddies, vertically-driven turbulent exchange and spring-neap adjustment of frontal position (§ 1.2.1). Estimated rates of nitrate supply due to the latter two processes were obtained for the frontal and stratified regions.

Pulsed nutrient supply in frontal region

Within the region of the front which undergoes spring-neap cycles of stratification, the nitrate supply can be estimated using the ambient nutrient concentration and the observed area of re-stratification (Loder and Platt, 1985). The ambient nitrate concentration in the mixed water during spring tides was around 2.4 mmol m^{-3}. If it is assumed that the phytoplankton population completely utilise the nitrate trapped near the surface during the neap-tide period, the depth of the near surface stratified region can be used to obtain an upper estimate on the new production. Given an 18-22m thick near surface stratified region as observed during the second SeaSoar survey (*Fig.3.2*), an average supply rate per spring-neap cycle of 3.1-3.8 mmol N m^{-2} d^{-1} was calculated. This flux was comparable to the values of 2.9 mmol N m^{-2} d^{-1} calculated by Loder and Platt, (1985) and 2.6 mmol N m^{-2} d^{-1} calculated by Morin et al. (1993).

Nitrate flux driven by turbulent mixing within thermocline

A marked minimum of turbulent dissipation and diffusivity was associated with the sharp thermocline, nutricline and pronounced DCM observed at the U2 site (*Figs. 3.3 & 3.5*). Vertical nutrient fluxes in these highly stratified regions will be dependent on mixing across the thermocline. The nitrate flux at U2 was thus estimated by combining the observed time series of turbulent dissipation rates (*Figs. 3.3 & 3.5b*), buoyancy frequencies and estimates of the vertical nitrate gradient (Eq. 2.5 & 2.6).

In order to use (Eq. 2.6) it was necessary to calculate the nitrate gradient $\Delta N/\Delta z$ at scales comparable to those of the thermocline. This was accomplished by using a combination of data from the SUV-6 *in-situ* nitrate spectrophotometer and discrete bottle samples. Due to drift in the SUV-6 sensor and each data point being an average of the previous 8 seconds sampling at 1Hz, this instrument could not be used to directly estimate absolute nitrate values or gradients. However, regions of strong nitrate gradient were clearly evident in the SUV-6 data (*Fig 3.5c* & Sharples et al. 2001a). Consequently the peak of the strong deep

chlorophyll maximum (DCM) observed at this station was found to be associated with the top of the nitracline as has previously been observed for the shelf sea thermocline (Holligan et al. 1984b; Sharples et al. 2001a).

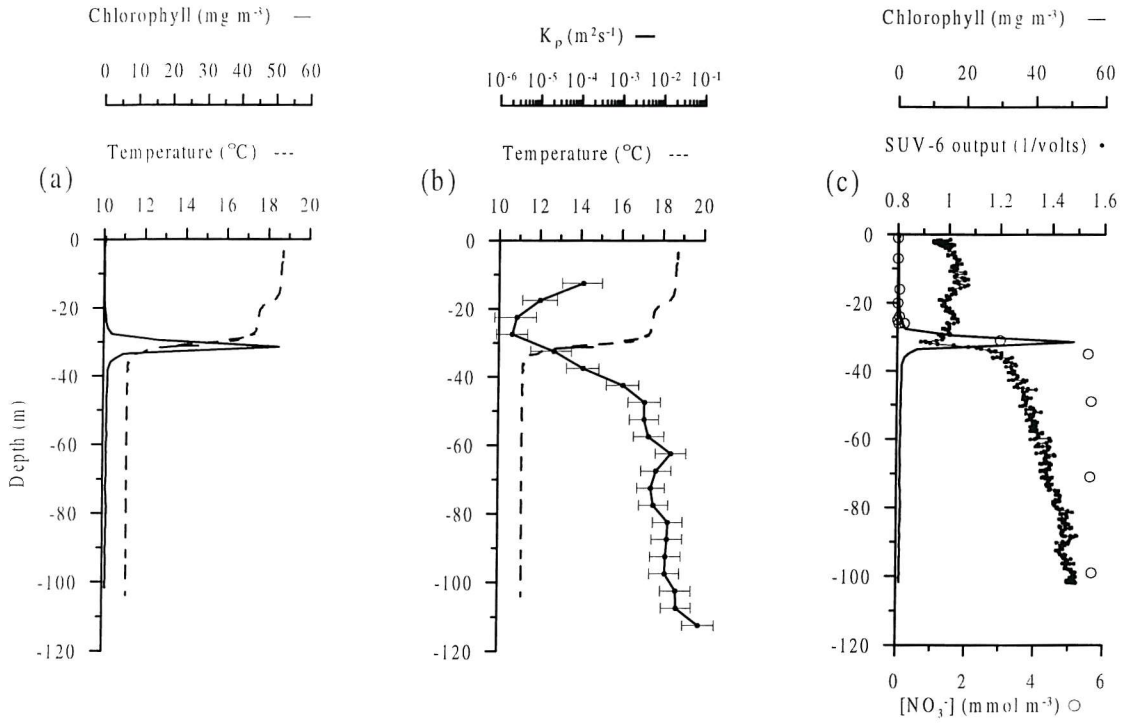

Fig. 3.5 Physical forcing, chlorophyll and nutrient distributions at U2. (a) representative profiles of temperature (dotted) and chlorophyll (solid) from CTD/FRRF profile around 1200 h at U2 on 9th August 1999. Chlorophyll is from calibrated FRRF F_M value (see *Appendix 4*). (b) temperature (dotted) and diffusivity (symbols) from CTD/FLY pair around 1200. Error bars for diffusivity are 95% confidence intervals approximated using a Bootstrapping technique (Effron and Gong, 1983) (c) chlorophyll (solid) and raw data output from SUV-6 sensor (filled symbols) and discrete samples analysed for nitrate (open symbols) at 1200 on 9th August 1999.

The extent of the nitracline (Δz) was therefore estimated as the distance between the peak chlorophyll concentration and the top of the bottom mixed layer. It was assumed that mixing due to tidally generated turbulence within the sub-thermocline region would have been sufficient to destroy any nutrient gradients here. Calculated in this way Δz ranged from about 1-3m. Discrete bottle samples consistently gave nitrate values of 5.7 mmol N m^{-3} in the bottom mixed layer, while nitrate levels were undetectable in the surface (*Fig. 3.5b*). The ΔN term was thus assumed to be constant at 5.7 mmol N m^{-3} and associated nitrate gradients therefore lay between 5.7 and 1.9 mmol N m^{-4}.

Estimated diffusivities (K_ρ) within the thermocline were low and in the range of 1×10^{-6} - 1×10^{-5} $m^2 s^{-1}$ (*Fig. 3.5b*). Combining estimates of nitrate gradients with observations of K_ρ over the full 25hr time series enabled a mean vertical nitrate flux of 2.0 mmol N m^{-2} d^{-1} (0.8 – 3.2 mmol N m^{-2} d^{-1}, 95% bootstrap confidence intervals, Efron and Gong, 1983) to be calculated (Sharples *et al.* 2001a). The low concentrations of nitrate above the DCM at this site suggested that this flux was utilised by phytoplankton within the thermocline and was therefore not available to the surface populations.

3.2.4 Controls on light availability

The mean diffuse attenuation coefficient for irradiance (k_d) calculated from the vertical PAR profiles at the M and U2 sites ranged from 0.09 m^{-1} at U2 to 0.15 m^{-1} at M, with little difference between the values calculated during M2 and M3. Surface layer phytoplankton populations at U2 were thus maintained at relatively high light levels above 10% of surface irradiance throughout the day. Thermocline populations at U2 would also have experienced relatively high light levels. Calculating the 1% light depth assuming a k_d of 0.09 m^{-1} would result in a value of ~50 m. However the attenuation coefficient will vary depending on the phytoplankton concentration (§ 1.3.1). As a result of the high chlorophyll concentrations in the thermocline at U2, large variations in k_d were apparent (*Fig. 3.6*). The peak of the sub-surface chlorophyll maximum was therefore generally just above the 1% light depth, with the whole sub-surface maximum contained within depths corresponding to around 7 and 0.3% of surface irradiance (*Fig. 3.6*).

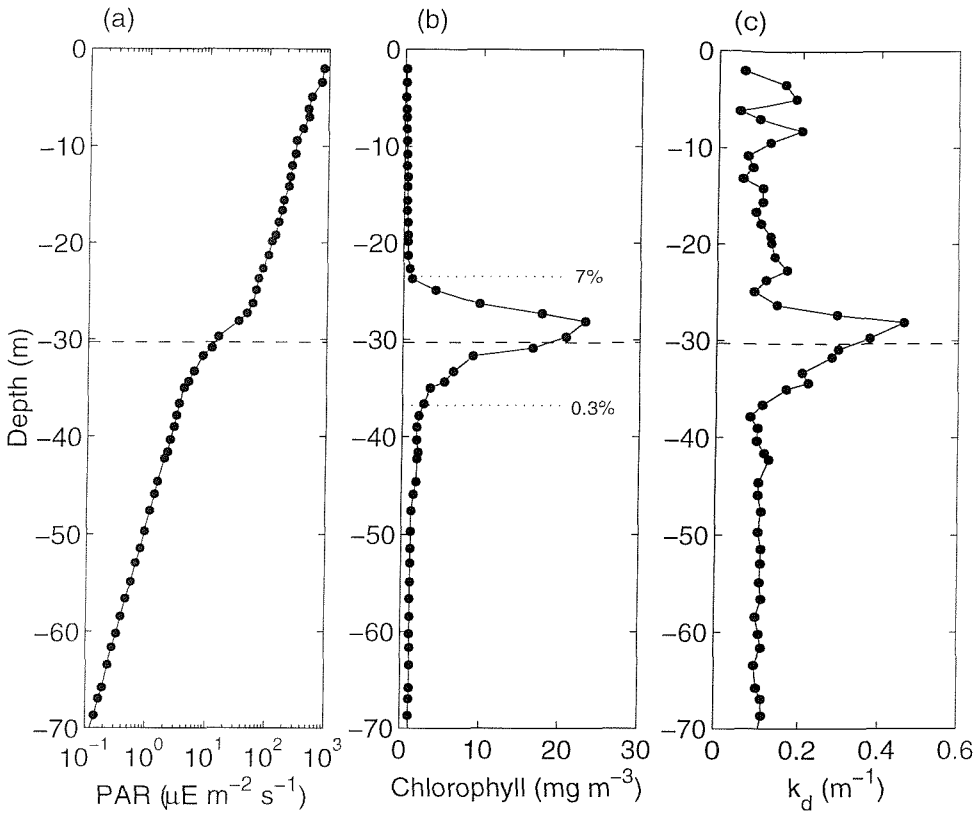

Fig. 3.6 Vertical light attenuation and chlorophyll distribution from a representative CTD/FRRF profile at 15:56 on 8th August 1999, all data are from CTD downcast only. (a) PAR profile with significant change in attenuance around depth of DCM. (b) vertical chlorophyll profile from calibrated FRRF fluorescence) indicating sharp DCM. (c) vertical profile of k_d calculated as $k_d = \Delta(\ln(PAR))/\Delta z$. The vertical attenuation coefficient was correlated to the chlorophyll concentration (k_d = 0.0908 + 0.0153 chl a, R^2 = 0.7566, n=60, p<0.001). Horizontal dashed line indicates 1% light depth, 0.3 and 7% light depths are also indicated in (b).

On the mixed side of the front, deep vertical mixing will significantly affect the integrated daily irradiance experienced by the phytoplankton. As an example during the M3 station, k_d was uniform throughout the water column, the 0.1% light level being just above mid-depth at 46m. Simple scaling arguments can be used to derive an estimate of the mixing time-scale over a distance L within a mixed water column, $t_{mix} = L^{2/3}\varepsilon^{1/3}$. (Denman and Gargett, 1983, see *Appendix 1*). Thus choosing a typical dissipation rate of between 1×10^{-6} - 1×10^{-7} m^2 s^{-3} (*Fig. 3.5*), phytoplankton cells at M3 could be expected to be mixed through the whole water depth on time-scales of order 1-2hours. On average, individual cells would therefore have spent a greater proportion of the daily period below the 0.1%

light level than above. Irradiance was thus likely to have been the dominant factor controlling phytoplankton photosynthesis towards the mixed side of the front.

3.2.5 Summary and inferences for growth limiting factors

In summary, nutrient concentrations were maintained at relatively high levels (>1 mmol N m^{-3}) in the mixed regions and decreased towards the stratified side. Estimated nitrate supply rates to the frontal zone and to the thermocline suggested that the phytoplankton populations in these regions were provided with a regular physically driven flux of nitrate. Surface populations on the stratified side of the front experienced very low ambient nutrient concentrations and an estimated low nutrient supply rate, but high mean light levels. Conversely phytoplankton on the mixed side of the front experienced low mean irradiance levels due to deep tidally driven mixing.

The detailed physical data therefore supported the standard hypothesis that phytoplankton growth rate may be limited by light in the mixed region, and by nutrients in the stratified regions of the front (e.g. Holligan, 1981). This hypothesis is now further investigated in the context of observations of phytoplankton physiology.

3.3 Results 2: Impact of physical forcing on phytoplankton physiology

3.3.1 Frontal scale variations in physiology

Clear relationships were observed between the large-scale physical structure and the physiology of the phytoplankton populations associated with various regions of the front during the CTD survey on 9^{th}-10^{th} August 1999 (*Fig. 3.7*).

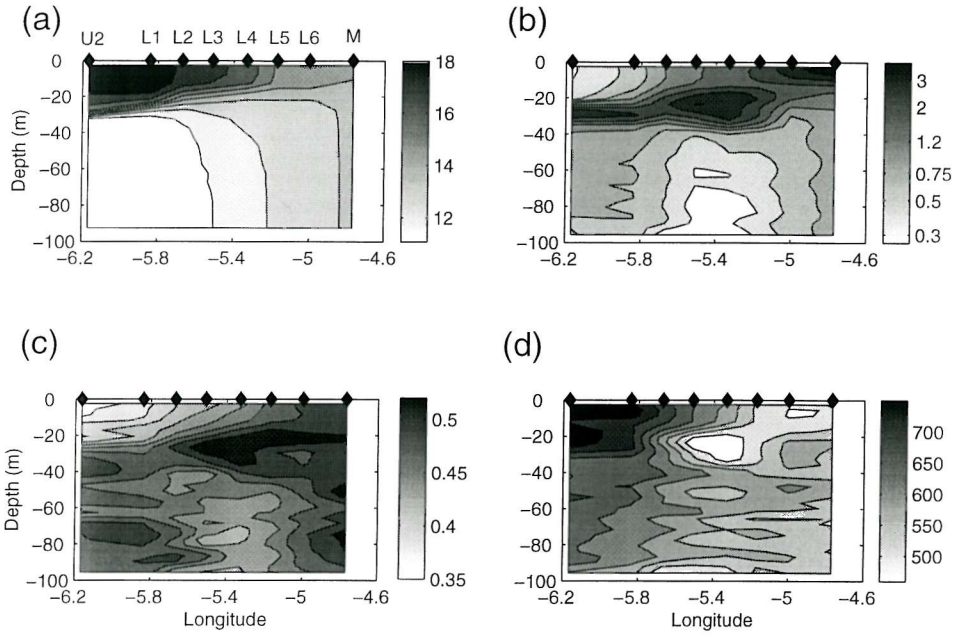

Fig. 3.7 Contoured CTD/FRRF data from cross frontal transect overnight on 9th-10th August 1999. (a) Temperature (°C), (b) Chlorophyll (mg m^{-3}), (c) F_v/F_m, (dimensionless), (d) σ_{PSII} ($Å^2$ $quanta^{-1}$). Chlorophyll values are FRRF F_M calibrated against discrete bottle samples. Positions of vertical casts indicated by filled diamonds. Station names indicated in (a).

The broad scale patterns of F_v/F_m and σ_{PSII} indicated marked physiological differences between populations on the mixed and stratified side of the front. Vertical variations associated with populations within and above the thermocline were also apparent (*Fig. 3.7*). The broad scale patterns of physiological variability were investigated at higher resolution using the FRRF on the SeaSoar undulator (*Fig. 3.8*). The data revealed smaller scale physiological differences, associated with physical variability (*Fig. 3.8*).

Populations on the mixed side of the front had high values of F_v/F_m (e.g. mean $\pm$ s.d. = 0.54 $\pm$ 0.02 and 0.56 $\pm$ 0.02 for the first and second SeaSoar runs respectively) (*Fig 3.8*). Relatively high values were associated with the thermocline and the surface region of the transitional zone (*Figs. 3.7 & 3.8*). The lowest photochemical efficiency was associated with the surface population on the highly stratified side, with $F_v/F_m = 0.35 \pm 0.02$ for the upper 5m at U2. Populations trapped beneath the thermocline in the middle portion of the front also had lower values of F_v/F_m (0.42 $\pm$ 0.03). Strong horizontal gradients in F_v/F_m were associated with the horizontal temperature gradients of the front (*Fig 3.8*).

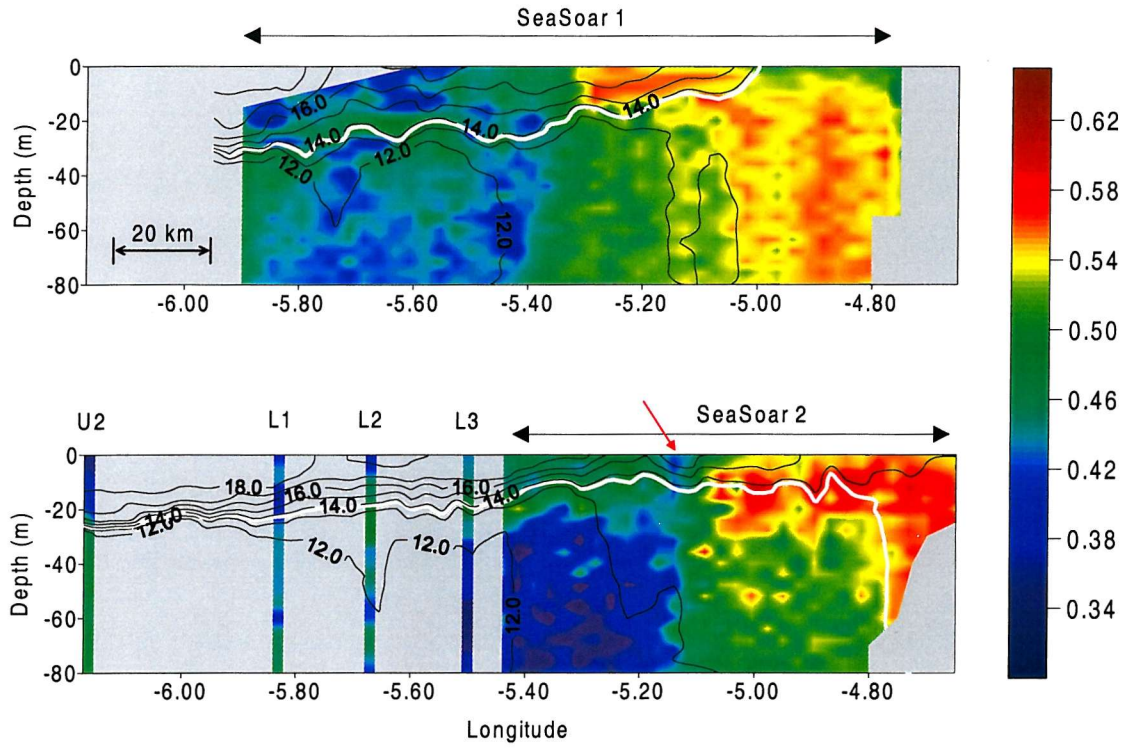

Fig. 3.8 Frontal cross sections of F_v/F_m and temperature during spring (top, 2nd August 1999) and neap (bottom, 8th – 9th August 1999) tidal conditions. Black lines are isotherms contoured every 1°C (see *Fig. 3.2*), the 13.7°C isotherm is additionally contoured (white) to provide added reference to the frontal position. Data collected during night-time from two SeaSoar runs across the front and during the CTD transect overnight on 9th August (see *Table 3.1*). During the second SeaSoar run (M – U2) the FRRF instrument failed around 5.45°W during the second SeaSoar run. Plots of FRRF data from the SeaSoar runs were generated using over 5000 (top) and 3000 (bottom) individual data points respectively. The red arrow indicates the position of a small (O(20km)) frontal eddy or filament structure with associated physiological variability.

Night-time (dark-adapted) values of σ_{PSII} were also significantly different between the stratified and mixed regions of the front (*Fig 3.7*). The highest values around 750 $Å^2$ $quanta^{-1}$ were found in the surface regions at U2. With lower values of σ_{PSII} towards the mixed side. A distinct minimum in σ_{PSII} was apparent within the deep population in the frontal region at around 5.4°W during the CTD survey (*Fig. 3.7*). The patterns of variability were thus similar to those described by Kolber *et al.* (1990) for a front the Gulf of Maine. However some differences were apparent, in particular Kolber *et al.* (1990) reported relatively low values of F_v/F_m and higher values of σ_{PSII} towards the mixed side of the front. These authors suggested such observations were indicative of a poorly developed physiological apparatus under conditions of low mean irradiance. For the current study, prolonged high irradiance was likely to have been experienced by a proportion of the *in situ* population at some stage in the previous 14 days, due to the spring-neap stratification

cycle. Some phytoplankters are known to be able to maintain high F_v/F_m under prolonged periods of darkness (Berges and Falkowski, 1998)

3.3.2 Relationship of physiological variations to nutrient availability

Both F_v/F_m and σ_{PSII} will be affected by the supply of nutrients, with higher values of σ_{PSII} and lower values of F_v/F_m tending to be associated with nutrient limitation (Kolber *et al.* 1988; Kolber *et al.* 1990). This relationship appeared to hold within the frontal region as F_v/F_m decreased and σ_{PSII} increased towards the low nutrient regions (*Figs. 3.4, 3.7 & 3.8*).

The decrease of F_v/F_m at low nutrient concentrations could be illustrated by considering how both F_v/F_m and nitrate were related to temperature within the front. Nitrate concentration generally decreased with increasing temperature (*Fig. 3.9a*).

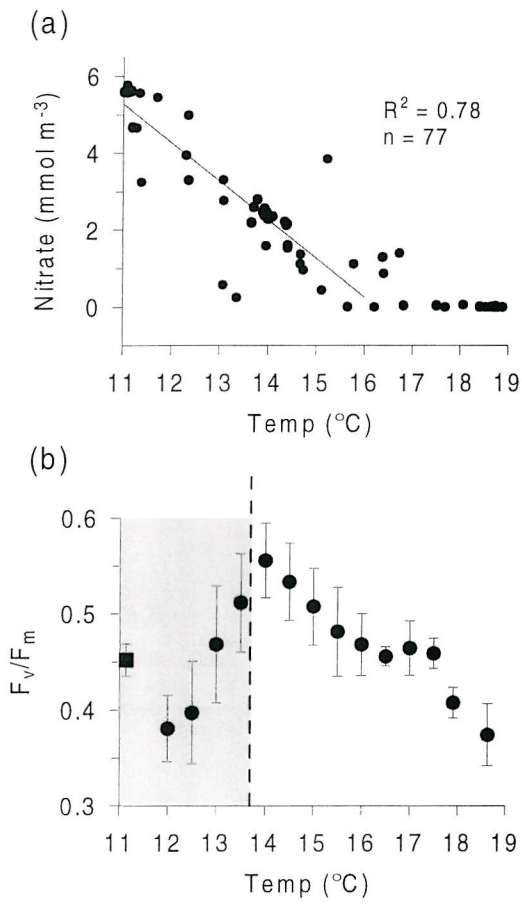

Fig. 3.9 Nitrate concentration and F_v/F_m vs. temperature for frontal region.
(a) Nitrate concentrations are from bottle samples collected at M and U2 and during CTD transect performed on 9th – 10th August 1999. Concentrations are plotted against *in situ* temperature recorded by CTD.
(b) F_v/F_m against temperature:
(●) Night-time measurements from SeaSoar run 2 (8th August 1999) and from above the thermocline at U2 (8th – 9th August 1999); F_v/F_m and temperature were interpolated onto a regular grid. Values shown are (mean ± s.d.) binned into temperature ranges of 0.5°C every 0.5°C.
(■) Night-time measurements from below the thermocline at U2, mean temp = 11.14 (± 0.003).
The vertical dotted line at 13.7°C corresponds to a temperature towards the base of the thermocline (see Fig 3.3b).
The shaded area thus corresponds to the sub-thermocline region.
For temperatures above the 13.7°C, F_v/F_m was highly correlated with temperature,
$F_v/F_m = 1.026 - 0.0342\ T$, $R^2 = 0.92$

Above the thermocline F_v/F_m decreased with increasing temperature, in accordance with the decreasing nitrate concentration (*Fig. 3.8b*). Phytoplankton populations sampled in

regions with mean temperatures less than around 13.7°C were generally trapped below the thermocline and had lower values of F_v/F_m (*Fig. 3.8b*). Phytoplankton found in the bottom mixed layer at U2 had a relatively high photochemical efficiency (0.45 ± 0.02).

3.3.3 Relationship of physiological variations to light 1: Diel variability

In addition to physiological variations caused by nutrient supply, variations in both F_v/F_m and σ_{PSII} (or under conditions of ambient light $\Delta F'/F_M'$ and σ_{PSII}') may be indicative of photoacclimation at various timescales and, for σ_{PSII}, of differences in species composition. Diel variations in both σ_{PSII}' and $\Delta F'/F_M'$ were observed in the 25hr time-series obtained at all the fixed stations (*Fig. 3.10*) and were closely related to both diel changes in irradiance and variations due to cloud cover etc.

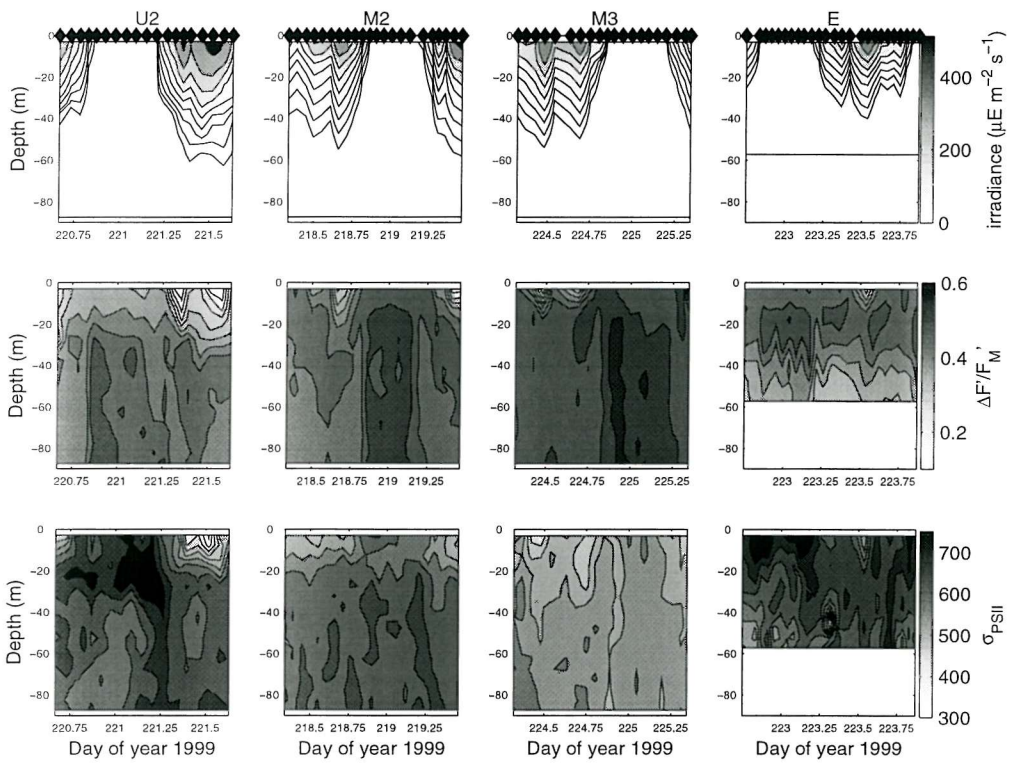

Fig. 3.10 Diel variability of $\Delta F'/F_M'$ and σ_{PSII}' during all four 25hr stations. (Top) variations of PAR measured from sensor attached to CTD/FRRF frame, PAR is contoured at 2,4,8,16,32,64,128,256 and 512 µ E m^{-2} s^{-1}. (Middle) Diel variations of $\Delta F'/F_M'$ measured *in situ* in chamber of FRRF exposed to ambient irradiance. (Bottom) Diel variations in σ_{PSII}' ($Å^2$ $quanta^{-1}$) measured *in situ*. Data were averaged into 5m bins and smoothed over two casts before contouring. Filled diamonds indicates times of individual vertical casts.

Both $\Delta F'/F_M'$ and σ_{PSII}' declined during the day and displayed minima associated with the peak irradiance around midday. Values of $\Delta F'/F_M'$ and σ_{PSII}' from near surface (<15m) waters were significantly negatively correlated with the instantaneous irradiance during all four stations (*Fig. 3.11*). Maximal reductions in $\Delta F'/F_M'$ ranged from 63% in the surface at U2 to around 61% at station M during neap tides (M2) and 45% during springs (M3). Reductions of $\Delta F'/F_M'$ during a generally cloudy day at E were around 37% at peak irradiances. At U2 σ_{PSII}' was around 51% lower at midday irradiances than during the dark, whereas reductions of around 30% were observed during M2,M3 and E.

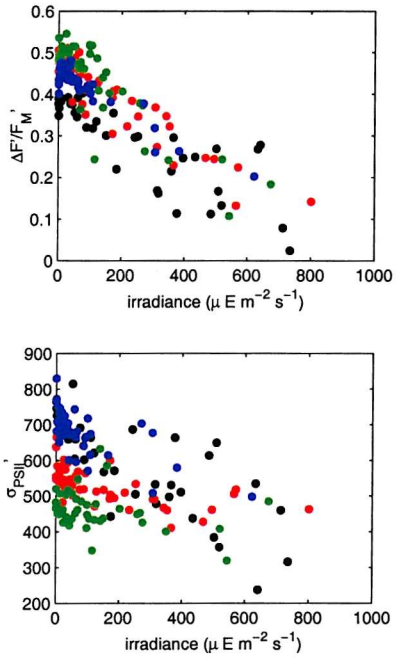

Fig. 3.11 Relationship of phytoplankton physiology to instantaneous irradiance within upper region (15m) of water column during all four 25hr stations. (Top) $\Delta F'/F_M'$ as a function of irradiance. (Bottom) σ_{PSII}' as a function of irradiance. Points correspond to data gathered at U2 (black), M2 (red), M3 (green) and E (blue).

Unexpectedly, diel variability, particularly with regards to $\Delta F'/F_M'$ (F_v/F_m) was also apparent in the deep sub-photic zone portions of the water column, even at the highly stratified U2 site (*Fig. 3.10*).

3.3.4 Relationship of physiological variations to light 2: σ_{PSII}, photoacclimation and mixing

Besides the short term diel changes in physiology, phytoplankton have the ability to acclimate their photosynthetic apparatus over longer time-scales to the mean daily irradiance they experience (Falkowski, 1984). In addition different groups or species of phytoplankton may have specific adaptations to differing light conditions. Currently few

studies have investigated species-specific variations in σ_{PSII}, which are likely to be related to variations in the pigment composition of the antenna complex (Kolber *et al.* 1988; Olson *et al.* 1996).

Photoacclimation and mixing

The vertical distribution of σ_{PSII}' observed within a water column will be dependent on the relative magnitudes of the vertical mixing rate and the rates at which phytoplankton alter σ_{PSII}' at both short and long time-scales (Falkowski, 1983; Lewis *et al.* 1984a; Kolber *et al.* 1990). If mixing causes cells to be moved through the vertical light gradient faster than they can alter their photosynthetic apparatus, the distribution will tend to be uniform with depth. Conversely if the acclimation rate is much faster than the mixing rate, cells will generally be fully acclimated to the light regime and there will be vertical heterogeneity in the parameter.

Microstructure measurements with FLY provided some measure of vertical mixing rates at three of the fixed 25hr stations. Profiles of σ_{PSII}' at these three stations showed significant differences in the degree of vertical variability (*Figs.3.10 & 3.12a*). Generally the vertical variation in σ_{PSII}' decreased from U2 - M2 - M3 in accordance with increasing vertical mixing (*Fig. 3.5 b,d &f*), this being consistent with an explanation based on photoacclimation. These results are now interpreted in terms of a simple photoacclimation - mixing model (Lewis *et al.* 1984a; Cullen and Lewis 1988).

Photoacclimation – diffusion equation

Lewis *et al.* (1984a), derived a simple equation which relates the rate of change of an observed parameter (Γ) to the rate of vertical mixing:

$$\frac{\partial \Gamma(z)}{\partial t} = \frac{\partial}{\partial z} K_z \frac{\partial \Gamma(z)}{\partial z} + \gamma(\Delta\Gamma) \qquad (3.1)$$

where γ is the photoacclimation rate constant and $\Delta\Gamma$ is the difference between Γ at time t and the fully light acclimated value of Γ at the incident irradiance (Γ^{∞}).

Lewis *et al.* (1984b) tested the model of Lewis *et al.* (1984a) by measuring the vertical variability in the maximum rate of chlorophyll specific production (P^*_{max}) and the rate of turbulent dissipation (ε) within the water column. A similar analysis of the current data set resulted in a relationship between ε and the vertical gradient of σ_{PSII}' within the upper

water column which was qualitatively very similar to the results of Lewis *et al.* (1984b) (*Fig. 3.12b*). Vertical gradients in σ_{PSII}' were much lower under conditions of high mixing than under conditions of low mixing, the relationship being approximately hyperbolic, as predicted by the model (*Fig. 3.12b*).

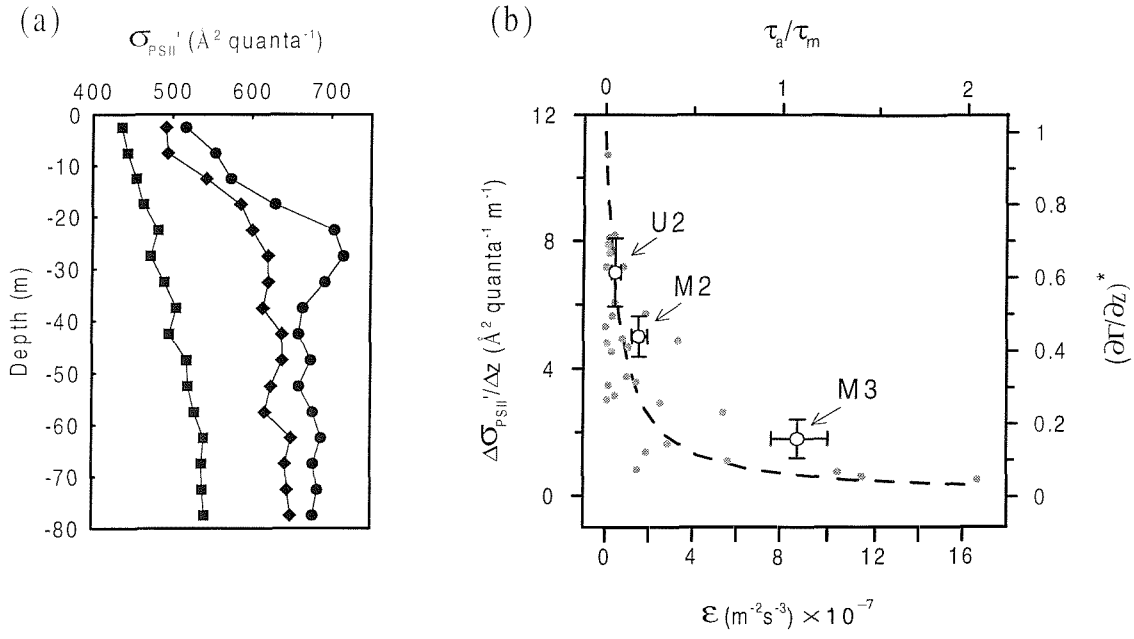

Fig. 3.12 Photoacclimation and mixing as controls on σ_{PSII}'. (a) Daytime mean vertical profiles of σ_{PSII} for the three stations where observations with the FLY profiler were collected, U2, (circles), M2, (diamonds) and M3 (squares). (b) Rate of dissipation of TKE (ε) against vertical gradient in σ_{PSII}' for the upper portion of the water column (<30m) during daytime at all three stations. Open symbols are the mean values calculated for the three stations, vertical error bars are ± 1 s.d. horizontal error bars are approximate 95% confidence intervals of the mean dissipation estimated using a bootstrapping technique (Effron and Gong, 1993). Filled symbols are individual values of depth mean ε vs. $\Delta\sigma_{PSII}'/\Delta z$ for all the FLY – CTD/FRRF pairs collected during the three stations. The dotted line is the normalised solution of a photoacclimation-diffusion equation (Lewis *et al.* 1984a), showing the expected relationship between the vertical variability in any photoadaptive parameter (Γ^*) and the ratio of the photoacclimation rate to the vertical mixing rate (τ_a/τ_m).

3.4 Discussion

Nutrient and light supply

As observed in previous studies the distributions of both nutrients and phytoplankton throughout the frontal region were strongly associated with physical forcing (Holligan, 1981, see *Fig. 3.2*). The lateral and vertical distribution of nutrients were consistent with nutrient limitation occurring in the surface stratified waters and light limitation within the mixed region (*Fig. 3.4*). Observations of the underwater irradiance field, combined with simple scaling arguments based on observed turbulent dissipation rates, also supported this hypothesis. It is suggested that the integrated daily irradiance experienced by phytoplankton in the different regions of the front progressed from highest levels within the surface stratified regions, through intermediate levels within the thermocline, to low levels within fully mixed water-columns.

The relatively high light levels within the thermocline/DCM, for example at U2 (*Fig. 3.6*), were likely to be a crucial factor in generating the high (>50 mg chl *a* m^{-3}, *Fig 3.5*) levels of phytoplankton within these regions. The presence of a tidally mixed bottom layer within shelf seas can cause the vertical position of the thermocline and associated nutricline to be determined by the strength of the tidal forcing, rather than by wind driven mixing and the input of buoyancy at the surface. It is therefore hypothesised that the position of the thermocline can be closer to the surface in such tidally dominated areas. This can increase the light climate experienced by phytoplankton and the biomass accumulation within the DCM in shelf seas as compared to open ocean systems.

Once nutrients have become depleted in the surface waters, new-production can only be supported by a cross thermocline flux of nitrate (Eppley and Peterson, 1979). Quantification of the physically driven turbulent cross thermocline flux at U2 indicated that the nitrate supply rate was around 2 mmol N m^{-2} d^{-1} (Sharples *et al.* 2001a). The estimated nitrate flux within the re-stratifying frontal region was of similar magnitude. The vertically driven nutrient flux is likely to vary throughout the frontal region as a complex function of the tidal energy dissipated in the bottom boundary layer and the changing stratification. The spring-neap cycle of tidal current amplitudes may also alter the nutrient flux at any one location. A cycle of thermocline deepening during neap tides followed by erosion during spring tides could cause additional enhancement of new-production (Sharples *et al.* 2001a). Such variation in thermocline thickness is an extension of the spring – neap

adjustment of frontal position mechanism into more stratified waters. The latter process was clearly evident in the current data set (*Fig. 3.2*).

Physiological variations

The high degree of correspondence between the physical structure of the front and the spatial variations in the photochemical efficiency (F_v/F_m) indicate that physical processes strongly affect the physiological state and growth of phytoplankton in frontal regions (*Figs 3.7 & 3.8*). Variations in F_v/F_m in regions within and above the thermocline were fully consistent with a reduction in photochemical efficiency under conditions of nutrient stress (*Fig.3.9*).

In regions below the thermocline, F_v/F_m generally decreased. This is often found and is thought to indicate senescence within the population (Babin *et al.* 1996). The marked exception to this occurred from around 5° 45' W to the stratified site at U2 (*Figs. 3.7 & 3.8*), and was associated with an elevated chlorophyll concentration of 0.8 – 1.2 mg m^{-3} below the thermocline (*Fig. 3.7*). The presence of a relatively high level of healthy phytoplankton in this region is the consequence of the regular removal of a population from the thermocline region by tidally generated turbulent mixing (see Sharples *et al.* 2001a & Chapter 6).

There was considerable smaller scale variability in the distribution of the physiological parameters measured, some of which appeared to be associated with physical forcing. An example was a region of lower photochemical efficiency in the surface around 5.14° W during the second SeaSoar run (*Fig. 3.8b*). In the middle of this patch F_v/F_m was 0.43 (s.d. =0.02, n=11) compared to a mean in the immediately adjacent region of 0.47 (s.d. =0.03, n=25). This region was also associated with a lens of slightly warmer surface water (*Fig. 3.8b*). It is suggested that the transect crossed a filament or eddy structure in the front at this position, with the warmer surface water and phytoplankton population with a lower photochemical efficiency having originated on the stratified side of the front. Such eddy structures have been hypothesised as being important for the cross frontal transfer of nutrients (Pingree *et al.* 1979). Small scale surveys with the SeaSoar/FRRF system may allow detailed examination of the development and biological consequences of such features.

Phytoplankton communities associated with the mixed and transitional regions of the front showed significant variability associated with the spring-neap variation in frontal position

(*Fig. 3.8*). Temporal variation in the regions of physiologically distinct communities closely followed the patterns of frontal movement. Furthermore the highest values of F_v/F_m observed throughout the cruise (mean $\pm$ s.d. = 0.57 $\pm$ 0.03) were associated with the thermocline in the newly re-stratified region of the front during neap tides (*Fig. 3.8b*). Thus, the photosynthetic capacity of the phytoplankton populations associated with the front appeared to be enhanced by springs-neaps adjustment, providing strong evidence that tidally driven variability is one of the principal mechanisms for enhanced growth and biomass within the system.

Observations of the functional absorption cross section can be more difficult to interpret as this parameter depends on both the light history and the nutrient status of the cells (Kolber *et al.*, 1990; Falkowski 1992). Dark adapted values of σ_{PSII} were consistent with nutrient limitation of phytoplankton within the upper water column at U2 as opposed to M2 and M3 (*Fig. 3.7*). However nutrients alone could not explain the variation between the dark adapted values of σ_{PSII} during the M2 and M3 stations (*Fig. 3.10*). The mean values of σ_{PSII} below 20m (i.e. below any stratification) reduced from 640 $\pm$ 20 $Å^2$ $quanta^{-1}$ during M2 to 510 $\pm$ 10 $Å^2$ $quanta^{-1}$ during M3 while the values of F_v/F_m and the nutrient concentrations remained approximately constant.

Variations in σ_{PSII} (or σ_{PSII}') as a function of the irradiance experienced are likely to be complex due to the variety of different processes (acting over different time-scales) which phytoplankton can employ to alter the absorption cross-section (§ 1.3.3 and refs. therein). The observed diel variability in $\Delta F'/F_M'$ and σ_{PSII}' was likely to be a result of non-photochemical quenching (NPQ) processes. NPQ caused by de-activation of PSII reaction centres reduces $\Delta F'/F_M'$ without a change in σ_{PSII}' while thermal dissipation of excitation energy within the antenna complex reduces σ_{PSII}' (Falkowski *et al.* 1994; Vassiliev *et al.* 1994). Quenching within the pigment bed has been observed to reduce σ_{PSII}' by up to 50% during the day, which is comparable to the 30-50% reductions observed during the 4 time series stations in the present study (Olaizola *et al.* 1994; Falkowski *et al.* 1994; Vassiliev *et al.* 1994). Differentiating between reaction centre and antenna quenching is difficult as both processes may be occurring simultaneously (Falkowski *et al.* 1994). Changes in $\Delta F'/F_M'$ and σ_{PSII}' were positively correlated within near surface waters, particularly at U2. Thus both antenna and reaction centre quenching may have been present.

Over longer time-scales, photoacclimation to the mean daily irradiance has been observed to cause up to 3-fold changes in σ_{PSII} (Ley and Mauzerall, 1982; Kolber *et al.* 1988).

Longer time-scale photoacclimation may well have been a factor affecting the observed distribution of σ_{PSII} and σ_{PSII}'. However interpretation is confounded due to variations in nutrient status and community structure which were likely to have concurrently altered the absorption cross-section between the sites studied.

The observed vertical distribution of σ_{PSII}' as a function of both short-term (non-photochemical quenching) and long-term (photoacclimation) responses to light will also be affected by the vertical mixing rate (Falkowski, 1983; Lewis *et al.* 1984a&b). The combined data on σ_{PSII}' and ε represents one of the few examples of a photoacclimation model being tested against a relatively direct estimate of vertical mixing rates (ε) and the first in tidally dominated waters (*Fig. 3.12*). The results of the present study indicate that phytoplankton were not able to adjust their photosynthetic apparatus to the instantaneous light level within the mixed region of the front, as the mixing time-scale was faster than the acclimation time-scale (*Fig. 3.12*). It is suggested that phytoplankton are unable to maximise growth within the mixed water column due to an inability to adjust their photosynthetic apparatus sufficiently quickly to fluctuations in the light environment. Deep mixing therefore exerts a fundamental control on growth, both by reducing the daily integrated irradiance experienced by phytoplankton and by reducing the potential for individual cells to fully exploit the periods of high light.

Relationships to growth rates

The physiological variability so far discussed will have a direct effect on the growth rate of the phytoplankton populations associated with the different regions of the front. The quantum yield of photosynthesis is directly related to the efficiency of light harvesting and photochemistry in PSII, as all the electrons generated by the oxidation of water or used in the reduction of carbon have to pass through PSII (Babin *et al.* 1996; Falkowski and Raven, 1997). The use of FRRF derived physiological parameters to calculate photosynthetic electron transport rates and carbon fixation rates is addressed in Chapter 5. Comparisons between such estimates of primary production rates and the nutrient flux based inferences of new production rates are considered in Chapter 6.

Summary and conclusions

Based on detailed physical and biological observations obtained during a field study in the region of a tidal mixing front, it was ascertained that physical forcing had a pronounced influence on the light and nutrient regime of the associated phytoplankton communities. The FRRF instrument was used to obtain information on phytoplankton physiological

responses at scales comparable to both physical forcing and observations, enabling investigation of whether such physically driven controls on nutrient and light availability also control phytoplankton physiology and hence growth rate in the region.

Observed variability in phytoplankton physiology was consistent with nutrient limitation within the surface stratified regions, while deep vertical mixing caused light limitation within the mixed region. These limitations were relaxed within the transition region of the front. The physiological data thus points to environmental conditions limiting the growth rate of the phytoplankton populations away from the front. Such physiological data is free from the ambiguities associated with inferences based on observations of phytoplankton distributions. The enhancement of phytoplankton biomass in such fronts is therefore at least partly due to increased *in situ* growth (Pingree *et al.* 1975,1977; Holligan, 1981) rather than simply passive accumulation or lower loss terms such as a relaxation of grazing pressure (Lefevre, 1986; Franks, 1992a&b).

The full range of dynamical process driving variations in nutrient and light supply to the frontal region were not completely captured within the current study. Only one of the fixed stations was occupied during spring and neap conditions (M) and only two cross-frontal transects were possible with SeaSoar. Further work utilising the same techniques and sampling strategy should enable a fuller understanding of the dynamics of resource supply and phytoplankton response within such tidal mixing fronts, as well as other dynamically active marine ecosystems.

4. Biological - physical interactions 2: Field studies of internal tides

4.1 Introduction, study region and sampling strategy

Two cruises to the Northeast New Zealand continental shelf were undertaken during Nov-Dec 1998 and Nov-Dec 2000 in order to investigate the influence of internal tides on phytoplankton physiology and growth in the region (*Fig. 4.1*).

The observational strategy employed for the two cruises included the deployment of mooring arrays to evaluate the dynamics of the internal motions. Details of the moorings deployed are presented in sections 4.2.1 & 4.3.1 below. Ship board observations of hydrography, biology and mixing parameters using CTD, FRRF and SCAMP instruments were also obtained (see Chapter 2 for general methods and instrument descriptions). Dates of shipboard occupations of sites during both cruises, and data collected are presented in *Table 4.1*. Vertical profiles of temperature gradient microstructure and hence estimates of turbulent mixing rates were obtained using the SCAMP during both cruises. Unfortunately, due to the failure of the FRRF instrument, no physiological data were available for the 1998 cruise.

After a brief introduction to the study region, the data obtained during the 1998 cruise are presented (§ 4.2). Analysis of the 1998 data set was principally concerned with evaluating the vertically driven flux of nitrate resulting from the dissipation of internal tidal energy on the shelf. Data from the 2000 cruise are then analysed (§ 4.3). The dynamics of the observed motions are described and vertical nutrient fluxes are quantified. A description of the physical processes responsible for the observed physiological variability is then provided. The influence of large amplitude internal motions on the light climate of the associated phytoplankton communities is also discussed (§ 4.4).

Brief background to physical oceanography of region

The study region is a narrow shelf sea, ranging from around 30-80 km in width. A western boundary current referred to as the East Auckland Current (hereafter EAuC) persists offshore of the continental shelf (Heath, 1980; Denham et al. 1984, *Fig. 1.1*). Upwelling is common in the region, and can result from either favourable wind conditions or the

presence of the quasi-geostrophic EAuC (Sharples *et al.* 1996). Current-driven upwelling at western ocean boundaries results from friction at the seabed slowing the current and thus breaking the geostrophic balance. A near bed current is then forced shoreward down the pressure gradient (Hseuh and O'Brien, 1971). Water from mid depths off-shore is thus upwelled near the coast (Hseuh and O'Brien, 1971; Sharples *et al.* 1996). During late November and early December, the surface sub-tropical waters of the EAuC (characterised by a salinity of >35.5 – 35.6) can penetrate onto the continental shelf (Sharples 1997). The timing of this cross shelf movement depends on local wind conditions (Sharples 1997).

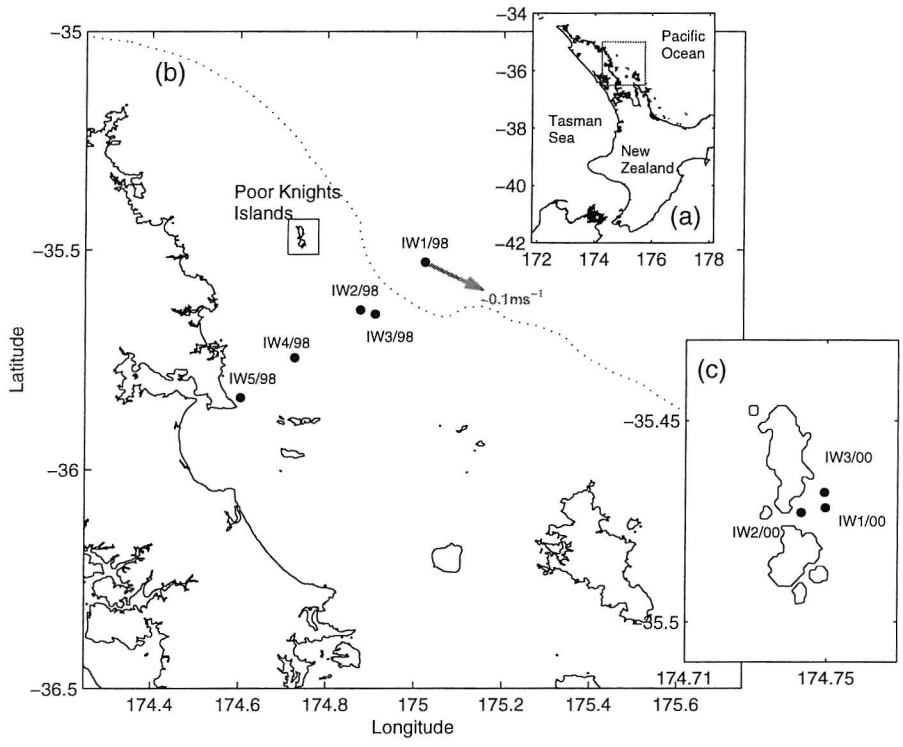

Fig. 4.1 Study region and positions of moorings deployed during Nov-Dec 1998 and 2000. (a), Location of study region in general context of North East New Zealand Shelf. (b), (see box in (a)) Positions of moorings deployed for 1998 cruise, dotted line is 200m contour. (c), Moorings positioned near Poor Knights Islands (see box in (b)) for 2000 cruise. The PK anchor station occupied during the 2000 cruise was adjacent to the IW1/00 mooring. Grey arrow in (b) is the mean flow measured at a depth of 58m on the IW1/98 mooring from 1st – 8th Dec 1998 and indicates influence of East Auckland Current (EAuC).

Previous evidence for internal wave activity in region

The study region was chosen as previous data had indicated that large amplitude internal waves were being generated at the shelf edge and propagating on-shelf. Data from moorings, CTD surveys and synthetic aperture radar (SAR) all indicated the presence of internal waves (*Fig. 4.2*).

1998 cruise : KAH9808, RV *Kaharoa*			
Moorings deployed from 25th November 1998 – 8th December 1998			
Location	**Date/Time**	**No./Type of Obs**	**Additional Info.**
IW4/98	02 Dec 1998 0845 – 1910	17 SCAMP casts 4 CTD casts	8 chl a, 12 nit
IW2/98	05 Dec 1998 0630 – 1907	18 SCAMP casts 15 CTD casts	18 chl a, 20 nit
IW2/98	06 Dec 1998 0651 – 1602	15 SCAMP casts 20 CTD casts	6 chl a, 6 nit
IW4/98	07 Dec 1998 0622 – 1906	20 SCAMP casts 24 CTD casts	26 chl a, 36 nit
2000 cruise : KAH0012, RV *Kaharoa*			
Moorings deployed from 21st November 2000 – 3rd December 2000			
Location	**Date/Time**	**No./Type of Obs**	**Additional Info.**
PK or IW1/00 (PK1)	26 Nov 2000 0420 – 1952	13 CTD/FRRF casts	19 chl a, 16 nit, 9 PE
" (PK2)	27 Nov 2000 0707 – 1910	22 SCAMP casts	
" (PK3)	28 Nov 2000 0422 – 1058	7 CTD/FRRF casts	14 chl a, 11 nit, 3 PE, †
" (PK4)	30 Nov 2000 0416 – 1922	17 CTD/FRRF casts 15 SCAMP casts	19 chl a, 15 nit, 9 PE
" (PK5)	01 Dec 2000 0429 – 1953	21 CTD/FRRF casts 19 SCAMP casts	18 chl a, 18 nit
" (PK6)	02 Dec 2000 0427 – 1946	17 CTD/FRRF casts 13 SCAMP casts	22 chl a, 22 nit, 9 PE
Initial CTD survey: 15 stations, around PK	25 Nov 2000	15 CTD/FRRF casts	51 chl a, 14 DFRRF
Final CTD survey: 35 stations, PK to shelf edge	03 Dec 2000	35 CTD/FRRF casts	11 chl a, 4 nit

Table 4.1 Sampling performed during internal wave cruises. *Notes:* chl a – chlorophyll a sample, nit – nitrate sample, PE – ^{14}C P* vs. E curve, DFRRF – dark acclimated FRRF sample collected. † CTD winch failed on 28th Nov 2000 at PK. Sampling for remainder of 28th November and 29th November was therefore abandoned while a port call was made for repairs. Positions of moorings are marked in *Fig 4.1*.

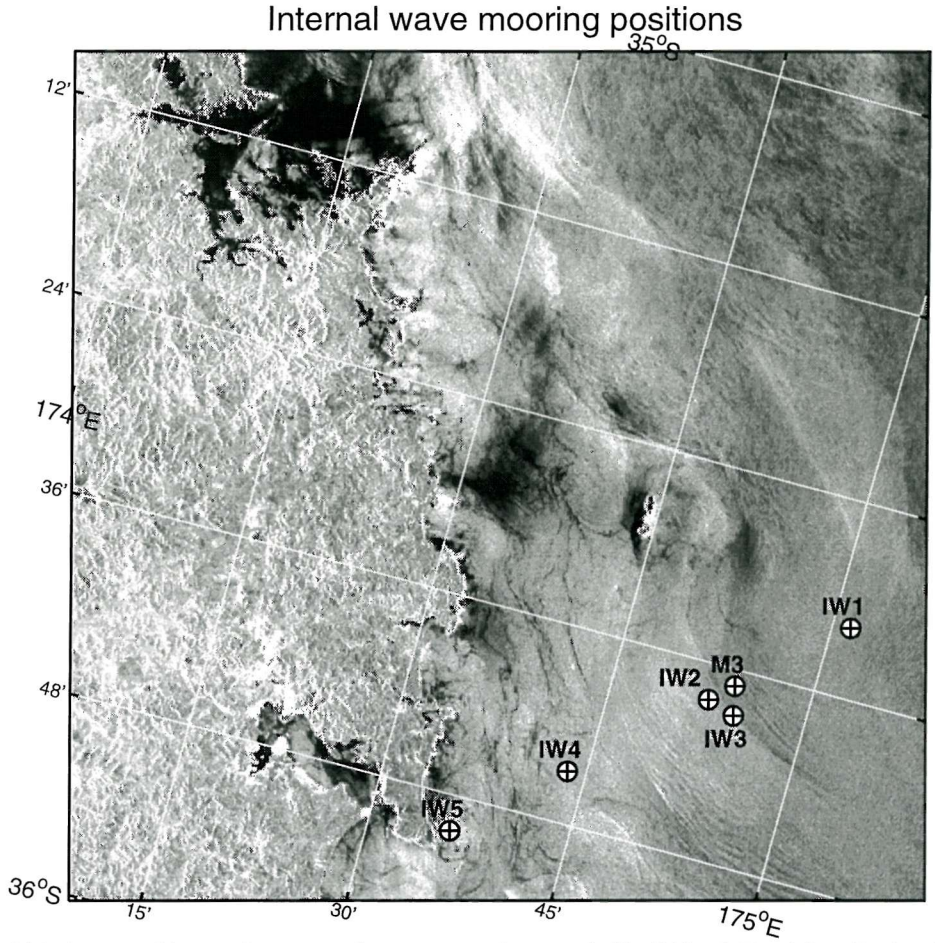

Fig. 4.2 SAR image of internal wave packets propagating on-shelf off North East New Zealand. The ERS-1 SAR image was collected on 17 November 1995. Internal waves in SAR imagery are usually apparent as bands of dark and/or light (e.g. Vesecky and Stewart, 1982; Alpers, 1985). Note moorings IW2/98 and IW4/98 are around a wavelength apart. M3 indicates the position of an additional long term mooring located in the study region. Not to be confused with the M3 station occupied during the 1999 (tidal mixing front) cruise.

4.2 1998 study: Internal tide dissipation and nitrate flux

4.2.1 Moorings

The design of the mooring array deployed for the 1998 experiment is shown in *Fig. 4.3*. No useful current data were recovered from the ADCP on the IW2/98 mooring.

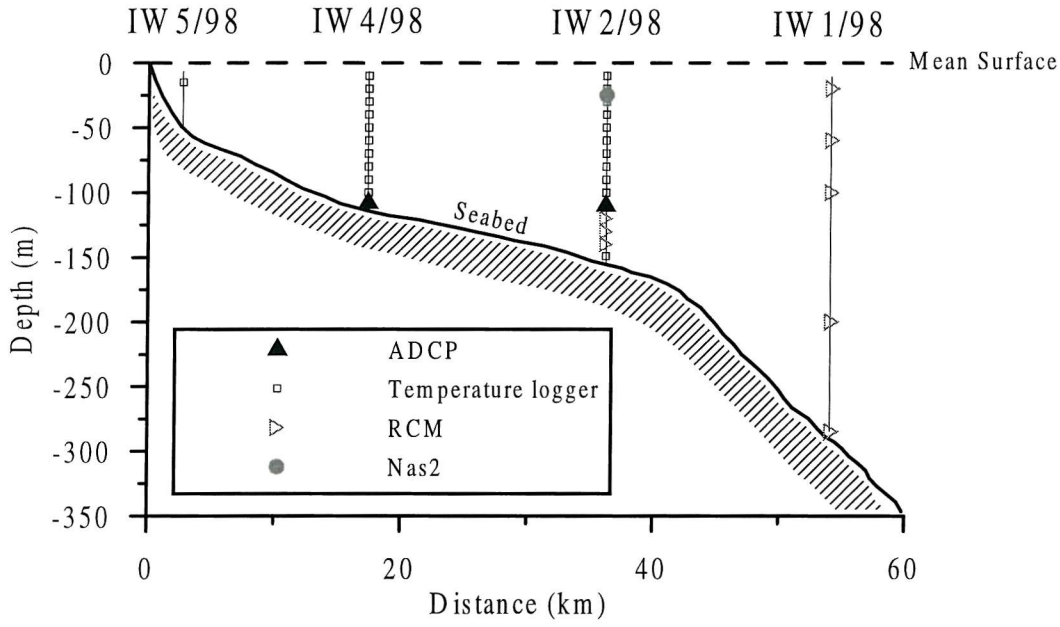

Fig. 4.3 Set-up and instrumentation used on mooring transect during 1998 experiment. Two upward facing ADCP's were deployed on the principal moorings (IW2/98 & IW4/98) in order to provide a detailed description of the current field. A series of temperature loggers and recording current meters (RCM's) also provided observations of the vertical temperature structure across the shelf. In addition a NAS-2 nitrate auto-analyser was deployed at a depth of 25m on the IW2/98 mooring. The IW3/98 mooring (*Fig. 4.1b*) consisted of an autonomous vertical profiler (APV) which failed soon after deployment. All instruments were sampled at 1 minute intervals excepting RCM's and NAS-2 auto-analyser, which were sampled every 5 and 30 minutes respectively.

General structure

Time series of temperatures from the moorings IW2/98 and IW4/98 provided a detailed description of the vertical water column structure over the deployment period (*Fig. 4.4*). Semi-diurnal variability in the thermal structure of the water column was apparent at both sites indicating the presence of an internal tide with amplitudes ranging from 10-35m at IW2/98 and 10-20m at IW4/98. During the period from 28-29th November 1998 a large storm passed through the region, causing complete mixing of the water column at IW4/98 and a pronounced deepening of the upper mixed layer at IW2/98 from 30m to around 70m (*Fig 4.4*). Re-stratification of the water column at both sites occurred after the storm subsided.

The semi-diurnal internal tidal signatures were not apparent during the storm event due to the break-down of stratification (*Fig. 4.4*). Times during which internal tidal motion dominated included the initial deployment period before the storm event (25th-27th Nov),

and after re-stratification (1st-5th Dec). The period after the 6th Dec appeared to be dominated by strong inertial motions (Sharples *et al.* 2001b).

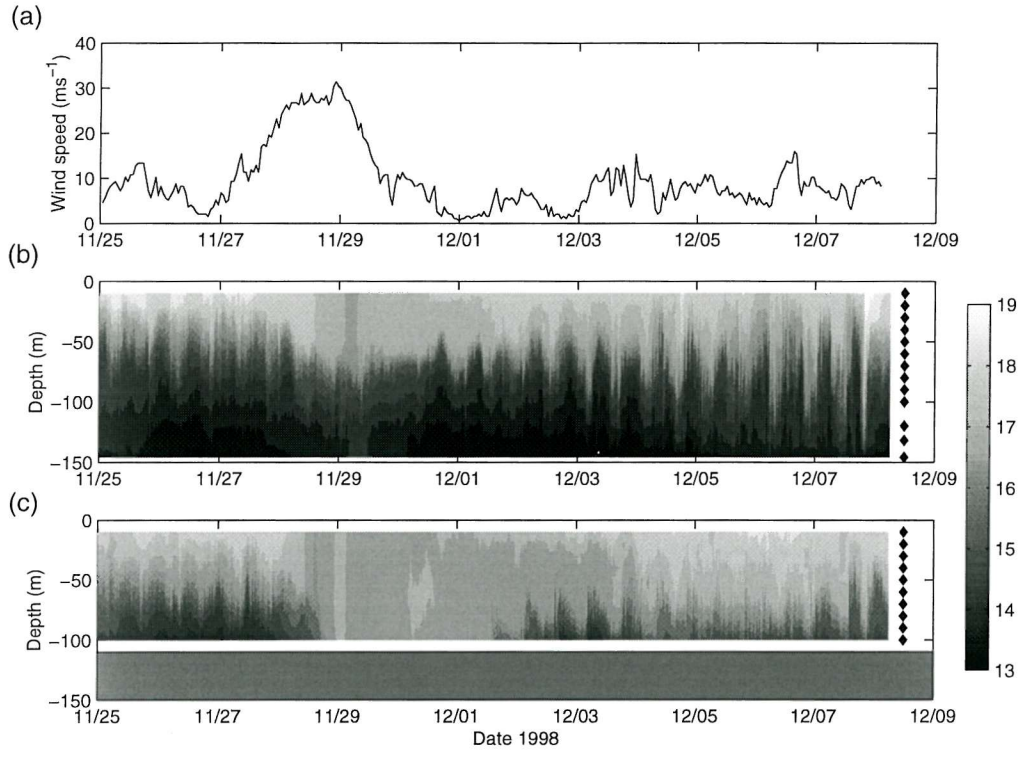

Fig. 4.4 Time series of surface wind speed and water column vertical thermal structure at the two principal moorings. (a) Wind speed measured during mooring deployment. Measurements were obtained from Mokohinau Islands (175.1°E 35.9°S, see *Fig. 4.1*) (b) Time series of vertical water column temperature (°C) at IW2/98. Filled diamonds to right show depths of temperature loggers and current meters. (c) as (b) but for IW4/98. Shaded region indicates seabed at this site.

Power spectra

The dominance of semi-diurnal variability in the observations was confirmed by the power spectra (*Fig. 4.5*). Significant peaks at the M2 tidal frequency (12.42 hr period) were apparent in temperature records from both moorings (*Fig. 4.5a*). As horizontal gradients in temperature between the two moorings were weak (on the order of 0.01°C km^{-1}) such semi-diurnal temperature variance must have resulted from vertical oscillations of the thermocline. The height of the peak in temperature variance at semi-diurnal frequencies was generally greater at IW2/98 than for similar depths at IW4/98. Power spectra of the time series of baroclinic currents calculated by removing the depth mean currents from the ADCP observations at IW4/98 also showed a significant peak at the M2 tidal frequency (*Fig. 4.5b*).

A broad peak of energy in both the temperature and current variance was also observed at periods between 10 and 30 minutes. Such higher frequency variability indicated the presence of shorter period internal waves as were visible in the SAR image (*Fig. 4.2*).

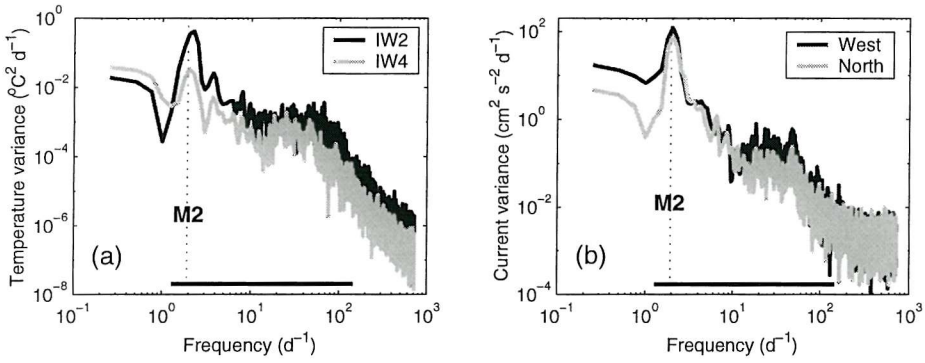

Fig. 4.5 Temperature and current variance spectra for the IW2/98 and IW4/98 moorings. (a) Variance in the temperature record at 60m from IW2/98 (black) and IW4/98 (grey) for the period 1st – 5th Dec 1998. (b) Variance in the northward (grey) and eastward (black) baroclinic components of the currents measured at a depth of 24m at IW4/98 using the ADCP. Baroclinic currents were estimated by removing the depth mean current from individual depth bins at every time throughout the time-series. Horizontal black line indicates integration limits for internal wave potential energy calculations (periods of 17hrs to 10 minutes, see below).

Vertical shear and Richardson no.

The observations of baroclinic currents and water column thermal structure at the two principal moorings suggested that the internal wave steepened as it propagated on-shelf, some of the energy being transferred to higher frequency internal solitons which then break. In order to evaluate whether enhanced shear and hence mixing may have been generated within the water column, the vertical current shear measured using the ADCP at the IW4/98 mooring was calculated as:

$$shear^2 = \overline{\left(\frac{\partial u}{\partial z}\right)^2 + \left(\frac{\partial v}{\partial z}\right)^2} \qquad (4.1)$$

where u and v are the eastward and northward components of the currents and the overbar denotes averaging over some period.

The Richardson number (R_i) which provides an index of stability, was calculated according to:

$$Ri = \frac{N^2}{shear^2} \tag{4.2}$$

where N^2 is the buoyancy frequency (Eq. 2.4).

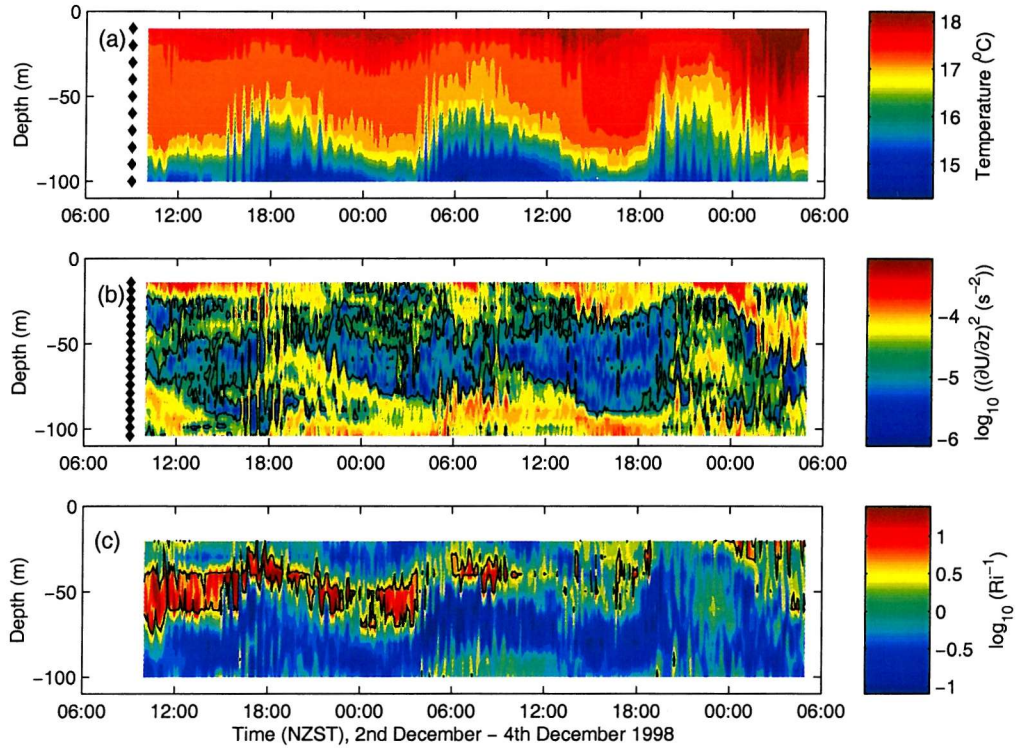

Fig. 4.6 Temperature structure, shear and Richardson number for the period from 1000 on 2nd December to 0500 on 4th December 1998 at IW4/98. (a) Contours of temperature from the thermistors on the IW4/98 mooring. (b) Squared current shear averaged over 5 minute intervals from ADCP. Black contour is at 2×10^{-5} s^{-2}. (c) Log_{10} of the inverse Richardson number. Black contour indicates $R_i = 0.25$. $R_i < 0.25$ is typically taken to be a necessary condition for instability, (i.e. $\log_{10}(R_i^{-1})>0.6$), thus red regions (inside black contour) may be unstable. Depths of the temperature loggers and ADCP bins are shown by black diamonds in (a) and (b) respectively.

An example time series of the 5 minute averaged squared current shear and R_i is given in *Fig. 4.6*. High levels of current shear were associated with the surface and seabed throughout the record (*Fig. 4.6* & Sharples *et al.* 2001b). Relatively high levels of shear were observed within the water column at times associated with the passage of internal waves. Calculated R_i numbers indicated that at certain stages the internal waves caused the necessary condition for instability to be satisfied ($R_i<0.25$) within the water column , e.g. around 01:00 on 3rd December 1998 (*Fig. 4.6*).

Internal tidal energy and dissipation

The temperature data from the IW2/98 and IW4/98 moorings was used to calculate a vertical profile of the internal wave potential energy according to Largier, (1994):

$$PE(z) = \frac{g \, \partial\rho/\partial T}{2 \, \partial T/\partial z} [\Delta T]^2 \tag{4.3}$$

where $\partial T/\partial z\,(z)$ is the mean vertical temperature gradient over the period in question, $\partial\rho/\partial T$ is the mean value of density as a function of temperature (≈ 0.206, *Fig. 4.7*) and $[\Delta T]^2(z)$ is the temperature variance calculated by integrating the observed temperature spectra for each depth (*Fig. 4.5a*). Integration limits for the spectra (from periods of 17 hrs to 10 minutes) were chosen to span the M2 tidal frequency and the shorter period waves in order that the energy contained in the solitons would also be included in the calculation (*Fig. 4.5a*).

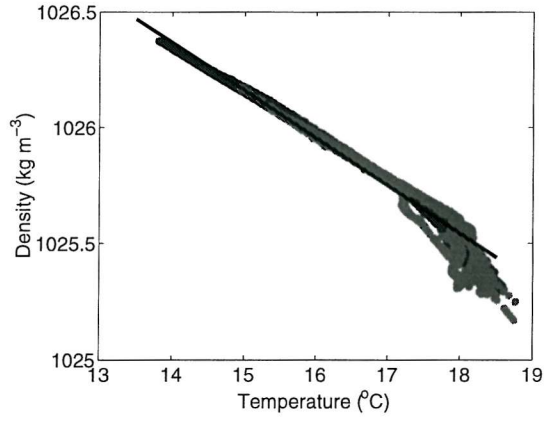

Fig. 4.7 Temperature density relationship from CTD data collected at the locations of both the IW2/98 (black) and IW4/98 (grey) moorings.
Black line indicates the derived relationship, Dens = 1029.25 – 0.206 ×Temp, $R^2 = 0.973$, n = 8800

In a similar manner the internal wave kinetic energy profile was calculated from the observed baroclinic currents at IW4/98 using:

$$KE(z) = \frac{1}{2} \rho \left[u(z)^2 + v(z)^2 \right] \tag{4.4}$$

where $u(z)^2$ and $v(z)^2$ are the eastward and westward components of the current variance calculated by integrating the observed current spectra over the same limits as the temperature spectra (*Fig. 4.5b*). These calculations were performed for the period between 1st and 5th December 1998 when internal tidal energy dominated over inertial oscillations (Sharples *et al.* 2001b).

The resultant profiles of PE and KE showed the expected vertical structure (*Fig. 4.8*). KE increased towards the surface and seabed boundaries at IW4/98, while maximal values of PE were found in the middle of the water column at both sites.

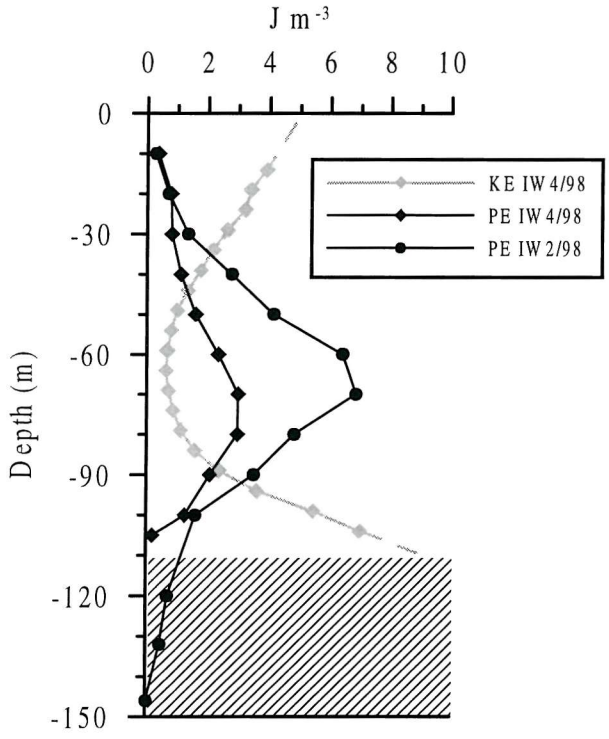

Fig. 4.8 Mean vertical profiles of internal wave energies at IW2/98 and IW4/98 for the period 1st – 5th December 1998.
Diamonds are profiles of potential energy (black) and kinetic energy (grey) at IW4/98.
Circles are potential energy at IW2/98. (see legend)
Dotted grey lines indicate KE extrapolated to surface and seabed. Hashed area indicates bottom depth at the shallower (IW4/98) mooring position

In addition the PE calculated for the offshore (IW2/98) mooring was larger than that for the inshore mooring. Integrated water column potential energy was 350 J m^{-2} at IW2/98 and 160 J m^{-2} at IW4/98. The vertical profile of internal wave kinetic energy at IW4/98 was extrapolated to the surface and seabed before calculating the water column integral (*Fig. 4.8*). The mean water column kinetic energy at IW4/98 was estimated to be 300 J m^{-2}. Neglecting the increase of KE in the regions towards the boundaries, where ADCP data was not available, would have caused the water column kinetic energy to have been underestimated by around 25% (Sharples *et al.* 2001b).

The total energy of the internal wave field is the sum of the kinetic and potential energies. The ratio of PE to KE can be predicted from linear theory as:

$$\frac{PE}{KE} = \frac{(\omega^2 - f^2)}{(\omega^2 + f^2)} \qquad (4.5)$$

where ω is the wave frequency and f is the Coriolis parameter (Fofonoff, 1969). For the dominant waves at tidal frequency the predicted ratio of PE:KE is 0.46, which compares

well with the observed value of 0.51 at IW4/98. A second calculation was performed to estimate the proportion of internal wave energy at tidal frequencies as opposed to the shorter period waves, by integrating the observed temperature and baroclinic current spectra over narrower limits (17hrs – 2hrs). The shorter period waves were thus estimated to contain around 25% of the PE contained in the internal tide at both moorings and 16% of the KE at IW4/98. This increase in the ratio of PE:KE at IW4/98 for higher frequency waves is consistent with linear theory (Eq. 4.5) and may explain why the total PE:KE ratio is slightly higher than the value predicted for pure tidal frequencies.

The total internal wave energy at the two sites was therefore calculated as the sum of the PE and KE and using the theoretical ratio of 0.46 to estimate the KE at IW2/98. Total wave energies at the two sites decreased from 1100 J m^{-2} at IW2/98 to 460 J m^{-2} at IW4/98. The mean internal wave dissipation rate between the two moorings could then be calculated once the mean wave propagation speed was known (Largier, 1994). This was estimated to be 40 cm s^{-1} by considering the phase of the temperature variations between the two moorings and noting that the wave propagation direction was essentially parallel to the mooring array, the moorings being around a wavelength apart (*Fig. 4.2*, see also Sharples *et al.* 2001b). Thus the energy loss of 640 J m^{-2} over 12.5 hrs, in a mean depth of 130m, was estimated to have driven a mean energy dissipation rate of 1.1×10^{-7} m^2 s^{-3} (1.5×10^{-2} W m^{-2}) between the two moorings from 1st – 5th December 1998. Taking the observed mean water column buoyancy frequency of 6×10^{-5} s^{-2} for this period and using (Eq. 2.5), a mean eddy diffusion coefficient $K_\rho = 4 \times 10^{-4}$ m^2 s^{-1} was thus calculated. Sharples *et al.* (2001b) calculated the same values using harmonic analysis of the current and temperature records in contrast to the spectral technique used here. The harmonic analysis additionally allowed a time series of potential and baroclinic energies at the tidal frequency to be calculated. Sharples *et al.* (2001b) thus calculated that the internal tidal energy and hence diffusivity varied by around 70% during the period from 1st – 5th December.

4.2.2 Microstructure observations and nutrient fluxes

Microstructure measurements

Microstructure data were obtained on four days at the sites of the two principal moorings. IW2/98 was occupied on 5th and 6th December and IW4/98 on 2nd and 7th December 1998 (*Table. 4.1*). Sampling was performed over 12.5hrs and internal tidal signals were generally dominant on all days where microstructure measurements were obtained. Microstructure data were averaged into 5m vertical depth bins from 10m to around 75m.

The near surface data was discarded due to possible contamination form the ship's wake. Additionally all the data collected at a site (32 – 37 individual profiles) was averaged over time to provide tidally averaged profiles of diffusivity collected over two tidal periods (*Fig. 4.9*). The resulting vertical profiles of K_T indicated higher diffusivities at the more off-shore site ($6 \pm 1 \times 10^{-4}$ m^2 s^{-1}, mean ± 95% C.I. depth mean value for all data at IW2/98) than the inshore site ($2 \pm 0.5 \times 10^{-4}$ m^2 s^{-1}, mean ± 95% C.I. for IW4/98).

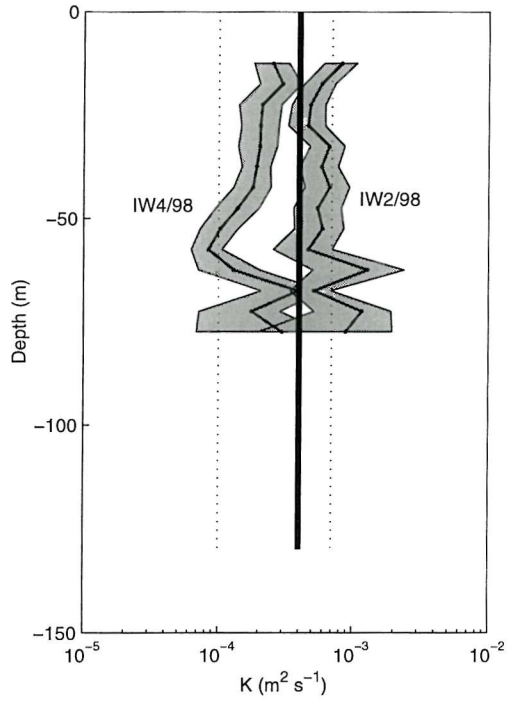

Fig, 4.9 Tidally averaged diffusivity profiles from microstructure data and comparison with mooring based estimate. Grey shaded regions indicate 95% confidence intervals (Effron and Gong, 1983) of microstructure diffusivity estimates for the two sites, with circles indicating the average values. Thick vertical line indicates the mean diffusivity calculated from the mooring data. Vertical dotted lines indicate the possible range of variability over 1st – 5th December 1998 (Sharples *et al.* 2001b).

Microstructure estimates of K_T compared well with the mean value calculated from the mooring data (*Fig. 4.9*). Higher diffusivities at IW2/98 were consistent with enhanced internal tide dissipation at this site associated with the higher energy flux observed at the shelf edge.

Nitrate fluxes

The vertical distribution of nitrate as observed using discrete bottle sampling from the CTD showed an increase in concentration with depth at both sites (*Fig. 4.10a*). Nitrate levels decreased from around 10 mmol m^{-3} near the seabed at IW2/98, to low levels (approaching 0.1 mmol m^{-3}) in the near surface regions associated with higher chlorophyll concentrations (*Fig. 4.10a & b*). Nitrate gradients were typically around 0.1 mmol m^{-4}, increasing to around 0.3 mmol N m^{-4} at depths associated with the base of the higher chlorophyll regions (*Fig. 4.10c*).

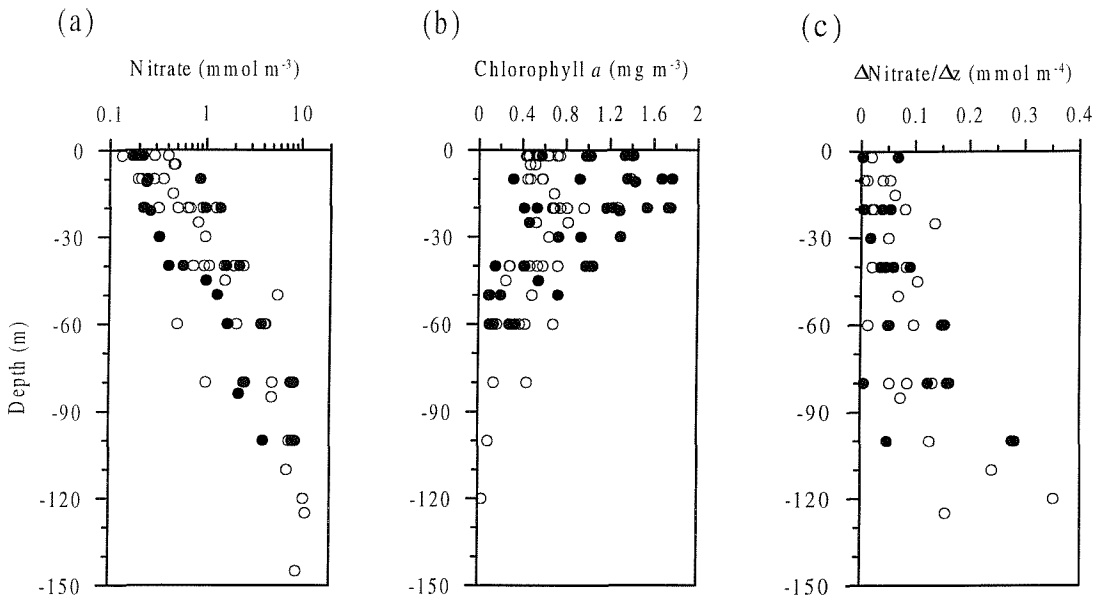

Fig. 4.10 Vertical distributions of nitrate, chlorophyll and nitrate gradients. (a) Nitrate concentration against depth for all bottle samples collected at IW2/98 (open symbols) and IW4/98 (closed symbols). (b) Fluorometrically derived chlorophyll *a* from discrete bottle samples, symbols as in (a). (c) Estimated vertical nitrate gradient based on bottle data, symbols as in (a).

Taking representative nitrate gradients of around 0.2 ± 0.1 mmol m^{-4} for both sites maximal vertical nitrate fluxes are now estimated using the observed diffusivities (Eq. 2.6). Vertical nitrate fluxes driven by the internal tide are estimated to be around 10 ± 5 mmol N m^{-2} d^{-1} at IW2/98 and 3.5 ± 1.7 mmol N m^{-2} d^{-1} at IW4/98. A mean value of around 4 – 7 mmol m^{-2} d^{-1} was representative of the region between the two moorings using the energy lost by the internal tide.

4.2.3 Possible consequences for phytoplankton nutrient and light climate

The high inferred rate of nutrient supply to the near surface phytoplankton populations was likely to have resulted in conditions where nutrient limitation was of relatively low importance for growth limitation through much of the water column. The large vertical motions of the internal tide would have caused rapid and significant variations in the light levels experienced by phytoplankton populations. Surface populations would have been drawn down to low light levels at certain times, while deeper populations at higher ambient nutrient concentrations would have experienced movement into regions of high light during the opposite phase of the tide.

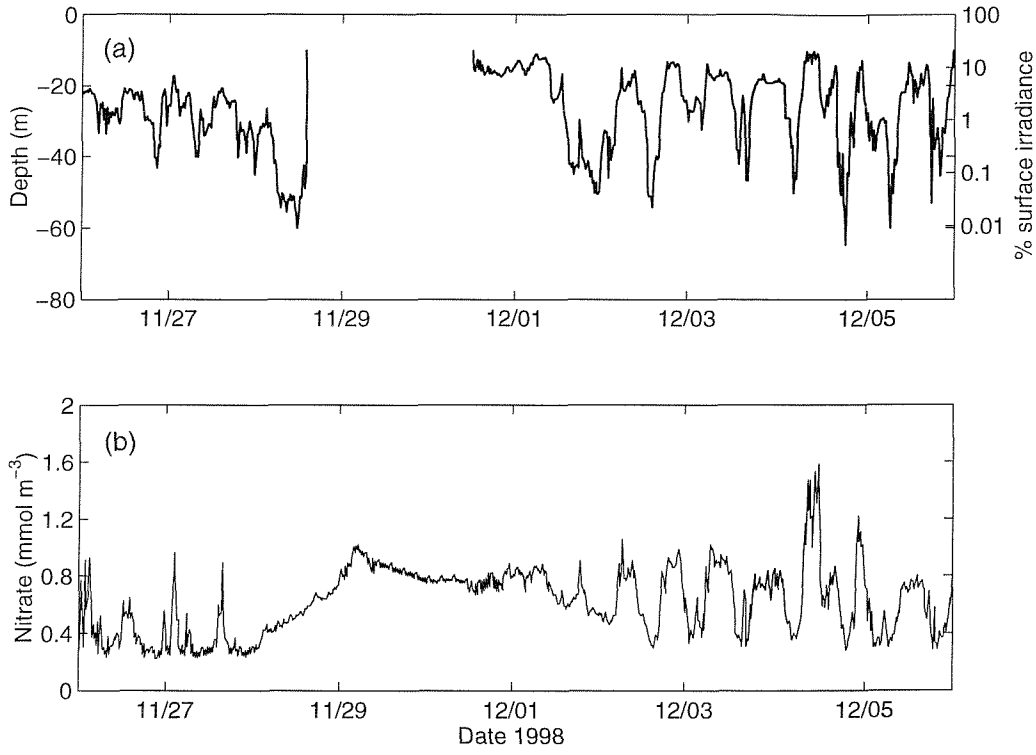

Fig. 4.11 Light depth and nitrate variability driven by internal tide vertical motions. (a) Time series of the depth and percentage surface irradiance experienced at the 18°C isotherm at IW2/98. The time series of thermal structure at the IW2/98 mooring was used to calculate the depth of the 18°C isotherm, then converted to % light depth using the mean diffuse attenuation coefficient of 0.155 m^{-1} measured during CTD casts at this site. (b) Time series of nitrate concentration at a depth of 25m at IW2/98 as measured by the NAS2 auto-analyser. The NAS2 data was calibrated against nitrate samples taken from the CTD, with an offset of around 0.3 mmol m^{-3} observed between the two methods.

These vertical motions and associated irradiance variations are illustrated in *Fig. 4.11*. The correlation between vertical oscillations of the thermocline and the nutrient concentration at 25m depth is clear. Depending on the position of phytoplankton within the density structure of the water column, individual cells could have experienced between 20-30% and <0.1% of surface irradiance at different stages of the tide.

The effect of such variations in irradiance and nutrient supply on the physiology and growth of phytoplankton will depend on the ability of the *in situ* population to adapt and acclimate to the changing conditions. Observations of the physiological response of phytoplankton to large vertical perturbations were obtained during the 2000 cruise.

4.3 2000 study: Internal bores and physiological response

4.3.1 Mooring data and internal dynamics

Set-up

The site chosen for the second internal wave study was close to a group of islands near the continental shelf edge (*Fig. 4.1*). It was expected that the sloping bottom in this region would cause steepening of internal waves and hence large vertical motions. Such an effect had been indicated in historical mooring data from the site.

The design of the mooring array deployed for the 2000 experiment is shown in *Fig. 4.12*. The two principal moorings consisted of upward facing ADCP's and thermistors, arranged to provide a detailed description of the vertical temperature and velocity fields throughout the experiment. A third mooring, IW3/00, consisting of an autonomous profiling vehicle (APV), which failed after four days and a temperature logger held at a mean depth of 11m, was also deployed (*Fig. 4.1*).

Good data were recorded from all instruments with the exception of near surface daytime ADCP data at the outer mooring (IW1/00). High errors in the current measurements and low backscatter strengths led to data for depths less than around 50m being rejected. The low signal strength was likely to have been caused by the vertical migration of scatterers (zooplankton) away from the upper portions of the water column during daylight.

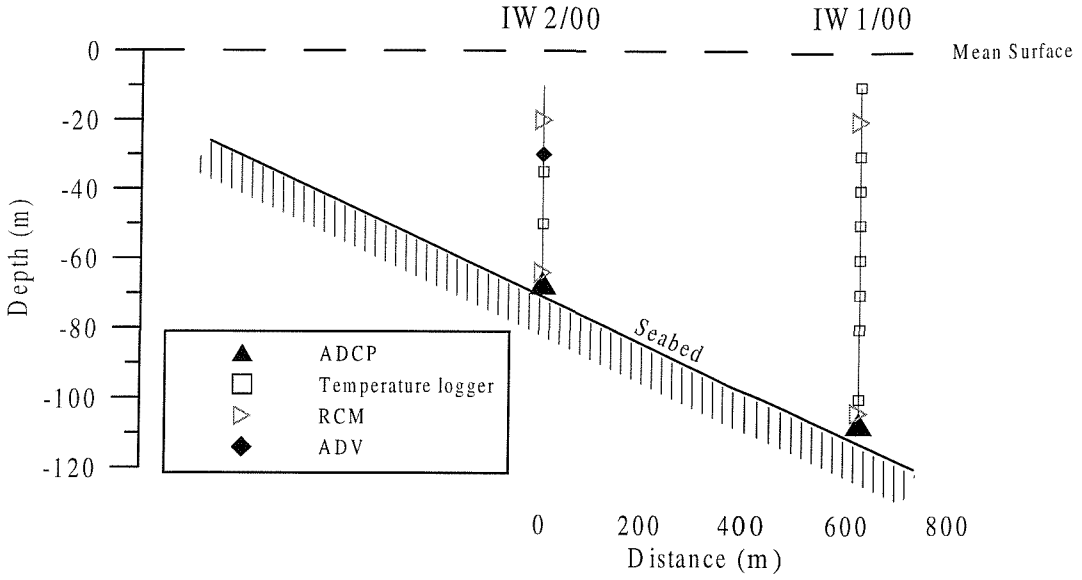

Fig. 4.12 Set-up and instrumentation used on two principal moorings during 2000 experiment. Two upward facing ADCP's were deployed near the seabed in order to provide a detailed description of the 3 components of the current field. A series of temperature loggers and RCM's also provided observations of the vertical temperature structure at the two sites. All instruments were sampled at 1 minute intervals. ADCP's provided vertical current profiles at 5m resolution.

General structure

The vertical thermal structure throughout the deployment period and an example of the thermal structure and current vectors for one day illustrate the presence of large bore like internal motions (*Figs. 4.13*, see also *Appendix 6*).

The observed internal motions showed similarities with the observations of Pineda, (1994, 1999) and with laboratory studies of internal waves running-up on slopes (Helfrich, 1992; Michallet and Ivey, 1999). The direction and phase speed (speed of propagation) of the internal bore front as it moved up the slope was calculated using cross correlation of the temperature records from the three moorings (e.g. Pineda, 1999). Maximal correlation between the temperature records at IW1/00 and IW2/00 was found with a delay of around 54 minutes, while the temperature record at IW3/00 preceded that at IW1/00 by 6 minutes. Assuming a linear bore front, a mean constant phase speed of 20 (±3) cm s^{-1} was calculated. Such phase speeds are similar to those calculated by Pineda, (1999) albeit for a bore in much shallower water. The propagation direction was estimated to be around 5° (±1°) counter-clockwise of a line from IW1/00 to IW2/00

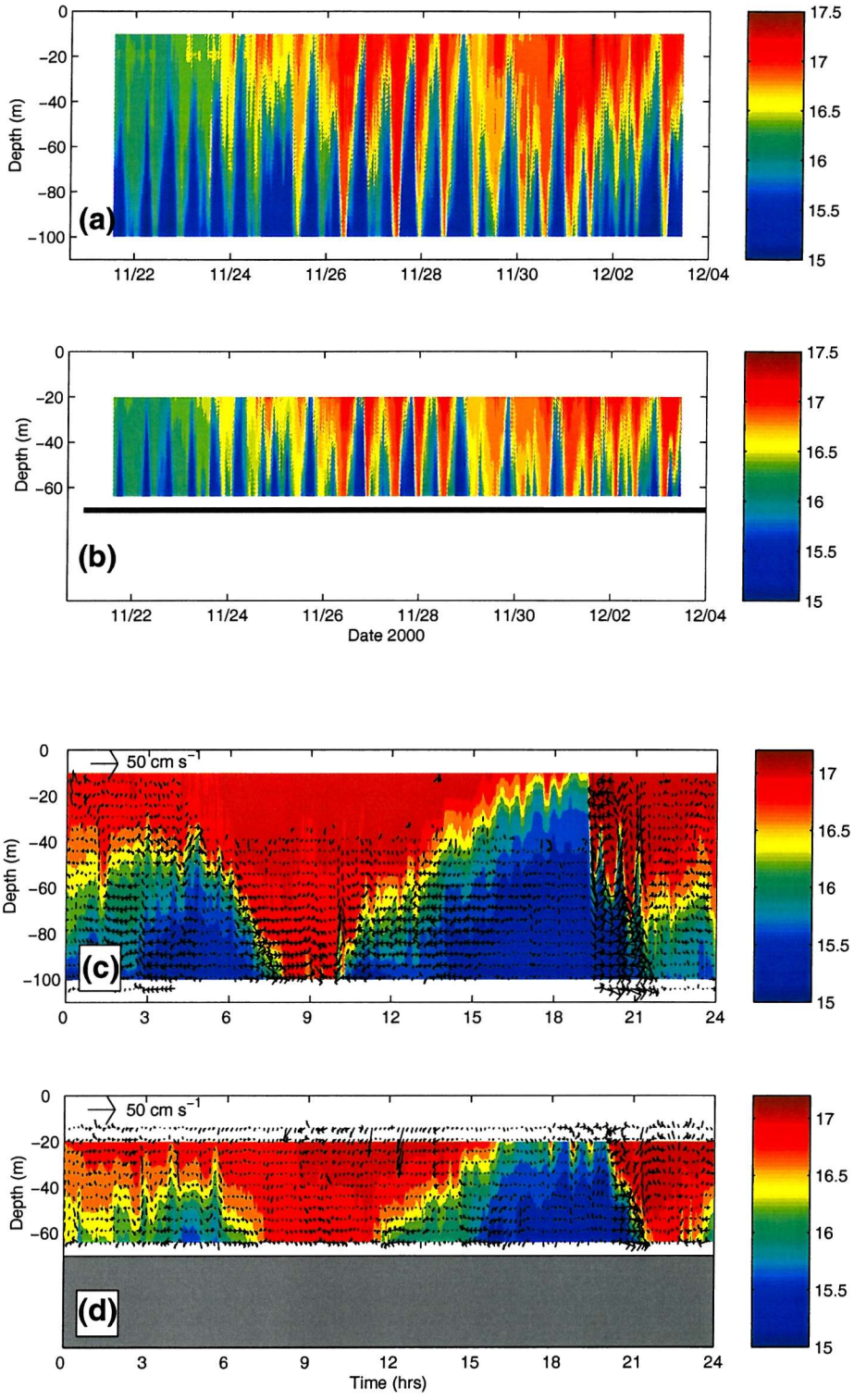

Fig. 4.13 Time series of thermal structure in 2000 (Temperature, °C). (a) Data from entire deployment for IW1/00, (b) Data from entire deployment for IW2/00. Thick horizontal line in (b) indicates bottom depth at this site. (c) Temperature variability and current vectors for 26 November 1998 at IW1/00, Colours are temperature contours (°C), arrows are current vectors plotted every ten minutes, vertical being vertically up, left indicating offshore (relative to bore direction, see text). (d) as (c) for IW2/00.

The internal bore was characterised by a 'warming phase' e.g. from around 0300 – 0900 on 26th November (*Fig. 4.13 c & d*), where water was drawn down the slope and off shore at depth to be replaced by warmer water being advected in-shore and then down at the surface. This was followed by a 'cooling phase', where cooler, denser water moved in-shore and up the slope at depth, with off-shore flow in the surface (*Fig. 4.13 c & d*, see also *Appendix 6*).

Observed variations in temperature were not dominated by vertical motions at all times. This contrasted with the more open shelf study in 1998 and resulted from the large degree of horizontal advection and relatively high lateral temperature gradients during certain periods. Horizontal temperature gradients, as measured by comparing the records at the two principal moorings, were at times >1 °C km^{-1}. When combined with horizontal velocities of around 20 cm s^{-1}, temperature variability was often a strong function of lateral as well as vertical components. In particular during the 'warming phase' vertical motions tended to dominate, while during the 'cooling phase' as denser water moved up the slope, horizontal advection was dominant. The relative contribution of horizontal and vertical motions was confirmed by tracking water parcels using the ADCP vertical velocities, then comparing the results to the observed isotherm displacements (*Appendix 6*).

A general warming trend was observed throughout the mooring deployment period (*Fig. 4.13a & b*). In addition following 1st December the amplitude of the internal motions decreased.

Soliton packets, shear and R_i

In addition to the large internal bore events, higher frequency internal waves were observed throughout the record (see e.g. *Fig. 4.13c* around 2000 hrs). The shorter period internal motions propagated as packets of solitary waves and were associated with relatively high vertical velocities between 5-10 cm s^{-1} (*Fig. 4.14*). The occurrence of soliton packets throughout the time series was intermittent.

The time series of squared vertical current shear (Eq. 4.1) displayed enhanced shear within the water column associated with the passage of the internal bore events (*Fig. 4.15*). Regions of strong internal shear were associated with the regions of maximal vertical thermal gradient at times corresponding to both up and down slope currents in the lower water column (*Fig. 4.15b*). Much of the enhanced internal shear was also associated with the higher frequency internal waves.

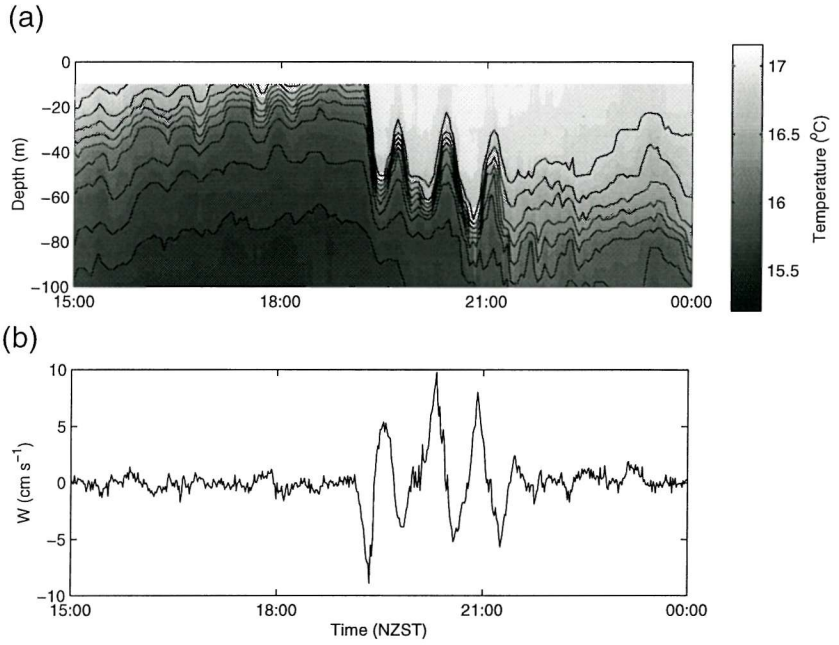

Fig. 4.14 Detailed structure of a soliton packet on 26th December 2000. (a) Temperature from thermistors on IW1/00 mooring. (b) Vertical velocity at 54m as measured by ADCP on IW1/00 mooring.

Richardson numbers, calculated using the temperature and current time series, were low near the seabed and also low in the interior of the water column during certain periods (*Fig. 4.15c*). Variability in R_i was associated with the internal motions, with lower R_i at mid-depths closely related to the passage of the 'warm phase' of the bore. The necessary condition for instability ($R_i<0.25$) was frequently satisfied within the bottom layers and periodically (at approximately tidal frequencies) within the upper water column. Sub-critical Richardson numbers were also observed to be associated with some periods of higher frequency wave passage (*Fig 4.15b*).

Generally R_i within the region of maximal thermal gradients indicated stability. However the introduction of artefacts due to the sampling resolution of the moorings could not be ruled out. In particular the region of maximal thermal gradients was generally narrower than the vertical resolution of the thermistors and ADCP depth bins. Additionally shear and R_i calculations performed over 5 minute intervals may have been insufficient to resolve the short instability events which may have been associated with the 20 minute period solitons.

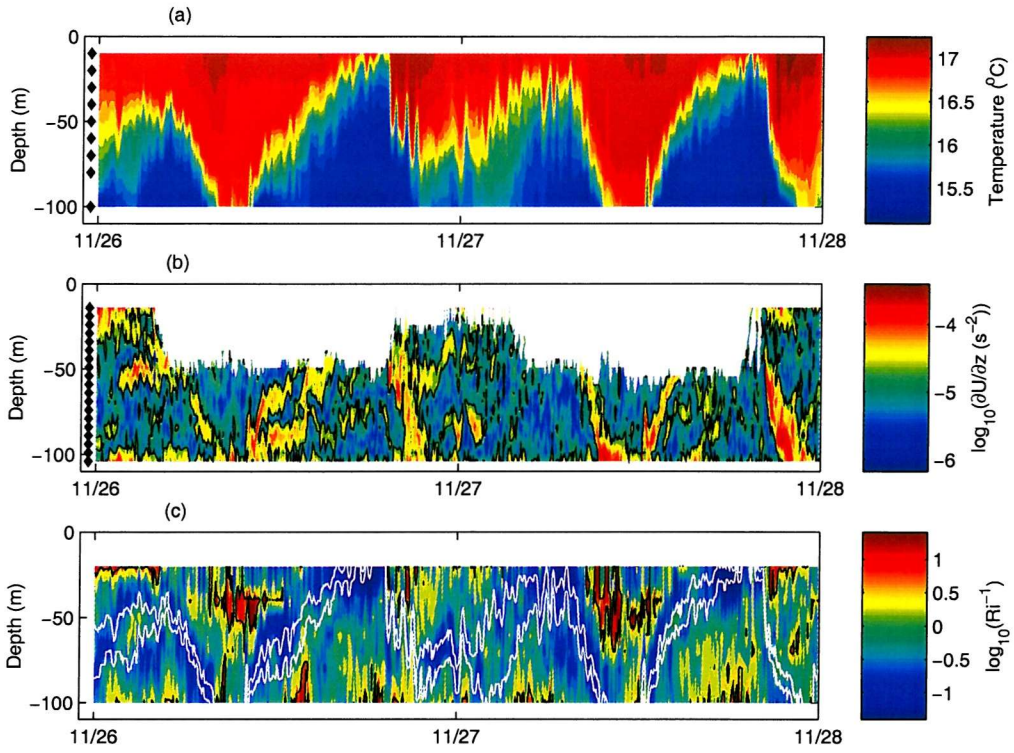

Fig. 4.15 Vertical temperature, shear and R_i number variability for a 48hr period from 26th – 28th December 2000 at IW1/00. (a) Temperature from thermistors on IW1/00. (b) Squared current shear averaged over 5 minute intervals from ADCP. Black contour is at 2×10^{-5} s^{-2}. (c) Log_{10} of the inverse Richardson number. Black contour indicates $R_i = 0.25$ (see *Fig. 4.6*). White contours are the 16 and 16.5°C temperature contours provided for reference. Depths of the temperature loggers and ADCP bins are shown by black diamonds in (a) and (b) respectively. The Richardson number calculated in (c) utilises both the ADCP currents and the RCM situated at a depth of 20m in order to recover values of shear for the upper water column during daylight hours.

4.3.2 Microstructure, mixing and nutrient fluxes

Microstructure and mixing

Microstructure measurements were obtained on four days during the anchored occupation of the IW1/00 mooring site by ship, (PK2) 27th & (PK4) 30th November and (PK5) 1st & (PK6) 2nd December 2000 (*Table. 4.1*). Microstructure data were averaged into 5m vertical depth bins from the surface to around 85m.

Spatial and temporal variability in the patterns of turbulent dissipation (ε) and diffusivity (K_T) were closely linked to the dynamics of the internal tide/bores (*Fig. 4.16*). Higher dissipation was observed in the regions of the maximal vertical thermal gradients and

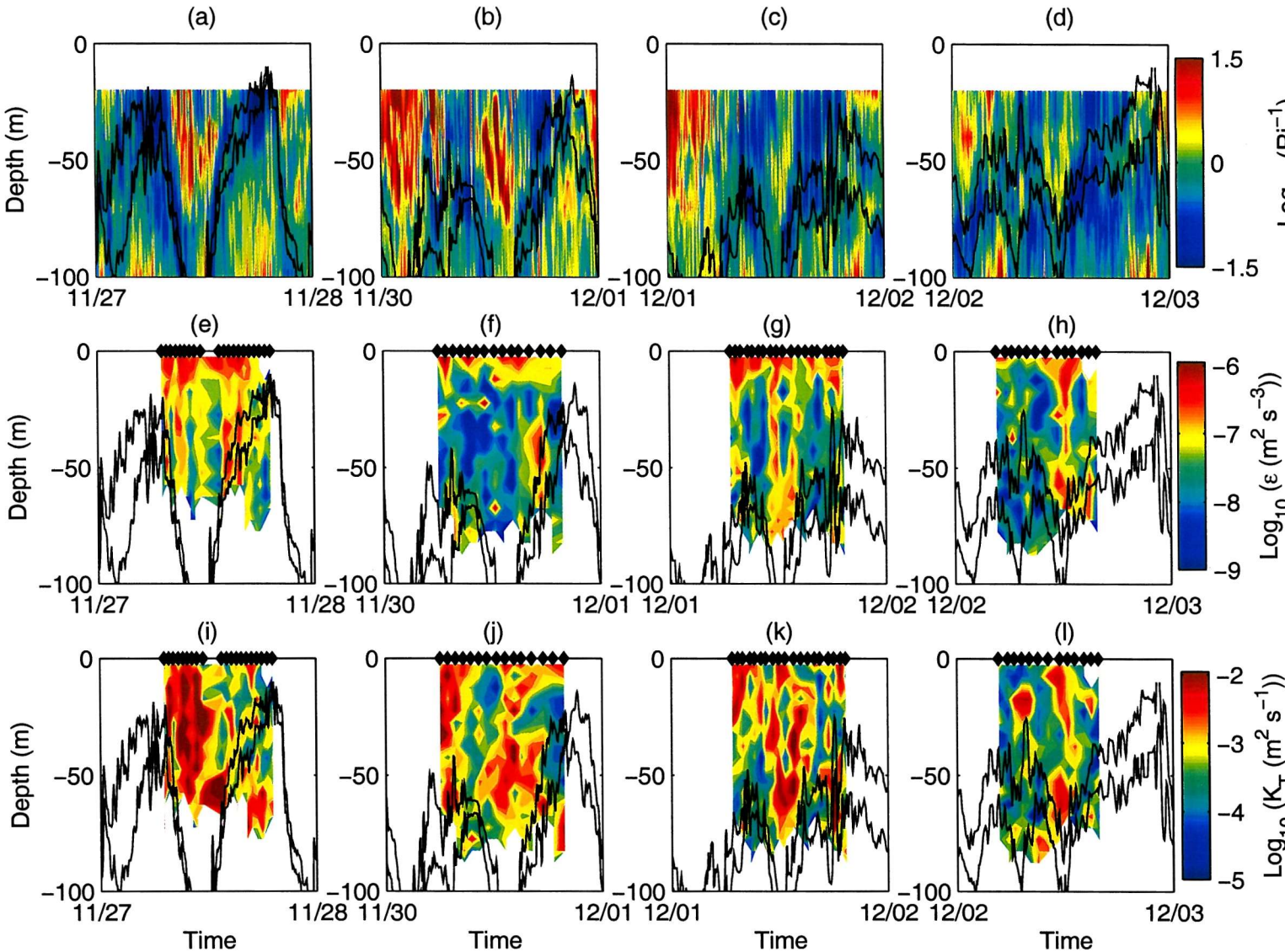

Fig. 4.16 Observations of mixing parameters from ADCP and microstructure measurements during ship occupation of site PK 27th November - 2nd December 2000. (Top, a,b,c,d), Time series of Log_{10} of the inverse Richardson number calculated from ADCP and thermistors, averaged every 5 minutes. (Middle, e,f,g,h), Time series of rate of dissipation of turbulent kinetic energy $\log_{10}(\varepsilon\ (m^2\ s^{-3}))$ as measured by SCAMP profiles of temperature gradient microstrucutre. (Bottom, i,j,k,l), Time series of vertical temperature diffusivity $\log_{10}(K_T\ (m^2\ s^{-1}))$ as measured by SCAMP. Black lines in all plots are depths of the 16 and 16.5C isotherms to provide reference of internal tide phase. Times of individual vertical SCAMP profiles are indicated by filled diamonds.

hence higher internal shear (*Fig. 4.15 & Fig. 4.16*). Mean water column dissipation rates were around 1×10^{-7} m^2 s^{-3}, this value being similar to the offshore sites sampled during 1998. Vertical diffusivities as estimated using (Eq. 2.1) were high. Mean water column values ranged from 10^{-3} - 10^{-1} m^2 s^{-1} with the average diffusivity over the sampling period ranging from 2×10^{-2} m^2 s^{-1} on 27th November to 4×10^{-3} m^2 s^{-1} on 2nd December 2000. Maximal K_T within the upper water column was associated with the passage of the 'warm phase' of the internal tide/bore, while K_T was higher in the bottom layer during the period when cooler water ran-up the slope. Within the regions of maximal thermal gradients (as signified by the 16 – 16.5°C isotherms in *Fig. 4.16*), K_T was frequently lower. In general the patterns of variability of K_T closely matched variations in R_i, with higher K_T associated with lower R_i (<0.25) as expected (*Fig. 4.16*). The decrease in diffusivity from 27th November to 2nd December was associated with a reduction in the energetics of the internal motions.

Mixing and nutrient flux

Nitrate concentrations measured on discrete samples collected using the CTD rosette typically increased with depth and were highly correlated with temperature (*Fig. 4.17*).

Nitrate concentrations decreased from over 7 mmol m^{-3} in the coldest water to approaching zero in the warmest near surface waters. Due to the strong temperature nitrate relationship, the vertical nitrate gradient ($\partial N/\partial z$) could be estimated from the vertical temperature gradient ($\partial T/\partial z$) using:

$$\frac{\partial N}{\partial z} = \frac{\partial N}{\partial T}\frac{\partial T}{\partial z} \tag{4.6}$$

where $\partial N/\partial T$ is taken to be a constant (= 3.348 mmol N m^{-3} $°C^{-1}$) from the slope of the regression (*Fig. 4.17*).

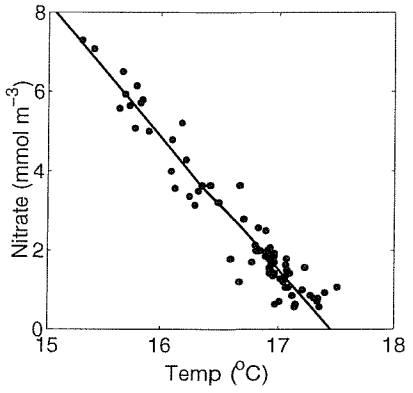

Fig. 4.17 Nitrate temperature relationship for 2000 cruise. The line is a model II linear fit, Nitrate = 58.429 – 3.348 Temp, $R^2 = 0.930$, n = 75, $p < 0.001$

A time series of vertical nitrate distribution and vertically driven nitrate flux using the values of diffusivity estimated from the SCAMP profiles (Eq. 2.6), could therefore be calculated. The nitrate distribution was obviously highly dependent on the phase of the internal motions (*Fig. 4.18a*). Estimated vertical nitrate gradients ranged from 0.001 mmol N m^{-4} within the nearly isothermal regions associated with the passage of the internal bore 'warm phase', to greater than 0.3 mmol N m^{-4} in the regions of maximal thermal gradients (*Fig. 4.18c*). Estimated vertical nitrate fluxes were highly variable and patchy. Some variability associated with the passage of the internal motions was evident. Values of estimated fluxes ranged from 0.01 mmol N m^{-2} hr^{-1} to around 10 mmol m^{-2} hr^{-1} in regions where relatively high nitrate gradients coincided with patches of enhanced mixing (*Fig. 4.18d*).

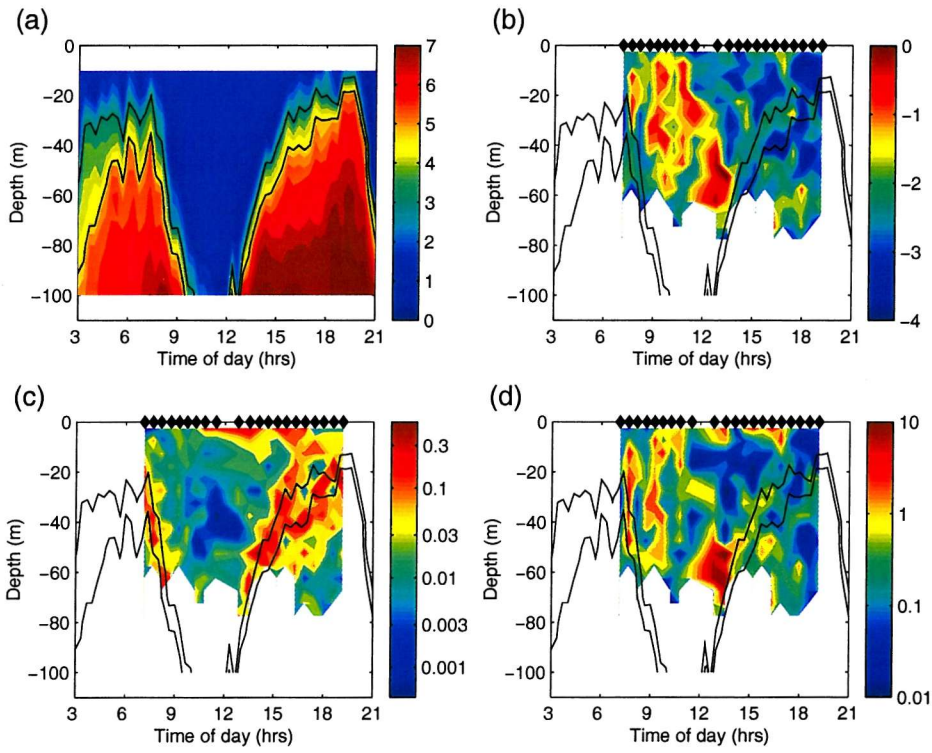

Fig. 4.18 Example time series of calculated nitrate distributions and fluxes, from 27th November 2000 at the site of the IW1/00 mooring. (a) Time series of nitrate concentration (mmol N m^{-3}) calculated from thermistor time series of temperature and the temperature nitrate relation (*Fig. 4.17*). (b) Vertical heat diffusivity ($\log_{10}(K_T\ (m^2\ s^{-1}))$), from SCAMP profiles (see *Fig. 4.16*). (c) Vertical nitrate gradient (mmol N m^{-4}) estimated using (Eq. 4.6) and SCAMP based measurements of $\partial T/\partial z$. (d) Vertical nitrate flux (mmol N m^{-2} hr^{-1}) estimated using (Eq. 2.6) i.e. the product of the nitrate gradient and the diffusivity. Diamonds in (a-c) indicate times of individual SCAMP profiles. The depths of the 16 and 16.5°C isotherms are shown in black on each plot.

The mean daily vertical nitrate fluxes calculated for the four days ranged from 22 mmol N m^{-2} d^{-1} (16 – 32 mmol N m^{-2} d^{-1}, 95% CI) for 27th November to 7 mmol N m^{-2} d^{-1} (4 – 10 mmol N m^{-2} d^{-1}, 95% CI) on 2nd December 2000. SCAMP profiles typically did not sample to the bottom of the water column (*Figs. 4.16 & 4.18*). High shear between currents and the sea-bed was likely to have resulted in the highest mixing occurring within the bottom boundary layer. Additionally, due to the internal bore dynamics, the regions of high nitrate and temperature gradient were likely to have intersected the bottom boundary at certain times (*Fig. 4.18*). The daily nitrate fluxes may therefore have been underestimated. A general decrease in the vertical nitrate flux occurred from the first to the last day of microstructure measurements, in keeping with the decreasing magnitude of the internal motions observed.

4.3.3 Phytoplankton distribution

Chlorophyll distribution and variation

Values of fluorescence from the CTD fluorometer and values of F_M (F_M') from the FRRF instrument were well correlated with the values of chlorophyll measured on discrete samples ($R^2 > 0.7$ see *Appendix 7*). The relationship between chlorophyll concentration and *in situ* fluorescence could be further improved by using an empirical expression to account for fluorescence quenching in the near surface (e.g. Strass, 1990). The value of transmittance measured by the CTD package was inversely related to chlorophyll concentration throughout the study ($R^2 = 0.841$, $n = 56$, $p < 0.001$, see *Appendix 7*).

Discrete samples and both fluorescence and transmissometer data collected during the initial spatial survey on 25th November indicated decreasing concentrations of chlorophyll away from the coast (*Fig.4.19*). Surface chlorophyll concentrations measured on discrete samples decreased from 3.7 mg m^{-3} at station B to around 0.6 mg m^{-3} in the vicinity of the Poor Knights islands and <0.1 mg m^{-3} at station C. Along shelf gradients in chlorophyll as indicated by transmittance were relatively weak (*Fig. 4.19g*).

The combined data from discrete samples and the time series of transmittance and fluorescence collected at the fixed station (PK), indicated that chlorophyll concentrations increased from surface values of around 0.6 mg m^{-3} on 25th November 2000 to >2 mg m^{-3} on 2nd December 2000 (*Fig. 4.20*).

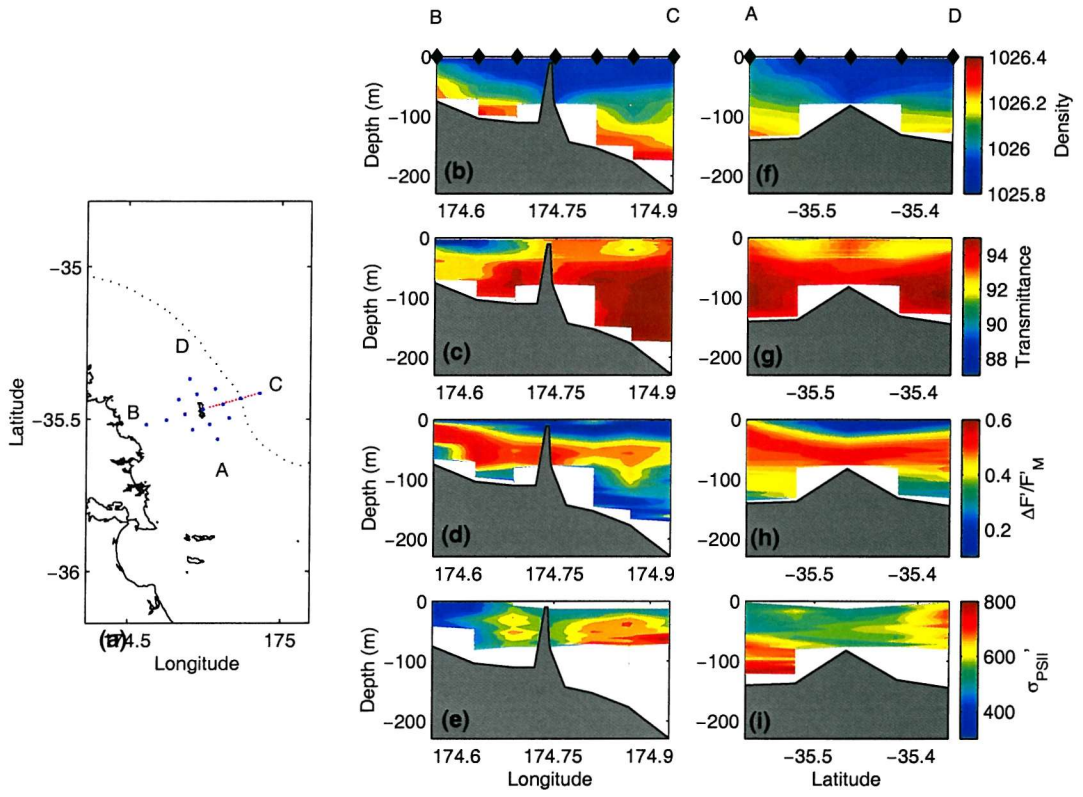

Fig. 4.19 Data from initial survey on 25th November 2000. (*a*) Positions of CTD stations occupied on 25th November 2000 (blue) superimposed on map of study region. Dotted line indicates position of 200m Isobath. CTD stations occupied during final survey (PK – C) on 3rd December 2000 are also indicated (red). Contoured sections of data from lines (B – C) and (A – D) are presented in (b – e) and (f – i) respectively.

(b & f) Density (kg m^{-3});

(c & g) Transmittance (a.u.);

(d & h) $\Delta F'/F_M'$;

(e & i) σ_{PSII}' ($Å^2$ $quanta^{-1}$).

Black diamonds indicate positions of CTD stations in (b & f).

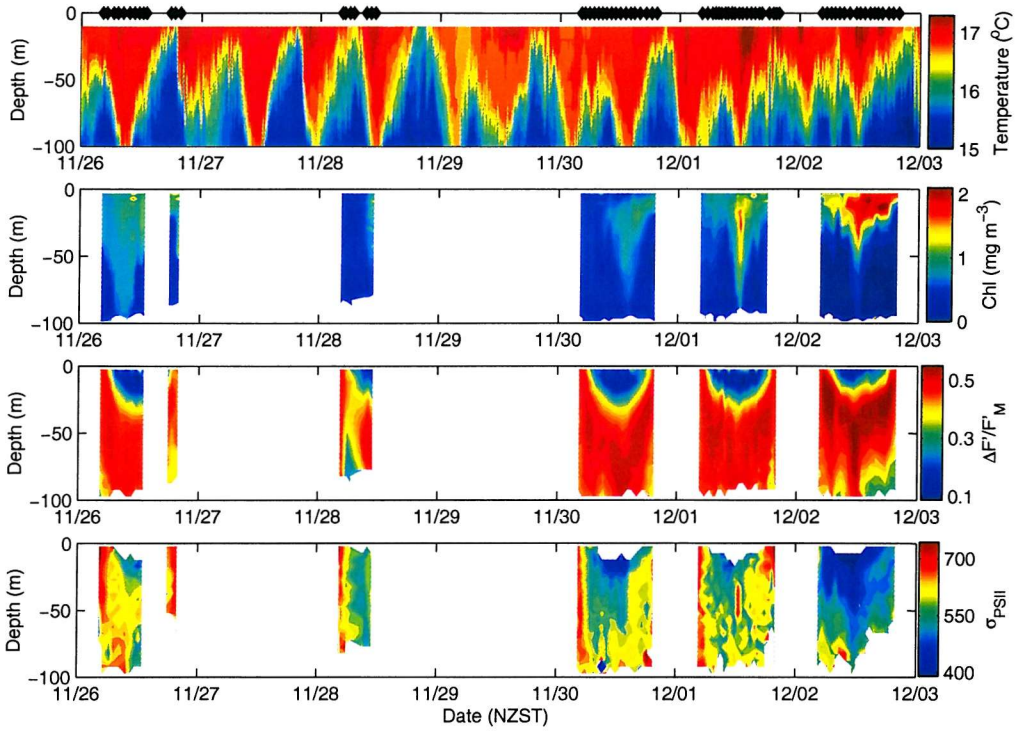

Fig. 4.20 Time series of phytoplankton distribution and physiology during on station sampling at PK from 26th November – 3rd December 2000. (a) Temperature (°C) time series from IW1/00 mooring showing presence of internal waves (bores), times of individual vertical (Yo-Yo) profiles with CTD/FRRF package are indicated by filled diamonds. (b) Time series of chlorophyll concentration (mg m^{-3}) as inferred from transmittance calibrated against discrete chlorophyll samples (*Appendix 7*). (c) Time series of $\Delta F'/F_m'$ from FRRF. (d) Time series of σ_{PSII}' ($Å^2$ $quanta^{-1}$) as measured by FRRF.

Satellite data suggested that the high chlorophyll concentrations observed near the coast during the initial survey and the high concentrations at PK on 2nd and 3rd December 2000 were the result of a coastal bloom (*Fig. 4.21*). Size fractionated chlorophyll measurements performed on samples collected at PK indicated that the increase in chlorophyll on 2nd December 2000 was associated with a shift of community composition. The smaller (0.2 – 2 μm) size fraction accounted for 55-60% of the population up until 1st December 2000, whereas the largest (>20 μm) fraction accounted for >60% of the population on 2nd December 2000.

The high chlorophyll waters of the coastal bloom had lower temperatures and salinities than offshore surface waters. For example, during the initial survey on 26th November, the surface water at the inshore station (B) was characterised by a salinity of around 35.32. This corresponded to the salinity at a depth of around 150 m at station C, suggesting that

the bloom was associated with upwelling near the coast, the water originating from mid-depths offshore.

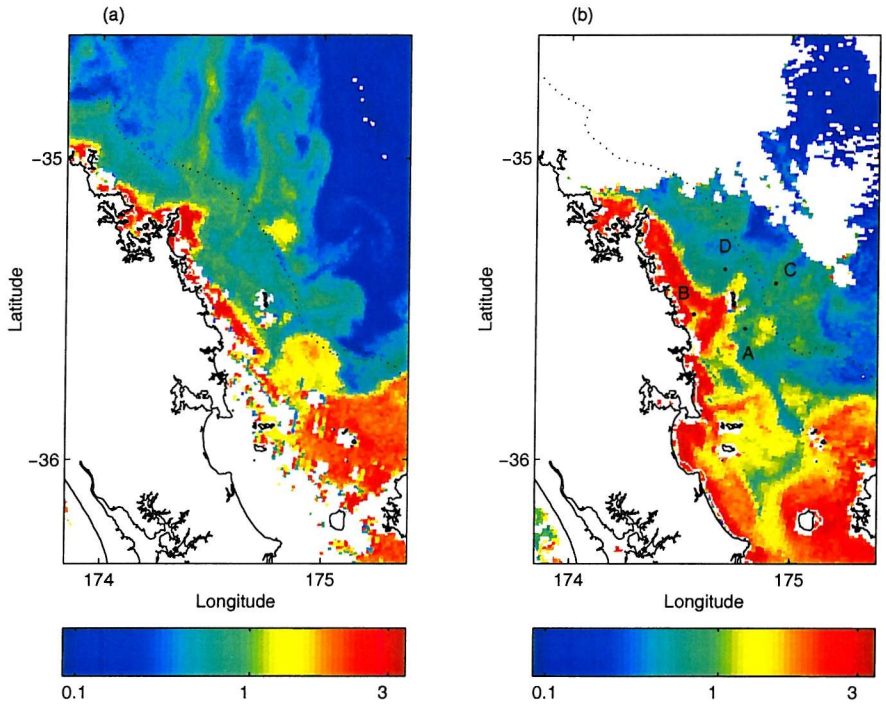

Fig. 4.21 Sea surface chlorophyll concentration (mg m^{-3}) derived from SeaWifs observations of ocean colour for North Eastern New Zealand continental shelf on (a) 26th November 2000 and (b) 3rd December 2000. Dotted line indicates position of 200m depth contour. Positions of CTD stations A-D occupied during initial survey are indicated in (b). Anchor station PK is adjacent to the Poor Knights Islands located at centre of initial survey. The coastal bloom, as indicated by enhanced chlorophyll concentrations (> 1.5 mg m^{-3}), covered a greater proportion of the shelf on 3rd December. Eddy activity is also evident both on and off shelf.

The vertical distribution of chlorophyll at PK was closely associated with the vertical and horizontal water motions associated with the internal tide (*Fig. 4.20*). Concentrations of chlorophyll were low (<0.1 mg m^{-3}) at depth during the cool phase of the internal tide and increased in the warmer (surface) waters. Overall, chlorophyll concentrations increased with temperature (*Fig 4.22*). A linear relationship was evident throughout the entire period for temperatures below 16.8°C. Above 16.8°C a marked increase on 2nd December again indicated the arrival of the bloom containing water mass.

Due to the association of higher chlorophyll with the warmer (less dense) surface waters at PK, the time series of the chlorophyll concentrations for individual days typically showed peaks within the warm 'trough' of the internal tide (*Fig. 4.20*).

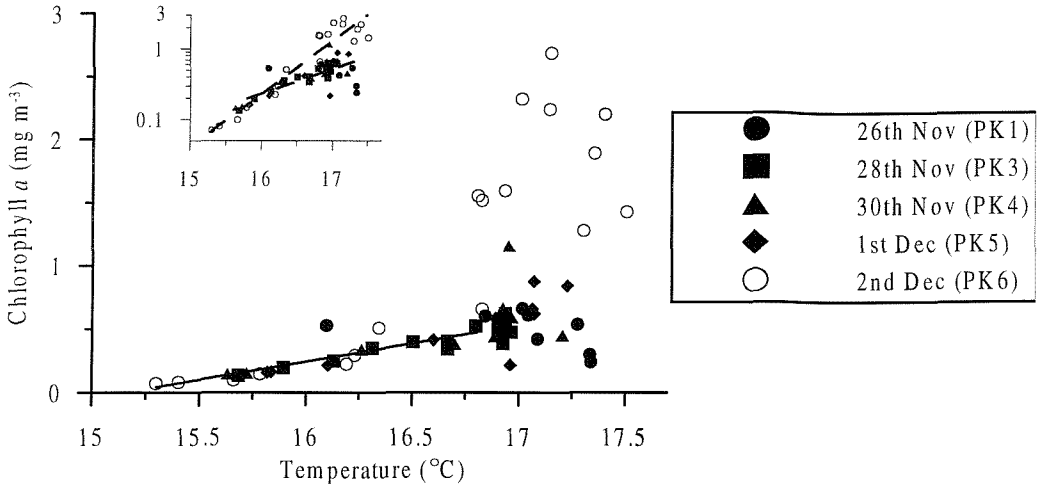

Fig. 4.22 Chlorophyll temperature relationship during anchored occupation of the PK site adjacent to Poor Knights Islands. (Main) *In situ* temperature versus chlorophyll *a* as determined on discrete samples for five days of CTD profiling. Solid line is linear fit of chlorophyll vs. temperature for all days for temperatures ≤ 16.8°C (R^2 = 0.728, n = 24). (Inset) Data as in main with $\log_{10}$ axis for chlorophyll. Dotted lines are fits for all data before 2nd Dec (R^2 = 0.551, n = 46) and on 2nd Dec (R^2 = 0.907, n = 18).

4.3.4 Physiological variability

Spatial variability

The *in situ* data collected during the initial survey on 25th November 2000 (see *Table 4.1*) indicated low functional absorption cross-sections (σ_{PSII}') around 400 Å^2 quanta^{-1} within the coastal bloom. Values of σ_{PSII}' increased off-shore and were maximal (>700 Å^2 quanta^{-1}) at depth towards the shelf edge (*Fig. 4.19e*). A local minimum in σ_{PSII}' was apparent in the vicinity of the Poor Knights Islands. Values of $\Delta F'/F_M'$ taken from the *in situ* FRRF profiles generally decreased off-shore. Low $\Delta F'/F_M'$ in the near surface waters probably resulted from both photochemical and non-photochemical quenching (*Fig. 4.19d*).

The cross-shelf distribution of physiological properties on 25th November 2000 was also investigated using a series of discrete samples. These samples were collected from various depths and held in dark bottles within a water bath cooled to sea-surface temperature for >15minutes before being analysed (e.g. Kolber et al. 1990). Dark acclimated values of the functional absorption cross-section (σ_{PSII}) again displayed a general off-shore increase and small minimum around the islands, confirming the distribution observed in the *in situ* data (*Fig. 4.23*). A strong negative correlation was observed between salinity and σ_{PSII} for the

complete set of discrete samples ($R^2 = 0.792$, n=14, $p < 0.001$). This correlation was dominated by the cross shelf gradients in both salinity and σ_{PSII}.

The photochemical efficiency (F_v/F_m) could also be measured on the dark-acclimated samples and indicated a small off-shore decrease from values of 0.47 within the coastal bloom to <0.35 at the shelf edge. As a result of quenching processes, differences between F_v/F_m measured on discrete samples and $\Delta F'/F_M'$ measured *in situ* were a function of the irradiance at the time of sampling (*Fig. 4.23*). Values of σ_{PSII}' measured *in situ* were also lower than σ_{PSII} measured on discrete samples (*Fig. 4.23*). This was also likely to have been due to quenching, the magnitude of the difference again being related to irradiance.

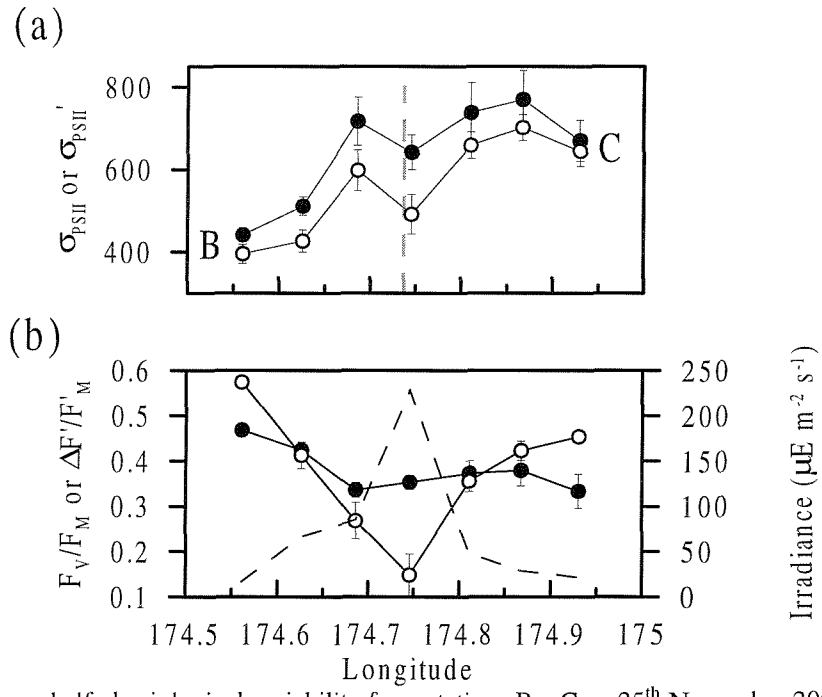

Fig. 4.23 Cross shelf physiological variability from stations B – C on 25th November 2000. (a) Functional absorption cross-section measured on discrete dark acclimated samples (σ_{PSII}, filled symbols) and measured *in situ* at sampling depth (σ_{PSII}', open symbols). Error bars indicate ± 1 s.d. of 16 analyses for discrete samples or for *in situ* data ± 1 s.d. of the 5m depth bin containing the sample depth. Grey dotted line indicates position of Poor Knights Islands. (b) F_v/F_m measured on dark acclimated samples (filled symbols), $\Delta F'/F_M'$ measured *in situ* (open symbols) and irradiance at sampling depth (dotted line). Error bars as in (a). Differences between $\Delta F'/F_M'$ and F_v/F_m and σ_{PSII} and σ_{PSII}' were both correlated with (log) irradiance, $R^2 = 0.962$ & 0.912 respectively. A number of samples were collected from a variety of depths at each station, the data displayed comprise a representative subset collected from depths between 15 and 50m.

Along shelf variability on 25th November in both $\Delta F'/F_M'$ and σ_{PSII}' was relatively low although a decrease in $\Delta F'/F_M'$ and an increase in σ_{PSII}' was apparent at the most northern

station D (*Fig. 4.19h & i*). Lower values of σ_{PSII}' and higher values of $\Delta F'/F_M'$ tended to be associated with regions where denser water approached the surface.

Strong cross shelf horizontal gradients in σ_{PSII}' were also apparent during the second CTD survey consisting of two transects performed on 3rd December 2000 (see *Table 4.1*). By this stage the bloom of large cells dominated in the region of the Islands. Low values of σ_{PSII}' around 450 $Å^2$ $quanta^{-1}$ were observed around the islands, increasing to >750 $Å^2$ $quanta^{-1}$ towards the shelf edge during the second transect (*Fig. 4.24*). Lower values of $\Delta F'/F_M'$ were also observed at the furthest off-shore station, with the near surface distribution of $\Delta F'/F_M'$ again being controlled by the irradiance field (*Fig. 4.24*).

The temporal variability in temperature, salinity and density was marked between the two transects (*Fig. 4.24*). During the second transect, surface values of temperature and salinity around 5-15 km offshore of the islands had increased by 0.5°C and 0.04 to > 18°C and >35.62 respectively. The higher values of σ_{PSII}' were again associated with the higher salinity water (*Fig. 4.24*). As an example, for mid-depths (35-55 m), i.e. away from the effects of surface quenching on σ_{PSII}' and the low chlorophyll bottom water, salinity and σ_{PSII}' were highly correlated ($R^2 = 0.764$, n = 165, $p<0.001$).

Considerable problems are associated with the interpretation of these transects of hydrographic properties in regions dominated by large internal motions, as the observation point moves on time-scales comparable to those of the physical variability. Each transect took around 5hrs from PK to C and individual stations were sampled around 7hrs apart. CTD stations are therefore representative of the two opposite phases of the internal tide, however considerable aliasing of the broad structure of the internal motions is likely in the contoured transects.

Although the possibility of along shelf advection and movement of the coastal (upwelled) water mass cannot be discounted, the large difference in water properties between the first and second transect could be interpreted as the shoreward propagation of a front (*Fig. 4.24*). Assuming that the frontal propagation direction was along the transect line (i.e. perpendicular to the shelf) and taking into account the timings of the CTD stations, a frontal propagation speed of 40cm s^{-1} was calculated.

A striking high frequency internal wave feature was also observed during the second transect on 3rd December at 174.7984°E (*Fig. 4.24e-h*). The internal wave was associated

with the shoreward edge of the sharp front observed during the second transect. The large depression of the thermocline was associated with a region of low $\Delta F'/F_M'$ at intermediate depths and was also in the region of the strongest horizontal gradients in σ_{PSII}'.

Temporal variability at anchor station

The photochemical efficiency as indicated by F_v/F_m for the five days of CTD sampling at PK was inferred from the initial pre-dawn profile, when both photochemical and non-photochemical quenching were likely to have been minimal. Values of F_v/F_m were around 0.47 above 10m depth on all days with low vertical variability except for a decrease in the low chlorophyll 'deep' waters (*Fig. 4.20*).

The dark acclimated functional absorption cross-section (σ_{PSII}) was also taken from the initial pre-dawn cast at PK. Values of σ_{PSII} were approximately uniform with depth on most days, although a 20-30% linear decrease from the surface to bottom was observed on 26th and 28th November (*Fig. 4.20*). A decreasing trend in σ_{PSII} for both surface and deeper regions was observed. Surface pre-dawn values of σ_{PSII} decreased from 740 ($\pm$ 40) to 580 ($\pm$ 30) Å^2 quanta^{-1} from 26th November to 2nd December 2000. The largest changes coincided with the arrival of the large cell dominated bloom at the sampling site (*Fig. 4.20*).

Diel physiological variability

Strong diel signals in $\Delta F'/F_M'$ and σ_{PSII}' were observed on all CTD sampling days (*Figs. 4.20 & 4.25*). Both $\Delta F'/F_M'$ and σ_{PSII}' decreased to minimum values at midday irradiances. Reductions in near surface values of $\Delta F'/F_M'$ were around 70-80%, while reductions of σ_{PSII}' reached around 35%. Negative correlations between irradiance and both $\Delta F'/F_M'$ and σ_{PSII}' were found on all days. Diel variability in the value of F_M was also observed in the near surface (*Fig. 4.25c*).

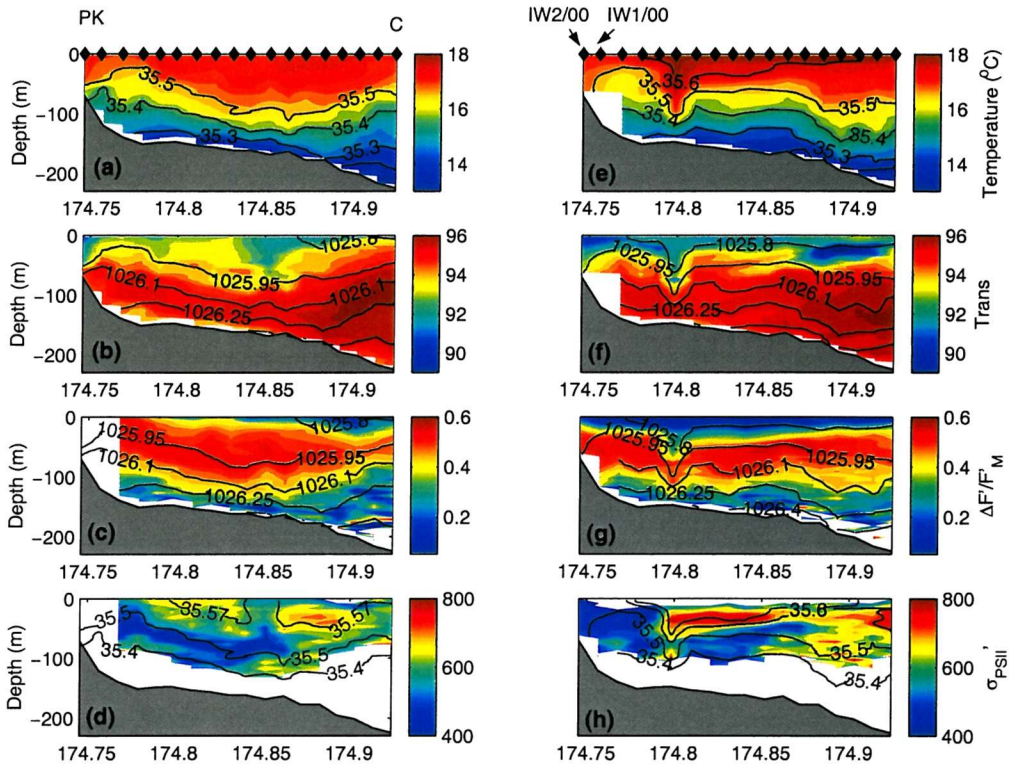

Fig. 4.24 Data from cross shelf survey (from PK – C) on 3rd December 2000. Data were collected during two transects from 0430 – 0942 (a-d) and 1157 – 1628 (e-h). Individual stations were thus occupied twice around 7hrs apart. Colours are contoured: (a & e) Temperature (°C), (b & f) Transmittance, (c & g) $\Delta F'/F_M'$, (d & h) σ_{PSII}' ($Å^2$ $quanta^{-1}$). Black contours are Salinity in (a, d, e & h) and density (kg m^{-3}) in (b, c, f and g). Diamonds indicate positions of CTD/FRRF casts in (a & e). Positions of the IW1/00 and IW2/00 moorings are indicated in (e).

The influence of the internal motions was also apparent in the physiological time series data. Patterns of $\Delta F'/F_M'$ variability were typically symmetric about midday and highly correlated with the instantaneous irradiance (*Figs. 4.20c & 4.25d & e*). Conversely σ_{PSII}' displayed variability associated with the horizontal and vertical movements caused by the internal tide (*Fig. 4.20d & 4.25f*). Such variability could have partially resulted from the time-scale for photo-responsive change in σ_{PSII}' being slower than the time-scale for the vertical motions. Horizontal advection of the significant horizontal gradients in σ_{PSII}', by the high currents associated with certain stages of the internal bore, was also likely to have been important.

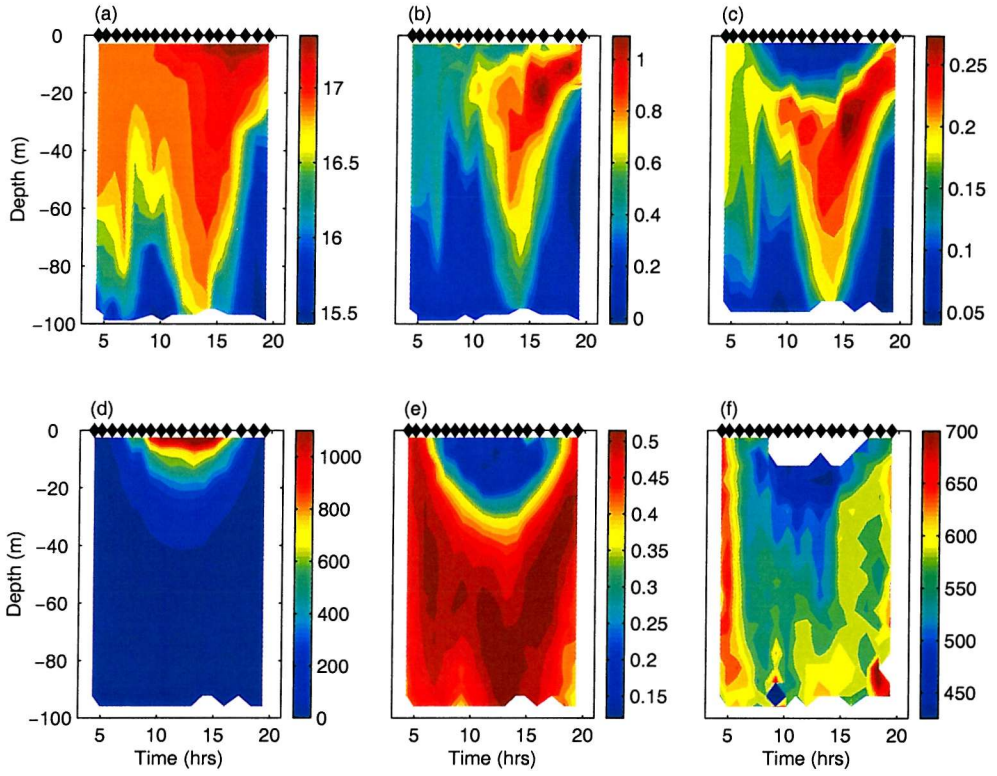

Fig. 4.25 Detailed time series of observations for 30th November 2000. (a) Temperature (°C) showing passage of large internal motions. (b) Chlorophyll (mg m^{-3}) as indicated by calibrated transmissometer readings. (c) F_M (a.u.) from FRRF, near surface quenching of F_M is evident. (d) PAR (μmol quanta m^{-2} s^{-2}). (e) $\Delta F'/F_M'$ as measured from *in situ* FRRF. (f) σ_{PSII}' ($Å^2$ $quanta^{-1}$) measured by FRRF. Diamonds on top of plots show mean times of individual Yo-Yo profiles.

Time-scales of photo-acclimation

In order to investigate the time-scales over which both F_v/F_m and σ_{PSII} acclimate to changes in irradiance, a series of light manipulation experiments were performed. Samples were collected from a variety of depths whilst at the PK anchor station (see Chapter 2 §2.2.1). Time series of changes in F_v'/F_m' and σ_{PSII}' in response to step shifts in irradiance were fitted to a simple first order rate model (e.g. Falkowski, 1983; Lewis *et al.* 1984a; Cullen and Lewis, 1988; Claustre *et al.* 1994):

$$\Gamma(t) = \Gamma(\infty) + (\Gamma(0) - \Gamma(\infty))e^{-\gamma t} \tag{4.7}$$

where $\Gamma(t)$ represents the value of the physiological parameter (i.e. F_v'/F_m' or σ_{PSII}') at time t, $\Gamma(0)$ and $\Gamma(\infty)$ represent the initial and fully acclimated value of the parameter and γ is the rate constant (*Fig. 4.26*).

Half times for acclimation ($\tau_{a1/2} = 0.693/\gamma$) for all the irradiance shifts where a clear trend was observed were highly variable for both σ_{PSII}' and F_v'/F_m' ranging from 2 minutes to > 80 minutes. Mean values of $\tau_{a1/2}$ excluding extreme values (outside 2 s.d.) were 20 ± 16 and 21 ± 19 minutes for F_v'/F_m' and σ_{PSII}' respectively. A value for $\tau_{a1/2}$ of around 20 minutes was therefore representative of the majority of shifts for both parameters.

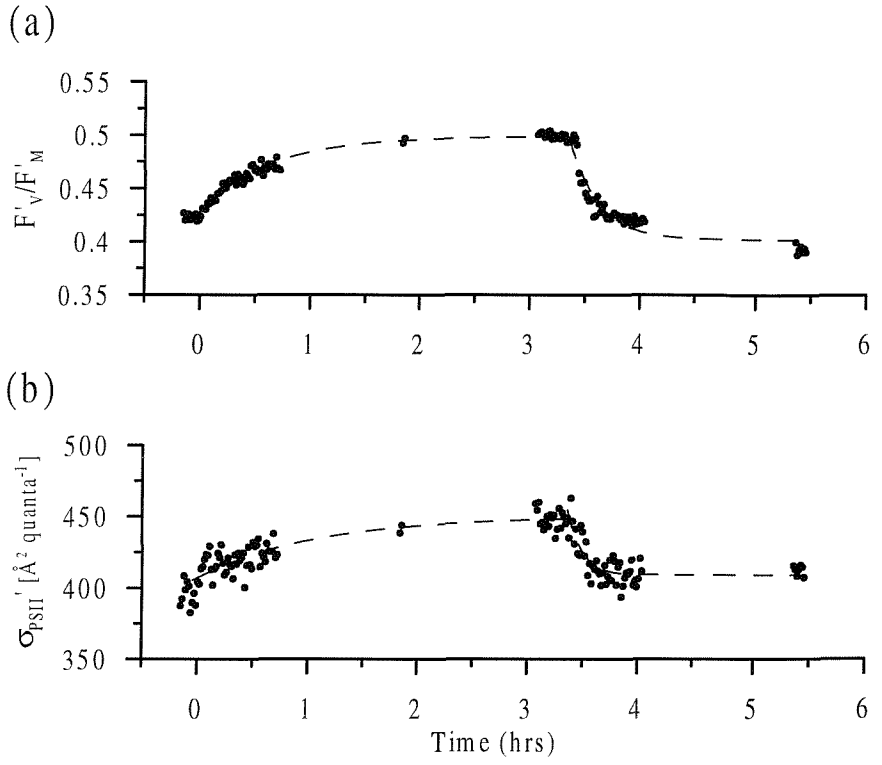

Fig. 4.26 Example of results of irradiance shift experiments performed on a sample collected from a depth of 5m on 2nd December 2000 at PK. (a) Time series of values of F_v'/F_m' following a shift from high (~500 μE $m^{-2}s^{-1}$) to low (~60 μE $m^{-2}s^{-1}$) then back to high irradiance. (b) Time series of σ_{PSII}' following same shifts. Time is in hours after first light change, second light shift performed at 3.4 hrs. Each point is the mean of 10 consecutive individual FRRF measurements. Dotted lines indicate fits to (Eq. 4.7), for (a), $\tau_{a1/2} = 27$ ($R^2 = 0.97$) and 11 ($R^2 = 0.89$) minutes for first and second shifts respectively, for (b), $\tau_{a1/2} = 45$ ($R^2 = 0.78$) and 6 ($R^2 = 0.66$) minutes

4.4 Discussion

Physical setting and nature of internal motions

A detailed physical description of the generation and propagation mechanisms for internal motions in shelf seas is beyond the scope of the present work, hence only a brief summary of the observed motions now follows. For a more detailed physical description see Sharples *et al.* 2001b and Stevens *et al.* (*In prep*).

Large amplitude internal motions with dominant tidal frequencies were observed on the Northeast New Zealand shelf at a variety of locations. These internal motions were related to the internal tide generated at the shelf edge by the interaction of the barotropic tide with steep bathymetery. The subsequent propagation of these internal motions on-shelf and the evolution of the wave form was complex and varied between the open shelf region (1998 cruise) and in the vicinity of an island group at the shelf edge (2000 cruise).

Within the open shelf region the internal tide propagated on-shelf as a large amplitude depression of the thermocline (*Fig.4.4)*. The internal tidal energy decreased during on shelf propagation (*Fig 4.8*) and non-linear solitons were generated as the internal tide disintegrated, presumably by dispersive processes (Lamb, 1994; Stanton and Ostrovsky, 1998). Enhanced shear generated within the water column, possibly as a result of interactions between the higher frequency non-linear waves and the internal tide, resulted in enhanced mixing, as evidenced by sub-critical Richardson numbers and microstructure observations (*Fig. 4.6)*. Estimates of mixing from microstructure observations were consistent with the observed loss of internal energy during on shelf propagation (*Fig. 4.9*).

In the vicinity of the Poor Knights Islands the internal tide was best described as a bore like structure propagating up slope (*Figs. 4.13, 4.20 & 4.24*). A marked front was usually observed at the leading edge of the bore, often associated with a packet of high frequency (~ 20 – 30 min period), large amplitude (>30m) solitons. Detailed examination of the time series of temperature from the two moorings close to the islands indicated that the form of the internal bore was, to a large extent, unaffected by the presence of the islands.

Estimated bore propagation speeds (phase speeds) between the two moorings were around 20 cm s^{-1}. In contrast the estimated frontal propagation speed from the final CTD survey was around 40 cm s^{-1}. The former value is consistent with the magnitude of the maximum currents observed at the moorings and estimated internal tidal bore phase speeds from other studies (Pineda, 1994,1999). It may be possible to reconcile these two estimates if it is assumed that the front/bore slows as it moves in to shallower water on the shelf. However along shelf advection and movement of the coastal water body may have been important.

Late November and early December represents the period when the sub-tropical waters of the EAuC, which are characterised by a salinity of > 35.5 – 35.6 and higher temperatures approaching 18°C, can penetrate onto the continental shelf (Sharples 1997). It is suggested that the Poor Knights study was performed during the period of subtropical water cross-shelf intrusion for the year 2000. Such a view is supported by the observed salinity which

was >35.55 in the region surrounding the Poor Knights on 25th November and >35.6 during final CTD transect on 3rd December. The time series of sea-surface temperatures, as observed using AVHRR satellite imagery, also provide information on the movements of the EAuC during the study period (*Fig. 4.27*).

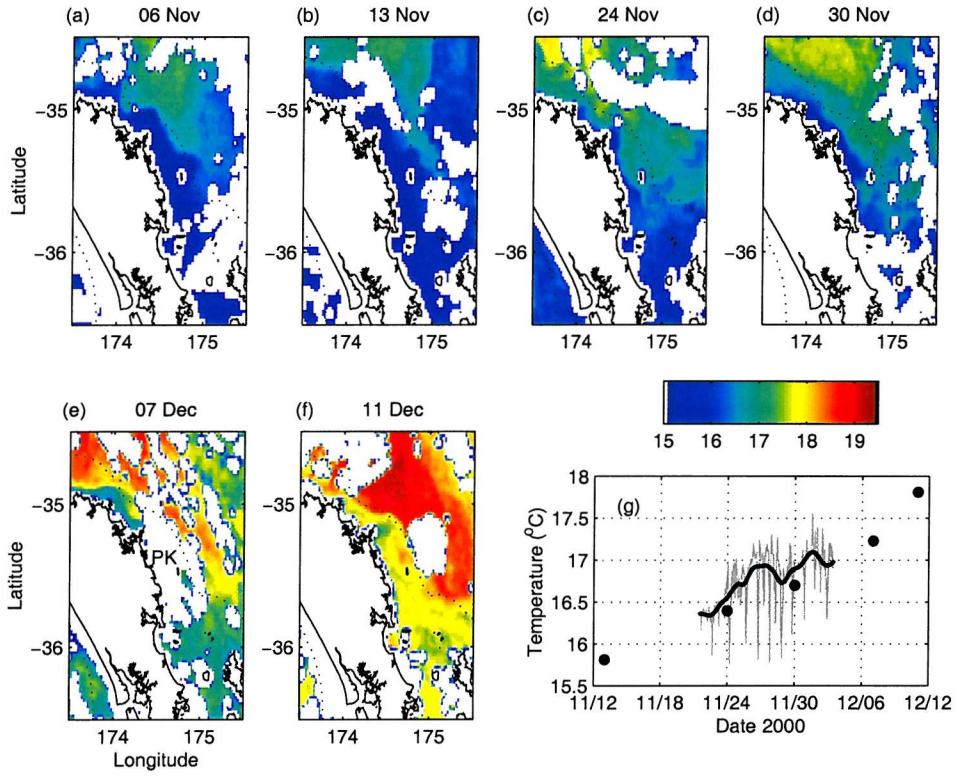

Fig. 4.27 AVHRR derived sea surface temperature around the period of the Poor Knights cruise 2000. Time series of AVHRR images on (a) 6th, (b) 13th, (c) 24th, and (d) 30th November and (e) 7th and (f) 11th December 2000. Dotted line indicates 200m isobath. (g) Time series of temperature in the vicinity of the Poor Knights Islands, grey line, raw temperature from 20m at IW1/00, black line, temperature at 20m filtered with a 48hr low pass window, solid circles, SST from AVHRR data.

Both AVHRR and *in situ* data indicated a general warming trend throughout the region with the highest temperatures to the North East of the study region. Much of the warming both on and off shelf may have resulted from direct surface heating. The effect of surface heating can be calculated using $\Delta\theta = Q\Delta t/\rho hc$, where ($Q$) is the heating rate, ρ is the sea water density, h is the depth of the sea water layer undergoing the change in temperature, c is the specific heat capacity of seawater and Δt is the time taken for a change of temperature $\Delta\theta$. The period of 28 days from the 13th November to 11th December 2000 would have been sufficient for a typical solar heating rate of around 300 W m^{-2} at the sea

surface (Sharples, 1997), to increase the upper water column temperature by 2 °C. Thus the increasing trend in sea surface temperature could be entirely accounted for by local heating. Along shelf advection and cross shelf movements of the subtropical water are superimposed on this warming trend.

The EAuC is apparent in the SST data as the region of higher temperatures towards the North East of the study area (*Fig. 4.27*). A front at the shelf edge was observed to separate the cooler shelf waters from the warmer subtropical water throughout much of the study period. Comparing images from the 13th, 24th and 30th November with the *in situ* record at IW1/00, it is suggested that an initial cross shelf intrusion occurred around the 23rd-24th November and passed the Poor Knights islands at the shelf edge (*Fig. 4.27c*). Cooler shelf water then arrived back in the region of the islands (*Figs. 4.27d & 4.21b*), causing a series of decreases in mean temperature at IW1/00. The cooler water was likely to have resulted from upwelling and was responsible for the arrival of the large cell dominated bloom population at PK around 2nd December. It is therefore proposed that subtropical water was a major influence during the initial period of on site occupation at PK (26th Nov – 1st Dec), while upwelled shelf water dominated in the region of PK on 2nd and 3rd December.

The general circulation pattern on the shelf was therefore complex. Additionally the precise nature of the interaction between the internal tide/bore and the inevitable changes in stratification brought about by the movement of different water masses on and off the shelf is not clear from the present study.

As in the open shelf location, high levels of interior water column shear and sub-critical Richardson numbers indicated dissipation of internal tidal energy as the internal bore moved past the islands. Considerable mid water column mixing observed using the microstructure profiler confirmed this view (*Fig. 4.16*). Lower stratification was observed in the region of the islands, this being consistent with enhanced localised mixing (*Fig. 4.19*)

Nutrient fluxes and consequences for phytoplankton

Nutrient concentrations both in the open shelf region and adjacent to the islands decreased towards the surface. Lowest observed concentrations were often still above the detection limit, indicating that complete utilisation of surface nutrients had not occurred. However, as samples were frozen and returned to lab, the possibility of contamination cannot be discounted.

The enhanced mixing generated by the internal tide was responsible for driving high vertical nitrate fluxes at all the sites studied. Quantification of the magnitude of the vertically driven nitrate flux was attempted using observations of the vertical nitrate gradient and the estimated diffusivity. Microstructure measurements from both cruises and, for the 1998 study, the loss of internal tidal energy during on-shelf propagation of the internal tide, were used to estimate diffusivities. Vertical fluxes of around 3.5 and 10 mmol N m^{-2} day^{-1} were calculated for an inner shelf (IW4/98) and outer shelf (IW2/98) station during the 1998 cruise and a mean flux of 12 mmol N m^{-2} day^{-1} for PK (IW1/00) during the 2000 cruise. These estimated fluxes were all of comparable magnitudes and suggested an increasing flux towards the shelf edge and in regions of steep bathymetry. The hypothesis of enhanced nutrient fluxes at the shelf edge, driven by the internal tide, is therefore supported by the data presented here (Pingree and Mardell, 1981; Pingree *et al.*, 1986; New and Pingree, 1990; Mazé and Tareau, 1990).

The presence of the warm EAuC is one possible reason why a region of cooler water caused as a result of internal mixing is not observed at the North East New Zealand shelf edge (*Fig. 4.27*). Additionally much of the narrow shelf is influenced by upwelling and internal mixing, thus limiting the potential for warmer surface temperatures to form inshore of the shelf break.

The high vertical nitrate fluxes were likely to have resulted in a regular supply of nutrients for phytoplankton growth. Nutrient limitation may therefore be of minor importance in controlling the maximal growth rates and biomass within the study region at this time of year. Circumstantial evidence for the lack of near surface nutrient limitation was provided by the vertical chlorophyll profiles. Chlorophyll concentrations often showed no decrease towards the surface. Where a sub-surface chlorophyll maximum did exist, surface chlorophyll concentrations were not reduced to the very low levels associated with undetectable nitrate concentrations in highly stratified regions of shelf seas (see Chapter 3 and also e.g. Holligan *et al.* 1984b; Sharples *et al.* 2001a).

The vertical nutrient flux will however exert an upper limit on the amount of new and export production which can occur throughout the summer months (Dugdale and Goering, 1967; Eppley and Peterson, 1979; Sharples *et al.* 2001b). The balance between nitrate supply and the estimated productivity of the region is further addressed in subsequent chapters.

Light variability

Vertical motions of the thermocline will transport phytoplankton cells through the vertical light gradient. The time scale of such changes in light will be dependent on the frequency of the internal motion. The larger scale internal tide caused changes in the % surface irradiance experienced by phytoplankton which spanned 2-3 orders of magnitude over time-scales of hours (*Fig. 4.11a*). The largest amplitude soliton packets caused changes in irradiance of the same magnitude over time-scales of 10 minutes.

Quantifying the degree to which such highly non-linear vertical motions affect the integrated daily irradiance of phytoplankton is complicated by the timing of such motions compared to the daily photo-period (Kamykowski, 1974) and the problem of defining the un-perturbed displacement depth. The assertion by Lande and Yentsch (1988) that any vertical perturbation about a mean depth will increase the daily integrated irradiance is in general only valid for linear perturbations of relatively small amplitude.

In order to illustrate these problems the following simple model based on a subset of the field observations is considered. The observed 24hr temperature field from the IW2/98 mooring on 3rd December 1998 was taken to represent an example of a location and period when internal tidal motions dominated and when vertical displacements of the thermocline could be estimated from temperature variability. The displacements of the thermocline inferred from the temperature time series were then used to estimate the mean daily irradiance which would be experienced by phytoplankton advected vertically by the internal motions.

Surface irradiance is modelled by a simple sinusoidal function, while decreasing irradiance with depth is calculated using a constant diffuse attenuation coefficient of 0.155 m^{-1}. Four model situations are considered where the timing of the daily photo-period is shifted in phase to the internal motions by 6hrs (*Fig. 4.28a*). The depth of the 18.2, 18, 17.8 and 17.6°C isotherms, chosen to span the euphotic zone, are calculated every 2 minutes via linear interpolation of the vertical temperature profile from the thermistors and RCM's on the IW2/98 mooring (*Fig. 4.28b*). The instantaneous irradiance that would be experienced by phytoplankton passively transported on each of these isotherms is then calculated for each time-step (*Fig. 4.28c*), and hence the mean daily irradiance calculated.

Resulting increases in daily irradiance for the four runs with different phase relationships between the internal motions and the photo-period are presented in (*Fig. 4.28d*). These models were compared with mean daily irradiances calculated assuming no vertical

motions. The mean depth for each of the 4 isotherms chosen was calculated from the 24hr time series. Three calculations were then performed. Firstly it was assumed that, in the absence of vertical motions, the temperature structure would conform to the mean temperature. Secondly, it was assumed that the mean temperature structure would be offset by 7m negatively and thirdly by 7m positively. These depth offsets were chosen arbitrarily in order to illustrate the sensitivity of the daily irradiance to the mean (un-disturbed) depth.

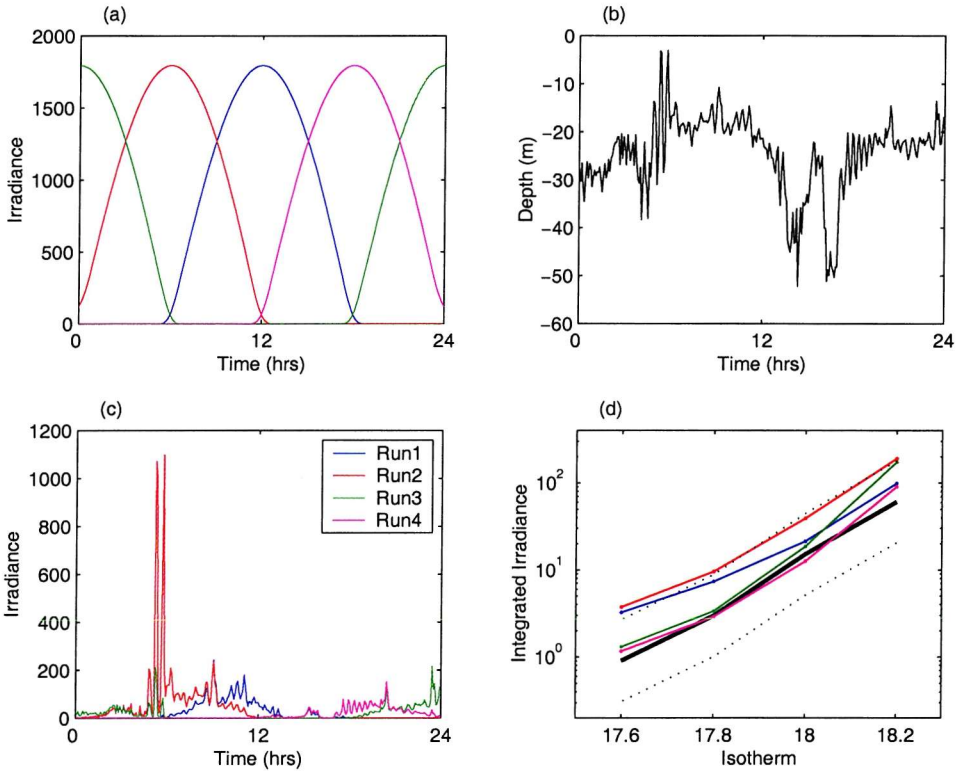

Fig. 4.28 Results from simple model for quantifying increase in irradiance due to internal motions. (a) Surface irradiance field used for the four model runs. Photo-period is phase shifted by 6hrs for each run. (b) Depth of the 18°C isotherm as calculated using the temperature data from the IW2/98 mooring for the 3rd December 1998. The upper 10m of the water column was assumed to be isothermal and the vertical temperature profiles were smoothed with a 20m window before calculating the isotherm depth via linear interpolation. A high frequency soliton packet around mid morning (0600 hrs) is superimposed on the general internal tidal motion. (c) Modelled irradiance experienced by the 18°C Isotherm for the four model runs. (d) Mean daily irradiance experienced by the 17.6, 17.8, 18 and 18.2°C Isotherms for the four model runs. Results are compared to calculations assuming no vertical motions. The three considered cases are (thick black line) mean depth of isotherms taken from temperature data and (dotted black lines) mean depth ± 7m.

Estimated increases in daily irradiance varied depending on the phase relationship between the internal tide and the photo-period. Maximal increases occurred when the high frequency soliton packet arrived at the time of maximal (noon) surface irradiance (*Fig. 4.28*). At any one location the phase relationship between the internal tide and the photo-period can be expected to cycle over a 15 day period due to the 12.42 hr internal tidal period and 24hr photo-period. The potential productivity at a fixed point may therefore also vary over such time-scales (Kamykowski, 1974).

Maximal increases in mean daily irradiance were around 3 times the value calculated assuming the mean isotherm depth would have been representative of the un-disturbed temperature field. This value was comparable to the results of Lande and Yentsch (1988). The sensitivity of the mean daily irradiance to internal motions was of similar magnitude to vertical movements of the undisturbed mean temperature field on the order of 7m.

High frequency internal solitons are often non-linear and hence do not oscillate about a mean depth, rather they propagate as a series of depressions of the thermocline (e.g. Stanton and Ostrosvsky, 1998). The lower frequency internal tide observed at many of the sites also had an amplitude which was comparable to the mean water depth and could therefore not be considered linear, this being particularly apparent adjacent to the Poor Knights Islands during the 2000 study (*Fig. 4.13*). Additionally the internal tides and associated non-linear waves can cause mixing and hence alteration of the stratification of the water column (Sherwin, 1988). It is therefore difficult to define a zero displacement depth by removing the internal signals from the *in situ* observations. Quantifying the potential increase (or decrease) in mean irradiance experienced is thus also complex. A final complication arises within the upper layers of the water column where the internal tide and wind driven surface mixed layer interact to govern the light available for phytoplankton.

Generally however some of the internal waves observed in the present study had the capacity to increase the mean daily irradiance experienced by phytoplankton and hence deepen the compensation depth (Lande and Yentsch, 1988). Phytoplankton populations living at depth and hence at higher ambient nutrient concentrations may therefore have been capable of substantially increased growth as a result of the internal motions (*Fig. 4.11*).

Physiological variability

Phytoplankton populations encountered during the occupation of the PK site were characterised by intermediate photochemical efficiencies (F_v/F_m) around 0.47 (*Fig. 4.20*). A decreasing offshore gradient in F_v/F_m ($\Delta F'/F_M'$) was apparent in both the spatial surveys (*Figs. 4.19 & 4.24*). For example values of F_v/F_m measured on discrete samples decreased from 0.47 ± 0.013 to 0.33 ± 0.038 from stations B – C on 25th November 2000 (*Fig. 4.23*). Unfortunately nitrate concentrations were not measured on samples for which the *in situ* ambient temperature was > 17.6°C and only on two samples collected at temperatures >17.4°C. The regression equation between nitrate and temperature suggested that nitrate would be depleted for temperatures above 17.45°C (*Fig. 4.17*). Thus the warmest offshore surface waters may have been low in surface nitrate, which would be consistent with lower F_v/F_m under conditions of nutrient stress.

The functional absorption cross section (σ_{PSII}) varied significantly between the high chlorophyll, large cell dominated bloom (sampled towards the coast during the first survey and at PK on 2nd December 1998) and the off-shore phytoplankton populations (*Fig. 4.23*). Values of σ_{PSII}' increased off-shore during both CTD surveys. The strong correlations observed between salinity and σ_{PSII} indicated that the off-shore (sub-tropical) water was dominated by a population with high absorption cross sections while the low salinity (upwelled) shelf water was dominated by cells with low absorption cross sections (*Figs. 4.19, 4.23 & 4.24*). This relationship between higher salinity water and σ_{PSII} was striking. The high values of σ_{PSII}' observed around 30-50m at 12:30 on 1st December, for example, were associated with a discrete patch of higher salinity water (>35.57) which was somehow subducted to this depth, presumably as a result of the internal bore (*Fig. 4.20*).

Taxonomic differences between the two populations were inferred from the change in size class dominance when the coastal water was sampled at PK. It was likely that the bloom within the upwelled coastal water was dominated by a diatom population. However it remains unclear whether the higher functional absorption cross sections observed in the off shore water were a result of nutrient limitation, photoacclimation or a taxonomic difference (Kolber *et al.* 1988; Kolber *et al.*, 1990; Falkowski *et al.* 1992).

Diel variability in the physiological state of the phytoplankton populations sampled at PK was pronounced in both $\Delta F'/F_M'$ and σ_{PSII}' (*Figs. 4.20 & 4.25*). Some variability in σ_{PSII}' was caused by the internal motions. Distinguishing between the influence of photoacclimation and horizontal advection on this parameter at PK was complicated as the

warm phase of the internal bore arrived toward the middle of the day throughout the survey (*Fig. 4.20*).

Conversely the near surface value of $\Delta F'/F_M'$ was closely related to irradiance throughout the majority of the 2000 study (*Fig. 4.20 & 4.25*). The photoacclimation time-scale for $\Delta F'/F_M'$ is therefore considered to be faster than the time-scale for internal motions in the majority of cases (Falkowski, 1983; Lewis *et al.* 1984a&b). The marked exception to this pattern was observed during the second transect of the final CTD survey (*Fig. 4.24g*). Horizontal gradients in $\Delta F'/F_M'$ (F_v/F_m) were much weaker than vertical gradients. The low values of $\Delta F'/F_M'$ observed around 45-65m at 174.8°E, were therefore probably the result of a rapid removal of a near surface, high light acclimated, population of phytoplankton to depth by the large amplitude internal soliton (*Fig. 4.24g*). The relationship between irradiance and $\Delta F'/F_M'$ for all the stations sampled during this transect supports this view. The station which sampled the soliton had a significantly different relationship to all the other stations (*Fig. 4.29*).

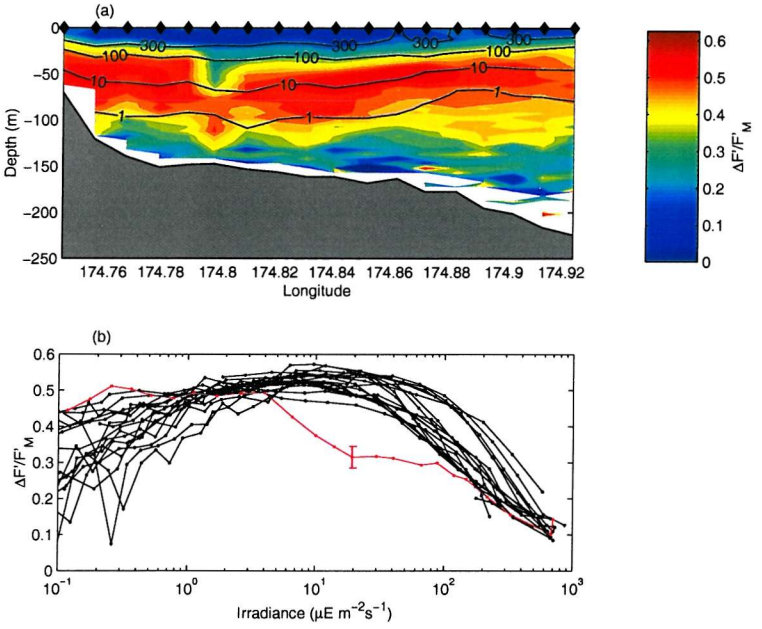

Fig. 4.29 Observed relationship between $\Delta F'/F_M'$ and irradiance during second CTD transect on 3rd December 2000. (a) Contoured $\Delta F'/F_M'$ (colours) and irradiance (black contours). Irradiance is contoured at 1, 10, 100 and 300 μE $m^{-2}s^{-1}$. (b) $\Delta F'/F_M'$ vs. irradiance for all profiles during transect. Profile collected within soliton at 174.8°E is indicated in red. Error bar indicates standard deviation for one 5m depth bin of *in situ* data, other error bars omitted for clarity.

In order to further verify whether the observed pattern of $\Delta F'/F_M'$ could reasonably have resulted from a soliton generated vertical movement of the thermocline, the time-scale for photo-acclimation, as estimated from the light shift experiments, was compared to the implied time-scale for vertical movement within this soliton. The maximum thermocline displacement within this internal soliton was around 50m. Assuming a photo-acclimation time-scale ($\tau_{a1/2}$) of around 20 minutes, it was estimated that a characteristic vertical velocity of 4 cm s^{-1} should have been capable of drawing the phytoplankton population away from the surface faster than it could acclimate to the changing *in situ* irradiance. This vertical velocity is comparable to the maximal values of 5-10 cm s^{-1} measured within internal solitons by the ADCP's on IW1/00 and IW2/00.

It is therefore concluded that the observation of the soliton during the second transect on 3rd December 2000 represented an example of a phytoplankton population which was not acclimated to the ambient irradiance field, due to rapid vertical motions. The absence of such events in the time-series data collected at PK most probably resulted from a lack of large amplitude solitons passing the anchor station towards the middle of the photo-period (*Fig. 4.20*). The short acclimation time-scales estimated from the light shift experiments, combined with the *in situ* observations of $\Delta F'/F_M'$ and σ_{PSII}' therefore suggested that the phytoplankton were generally acclimated to the ambient light field. As previously stated, longer time-scale photo-acclimation cannot be ruled out as a cause of the observed lateral gradients in σ_{PSII} and σ_{PSII}'.

As with the frontal study in the preceding chapter, the use of the observed FRRF derived physiological parameters to calculate carbon fixation rates and comparisons with inferred nutrient fluxes are postponed until later chapters.

Summary and conclusions

Detailed physical and biological observations were obtained at a number of sites on the North East New Zealand Continental Shelf, where the dominant cause of physical variability was large amplitude internal motions. The internal tides/bores and solitons were observed to affect both the nutrient and light climate of the phytoplankton populations in the region. The dissipation of internal energy was shown to be capable of producing significant vertical fluxes of nitrate at all the sites studied and hence provides a source of new nutrients for phytoplankton production and growth.

Vertical movements of the thermocline also affected the light climate of phytoplankton. General increases in irradiance may have resulted, although quantifying this effect is problematic. In particular the interaction between the internal tide and the 'background' stratification may be crucial in determining the long-term influence of the baroclinic motions on phytoplankton light climate.

High resolution physiological data collected during the second cruise indicated that phytoplankton were able to maintain their photosynthetic apparatus in a state acclimated to the ambient irradiance except under the most rapid shifts in light. The FRRF data was also at least partially consistent with a regular supply of nutrients for phytoplankton growth, as indicated by moderate photosynthetic efficiencies (F_v/F_m). Larger scale changes in the functional absorption cross section were closely related to circulation patterns on the shelf and in particular upwelling near the coast. However, it was unclear if the differences in the functional absorption cross section were taxon specific or due to nutrient effects.

The lack of phytoplankton physiological data from the first cruise, where the physical situation was simpler, hampered fuller investigations of the influence of internal motions on phytoplankton growth in the region. In general, the more complex physical system and lower quantity of ancillary information resulted in the interpretation of the FRRF data being more difficult for the studies on the North East New Zealand shelf than in the Western English Channel (Chapter 3). However, the physiological and physical observations provided a strong background against which the productivity measurements will be assessed (see below, Chapters 5 & 6).

The net effects of increased mixing and hence nutrient flux, as well as changes in integrated irradiance, may best be investigated using coupled biological-physical models of the shelf region which allow for internal motions. Observations of phytoplankton physiological variability in response to environmental forcing such as those presented here, may enable the biological aspects of such models to be better parameterised.

5. Comparisons between FRRF and ^{14}C P* vs. E derived physiological parameters and productivity estimates

5.1 Introduction and description of P* vs. E data sets

A number of ^{14}C P* vs. E experiments were run during the August 1999 (Chapter 3) and November-December 2000 (Chapter 4) cruises. These experiments allowed investigation of the relationship between fluorescence derived physiology and carbon fixation, as well as providing a comparison between FRRF and ^{14}C based productivity estimates. A series of ^{14}C simulated *in situ* experiments were also performed during the August 1999 cruise, the results from these are compared to FRRF derived productivity estimates in Chapter 6.

The two ^{14}C P* vs. E data sets are now introduced (§ 5.1.1) along with a brief discussion of how spectral variability in excitation sources can alter some of the derived parameters, specifically α^* (§ 5.1.2). The 1999 and 2000 data sets are then examined independently. The 1999 data set is extensively studied first (§ 5.2), with the 2000 data set subsequently analysed using similar ideas (§ 5.3). For each data set, relationships between FRRF and ^{14}C derived physiology are first investigated (§ 5.2.1 – 5.2.4 & 5.3.1 – 5.3.2). A series of models are then introduced for the derivation of production from *in situ* FRRF data. The models were designed to account for possible vertical and temporal variability in E_K (and P^*_{max}). The resulting P* estimates are then compared with ^{14}C P* vs. E derived values (§ 5.2.5 – 5.3.3).

5.1.1 ^{14}C P* vs. E determinations

Photosynthesis irradiance (P* vs. E) determinations were performed on discrete samples collected at a variety of times, locations and depths (*Table 5.1*). Sample treatments and incubation procedures varied between the two cruises (see Chapter 2). In particular a different range of light levels and lamps with different spectral characteristics were used. All curves of P* against irradiance were fitted to the model of Platt *et al.* (1980) in order to derive values for P^*_{max} and α^* (§ 2.4.2). Example data and fits from the two cruises are shown in (*Fig. 5.1*).

Cruise	Station	Date & Time	Depths (m)	Notes
1999, CH145	M (M2)	06/08/99 11:51	7, 43	a*
		07/08/99 06:00	9, 41	a*
	M (M3)	12/08/99 11:25	4, 10, 40	a*
		12/08/99 17:55	4, 20	a*
	U2	08/08/99 15:44	5, 29	a*
		09/08/99 06:10	25, 27, 29, 30	a*
	L3	10/08/99 09:00	5, 19	
	E	10/08/99 18:00	7, 30	
		11/08/99 18:37	7, 20	
		Total: 21	15 with a*	
2000, KAH0012	PK (PK1)	26/11/00 04:11	5, 19, 51	†
		26/11/00 12:16	5, 29, 55	†
		26/11/00 16:24	5, 20, 39	No FRRF
	(PK3)	28/11/00 04:13	5, 14, 29	
	(PK4)	30/11/00 04:10	3, 29, 70	
		30/11/00 11:48	4, 25, 49	
		30/11/00 17:00	5, 15, 45	
	(PK6)	02/12/00 04:16	30, 52, 51	
		02/12/00 11:45	4, 30, 60	
		02/12/00 17:26	5, 31, 60	
		Total: 30		

Table 5.1 Locations, sampling times and depths for discrete samples incubated for ^{14}C P* vs. E determinations. Times for 1998 are in GMT and for 2000 in NZST (=GMT + 12hrs). In notes, a* indicates phytoplankton chlorophyll specific absorption measurements available for this station. † indicates anomalous chlorophyll values measured on discrete samples. For these two profiles reported chlorophyll values from discrete samples decreased towards surface, while both FRRF and CTD fluorometers and the transmittance indicated increases. Chlorophyll values for normalisation were therefore taken from the calibrated CTD and FRRF fluorescence and CTD transmittance which all agreed well, reported values of P^*_{max} and α^* for these profiles should however be treated with caution.
No FRRF, indicates no FRRF data available for this profile.

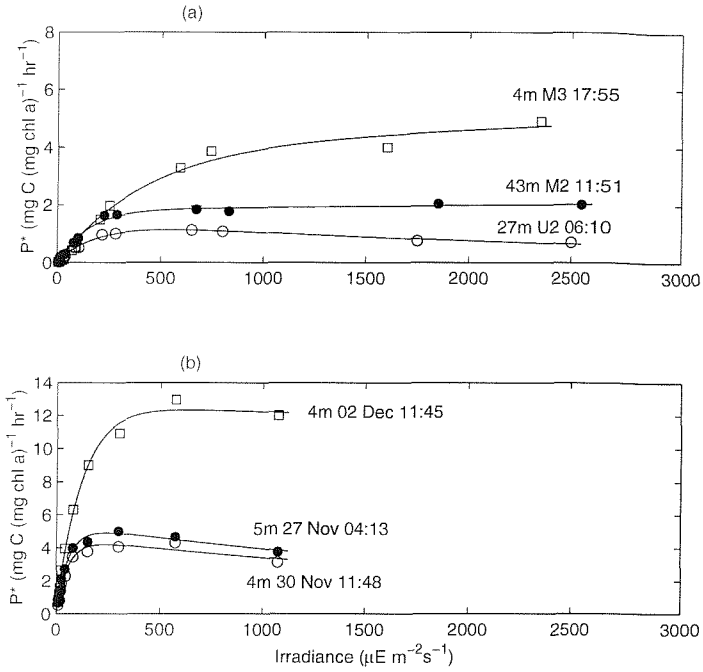

Fig. 5.1 Examples of P* vs. E data and fits for the (a) 1999 and (b) 2000 cruises. Note P vs. E measurements were made over a smaller range of irradiances during the 2000 (Poor Knights internal wave) cruise. Solid lines are fits of the data to the model of Platt *et al.* (1980).

Productivity rates (P*) measured on individual samples during the 2000 cruise were noticeably higher at all irradiances than those measured during 1999 (*Fig. 5.1*). Genuine physiological changes may have been responsible for these differences, however artefacts due to methodological differences have not been ruled out. Systematic bias introduced as a result of normalisation to HPLC (1999 cruise, Chapter 2) or fluorometrically (2000 cruise, Chapter 2) derived chlorophyll *a* could not have been responsible for these differences, as this would tend to increase P* for the 1999 cruise. Even if the possibility of errors due to poor quality data is neglected, differences in the spectral qualities of the lamp used could have been responsible for the marked contrast between the 1999 and 2000 cruises.

5.1.2 Spectral dependencies of σ_{PSII}, α^* and E_K

The parameters σ_{PSII} and α^* are dependent on the irradiance absorbed by phytoplankton cells. As the absorbance of phytoplankton varies over the PAR wavelength range both σ_{PSII} and α^* are spectrally dependent quantities ($\sigma_{PSII}(\lambda)$ and $\alpha^*(\lambda)$). Variability in the spectral quality of an excitation energy can therefore change the amount of light absorbed for a given irradiance (e.g. Dubinsky et al. 1986; Cleveland et al. 1989; Babin *et al.* 1996; Suggett *et al.* 2001). The spectral dependence of σ_{PSII} and α^* is important, as comparisons

between different techniques, as well as the use of P* vs. E or FRRF derived parameters for the estimation of *in situ* productivity, require normalisation for the spectral quality of the actinic and FRRF excitation sources (*Fig. 5.2*). For the current study, as with much previous work, values of α^* and σ_{PSII} were corrected to correspond to a 'white' spectrum where possible (1999 cruise) using the measured chlorophyll specific absorption and lamp spectra (e.g. Dubinsky et al. 1986; Cleveland et al. 1989; Babin *et al.* 1996; Suggett *et al.* 2001).

In order to compare FRRF and ^{14}C derived physiological parameters, the mean absorption coefficient for phytoplankton $\overline{a^*}$ (i.e. the absorption coefficient for white light) was calculated as:

$$\overline{a^*} = \frac{\int_{400}^{700} a^*(\lambda) d\lambda}{\int_{400}^{700} d\lambda} \tag{5.1}$$

where $a^*(\lambda)$ was the chlorophyll specific absorption spectrum measured for a sample. The weighted mean absorption which accounts for the spectral quality of the excitation source is:

$$\overline{a_{ex}{}^*} = \frac{\int_{400}^{700} a^*(\lambda) E_{ex}(\lambda) d\lambda}{\int_{400}^{700} E_{ex}(\lambda) d\lambda} \tag{5.2}$$

where $E_{ex}(\lambda)$ is the incident irradiance of the excitation source at λ (e.g. Dubinsky *et al.* 1986; Kyewalyanga *et al.*, 1997; Suggett *et al.* 2001).

Correction factors (X) to convert measured values of σ_{PSII} and α^* to values corresponding to a 'white' spectrum were therefore calculated as:

$$X = \frac{\overline{a^*}}{\overline{a_{ex}{}^*}} \tag{5.3}$$

Unfortunately phytoplankton absorption spectra were only available from three of the five stations for which discrete water samples for P* vs. E determinations were collected during the 1999 cruise (*Table 5.1*). Values of X calculated for the conversion of measured α^* to that for a white spectrum ranged from 1.9 for the surface at U2, to 1.5 at M3, with

significant depth variation (1.9-1.7) only apparent at U2. Corrected values of α^* for stations where absorption spectra were not obtained were therefore estimated using a mean value of X = 1.6. Errors introduced using this procedure on the entire 1999 data set were likely to have been < 20%. No absorption spectra were available for the 2000 cruise and additionally the lamp spectrum was not measured, thus no correction for spectral effects on α^* were possible for the second data set. All quoted values of α^* for the 1999 cruise have thus had a spectral correction applied whilst none of the values for the 2000 cruise have been corrected.

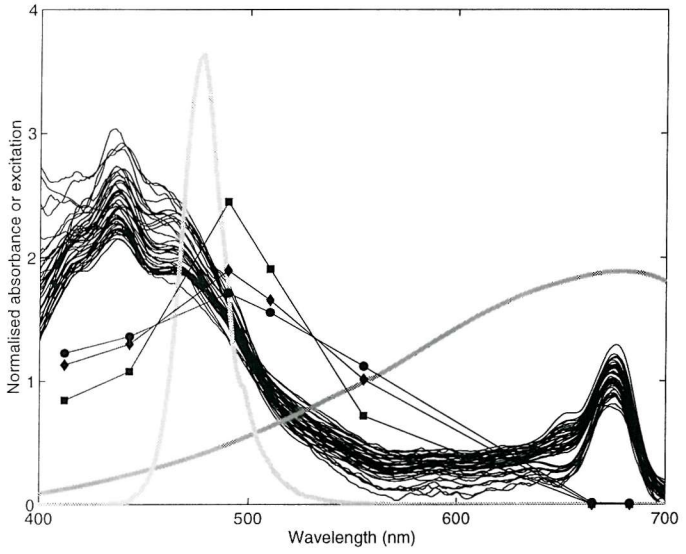

Fig. 5.2 Normalised excitation and absorption spectra. Thin black lines are chlorophyll specific absorption spectra for all the samples collected during the 1999 cruise. Thick grey lines are excitation spectra for the FRRF (light grey) and the photosynthetron lamp (dark grey) used during the 1999 cruise. Thin lines with symbols are representative of *in situ* spectra measured at depths of 10m (circles), 20m (diamonds) and 50m (squares) using an SPMR during the 2000 cruise. For comparison all spectra are normalised to the mean value with the exception of the FRRF excitation spectrum which was normalised then scaled by a factor of 1/3.
The excitation source of the FRRF is clearly more efficient at providing excitation energy to the phytoplankton as it overlaps the high wavelength end of the major phytoplankton absorption peak. Conversely the 'relatively red' photosynthetron lamp spectrum provides a majority of excitation in a region of low absorption (>550nm). The FRRF spectrum approximates the *in situ* irradiance field better at depth due to the higher penetration of blue-green light through the water column.

Conversion factors for σ_{PSII} to σ_{PSII}(white) calculated for the 1999 cruise ranged from 0.52 at U2 to 0.61 at M3 and were comparable to values of 0.53 – 0.58 calculated for an FRRF by Babin *et al.* (1996). A mean value of 0.57 was used to correct the remainder of the 1999 data set. Once again no correction was possible for the 2000 cruise due to the lack of

absorption data. In the interests of clarity and comparison between cruises, and consistent with the preceding chapters, all values of σ_{PSII} quoted will therefore be the uncorrected (i.e. measured) values. Corrections were only applied to the 1999 data when direct comparisons between FRRF and ^{14}C P* data were required, and this will be indicated in the quoted data.

Justification for use of data sets

Although spectral correction of the 2000 data set was not possible, it is reasonable to assume that any adjustment would increase rather than decrease the values of α^* calculated from the P* vs. E determinations. Thus, as with normalisation to HPLC or fluorometric chlorophyll *a*, spectral effects were unlikely to have accounted for the >6 fold difference between the values of α^* calculated from the 2000 and 1999 data sets (*Fig. 5.1*). Neither of the potential problems addressed above can explain the nearly three fold difference in the highest values of P^*_{max} for the two data sets.

As no cross comparison between the two P* vs. E data sets was possible, the observed relationships between the ^{14}C and FRRF derived physiological parameters and photosynthetic rates are initially interpreted separately for the two cruises. It is once again emphasised that true physiological variation between the populations sampled during the two cruises have not been ruled out and the possible consequences of such marked changes in P* and particularly P^*_{max} are discussed.

5.2 Comparisons for 1999 data set

5.2.1 Relationships between FRRF and ^{14}C physiological parameters

Physiological parameters calculated from the P* vs. E incubations performed on discrete samples were compared to parameters measured *in situ* by the FRRF at the time of sampling (*Fig. 5.3*). Weak significant correlations ($p < 0.05$) were observed between α^* and both F_v/F_m and σ_{PSII}'. Around 30% of the variance in α^* was explained by a positive correlation with F_v/F_m or a negative correlation with σ_{PSII}'. No significant relationship was apparent between F_v/F_m and P^*_{max}, however a striking and highly significant ($P < 0.001$) negative correlation accounting for over 89% of the variance, was observed between σ_{PSII}' and P^*_{max} (*Fig. 5.3d*).

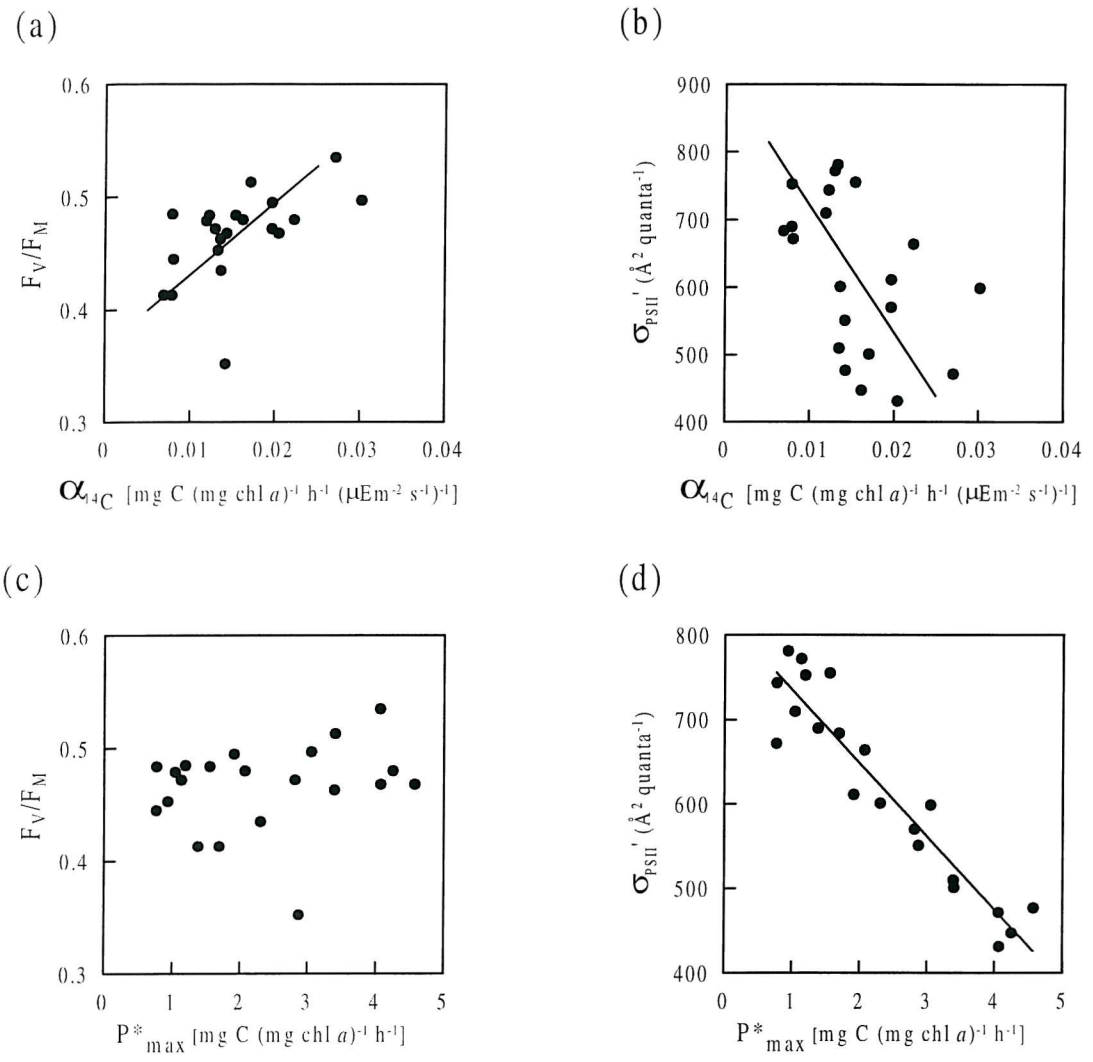

Fig. 5.3 Relationships between FRRF and ^{14}C (P* vs. E) physiological parameters from the August 1999 cruise. (a) F_v/F_m vs. α^*. Values of F_v/F_m for individual stations are taken from the night-time values at the sampling depth. (b) σ_{PSII}' vs. α^*. Values of σ_{PSII}' are from the instantaneous *in situ* measurement at the time of sampling. (c) F_v/F_m vs. P^*_{max} (d) σ_{PSII}' vs. P^*_{max}. Relationships for σ_{PSII} (i.e. taken from night-time observations) are similar to those for σ_{PSII}'. Lines indicate linear regressions where significant ($p < 0.05$).

Using (Eqs. 1.11 & 1.12) a FRRF based estimate of α^* can be calculated as:

$$\alpha^*_{FRRF} = A\frac{F_V / F_M \sigma_{PSII} n_{PSII}}{PQ} \tag{5.4}$$

with F_v/F_m and σ_{PSII} replacing $\Delta F'/F_M'$ σ_{PSII}' in (Eq. 1.11), as by definition α^* is the initial slope of the P* vs. E relationship before light saturation and should therefore correspond to irradiances below those which cause reductions in $\Delta F'/F_M'$ and σ_{PSII}'. A positive correlation between F_v/F_m and α^* (*Fig. 5.3a*) may therefore be expected and has previously

been observed on field populations by Boyd *et al.* (1997). A negative relationship between σ_{PSII} (or σ_{PSII}') and α^* is however contrary to what may be expected from (Eq. 5.4).

Possible causes/consequences of the observed relationship between P^*_{max} and σ_{PSII} are discussed further below (§ 5.4).

5.2.2 Estimation of n_{PSII}

In order to use (Eq. 1.11) or (Eq. 5.4) to derive the carbon specific productivity rate or α^* respectively, an estimate for the ratio of PSII reaction centres to chlorophyll *a* (n_{PSII}) is required (Kolber and Falkowski, 1993; Boyd *et al.* 1997; Suggett *et al.* 2001). Suggett *et al.* (2001) suggested a method for estimating n_{PSII} using observations of a^* using arguments similar to the following.

Assuming that F_v/F_m is a measure of the photochemical efficiency, σ_{PSII} should be related to the optical absorption cross section of PSII (a_{PSII}) by (Kolber et al. 1998):

$$\sigma_{PSII}(\lambda) = a_{PSII}(\lambda)\, F_v/F_m \tag{5.5}$$

It was then assumed that the optical absorption cross section of PSII is related to the chlorophyll specific optical absorption cross section (a*) by:

$$a_{PSII}\, n_{PSII} = a^* \tag{5.6}$$

noting that any variation in the proportion of chlorophyll that is associated with photosystem I will lead to some uncertainty in this relationship. Using (Eqs. 5.5 & 5.6) an estimate of n_{PSII} can thus be derived from measurements of $a^*(\lambda)$ and FRRF based measurements of F_v/F_m and σ_{PSII} using:

$$n_{PSII} = \frac{a^*(475)\, F_V/F_M}{\sigma_{PSII}} \tag{5.7}$$

the 475nm wavelength being chosen to coincide with the peak of the FRRF excitation spectrum. Suggett *et al.* (2001), originally derived this relationship using F_v/F_o rather than F_v/F_m as an index of active reaction centres (see Babin *et al.* 1996 their Appendix 1 for discussion).

Performing this calculation for the 1999 data set resulted in a mean value for n_{PSII} of 0.0019 ± 0.0003 mol PSII/mol Chl (or 1 PSII reaction centre for every 530 ± 80 molecules of

chlorophyll *a*) being calculated. This number is very similar to the value of 500 assumed by Kolber and Falkowski, (1993), which was based on laboratory studies of eukaryotic algal cultures. No significant variations in n_{PSII} were observed between the stratified and mixed side. The decreasing values of a^* from the stratified (U2) to mixed stations (M2 & M3) was accompanied by decreasing values of $\sigma_{PSII}/F_v/F_m$ (*Fig. 5.4*).

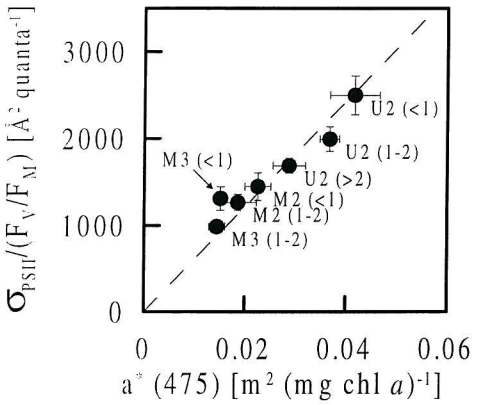

Fig. 5.4 Mean values of a* (475) vs. $\sigma_{PSII}/(F_v/F_m)$ for all three stations where phytoplankton absorption data were collected. The data were averaged into mean daily values in 1 optical depth vertical bins. Labels indicate the station during which samples were collected and the optical depth. Data are highly correlated ($r^2 = 0.987$, $p < 0.001$). Dashed line is regression through the origin indicating a constant n_{PSII}, the slope giving the value (see text). Error bars are one s.e.

The observed positive correlation between $\sigma_{PSII}/F_v/F_m$ and a^* lends confidence to the use of (Eq. 5.7) for the calculation of n_{PSII}, as does the similarity between the values derived using the method of Suggett *et al.* (2001) and those quoted for laboratory cultures (Dubinsky *et al.* 1986; Greene *et al.* 1991; Kolber and Falkowski, 1993; Berges *et al.* 1996).

5.2.3 Comparisons of α^* estimates by FRRF and ^{14}C

FRRF derived estimates of α^* were thus calculated using $n_{PSII} = 0.0019$ mol PSII/mol Chl and by assuming a constant PQ value. For simplicity and comparison with Suggett *et al.* (2001) the PQ value was assumed to be 1. PQ values in the ocean are expected to be around 1.4 (Laws, 1991) thus a slope >1 could be expected when performing regression between FRRF and ^{14}C α^* calculated in this way. Spectral correction of σ_{PSII} values was performed in order to calculate α^*_{FRRF} (§ 5.1).

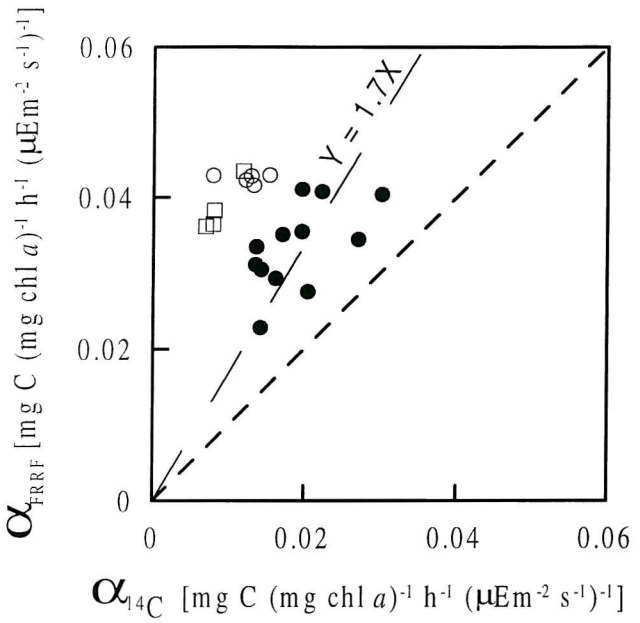

Fig. 5.5 Relationship between ^{14}C and FRRF derived estimates of α* from the 1999 cruise. Each point corresponds to α^*_{14c} calculated on a discrete water sample collected for a P* vs. E determination plotted against the value of α^*_{FRRF} calculated using (Eq. 5.4) applied to the FRRF data. FRRF α* has been spectrally corrected. Open circles are for the thermocline at U2, Open squares are from station E and solid circles for all other stations. Dotted line indicates 1:1 relationship, dashed line indicates regression through origin for points excluding U2 thermocline and E.

The relative magnitudes of both FRRF and ^{14}C derived α* estimates were comparable, however for the complete data set, no clear trend was observed (*Fig. 5.5*). FRRF derived values of α* were higher than ^{14}C derived values at all the stations and much higher for the thermocline at the highly stratified U2 site and the stratified site E. Absolute values for the remaining regions were similar, with a weak but significant correlation observed between the two methods ($R^2 = 0.338$, $n = 12$, $p < 0.05$).

Possible reasons for underestimation of P* by ^{14}C methods at site E and the thermocline of site U2 include 'bottle effects' and differences between the ambient *in situ* temperature to which phytoplankton were acclimated and the incubation temperature. Temperature differences between incubation and *in situ* temperatures were maximal for the thermocline at U2 and reached >5°C. However it is suggested that manipulation and enclosure of the very dense and virtually mono-specific community of coccolithophores found within the thermocline at this site (Sharples *et al.* 2001a), may well have resulted in artefacts being introduced into ^{14}C derived physiological values. Site E was further thought to have been

occupied during the declining stage of a near surface bloom of the coccolithophore *Emiliania huxleyi*. The possibility of artefacts caused by incubation and manipulation of a senescent population thus remains.

5.2.4 Calculation of E_K and sensitivity of FRRF productivity to E_K

Sensitivity of productivity calculations to E_K

Estimation of phytoplankton productivity using (Eq. 1.11 & 1.12), is essentially a two stage process. The ETR through PSII below the level of light saturation, i.e. in the 'α^* region' of the P* vs. E curve, is first estimated. However above light saturation the ETR can become decoupled from oxygen evolution or carbon fixation (Kolber and Falkowski, 1993; Flameling and Kromkamp, 1998; Gilbert *et al.* 2000). A correction therefore has to be applied when the ETR exceeds the maximal rate of electron transfer from PSII to the final stage of the electron transport chain (Kolber and Falkowski, 1993). In the case of carbon specific production the terminal stage is carbon fixation by the Calvin – Benson cycle (Kolber and Falkowski, 1993; Falkowski and Raven, 1997). FRRF derived productivity rates for irradiances above light saturation thus require some measure of the maximal turnover time of the photosynthetic apparatus (τ_{PSII}) or effectively the light saturation parameter (E_K) which is related to τ_{PSII} according to (Falkowski, 1992; Kolber and Falkowski, 1993):

$$E_K = \frac{1}{\sigma_{PSII}\tau_{PSII}} \tag{5.8}$$

In effect the maximal photosynthetic rate (P^*_{max}) is not measured by the FRRF technique, but rather is inferred from some knowledge of E_K and α^* (Kolber and Falkowski, 1993; Boyd *et al.* 1997).

FRRF derived productivity rates are therefore crucially dependent on the method for evaluating E_K or P^*_{max}. Both these parameters are known to vary both vertically within the water column and have been shown to display diel cycles (e.g. Babin *et al.* 1994; 1996; Falkowski and Raven, 1997; Behrenfeld *et al.* 1998). Careful consideration of such variability is therefore necessary before applying the FRRF technique to estimates of productivity.

Calculation of E_K from FRRF data

Calculation of the saturation light intensity using active fluorescence data has previously been accomplished by evaluating the irradiance at which photochemical quenching causes a sharp reduction of $\Delta F'/F_M'$ (Kolber and Falkowski, 1993; Boyd *et al.* 1997; Suggett *et al.* 2001). The principle behind this measurement is that as irradiance increases, the rate of re-oxidation of Q_a^- is decreased due to reduction of the PQ pool (*Fig. 1.1*). The turnover time for Q_a^- reduction may thus approach τ_{PSII}, with an increase in quenching accompanying this effect (Kolber and Falkowski, 1993)[1].

Studies which have previously compared active fluorescence and ^{14}C based productivity estimates within water columns have taken the saturation light intensity to correspond to the irradiance at the depth where marked reduction in $\Delta F'/F_M'$ is first observed (Boyd *et al.* 1997; Suggett *et al.* 2001). Suggett *et al.* (2001) formalised this procedure by fitting vertical profiles of $\Delta F'/F_M'$ and irradiance (E) to the following empirical form:

$$\Delta F'/F'_M = \Delta F'/F'_M\,(\max)\left(1 - e^{\frac{-E}{E_K}}\right)\frac{E_K}{E} \qquad (5.9)$$

where $\Delta F'/F_M'(\max)$ is the value of $\Delta F'/F_M'$ at low irradiance and thus approaches F_v/F_m. Such an empirical relationship corresponds to the mathematical equations used to describe the P* vs. E curve (e.g. Platt *et al.* 1980).

Examples of data from U2 fitted to (Eq. 5.9) revealed that estimated values of E_K using the model were considerably higher than those which may have been chosen if the point of initial inflection in $\Delta F'/F_M'$ were taken (see Boyd *et al.* 1997), (*Fig. 5.6*). General empirical agreement was found between E_K estimates using (Eq. 5.9) and from ^{14}C P* vs. E curves by Suggett *et al.* (2001). Hence in order to facilitate direct comparison between the current data set and that of Suggett *et al.* (2001), all estimates of E_K derived from the relationship between $\Delta F'/F_M'$ and irradiance were generated using (Eq. 5.9).

[1] An alternative method for calculating τ_{PSII} using active fluorescence derived estimates of τ_{Qa} may be possible (Kolber and Falkowski, 1993; Falkowski and Raven, 1997; Kolber *et al.* 1998). Using a suitable protocol the relaxation of fluorescence following saturation can be followed using the FRRF technique (Kolber *et al.* 1998). Thus the relaxation rate of the primary stable acceptor (τ_{Qa}) can be measured. This could be expected to equal τ_{PSII} at light saturation (Kolber and Falkowski, 1993). However this method has not been tested. Additionally current *in situ* estimates of τ_{Qa} using the FRRF technique appear to be inaccurate, probably as a consequence of the relaxation protocol, which must last O(ms) being of comparable length to the residence time of the sample in-front of the FRRF optics (Suggett, 2000).

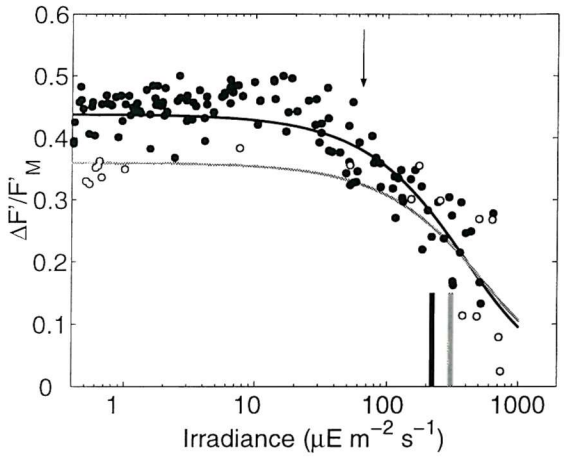

Fig. 5.6 Example of relationship between $\Delta F'/F_M'$ and irradiance for station U2 during CH145, August (1999). Symbols indicate all 5m binned data collected during the 25hr station at U2. Open symbols are data for surface 5m depth bin only. Black and grey lines are fits of data to (Eq. 5.9) for all the data ($R^2 = 0.697$) and only surface data ($R^2 = 0.744$) respectively. Thick vertical black and grey lines indicate the values of E_K derived using (Eq. 5.9) for the complete data set and the surface 5m, i.e. a higher E_K for the near surface region is calculated. Arrow indicates approximate (qualitatively chosen) first point of inflection in $\Delta F'/F_M'$.

Accounting for vertical and temporal variability in E_K

Previous comparisons between active fluorescence and ^{14}C derived productivity estimates have used individual vertical profiles of $\Delta F'/F_M'$ and irradiance in order to calculate a value for the 'water column' E_K from each profile (Boyd *et al.* 1997; Suggett *et al.* 2001). This method will differentiate the water column into a saturated and unsaturated fraction. The advantage of such a method is that diel variations in E_K (or P^*_{max}) may be detected and thus taken in to account in productivity calculations (*Fig. 5.7*). However, depth variability in E_K is neglected using this method. An alternative method would be to use the time series of $\Delta F'/F_M'$ and irradiance at each depth, generated by a series of vertical profiles, in order to calculate a vertical profile of E_K (*Fig. 5.7*). This method will, however, fail to take into account any diel variability.

Saturation light intensities for the four stations sampled over 25hrs during the 1999 cruise were therefore calculated in three ways. First, all the $\Delta F'/F_M'$ and irradiance data were fitted to (Eq. 5.9) in order to estimate a mean water column and daily E_K. Secondly individual depth profiles of $\Delta F'/F_M'$ and irradiance were fitted to (Eq. 5.9) in an attempt to evaluate any time dependent changes in E_K. Finally time-series of $\Delta F'/F_M'$ and irradiance at near surface depths were fitted to (Eq. 5.9) in order to evaluate any vertical variations in E_K (*Fig. 5.7*).

Estimated from all the profiles, mean daily E_K values for the four 25hr stations were 220 ± 20 (U2), 410 ± 25 (E), 377 ± 30 (M2) and 409 ± 41 (M3) μ E m^{-2} s^{-1}. Temporal variations in E_K were highest at the highly stratified U2 site (*Fig. 5.7a*), however no clear relationship between time of day or irradiance was observed. Vertical increases in E_K towards the surface were apparent at U2 and agreed well with the observed differences in deep and shallow ^{14}C derived estimates for E_K (*Fig. 5.7b*). Some near surface increase in E_K was also observed at station E, although no discernible trends were apparent during stations M2 or M3.

The data from the 4 25hr stations therefore demonstrated the potential for both temporal and vertical differences in E_K, as well as inter-site variability.

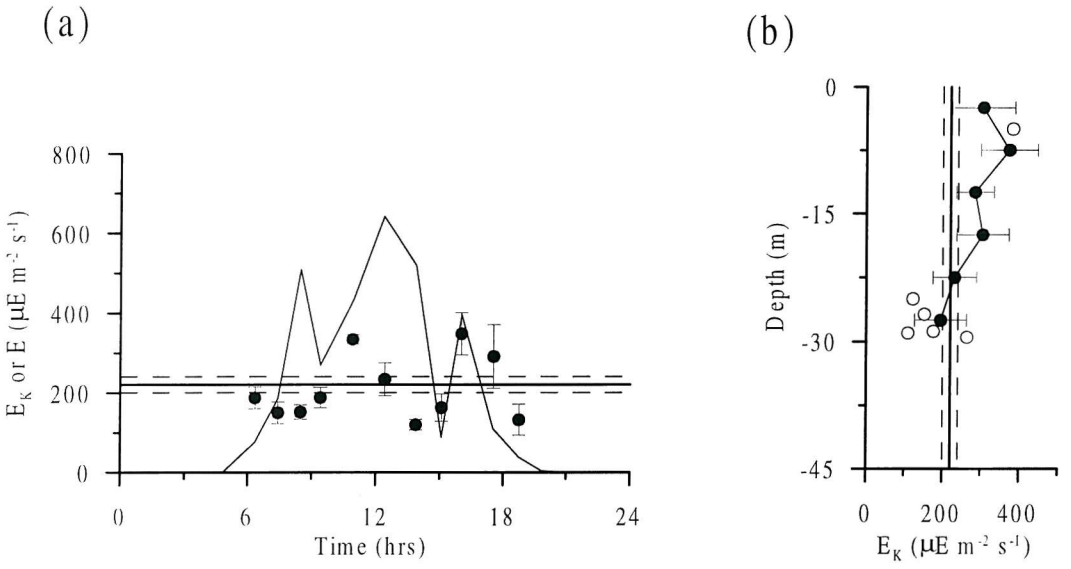

Fig. 5.7 Variability in FRRF derived E_K estimates at site U2. (a) Time series of E_K estimates calculated on individual vertical profiles (symbols) and mean irradiance (line) in upper 5m of water column. For E_K Symbols are mean ± 1.s.d. Solid horizontal line indicates depth and time mean value of E_K calculated for this station from complete data set of $\Delta F'/F_M'$ and irradiance (*Fig. 5.7*), with dashed lines indicating ± 1 s.d. (b) Vertical profile of E_K estimates calculated from time series of $\Delta F'/F_M'$ and irradiance in individual depth bins. Symbols are mean ± 1.s.d. Solid and dotted vertical lines indicate depth and time mean value of E_K as in (a). Open symbols are E_K from ^{14}C P* vs. E curves for this station.

5.2.5 FRRF vs. ^{14}C derived P*, models used and comparisons

Models used for comparison

As demonstrated in the previous section, no method for determining E_K for each individual time and depth from FRRF profile data is possible. Four models were therefore used to compare FRRF to ^{14}C P* vs. E derived productivity estimates.

All the models used were based on (Eqs. 1.11a & 1.12) and only differed in the calculation of E_K or in the way that FRRF productivity within a water column was treated for irradiances above E_K. Model I (hereafter, MI) assumed that the relationship between FRRF derived ETR and carbon fixation was linear even at high irradiances, i.e. (Eq. 1.6b) was neglected. Model II (MII) uses (Eq. 1.6b) for $E>E_K$ with E_K the depth and time mean value calculated for each of the 25hr stations (*Figs. 5.6 & 5.7*). Model III (MIII) was similar to MII, however in near surface regions where E_K values estimated using the FRRF technique on individual depth bins showed some increase, the higher values were adopted (*Fig. 5.7b*). Model IV (MIV) was empirical and used the observed relationship between σ_{PSII}' and P^*_{max} for the 1999 cruise ($P^*_{max} = 8.7\ (\pm 0.5) - 0.0103\ (\pm 0.0008)\ \sigma_{PSII}$', *Fig. 5.3d*), to convert *in situ* measurements of σ_{PSII}' to equivalent P^*_{max} values. For MIV, P* was thus calculated as in MI, however if P* was greater than the empirical P^*_{max}, P* was set equal P^*_{max}. Estimated production rates using a temporally varying E_K from individual profiles (*Fig. 5.7a*) were found to have very minor differences to MII estimates. Also the near surface increase in E_K (*Fig. 5.7b*) was likely to have caused greater variations in the higher production values. A separate model using E_K estimates from individual profiles was therefore not considered for comparison with ^{14}C derived estimates.

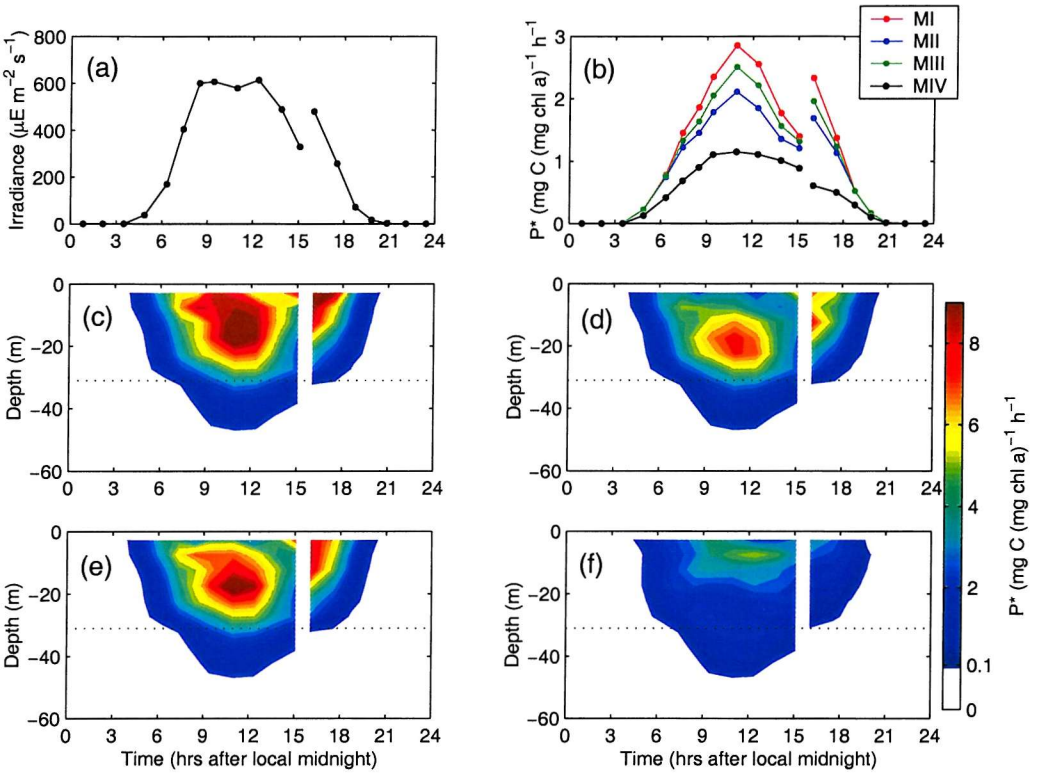

Fig. 5.8 Results of P* calculations based on FRRF data for the U2 site sampled on 8-9th August 1999. Data are presented against time relative to local midnight, note gap in data between around 15:00 and 16:00 hrs as sampling commenced at 16:00 on 8th August and ended at 15:10 on 9th August (a) Mean irradiance from 0-5m. (b) Depth mean P* for the four different models. (c-f) Depth vs. Time contours of FRRF productivity estimated using MI-MIV respectively. Dotted horizontal lines in (c-f) indicate mean depth of DCM associated with the base of the thermocline observed at this site (see Chapter 3).

Examples of productivity rates estimated using FRRF data for one of the 25hr stations indicated the sensitivity of such calculations to the chosen method for estimating E_K (*Fig. 5.8*). MI estimates were considerably higher than other models as would be expected if no light saturation occurred anywhere within the water column (*Fig. 5.8b & c*). MII and MIII estimates were generally similar, with some higher P* for MIII estimates resulting from the higher near surface E_K (*Fig. 5.8b,d & e*). The empirical MIV model generally estimated lower P* corresponding to the region above light saturation (*Fig. 5.8f*).

Comparison between P from FRRF and ^{14}C P* vs. E*

Instantaneous P* as estimated from the ^{14}C P* vs. E experiments and the irradiance measured at the time of sampling were compared to FRRF productivity estimates derived using the four models above (*Fig. 5.9*).

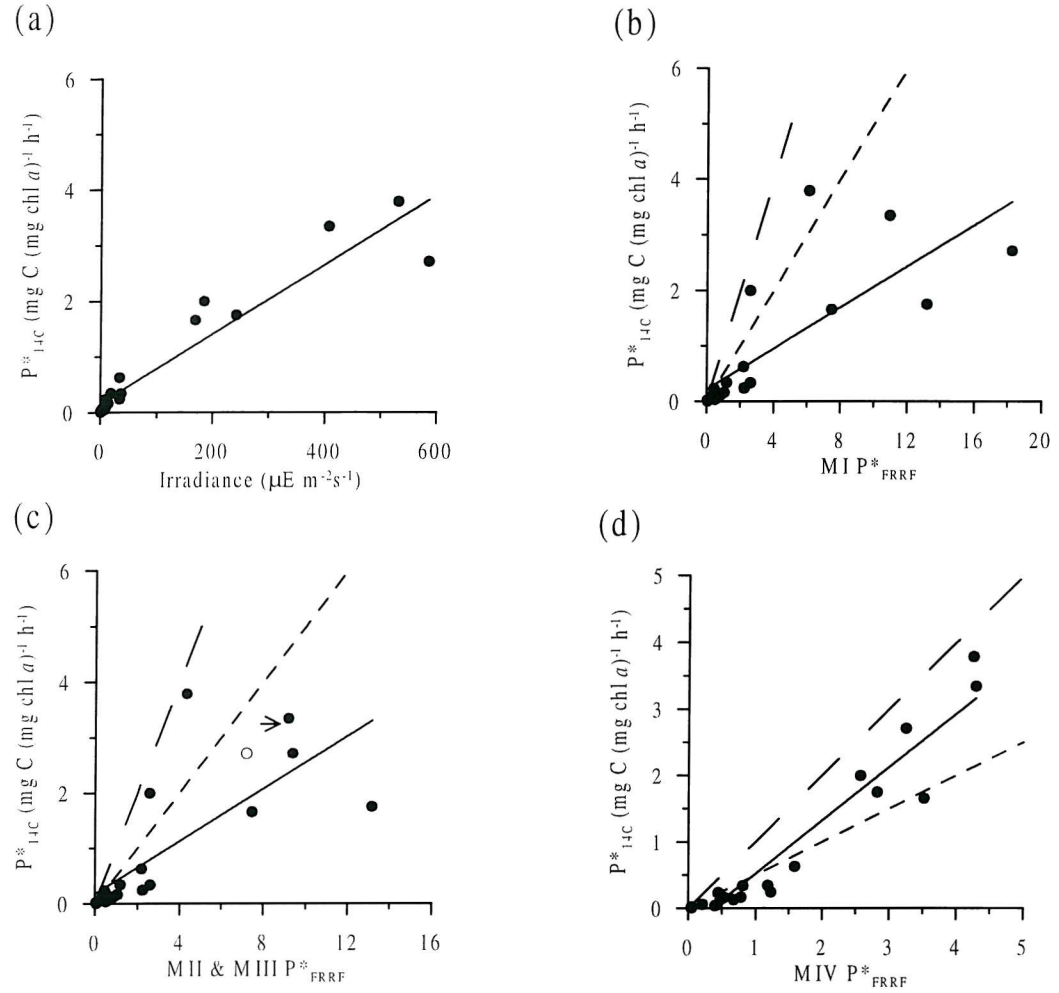

Fig. 5.9 Relationships between ^{14}C and FRRF derived P* and irradiance for 1999 cruise (a) ^{14}C derived P* vs. instantaneous irradiance at the time of sampling. (b) ^{14}C derived vs. FRRF (MI) derived P*. (c) ^{14}C derived vs. FRRF (MII (open symbols) and MIII (closed symbols)) derived P*. Note: MII and MIII values of P* only vary for a few data points, arrows indicate these pairs. (d) ^{14}C derived vs. FRRF (MIV) derived P*. Dashed lines in (b-d) indicate a 1:1 relationship while dotted lines indicate a 2:1 relationship. Thus the area between the dotted and dashed lines represents PQ values of 1-2. Solid lines are linear fits to the data. Percentage variances explained were: (a) 91% *(95%)*, (b) 60% *(88%)*, (c) MII 56% *(54%)*, MIII 54% *(87%)* and (d) 92% *(92%)*, ($p < 0.001$ for all). Values in parentheses are for log transformed data.

Linear relationships between FRRF and ^{14}C derived P* were found for all models. However, a large proportion of the variance in the ^{14}C derived P* could be explained by regression against the instantaneous irradiance at the time of sampling (*Fig. 5.9a*). Indeed ^{14}C derived P* was more highly correlated with irradiance than with FRRF derived P* for MI, MII & MIII. Only the empirical model (MIV) could account for a greater proportion of the variance than irradiance alone. These results reflected the high dependence of FRRF based estimates of production on the calculation of E_K. This conclusion was further

reinforced by the greater variance explained once the data had been log transformed, the relationship between FRRF and ^{14}C P* being closer at lower irradiances (*Fig. 5.9*).

Overall FRRF based estimates of P* were greater than ^{14}C based estimates by a factor of around 4 for the MI, MII & MIII models, and a factor of 1.4 for the empirical MIV model.

5.3 Comparisons for 2000 data set

5.3.1 Relationships between FRRF and ^{14}C physiological parameters

As for the 1999 data set, physiological parameters calculated from the P* vs. E incubations performed on discrete samples were again compared to parameters measured *in situ* by the FRRF at the time of sampling (*Fig. 5.10*). A significant ($P < 0.001$) negative correlation was again observed between σ_{PSII}' and P^*_{max} (*Fig. 5.10d*), although only 44% of the variance was explained by this relationship. No other clear patterns between FRRF and ^{14}C derived physiological parameters were observed within the 2000 data set. Any relations between F_v/F_m and either P^*_{max} or α^* may have been masked by the large horizontal and vertical advection of different water bodies which was occurring at the PK site. Values of F_v/F_m had to be inferred from the pre-dawn profiles each day and this period tended to coincide with the 'cool' phase of the internal tide (see *Fig. 4.20*). Conversely many of the samples collected for P* vs. E determinations were collected around midday or during the afternoon and thus coincided with the 'warm' phase of the internal tide. The low variability of F_v/F_m and hence by inference adequate nutrients at the PK site may also explain some of the lack of patterns displayed in *Figs. 5.10a & c*.

When separated into data for individual days, the observed relationship between P^*_{max} and σ_{PSII}' appeared to change, particularly between 30th November and 2nd December 2000 (*Fig. 5.10d*). Highest values of P^*_{max} were obtained on samples collected within the diatom bloom on 2nd December.

Although no overall relationship between σ_{PSII}' and α^* was apparent, the general decreasing trend of σ_{PSII}' from the 26th November – 2nd December was accompanied by increasing α^* (*Fig. 5.10b*). When subsets of data from individual days were considered, decreasing values of α^* and σ_{PSII}' towards the surface resulted in some indication of positive relationships between the two parameters.

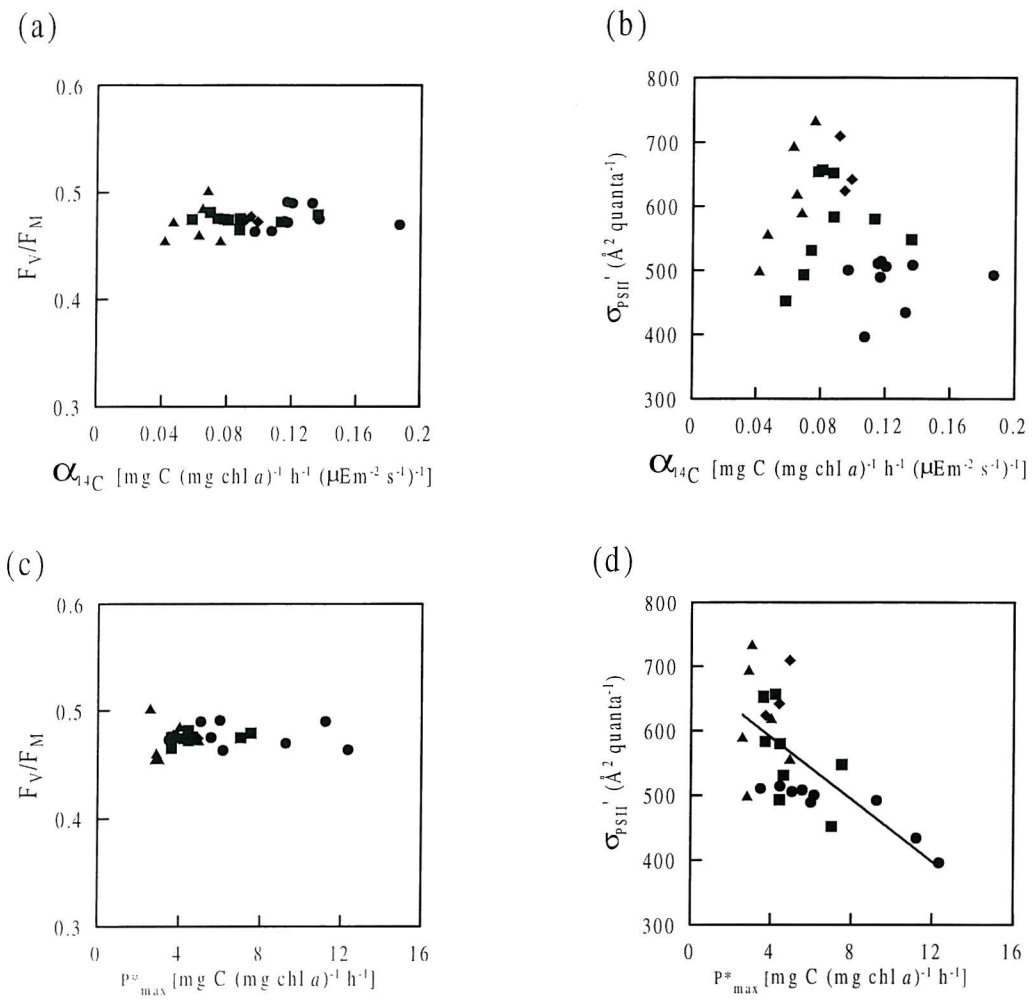

Fig. 5.10 As 5.4, Relationships between FRRF and ^{14}C (P* vs. E) physiological parameters from the November - December 2000 cruise. (a) F_v/F_m vs. α^*. Values of F_v/F_m for individual stations are taken from the pre-dawn values at the sampling depth. (b) σ_{PSII}' vs. α^*. Values of σ_{PSII}' are from the instantaneous *in situ* measurement at the time of sampling. (c) F_v/F_m vs. P^*_{max} (d) σ_{PSII}' vs. P^*_{max}. Data collected on different days are indicated in all plots. Triangles (▲) – 26th November, Diamonds (◆) – 28th November, Squares (■) – 30th November, Circles (●) – 2nd December.

5.3.2 Comparisons of α^* estimates by FRRF and ^{14}C and E_K calculations

Comparisons of α^* estimates

As no samples were taken for the determination of phytoplankton absorption spectra, estimation of n_{PSII} using (Eq. 5.7) was not possible and a value of 0.0020 mol PSII/mol Chl was therefore assumed, in agreement with the 1999 data set and Kolber and Falkowski, (1993). As previously mentioned, no spectral correction for differences in photosynthetron lamp and FRRF excitation source was possible.

No clear relationships between FRRF derived α* estimated using (Eq. 5.4) and ^{14}C derived values was apparent for the complete data set (*Fig. 5.11*). However for individual days some covariance of FRRF and ^{14}C α* estimates was observed. Additionally the ratio of FRRF:^{14}C derived α* decreased from the 26th November to 2nd December. Values of α* estimated using the FRRF technique were comparable to ^{14}C derived values on 26th November but had decreased to around 40% of the ^{14}C derived estimates by 2nd December (*Fig. 5.11*).

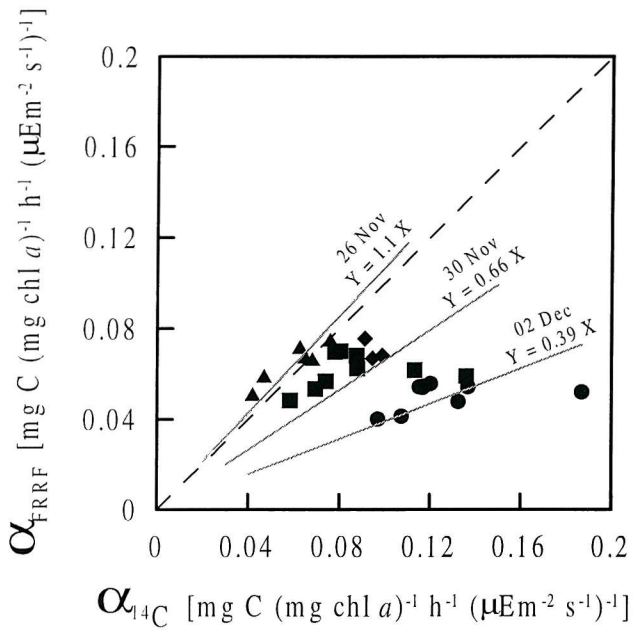

Fig. 5.11 Relationship between ^{14}C and FRRF derived estimates of α* from the 2000 cruise. As (*Fig. 5.6*), each point corresponds to α^*_{14c} calculated on a discrete water sample collected for a P* vs. E determination, plotted against the value of α^*_{FRRF} calculated using (Eq. 5.4). Symbols as in (*Fig. 5.11*), i.e. Triangles (▲) – 26th November, Diamonds (◆) – 28th November, Squares (■) – 30th November, Circles (●) – 2nd December. Dotted line indicates 1:1 relationship. Grey lines are regressions forced through the origin for data from 26th & 30th November and 2nd December 2000.

Calculation of E_K

Estimates of the saturation light intensity (E_K) for the 2000 data set were derived from the *in situ* FRRF measurements as described above for the 1999 cruise. Mean daily values of E_K estimated by fitting the whole time-series of $\Delta F'/F_M'$ and irradiance data to (Eq. 5.9) were 210 ± 10 (26th November), 206 ± 5 (30th November), 220 ± 10 (1st December) and 230 ± 10 (2nd December) µ E m^{-2} s^{-1}. Temporal variability in E_K as evaluated by fitting individual vertical profiles to (Eq. 5.9) was generally low on all days (e.g. *Fig. 5.12a*).

Some near surface increases in E_K could again be inferred from the slightly different $\Delta F'/F_M'$ vs. irradiance relationship within the upper water column on 26th & 28th November and 1st December (e.g. *Fig. 5.12b*).

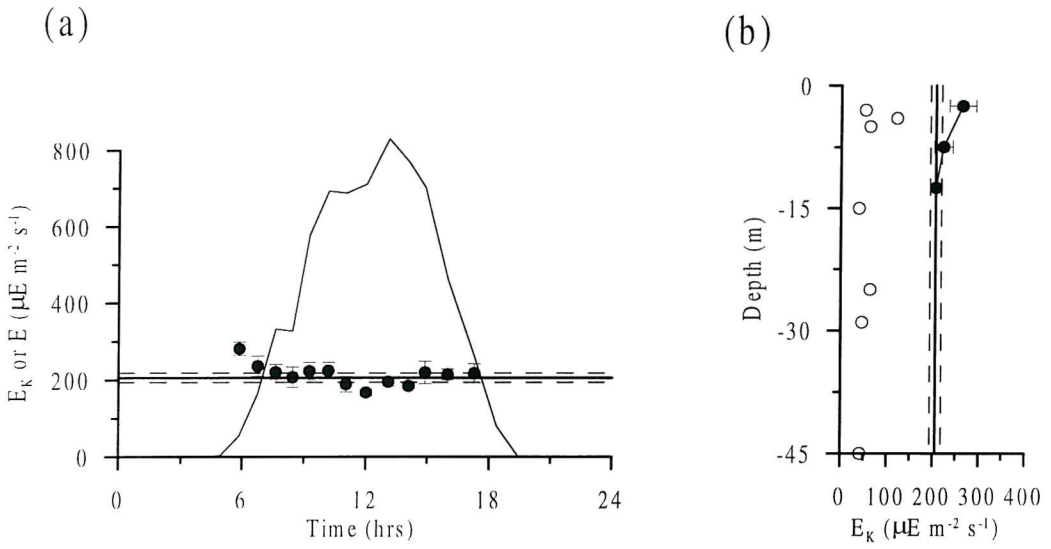

Fig. 5.12 Variability in FRRF derived E_K estimates at PK on 30th November 2000. As (*Fig. 5.8*) (a) Time series of E_K estimates calculated on individual vertical profiles (symbols) and mean irradiance (line) in upper 5m of water column. For E_K, symbols are mean ± 1.s.d. Solid horizontal line indicates depth and time mean value of E_K calculated for this station from complete data set of $\Delta F'/F_M'$ and irradiance, with dashed lines indicating ± 1 s.d. (b) Vertical profile of E_K estimates calculated from time series of $\Delta F'/F_M'$ and irradiance within individual depth bins. Symbols are mean ± 1.s.d. Solid and dotted vertical lines indicate depth and time mean (± 1 s.d.) value of E_K as in (a). Open symbols are E_K from ^{14}C P* vs. E experiments performed on discrete samples collected on this day.

In contrast to the 1999 data set, ^{14}C derived values of E_K were significantly lower than FRRF derived values calculated using (Eq. 5.9) by a factor of around 2-4 (*Fig. 5.12b*).

5.3.3 FRRF vs. ^{14}C derived P*

FRRF and ^{14}C derived estimates of P* were compared for the 2000 data set using the same models as for the 1999 data set. Models I-III (MI-MIII) were unchanged, while the empirical model (MIV) was simply altered such that the observed relationship between σ_{PSII}' and P^*_{max} for the 2000 cruise ($P^*_{max} = 21\ (\pm 3) - 0.028\ (\pm 0.005)\ \sigma_{PSII}'$, *Fig. 5.10d*), was used to convert *in situ* measurements of σ_{PSII}' to equivalent P^*_{max} values.

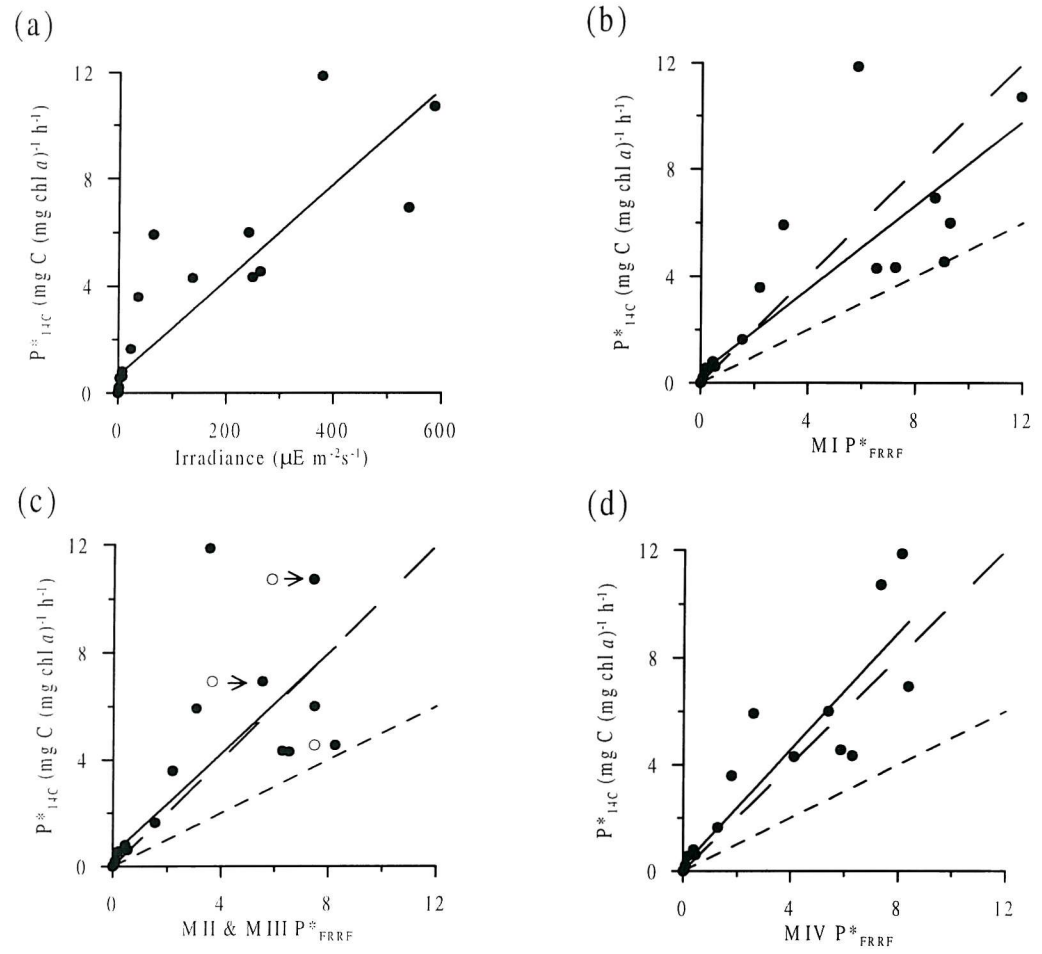

Fig. 5.13 Relationships between ^{14}C and FRRF derived P* and irradiance for 2000 cruise (a) ^{14}C derived P* vs. instantaneous irradiance at the time of sampling. (b) ^{14}C derived vs. FRRF (MI) derived P*. (c) ^{14}C derived vs. FRRF (MII (open symbols) and MIII (closed symbols)) derived P*. Note: MII and MIII values of P* only vary for a few data points, arrows indicate these pairs. (d) ^{14}C derived vs. FRRF (MIV) derived P*. Dashed lines in (c-d) indicate a 1:1 relationship while dotted lines indicate a 2:1 relationship. Thus the area between the dotted and dashed lines represents PQ values of 1-2. Solid lines are linear fits to the data. Percentage variances explained were: (a) 79% *(95%)*, (b) 74% *(96%)*, (c) MII 58% *(95%)*, MIII 62% *(95%)* and (d) 86% *(97%)*. ($p < 0.001$ for all) Values in parentheses are for log transformed data.

P* values calculated using all four models applied to the FRRF data were again significantly positively correlated with P* estimated using the ^{14}C data (*Fig. 5.13*). However as with the 1999 data set, only the empirical (MIV) model could explain a greater proportion of the variance in the ^{14}C data than could be explained by irradiance alone (*Fig. 5.13d*). Improved correlations for log transformed data once again emphasised the dependence of FRRF derived production at high light levels on evaluation of E_K. Overall the FRRF derived productivity rates were around the same magnitude as the ^{14}C derived rates for all the models.

5.4 Discussion

Empirical relationships between FRRF and ^{14}C derived physiology

Investigation into relationships between FRRF and ^{14}C derived physiology resulted in few general relationships being valid both within and across the two data sets (*Figs. 5.3 & 5.10*). The 1999 and 2000 P* vs. E data sets were collected under markedly different environmental conditions. The 1999 data was collected in summer and in a region dominated by barotropic tides and shelf sea fronts (Chapter 3), while the 2000 data set was collected during spring in a region dominated by internal tidal motions (Chapter 4). Differences in both the community structure and physiology of the phytoplankton populations may therefore have been expected. Additionally the 1999 data set consisted of samples collected at a variety of sites with widely varying nutrient and light conditions whilst the 2000 data were collected at a single site over a relatively short time period.

High mixing rates at the PK site in 2000 implied that nutrient limitation was unlikely (Chapter 4), thus the lack of variability in F_v/F_m was perhaps not surprising (*Fig. 5.10a*). Differences in α^* and P^*_{max} were apparent despite low variability in F_v/F_m,, indicating that photochemical efficiency was of minor importance in determining production and carbon fixation at PK during the study period. Conversely some of the sites sampled during the 1999 cruise had undetectable nutrient concentrations and lower F_v/F_m which was associated with lower α^* and also some indication of lower P^*_{max} (*Fig. 5.3*). Lower F_v/F_m under conditions of nutrient stress (starvation) is consistent with previous work (Kolber *et al.* 1988; Kolber *et al.* 1990; Parkhill *et al.* 2001) and the results from the 1999 cruise suggest that low photochemical efficiencies limited carbon fixation at some of the sites studied (*Fig. 5.3*).

The only relationship which appeared to be valid across the two data sets was a negative correlation between P^*_{max} and σ_{PSII}' (*Figs. 5.3d & 5.10d*). Different geographical sites, containing distinctly different phytoplankton communities were sampled during the 1999 cruise. The relationship between these two completely independently derived physiological parameters may therefore have been driven by taxonomic variability. The highest observed P^*_{max} and lowest values of σ_{PSII}' were generally associated with the region towards the mixed side of the front, where diatom and dinoflagelates dominated the community (Chapter 3). For the 2000 cruise all the P* vs. E experiments were run on samples collected at PK. Coastal (upwelled) water, containing a large cell dominated (diatom) bloom, and off-shore sub-tropical water, were sampled at different times during the occupation of PK

(Chapter 4). These two water bodies had associated phytoplankton communities characterised by different functional absorption cross sections and maximal photosynthetic rates. The highest values of P^*_{max} and lowest σ_{PSII} (σ_{PSII}') were associated with the diatom dominated coastal water sampled at PK on 2nd December (*Fig. 5.10d*).

It was therefore unclear from the present study whether the observed relationships between P^*_{max} and σ_{PSII} resulted from a gradient in community structure in response to varying environmental conditions, and/or was the result of a more fundamental physiological mechanism. For example diatom dominated communities during both cruises tended to be associated with higher maximal photosynthetic rates and lower functional absorption cross sections. Such a relationship is consistent with the hypothesis that diatoms are characterised by high growth rates and occupy ecological niches where relative high nutrients and adequate light are available. Whether the observed balance between σ_{PSII}' and P^*_{max} is a contributory factor to, or consequence of, such adaptations to environmental conditions is not clear. However subsequent to the work of Behrenfeld *et al.* (1998), the following possibility argued on physiological grounds is suggested.

Possible balances between electron transport rates and light utilisation

From (Eq. 5.8) the reciprocal of σ_{PSII} may be expected to vary with the saturation light intensity (E_K), particularly under conditions of a relatively constant turnover time for electron transport through PSII reaction centres (τ_{PSII}). Significant positive correlations between E_K and $1/\sigma_{PSII}$' were found for both the 1999 and 2000 data sets, although the observed relationships varied between the two cruises as a result of the large differences in the range of E_K estimates from the P* vs. E experiments (*Fig 5.14a*). As previously mentioned, no cross comparison between the two ^{14}C data sets was possible, additionally E_K values for the 2000 cruise would have been likely to change considerably if spectrally corrected. It was therefore not possible to determine whether genuine physiological differences or methodological problems were responsible for the very different E_K values. It is noted that when normalised to the mean a value of E_K for each data set, around 45% of the relative variance in all the ^{14}C derived saturation light intensities could be explained by regression against $1/\sigma_{PSII}$' (*Fig. 5.14b*).

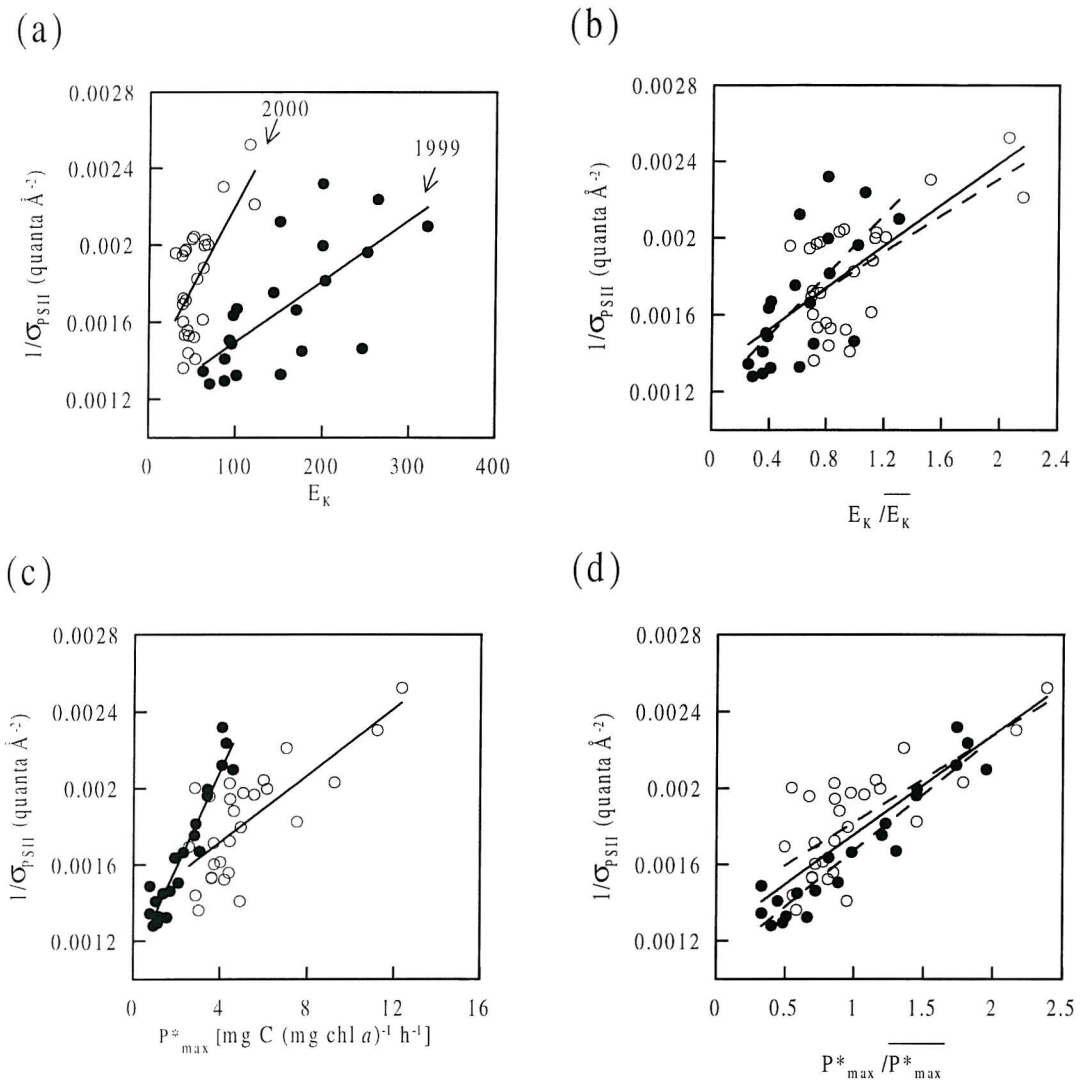

Fig. 5.14 Relationships between E_K, P^*_{max} and the reciprocal of σ_{PSII}' for both the 1999 and 2000 data sets. E_K and P^*_{max} are derived from the ^{14}C P* vs. E experiments, while σ_{PSII}' was measured *in situ* by FRRF

(a) $1/\sigma_{PSII}$' vs. E_K for 1999 (closed symbols) and 2000 (open symbols) solid lines indicate linear fits ($R^2 = 0.476$, n = 21, p = 0.001 & $R^2 = 0.419$, n = 27, $p < 0.001$ for 1999 and 2000 respectively).

(b) $1/\sigma_{PSII}$' vs. E_K normalised to the mean value for each data set, 1999 (closed symbols) and 2000 (open symbols). Dotted lines indicate linear fits for individual cruises, solid line indicates linear fit for all data ($R^2 = 0.450$, n = 48, $p < 0.001$).

(c) $1/\sigma_{PSII}$' vs. P^*_{max} for 1999 (closed symbols) and 2000 (open symbols) solid lines indicate linear fits ($R^2 = 0.899$, n = 21, $p < 0.001$ & $R^2 = 0.550$, n = 27, $p < 0.001$ for 1999 and 2000 respectively).

(d) $1/\sigma_{PSII}$' vs. P^*_{max} normalised to the mean value for each data set, 1999 (closed symbols) and 2000 (open symbols). Dotted lines indicate linear fits for individual cruises, solid line indicates linear fit for all data ($R^2 = 0.677$, n = 48, $p < 0.001$).

Rearranging (Eq. 5.8) P^*_{max} should be related to α^*, τ_{PSII} and σ_{PSII} according to (e.g. Falkowski 1992; Falkowski and Raven, 1997; Behrenfeld *et al.* 1998):-

$$P^*_{max} = \frac{\alpha^*}{\sigma_{PSII}' \tau_{PSII}} \tag{5.10}$$

Thus P^*_{max} should be inversely related to σ_{PSII}' if α^* and τ_{PSII} are constant or co-vary. Around 90% of the variance in P^*_{max} was explained by regression against $1/\sigma_{PSII}'$ for the 1999 data. For the 2000 data set, the explained variance in P^*_{max} increased from 44% for regression against σ_{PSII}' to 55% for regression against $1/\sigma_{PSII}'$ (*Figs. 5.14c*). Again the relationships varied significantly between cruises. Normalisation indicated that around 68% of the variance in relative P^*_{max} from both data sets could be explained by variability in $1/\sigma_{PSII}'$ (*Fig. 5.14d*). It is therefore suggested that the physiological and/or taxonomic response of the differing phytoplankton communities to changes in environmental conditions may have caused the value of α^*/τ_{PSII} (c.f. Eq. 5.10) to remain constant.

Values of τ_{PSII} were calculated using (Eq. 5.8) for the subset of the 1999 data for which spectral correction was possible and neglecting the thermocline at U2 where values of α^* were considered suspect (§ 5.2.3). A significant positive correlation was observed between α^* and τ_{PSII}, values of τ_{PSII} ranging from around 2 ms at low α^* to around 4.5 ms at high α^*. These values were comparable to previous estimates and provided further support for a constant α^*/τ_{PSII} whether it be in a physiological or ecological sense (Kolber and Falkowski, 1993; Behrenfeld *et al.* 1998). Accurate calculations of τ_{PSII} for the 2000 data set were not possible as spectral correction of the FRRF and photosynthetron light sources could not be performed. However a balance between α^* and τ_{PSII} was strongly implied (5.10, *Fig. 5.14c & d*).

Behrenfeld *et al.* (1998) showed that under conditions of photoinhibition, decreases in the number of functional reaction centres, and hence α^*, can be accompanied by a decrease in τ_{PSII}. Greene *et al.* (1991) reported an increase in σ_{PSII} and a decrease in P^*_{max} under iron limitation of a marine diatom, these changes being accompanied by an increase in both α^* and τ_{PSII}, again in agreement with (Eq. 5.10). Kolber *et al.* (1988) reported increases in relative σ_{PSII} and decreases in P^*_{max} under nitrate limitation of a marine diatom. At present the author knows of no similar studies relating changes of α^* to τ_{PSII} under conditions of longer term photo-acclimation, nor any comprehensive studies of taxonomic variations in σ_{PSII} and P^*_{max}. However the bulk of available evidence suggests that a physiological

mechanism was at least partially responsible for the observed inverse relationships between P^*_{max} and σ_{PSII}.

The differences in P^*_{max} as measured by ^{14}C P* vs. E experiments during 1999 and 2000 can now be re-addressed. It can be hypothesised that the marked change in carbon fixation physiology could have resulted from a change in the ratio α^*/τ_{PSII} between the phytoplankton populations studied during the two cruises. Regardless of whether this was the ultimate cause of the difference between the ^{14}C data sets, the possibility of balances between α^* and τ_{PSII} and/or marked changes in τ_{PSII} or α^*/τ_{PSII} has implications for the calculation of productivity from FRRF data which are discussed below.

FRRF productivity model and α^*

Previous comparisons between active fluorescence and ^{14}C derived productivity estimates have often concentrated on comparing estimates of P* (Kolber and Falkowski, 1993; Suggett *et al.* 2001). Within the majority of data sets both ^{14}C and FRRF derived P* will be highly dependent on irradiance (*Figs 5.9a & 5.13a*). Close agreement between the two methods may therefore merely reflect this dependence on irradiance (*Figs 5.9 & 5.13*). A more stringent test of the compatibility of the two techniques is thus to test whether physiological indices such as α^* are comparable for the two methods.

Such studies have been performed on field populations of phytoplankton using Pump and Probe fluorometery and ^{14}C P* vs. E experiments (Boyd *et al.* 1997). Field populations of microphytobenthos (Hartig *et al.* 1998), laboratory phytoplankton cultures (Gilbert *et al.* 2000) and field cyanobacterial blooms (Mesojidek *et al.* 2001) have been studied using Pulse Amplitude Modulated (PAM) fluorescence and O_2 evolution. For the PAM and Pump and Probe studies, changes in P* or α^* which could have resulted from alteration of σ_{PSII} could not be accounted for, as σ_{PSII} could not be measured. Suggett *et al.* (2001) compared FRRF estimates of α^* and P^*_{max} generated from a series of vertical profiles at three open ocean stations with ^{14}C P* vs. E derived values.

Results from these studies have been equivocal. Boyd *et al.* (1997) found significant correlations between F_v/F_m and ^{14}C based α^* but no significant relationship between fluorescence and ^{14}C based α^*. Conversely positive correlations between fluorescence and ^{14}C derived α^* were found by Hartig *et al.* (1998) and Mesojidek *et al.* (2001), although absolute values varied. Gilbert *et al.* (2000) found comparable absolute values for α^* but no correlations. These authors also emphasise that the differences between the empirical

models used to describe the P* vs. E relationship can cause marked changes in the photosynthetic parameters calculated. Suggett *et al.* (2001), found values of FRRF derived P^*_{max} and α^* were around 1.5-2.5 times higher than ^{14}C derived values, trends in parameters between the three sites studied were not consistent between the two techniques.

The FRRF technique may be expected to overestimate the carbon fixation rate for a number of reasons. Reducing power generated by the light reactions may be used for processes other than carbon fixation, for example nitrate reduction. This will alter the photosynthetic quotient (PQ) away from 1, with typical values in the marine environment tending to be close to the theoretical upper limit of 1.4 for nitrate as the N source (Laws, 1991). Although values of PQ greater than 1.4 may not theoretically be possible, reported values for natural phytoplankton populations measured by combined ^{14}C incorporation/O_2 evolution experiments are often found to be 2-3 (Holligan *et al.* 1984b; Williams and Robertson, 1991).

Physiological processes which act as sinks for electrons will also de-couple the ETR from both oxygen evolution and carbon fixation (Flameling and Kromkamp, 1998; Suggett *et al.* 2001). These processes include cyclic electron flow around PSII (Falkowski *et al.* 1986; Prasil *et al.* 1996), photorespiration (Raven and Johnston, 1991), mitochondrial respiration (Grande *et al.* 1989; Daneri *et al.* 1992) and the Mehler reaction (Kana, 1992). Cyclic electron flow around PSII and the Mehler reaction are likely to be the most important processes, however both are likely to be of greatest significance at irradiances approaching or exceeding E_K (Flameling and Kromkamp, 1998; Suggett *et al.* 2001).

Additionally when comparing the FRRF and ^{14}C techniques the limitations of the latter must be recognised. While the FRRF derived estimate of ETR is a completely *in situ* technique, the ^{14}C based estimates of carbon fixation require collection and manipulation of samples. The enclosure of natural phytoplankton communities during the incubation period can result in problems such as bottle effects and trace metal toxicity (Peterson, 1980; Carpenter and Lively, 1980; Fitzwater *et al.* 1987). Determining the influence of respiration on the ^{14}C derived carbon fixation estimate and hence the degree to which the ^{14}C technique measures net or gross photosynthesis is also problematic (Bender *et al.* 1987; Geider, 1992; Williams *et al.* 1996). The ^{14}C technique may therefore underestimate gross carbon fixation in many instances.

Absolute values of α^* estimated using the FRRF and ^{14}C techniques were comparable and weakly correlated for a subset of the 1999 data, with FRRF α^* a factor of around 1.7 times ^{14}C α^* (*Fig. 5.5*). This higher α^* using the FRRF technique is at least partially explainable by a PQ of around 1.4 (Laws, 1991; Kolber and Falkowski, 1993; Suggett *et al.* 2001). For site E and the thermocline at U2, FRRF derived α^* was around 3-4 times greater than ^{14}C derived α^* (*Fig. 5.6*). Interestingly both of these locations were either associated with, or in the declining stages of, blooms of coccolithoporids.

Spectral correction was not possible for the 2000 data set, however absolute values of α^* estimated using the two methods diverged in a direction which could not be accounted for by spectral effects (*Fig. 5.13*). Additionally no general patterns were observed between the two techniques. However some suggestion of trends on individual days, and differences between the coastal and sub-tropical phytoplankton populations was evident (*Fig. 5.13*). Some of this variability may have resulted from differences in the absorption characteristics of the two phytoplankton populations sampled during 2000. Again the possibility that the relationship between fluorescence based and carbon fixation based photophysiology is taxonomically dependent needs to be considered. The very different situation as regarded α^* for the 2000 data set was thus somewhat intractable due to the lack of spectral correction and the large discrepancy with the 1999 data.

Practicalities of comparing FRRF and ^{14}C estimates of physiological parameters

Attempts to compare *in situ* FRRF based estimates of production with ^{14}C carbon fixation based estimates derived by incubation of discrete samples must recognise the current limitations of/and differences between, the two techniques. Apart from the expected physiological differences between ETR and carbon fixation, vertical profiling using the FRRF cannot produce P^* vs. E curves for every depth and time. Additionally the FRRF provides a (near) instantaneous point measurement of the physiological state, while P^* vs. E incubations necessarily run over a finite time (typically O(1hr)). The time-scale for ^{14}C incubation experiments is thus comparable to the time-scales of the relaxation/ initiation of physiological processes such as non-photochemical quenching (Kolber and Falkowski, 1993, see also *Fig. 4.26*) and hence photo-acclimation can occur during the P^* vs. E measurement. Thus rather than being an instantaneous measure of the physiological state, the P^* vs. E experiment provides an integrated view of an evolving process.

A simple model illustrates this point and indicates the potential magnitude of artefacts that could be introduced if acclimation occurs during the course of a P^* vs. E experiment. The

collection and incubation of a sample containing a phytoplankton population was modelled in order to compare P* vs. E curves obtained after certain incubation periods, with the *in situ* physiological state of the population. The acclimation and photosynthesis of the sample within the photosynthetron was modelled using parameters derived from field data collected during both the 1999 and 2000 cruises. Model details are presented in *Appendix 8*.

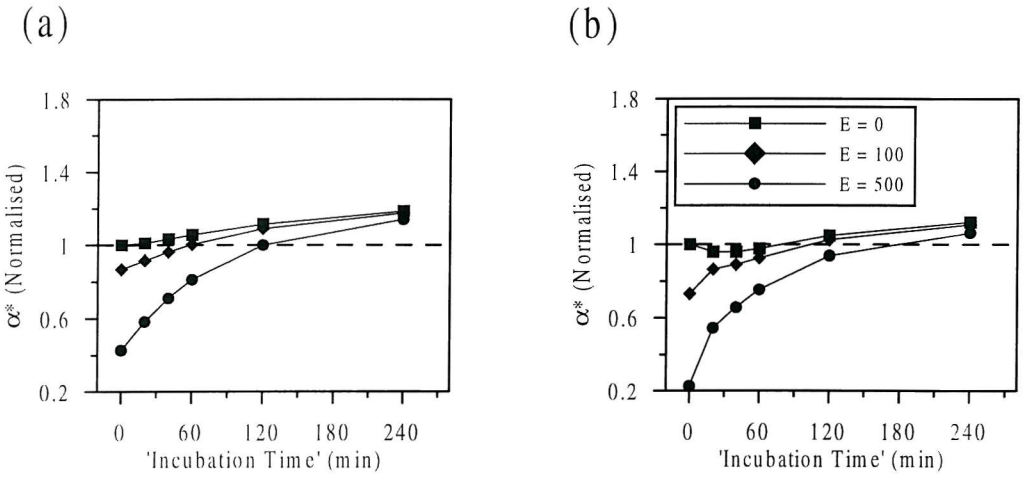

Fig. 5.15 Results from a simple model of photo-acclimation within a photosynthetron. Plots indicate the relative changes in α* as a function of incubation time for the simulated sampling of a population at a variety of *in situ* irradiances: 0 (squares), 100 (diamonds) and 500 (triangles) μ E $m^{-2}s^{-1}$. (a) and (b) simply differ in the modelled relationship between $\Delta F'/F_M'$ and irradiance (see *Appendix 8*).

The model reproduced patterns of variation in α* and photo-inhibition which were consistent with conceptual expectations and comparable to field data (see *Appendix 8* & Suggett *et al.* 2001). In order to investigate the possible magnitude of variations in α* between FRRF and ^{14}C techniques, results were normalised to the value of α* calculated using (Eq. 5.4) for FRRF data, i.e. to the value which would be calculated using F_v/F_m and σ_{PSII} (*Fig. 5.15*). A 'zero' incubation time thus corresponded to the value of α* which would be inferred if the *in situ* $\Delta F'/F_M'$ and σ_{PSII}' were substituted for F_v/F_m and σ_{PSII} in (Eq. 5.4). The model suggested that the largest discrepancies between the values of α* inferred from FRRF data (i.e. *in situ*) and those derived from ^{14}C would occur if a high light acclimated sample were incubated for a short time period, or under conditions of long incubation times (*Fig. 5.15*). The results also indicated that α* inferred from the instantaneous values of $\Delta F'/F_M'$ and σ_{PSII}' measured *in situ* could have been expected to

deviate significantly from the values calculated using F_v/F_m and σ_{PSII} and those inferred using P* vs. E incubations over realistic time-scales (1hr).

Overall deviations in the most extreme conditions approached 80%. However the model takes no account of the practical situation, where water samples are held for a short time in the dark within sampling bottles before the P* vs. E incubations are run. Indeed the results suggested that an extended period of dark acclimation of order 30 minutes, followed by a short time period incubation would be the optimal sampling strategy for comparing ^{14}C and FRRF derived α^* values. Artefacts introduced using such sampling strategies could be expected to be <20%.

Comparisons of FRRF and ^{14}C productivity rates: E_K and further practical considerations

As previously stated, generally high correlations between FRRF and ^{14}C derived productivity using a variety of methods for the calculation of E_K mainly reflected the dependency of P* on irradiance (*Figs. 5.9 & 5.13*). This was particularly evident for the 2000 data set, where the incompatibility of α^* calculated by the FRRF or ^{14}C techniques made little difference to the patterns of P* (*Figs. 5.11 & 5.13*). The major difference between the two ^{14}C data sets was only apparent when mean ratios of FRRF to ^{14}C derived P* were calculated. For both data sets, only the empirical models based on the observed relationships between P^*_{max} and σ_{PSII}' could predict carbon fixation as measured by the ^{14}C technique with more skill than could be achieved with the *in situ* irradiance alone.

The high dependence of FRRF derived productivity on the evaluation of E_K (or P^*_{max}), which are governed by the turnover time (τ_{PSII}) of the whole electron transport chain from water splitting to carbon fixation, is thus highlighted. This presents several potential weaknesses in the FRRF productivity technique. Firstly, even if it is assumed that the decrease in $\Delta F'/F_M'$ with increasing irradiance can be used to infer E_K (Kolber and Falkowski, 1993), no practical way of following variations in E_K both temporally and spatially presently exists. Secondly a number of studies suggest that the carbon fixation processes of the Calvin – Benson cycle actually limit photosynthesis at saturating light intensities (Sukenik *et al.* 1986; Falkowski and Raven, 1997). For example Sukenik *et al.*, (1986) demonstrated that the ratio of Rubisco to PSII reaction centres varies linearly with $1/\tau_{PSII}$ and thus the Rubisco catalysed carboxylation reaction may be the rate limiting step at light saturation. The question of whether/how the redox states of the members of the inter photosystem transport chain, are related to the enzymatically mediated reactions of the Calvin – Benson cycle then becomes of crucial importance if E_K is to be evaluated

using the $\Delta F'/F_M'$ and irradiance relationship (Kolber and Falkowski, 1993). For example cyclic electron flow around PSI could serve to de-couple the redox state of the PQ pool from the Calvin – Benson cycle and thus the relationship between quenching and E_K. The empirical relationships between P^*_{max} and σ_{PSII}' observed within the data sets studied here, which agreed with certain theoretical considerations, may represent a way around these problems. If verified, such a relationship allows P^*_{max} and hence E_K and/or τ_{PSII} to be inferred from σ_{PSII}' (Eqs. 5.8 & 5.10). However the dangers of forcing biophysical or empirical models of photosynthesis based on FRRF data to correspond to carbon fixation rates as measured by ^{14}C uptake must be recognised. This is clearly illustrated when an attempt is made to reconcile the FRRF P* and ^{14}C P* relationships within both data sets (*Fig. 5.16*).

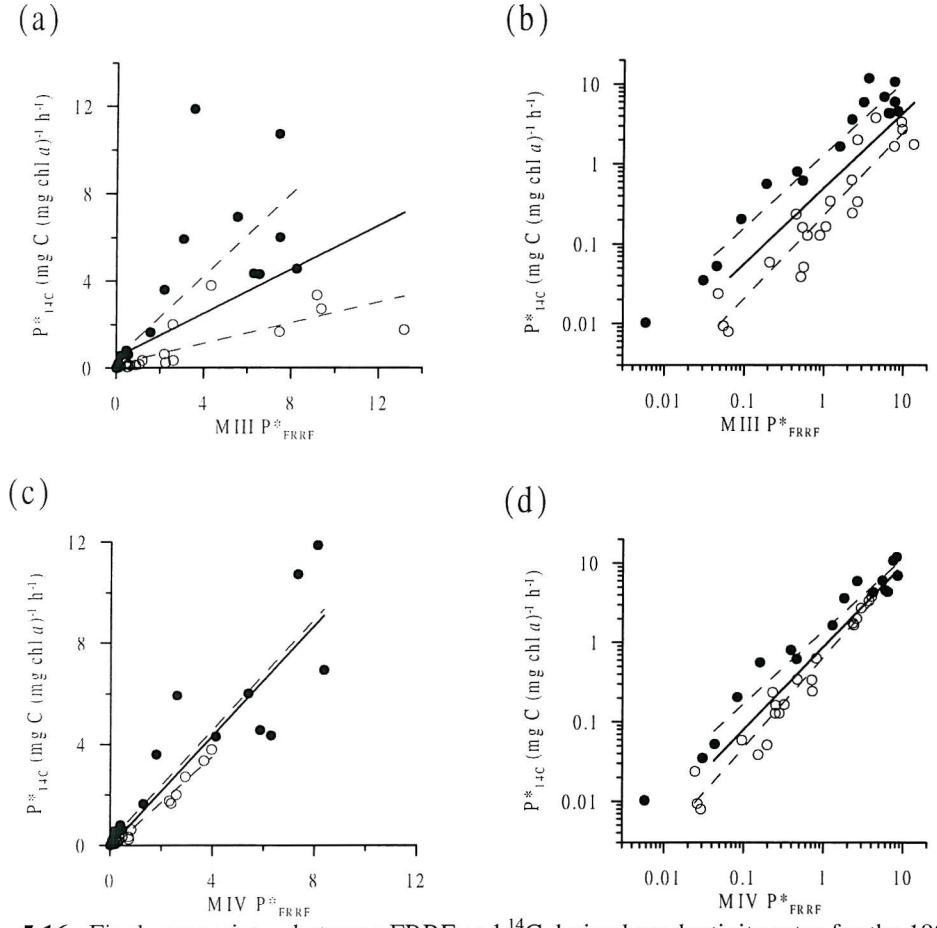

Fig. 5.16 Final comparisons between FRRF and ^{14}C derived productivity rates for the 1999 and 2000 ^{14}C P* vs. E experiments. (a) & (b) ^{14}C derived P* vs. MIII FRRF derived P* for the 1999 (open symbols) and 2000 (closed symbols) data sets. Dotted lines indicate linear regressions for the individual data sets, while solid lines indicate regressions for all the data. ($R^2 = 0.357$ for linear (a) or 0.750 for log transformed (b) data, $n = 47$, $p < 0.001$ for all). (c) & (d) ^{14}C derived P* vs. MIV FRRF derived P* for the 1999 (open symbols) and 2000 (closed symbols) data sets. Solid lines indicate regressions for all the data. ($R^2 = 0.867$ for linear (a) or 0.913 for log transformed (b) data, $n = 47$, $p < 0.001$ for all).

For the MIII model FRRF derived productivity rates are similar for the 1999 and 2000 data sets, but a clear offset is apparent between the ^{14}C derived rates between the two years (*Fig. 5.16a & b*). Conversely, using the empirical model (MIV), FRRF based P* estimates are forced to correspond to the ^{14}C derived values. A robust relationship is therefore obtained which can explain over 85% of the variance in all the data between the two techniques. However if systematic errors in one (or both) of the ^{14}C data sets were responsible for the large differences in ^{14}C derived carbon fixation rates, then using the empirical method propagates these errors into the FRRF based P* estimates.

Summary and conclusions

The FRRF technique measures physiological parameters related to light absorption and primary charge separation within PSII of phytoplankton. Using biophysical models of photosynthesis these measurements can be used to derive estimates of ETR and ultimately production (Genty *et al.* 1989; Kolber and Falkowski, 1993).

As expected, productivity rates were strongly controlled by the ambient irradiance. Estimates of productivity using the FRRF technique are then crucially dependent on the calculation and variability of E_K or P^*_{max}. Such a view is in keeping with the majority of recent studies, which suggest that ETR and production are tightly coupled at low irradiances, but deviate as irradiance approaches E_K (Prasil *et al.* 1996; Flameling and Kromkamp, 1998; Gilbert *et al.* 2000; Masojidek *et al.* 2001). Evaluation of the mechanisms responsible for such deviation is thus of primary importance. Specifically, as discussed by Flameling and Kromkamp (1998), the relative contribution of physiological processes such as the Mehler reaction, or rate limitation by the Calvin – Benson cycle must be evaluated. The latter process is crucially linked to the question of evaluating τ_{PSII} and/or E_K from fluorescence based measurements (Kolber and Falkowski, 1993).

The calculation of P* using the FRRF technique, and comparisons between FRRF and ^{14}C experiments, must take into account the practicalities of applying both techniques within a water column. Neglecting such considerations could result in discrepancies between techniques being falsely ascribed to physiological causes, when the very different sampling system was actually responsible.

The data presented here demonstrate that changes in PSII photo-physiology, as measured by the FRRF, were often accompanied by changes in physiological parameters relating to carbon fixation rates. Additionally certain of the observed relationships were consistent with current biophysical models of photosynthesis (Falkowski and Raven, 1997). However

few robust relationships were apparent between the two data sets. Further detailed study of the relationship between FRRF derived photophysiology and carbon fixation is required. Particular attention to possible variations across different taxonomic groups and environmental conditions may be required before FRRF based models of productivity can be applied with confidence across varying ecological systems.

6. Synthesis of productivity estimates

6.1 Introduction

The productivity of the sites studied during all three cruises was assessed using a variety of techniques. Productivity estimates were broadly divided into two principal types. First the *in situ* primary production was estimated using either ^{14}C uptake experiments or biophysical models applied to FRRF data. Second the potential for new production at a site was calculated by estimating the physically driven vertical nutrient (typically nitrate) flux, then assuming that the flux balanced the uptake. The FRRF and ^{14}C based *in situ* primary production estimates are compared. Estimates of primary production and new production are then combined to give an overview of the productivity of the sites/systems studied. Estimates of population growth rates are made, highlighting the problems of inadequate data on phytoplankton C:Chl ratios. Finally, possible physical mechanisms responsible for variations between regimes are considered.

6.2 ^{14}C and FRRF *in situ* primary productivity estimates from 1999 cruise

6.2.1 ^{14}C derived in situ productivity

The *in situ* productivity at the four 25hr stations (U2, E, M2 & M3) occupied during the 1999 cruise (Chapter 3) was estimated using on deck simulated *in situ* ^{14}C experiments (see Chapter 2 for method). Standard deviations of the productivity on individual samples incubated in triplicate were typically around 15%. Volume specific *in situ* productivity as measured by the ^{14}C technique was converted to profiles of chlorophyll specific productivity (P*) using the measured chlorophyll concentrations. Vertical profiles of ^{14}C derived simulated *in situ* productivity were of expected forms (*Fig. 6.1*). Chlorophyll specific productivity (P*) generally increased towards the surface, with a sub-surface maximum in production being apparent at some sites (*Fig. 6.1 a – d*). Increasing P* towards the surface resulted from increasing irradiance, while some depression at the highest irradiances was indicative of photoinhibiton. The maximum value of productivity within the water column corresponded to P^*_{opt}, the water column analogue of P^*_{max} (Behrenfeld and Falkowski, 1997; Falkowski and Raven, 1997). Vertical profiles of ^{14}C derived volume specific productivity (P) were influenced by the distribution of chlorophyll through the water column combined with the

increase of P* towards the surface (*Fig. 6.1 e – h*). The most striking feature was the strong maximum in volume specific production associated with the marked DCM within the thermocline at U2 (*Fig. 6.1e*).

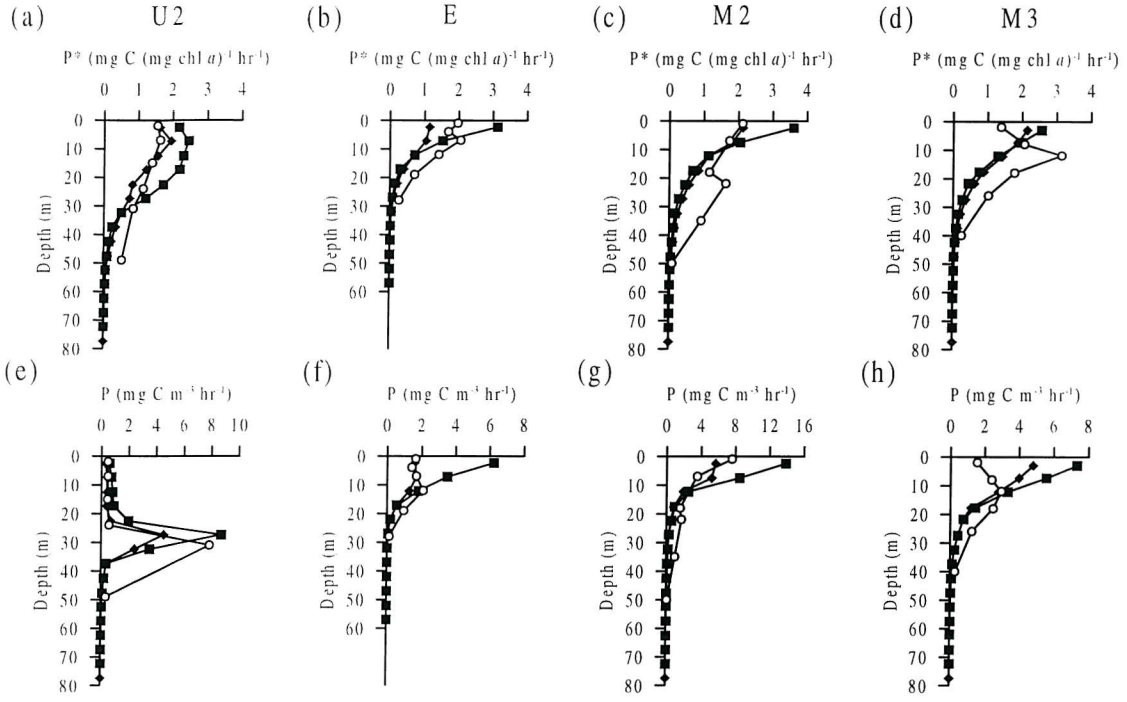

Fig 6.1 Vertical profiles of chlorophyll specific (P*, a-d) and volume specific (P, e-h) productivity from all four 25hr stations occupied during the 1999 cruise, U2 (a & e), E (b & f), M2 (c & g) and M3 (d & h). Open symbols are the mean of three replicates from ^{14}C simulated in situ incubations. Closed symbols are the mean daily productivity, calculated by applying the photosynthetic model (MIII, squares and MIV, diamonds) to the 24hr time-series of in situ FRRF data. Volume specific rates derived from the FRRF data were calculated using the observed time series of F_M calibrated against discrete chlorophyll samples (*Appendix 3*). Note: integration times varied for ^{14}C incubation experiments but were generally O (6 – 8 hrs), thus plotted values for ^{14}C experiments are averages over a fraction of day length while FRRF values are for integrals over 24hrs.

6.2.2 FRRF derived in situ productivity

Vertical profiles of chlorophyll specific productivity were also generated by applying two of the models (MIII and MIV) introduced in Chapter 5 to the *in situ* FRRF data. MIII was chosen as it attempted to account for the greatest degree of variation in E_K within the water column. The empirical model MIV was chosen as it displayed the best agreement with ^{14}C P* vs. E derived productivity estimates (see *Fig. 5.16*). The principal difference between MIV and MIII was that the former was tuned to the values of P^*_{max} derived from the P* vs. E

experiments. The photosynthetic quotient for estimation of *in situ* rates was assumed to be 1.4 (Laws, 1991). The mean daily productivity for each depth was calculated by integrating the time series of FRRF productivity estimates at that depth over 24hrs.

The derived vertical profiles of P* were similar in shape to the ^{14}C simulated *in situ* profiles, typically decreasing with depth with some near surface decrease apparent at U2 (*Fig. 6.1a-d*). Profiles of the volume specific productivity calculated form the FRRF technique were also similar to ^{14}C simulated *in situ* profiles, although FRRF derived values diverged from ^{14}C values in the near surface at E and M3. The peak in volume specific productivity at U2 was captured by both FRRF based models and the ^{14}C technique (*Fig. 6.1e*).

6.2.3 Overall comparisons between in situ productivity estimates

The *in situ* ^{14}C and FRRF derived productivity rates were positively correlated with >40 % of the variance in ^{14}C P* and >50% of the variance in ^{14}C volume specific production (P) explained using the models applied to FRRF data (*Fig. 6.2*). Logarithmic transformation of the data increased the variance explained to >75 % and >67% for chlorophyll (P*) and volume (P) specific production respectively (*Fig. 6.2*). The MIV FRRF model was capable of predicting ^{14}C derived productivity with greater skill than the MIII model, with 82% and 76% of the variance in log transformed data for P* and P being explained. Some deviation from a 1:1 relationship between the two methods was apparent at low light levels (*Fig. 6.2*).

6.2.4 Integrated daily productivity

The daily productivity ($\int P$) at the four 25hr stations was estimated by integrating the vertical profiles of volume specific production. Due to variable incubation times, ^{14}C derived integrated rates required scaling to 24hrs. Estimated errors in the integrated rates, taking into account the measured spread of samples run in triplicate, were typically < 10% for simulated *in situ* ^{14}C data. For the MIII and MIV models applied to the FRRF data, errors in individual estimates of $\Delta F'/F_M'$ and σ_{PSII}' as well as estimates of E_K needed to be accounted for in estimating the error in the integrated rate. A bootstrapping technique was eventually chosen whereby 100 replicated calculations of daily productivity for each site were performed using randomly generated 'noise' within the $\Delta F'/F_M'$, σ_{PSII}' and E_K values. The statistics of the 'noise' were chosen to conform to the observed errors in the measured parameters. Total errors in integrated rates were estimated to be around 10 – 15% using the bootstrapping technique.

Integrated daily rates were comparable using the ^{14}C and both the FRRF methods (*Table 6.1*). However absolute values varied, with MIII and MIV FRRF derived rates being around 1.3 and 2.1 times ^{14}C derived rates respectively (*Table 6.1*). The total range of production estimates (from 0.5 – 2.3 g C m^{-2} d^{-1}) was similar to previous values from the region (Holligan *et al.* 1984b; Videau 1987). Patterns of variation between sites were well replicated across techniques with the lowest productivity found at E and the highest at M2. Daily production at the other sites (M3 & U2) was intermediate, the ^{14}C and MIV FRRF estimates suggesting that M3 was marginally more productive than U2.

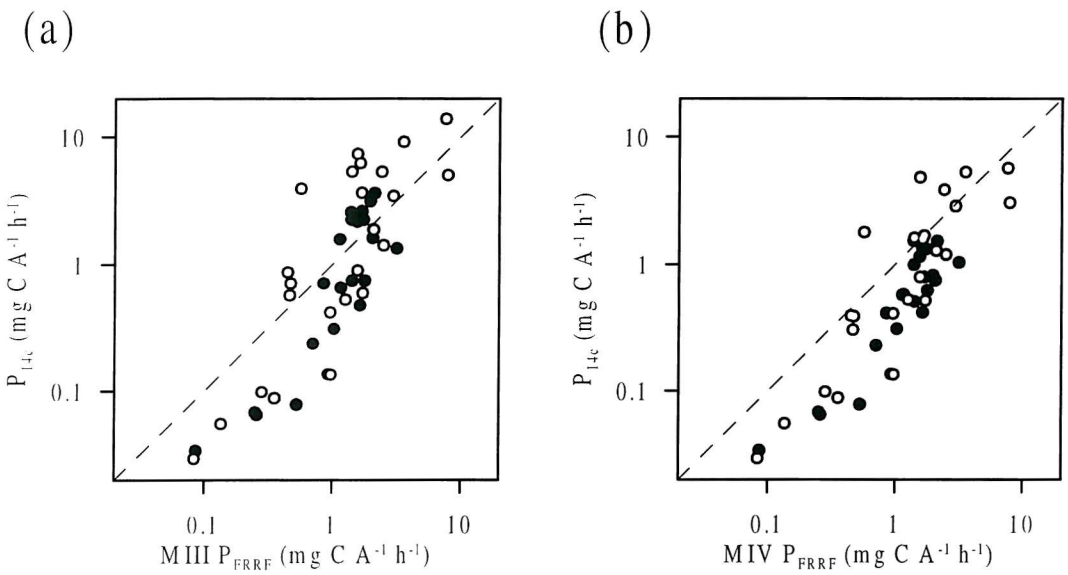

Fig. 6.2 Comparisons of FRRF and ^{14}C simulated *in situ* derived estimates of *in situ* productivity rates for four 25hr stations occupied during 1999. (a) FRRF MIII derived chlorophyll specific (P*, filled symbols, A = mg chl *a*) and volume specific (P, open symbols, A = m^3) productivity vs. simulated *in situ* ^{14}C values. (b) FRRF MIV derived productivity vs. ^{14}C values, symbols as in (a). Dotted lines indicate 1:1 relationship.

The possibility that some variations between the FRRF and ^{14}C derived *in situ* integrated rates resulted from deviations in PQ cannot be discounted. The assumption of a fixed PQ was likely to be invalid when considering sites with markedly different nutrient characteristics. For example Holligan *et al.* (1984b) found differences in PQ on the order of 50% around the Ushant front using combined ^{14}C and O_2 incubation experiments.

Station	∫P (^{14}C)	∫P (FRRF MIII)	∫P (FRRF MIV)
U2	0.8	2.0	1.1
E	0.5	1.1	0.5
M2	1.3	2.3	1.4
M3	0.9	1.8	1.4

Table 6.1 Estimated productivity (g C m^{-2} d^{-1}) at the four sites studied during the 1999 cruise. Values are integrated daily (24hr) rates using simulated *in situ* ^{14}C data and MIII and MIV applied to *in situ* FRRF data.

6.3 FRRF derived *in situ* productivity from the 2000 cruise: possible magnitudes of spectral effects

Daily mean productivity for the PK site studied during the 2000 cruise was calculated from the FRRF data as above using the MIII and MIV models (*Table 6.2*). The photosynthetic quotient (PQ) was again assumed to be constant = 1.4. Estimated production rates ranged from around 1.5-3 g C m^{-3} d^{-1} and were relatively insensitive to the model used for the 2000 data. *In situ* spectral data were available for the 2000 cruise. A second series of calculations were therefore performed in order to estimate the sensitivity of the *in situ* productivity calculation to differences between the spectral characteristics of the FRRF excitation source and the *in situ* irradiance field. Unfortunately no phytoplankton absorption spectra were available for the 2000 cruise. Correction factors to convert the values of σ_{PSII}' (and hence P*) measured by the FRRF to those values corresponding to the *in situ* light field were thus calculated assuming that the phytoplankton absorption spectra were similar to the mean spectrum from the 1999 cruise. Following the arguments in § 5.1, the weighted mean absorption accounting for the spectral quality of the excitation source was calculated according to (Eq. 5.2). The correction factor to convert FRRF measurements to equivalent *in situ* values was thus:

$$X = \frac{\overline{a_{insitu}}^{*}}{\overline{a_{FRRF}}^{*}} \qquad (6.1)$$

where $\overline{a_{insitu}}^{*}$ and $\overline{a_{FRRF}}^{*}$ were the weighted mean absorption coefficients for the *in situ* irradiance field and FRRF excitation source respectively (*Fig. 6.3*).

Station	∫P (FRRF MIII)	∫P (FRRF MIV)
PK1 (26 Nov 2000)	2.0	2.0
	(1.5)	(1.4)
PK4 (30 Nov 2000)	1.4	1.6
	(1.0)	(1.1)
PK5 (01 Dec 2000)	2.2	2.1
	(1.6)	(1.5)
PK6 (02 Dec 2000)	2.5	3.0
	(1.9)	(2.2)

Table 6.2 Estimated productivity (g C m^{-2} d^{-1}) at site PK during the 2000 cruise. Values are integrated daily (24hr) rates using MIII and MIV applied to *in situ* FRRF data. Values in parenthesis are estimated rates accounting for differences between spectra of *in situ* irradiance field and FRRF excitation source.

Mean values for the correction factor (X) were around 0.7. The FRRF technique may therefore overestimate the *in situ* productivity by around 30% when spectral effects are not taken into account. A vertical profile of the calculated correction factors showed some increase with depth as is expected, the FRRF excitation source better approximating the *in situ* spectral field at depth (*Fig. 6.3*).

Overestimates of *in situ* productivity using the FRRF technique were likely to have been of similar magnitudes during the 1999 cruise. Additionally spectral differences between the incubation irradiance field (on deck) and the *in situ* field may also have caused ^{14}C simulated *in situ* estimates to underestimate the 'true' productivity.

Unfortunately due to the lack of *in situ* spectral data from the 1999 cruise and the lack of phytoplankton absorption spectra from the 2000 cruise, no detailed comparisons were possible between data sets.

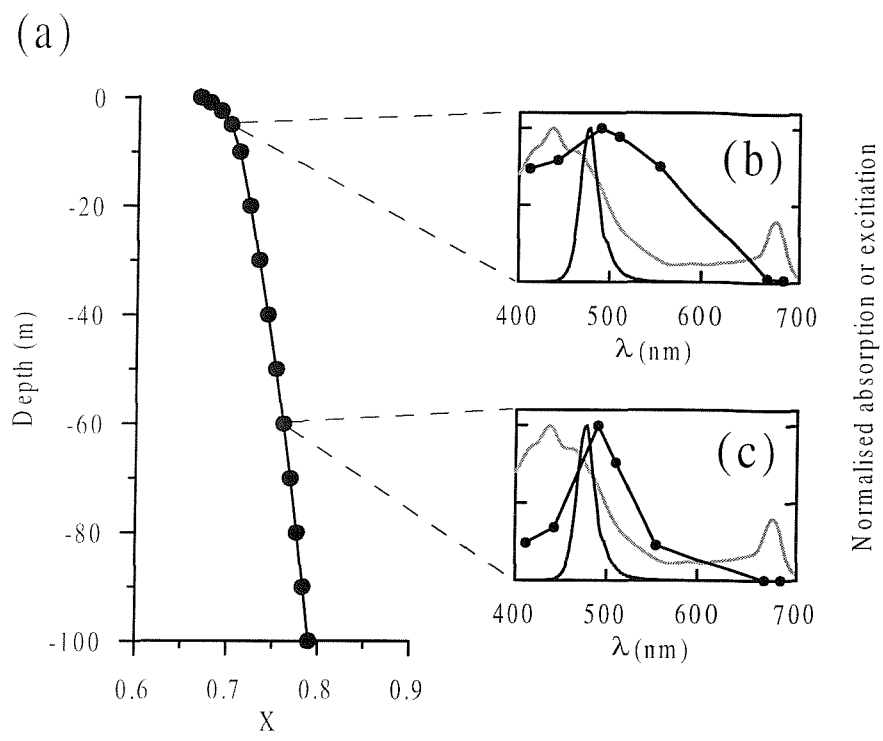

Fig. 6.3 Influence of differences between *in situ* and FRRF excitation spectra. (a) Vertical profile of correction factor to convert measured FRRF parameters (σ_{PSII}' etc.) to equivalent *in situ* values. Profile was calculated using the mean phytoplankton absorption spectrum from the 1999 cruise, the FRRF excitation spectrum and *in situ* irradiance data collected using an SPMR during the 2000 cruise on 26th November. (b & c) Normalised absorption and excitation spectra for 5m (b) and 60m (c). Symbols indicate the normalised irradiance for 7 wavelengths as derived from the SPMR data. Black line is the FRRF excitation spectrum, grey line is the mean phytoplankton absorption spectrum from the 1999 cruise.

6.4 Synthesis of productivity estimates, Nitrate fluxes and physiological indices

6.4.1 General inter site characteristics

The productivity of the four sites studied intensively during the 1999 cruise and the CTD/anchor station (PK) studied during the 2000 cruise is now considered in the context of the estimated vertical nitrate flux and changes in phytoplankton physiological indices between locations. Due to the dependence of FRRF derived productivity on the method used to estimate E_K (Chapter 5), the calculated productivity at each site using both the MIII and MIV methods is retained. Also, no further attempt was made to correct artefacts introduced to either ^{14}C or FRRF based productivity estimates as a result of the spectral quality of the *in situ*

irradiance field. In general terms spectral effects appeared to be capable of introducing discrepancies between FRRF and ^{14}C productivity estimates on the order of 30% (see above). However, such corrections were not applied, due to the lack of complete data for both cruises and in order to maintain comparisons between regions.

Biomass estimates (expressed as units of chlorophyll), nutrient concentrations and fluxes, key physiological indices and estimated productivity rates during all the 24hr occupations of fixed stations are summarised in *Fig. 6.4*. Sea surface chlorophyll variability was highest for the frontal system ranging from 0.3 (U2) – 3 (M3) mg chl *a* m^{-3}, while the sites dominated by internal tides had intermediate values ranging from around 0.5 – 1.5 mg chl *a* m^{-3} (*Fig. 6.4a*). The integrated water column biomass ($\int B$) was poorly related to the sea surface chlorophyll concentration at some sites. This was most obvious at U2 where the strong DCM resulted in a high integrated biomass despite the low sea surface chlorophyll.

Surface nitrate concentrations also displayed the highest range within the frontal system, ranging from undetectable at U2 to 2.2 mmol N m^{-3} at M3. During the two internal waves cruises (1998 & 2000), surface nitrate concentrations were intermediate, around 0.2-0.3 mmol N m^{-3} on the open shelf (1998) and around 1 mmol N m^{-3} at station PK during the 2000 cruise (*Fig. 6.4b*). Estimated vertical nitrate fluxes were generally lower within the frontal system than in regions dominated by internal tides. Lowest fluxes were calculated at the highly stratified U2 site (~2 mmol N m^{-2} d^{-1}), increasing slightly towards the transition region (~3.5 mmol N m^{-2} d^{-1}). Nitrate fluxes estimated for the PK site during the 2000 cruise were the highest (7 – 22 mmol N m^{-2} d^{-1}) (*Fig. 6.4b*), with fluxes for the open shelf internal wave dominated sites (1998 cruise) being intermediate (3.5 – 10 mmol N m^{-2} d^{-1}) the offshore site (IW2/98) having the higher estimate (Sharples *et al.* 2001b).

Physiological parameters for near surface phytoplankton populations varied markedly between stations (*Fig. 6.4c*). Low values of F_v/F_m (<0.42) were only observed at stations E and U2 corresponding to the lowest surface nutrient concentrations (<0.1 mmol N m^{-3}). These stations also had the lowest maximal photosynthetic rates and some of the highest values of σ_{PSII}. The increasing trend in P^*_{max} at PK during the 2000 cruise was accompanied by a decreasing trend in σ_{PSII}, but only minor changes in F_v/F_m.

Integrated daily productivity was lowest for station E during the 1999 cruise using all methods (^{14}C and both MIII and MIV models applied to the FRRF data) and generally highest for stations M2 and M3 for this cruise (*Fig. 6.4d*). Estimated productivity during the 2000

cruise was higher than during the 1999 cruise, particularly using the MIV model. Variability in the daily productivity at PK was associated with changes in the integrated biomass (chlorophyll). The highest productivity corresponded with the arrival of the coastal (upwelled) water and associated diatom bloom (see Chapter 4).

6.4.2 Biomass-specific integrated production rates and 'new production'

Water column biomass (chlorophyll) specific integrated production rates ($\int P/\int B$) were calculated for all the time series stations occupied during the 1999 and 2000 cruises. The water column specific rate was obtained by dividing the integrated productivity ($\int P$, *Fig. 6.4d*) by the integrated chlorophyll concentration ($\int B$, *Fig. 6.4a*). Additionally the maximal biomass specific rate within the water column (P^*_{opt}) was calculated from the mean vertical profiles of P^* estimated using ^{14}C and FRRF data.

Patterns of P^*_{max} and P^*_{opt} were similar, with much higher values observed during the 2000 cruise than the 1999 cruise (*Fig. 6.5*). As may be expected, higher water column integrated biomass specific productivity was generally found at those sites where values of P^*_{max} and P^*_{opt} were highest. Variation in $\int P/\int B$ between individual days and between cruises was well replicated using all the available techniques (*Fig. 6.5*). For the 1999 cruise, the highest biomass specific productivity using either ^{14}C or both models applied to FRRF data, was found at the frontal station (M2). Integrated biomass specific rates then decreased towards the stratified (U2) and mixed (M3) regions (*Fig. 6.5*). Integrated biomass specific productivity estimated using the FRRF data was generally greater during the 2000 cruise. In addition, the specific productivity increased towards the end of the occupation of PK, in accordance with an increasing P^*_{max} and the arrival of the diatom bloom at this site.

Fig. 6.4 (Overleaf). Synthesis of key biological characteristics of all the sites studied during the three cruises. (a) Integrated water column chlorophyll concentration (g chl *a* m^{-2}) and sea surface chlorophyll concentration (mg chl *a* m^{-3}). (b) Estimated nitrate flux (mmol N m^{-2} d^{-1}) and mean sea surface nitrate concentration (mmol N m^{-3}). (c) Maximal photosynthetic rates (P^*_{max}, mg C (mg chl *a*)$^{-1}$ h^{-1}), F_v/F_m, and σ_{PSII} ($Å^2$ $quanta^{-1}$). (d) Integrated water column daily production ($\int P$, g C m^{-2} d^{-1}). In the interests of clarity, error bars are only shown for the FRRF MIII estimate.

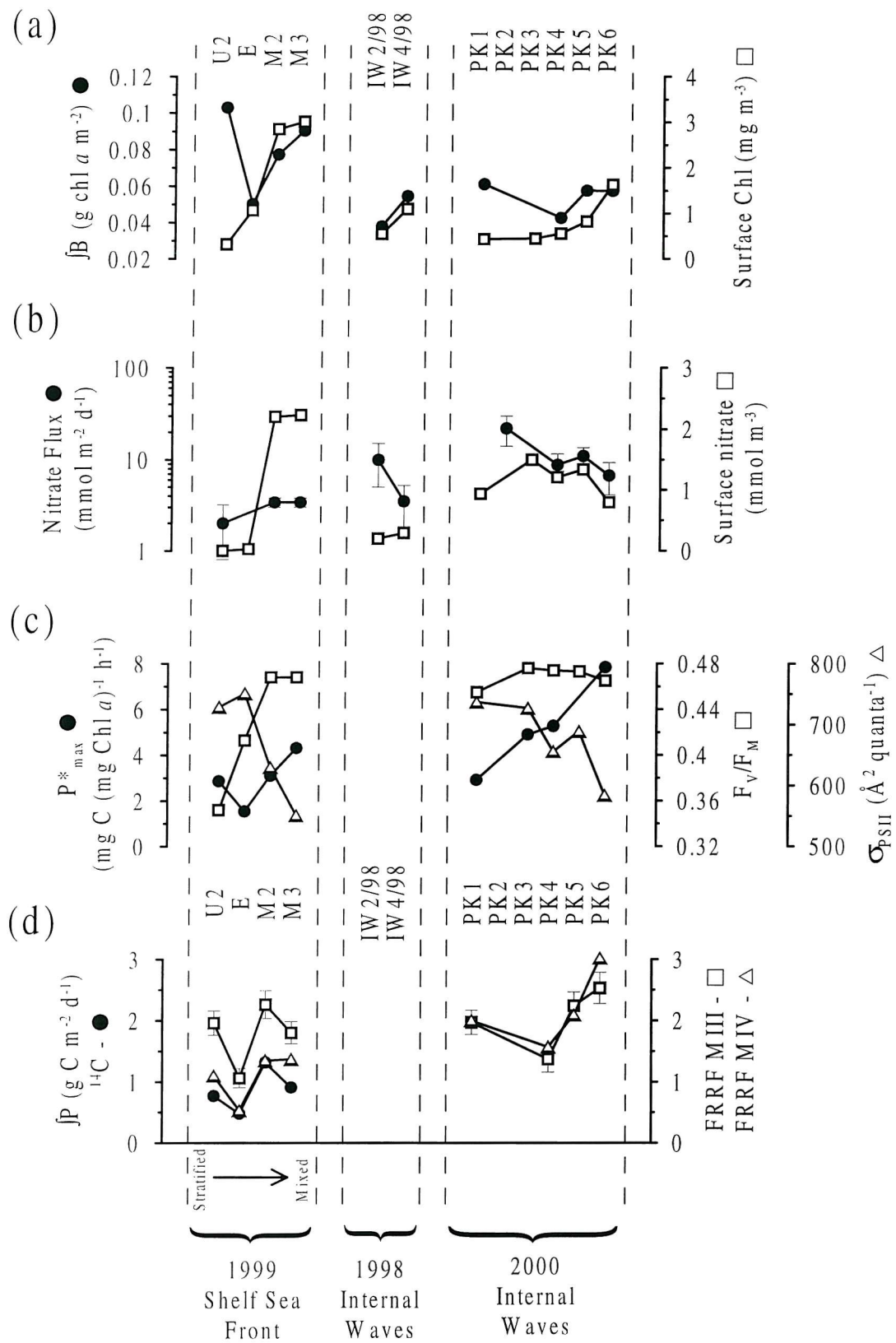

Fig. 6.4 Caption on previous page

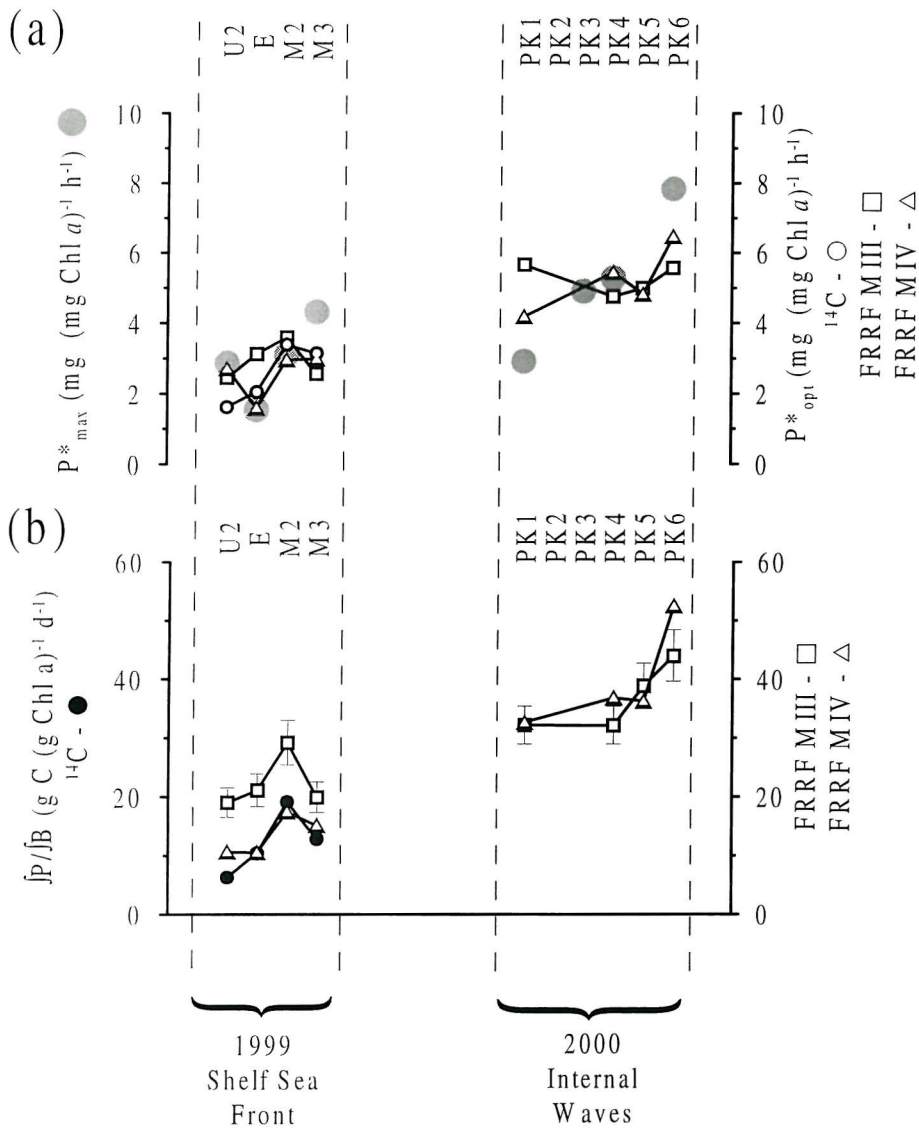

Fig. 6.5 Biomass (chlorophyll) specific productivity. (a) Surface values of P^*_{max} for all stations where ^{14}C P* vs. E experiments were performed and P^*_{opt} calculated from both simulated *in situ* ^{14}C and FRRF data (mg C (mg chl a)$^{-1}$ h^{-1}). (b) Integrated biomass specific productivity (∫P/∫B, g C (g chl a)$^{-1}$ d^{-1}) for all sites calculated from both ^{14}C and FRRF data.

The combined data on P^*_{max} (and P^*_{opt}) and the estimates of *in situ* productivity therefore suggested that higher specific production rates within the frontal region during 1999 and at the PK site during 2000, were a result of higher maximal photosynthetic rates (P^*_{max}). Additionally higher specific production rates and P^*_{max} values were generally calculated for those sites where the estimated vertical nitrate flux was higher (*Figs.6.4b & 6.5*).

Potential new production

Vertical fluxes of nitrate may be related to the potential for new production within a phytoplankton population (Dugdale and Goering, 1967; Lewis *et al.* 1986; Sharples *et al.* 2001a & b). Estimated vertical nitrate fluxes were converted into maximum potential new production rates by assuming that the C:N uptake ratio of the phytoplankton population was constant (= 6.6). It is noted that this assumption may not be valid, particularly over short time-scales O(hrs-days) (e.g. Sambrotto et al. 1993; Sambrotto and Langdon 1994; Bury *et al.* 2001). Incomplete uptake of newly available nitrate supplied to the euphotic zone could have resulted in the true new production rate being lower than that estimated using the nitrate flux.

The estimated potential new production was lowest at U2 (160 mg C m^{-2} d^{-1}), and highest at PK, reaching 1700 mg C m^{-2} d^{-1} during PK2 (27th November 2000), with an average value for the PK site of 960 mg C m^{-2} d^{-1} (*Table 6.3*). These estimates of new production were then combined with the estimated total productivity in order to derive the ratio of new to total production ('f-ratio', Eppley and Peterson, 1979). Again it is noted that this f-ratio is dependent not only on the assumption of a constant C:N uptake ratio and complete utilisation of the vertical nitrate flux, but also on the accuracy of the total production estimates using the various techniques. Additional supply routes of newly available nitrogen such as nitrogen fixation are also assumed to be negligible.

Estimated f-ratios calculated on the mean of the production estimates at each station ranged from 0.14 at the highly stratified U2 site in 1999, to 0.46 at the PK site during 2000 (*Table 6.3*). The f-ratios calculated for the frontal (1999) study were comparable to values measured in the same region at a similar time of year using combined nitrate and ammonium uptake experiments (Le Corre *et al.* 1993). These authors reported f-ratios of 0.15, 0.23 and 0.34 for highly stratified, frontal and mixed stations across the Ushant tidal mixing front.

	U2	M (M2 – M3)	PK
Nitrate Flux (mmol N m^{-2} d^{-1})	2 (0.8 – 3.2)†	3.4 (3 – 3.8) ††	9 (7 – 11) †
Production (g C m^{-2} d^{-1})	1.3 (0.3)	1.5 (0.2)	2.1 (0.2)
Biomass (g Chl a m^{-2})	0.103	0.084	0.055
Specific Production (P/B) (g C (g Chl a)$^{-1}$ d^{-1})	12 (4)	19 (2)	40 (3)
Potential New Prod. (g C m^{-2} d^{-1})	0.16 (0.1)	0.27 (0.04)	0.96 (0.5)
f – ratio	0.14 (0.03)	0.19 (0.02)	0.46 (0.05)

Table 6.3 Nitrate fluxes and new and total productivity estimates for the three stations, U2, M and PK. Data for station M corresponds to both occupations of this site (M2 and M3), thus representing a mean over the spring-neap cycle. For nitrate fluxes approximate upper and lower bounds are presented in parenthesis, † - calculated by combining observations of turbulent mixing parameters by microstructure profilers with observations of the vertical nitrate gradient, †† - calculated from the observed depth and nutrient concentration of the re-stratifying area due to springs-neaps cycle. All other values are means of all estimates obtained for each station using all techniques (i.e. ^{14}C and FRRF), values in parenthesis are s.e. of mean.

6.5 Estimated growth rates

6.5.1 Problems of calculating growth rates: the requirement for C:Chl estimates

Population growth rates can only be calculated from chlorophyll-specific productivity measurements once the ratio of phytoplankton carbon to chlorophyll (C:Chl) is known (§ 1.1.2, Eq. 1.4). This ratio can be highly variable ranging from ~20 to over 200 depending on both taxonomic differences and acclimation to changing growth conditions (e.g. Geider, 1987; Langdon, 1988; Cloern *et al.* 1995). No direct information on phytoplankton C:Chl

ratios was available from either the 1999 or 2000 cruises. More generally, the evaluation of the C:Chl ratio within the natural environment is highly problematic and may limit much of the current understanding of phytoplankton ecology (e.g. Eppley, 1972).

Many field studies find that C:Chl averages around 60 (e.g. Holligan *et al.* 1984a; Maranon *et al.* 2000). Holligan *et al.* (1984a) obtained C:Chl ratios from sites in the Western English channel which were highly analogous to those visited during the 1999 cruise, the data also being collected at the same time of year. These authors found relatively low inter-site variations in the water column mean of phytoplankton C:Chl, values of 60, 70 and 50 for a mixed, frontal and stratified site respectively being calculated from their Table 5. However the dominant species found at the hydrographically different sites, particularly U2, were not the same during 1999 as those reported by these authors. Additionally the method used for evaluation of the C:Chl ratio by Holligan *et al.* (1984a) involved the estimation of phytoplankton carbon from cell counts. Within certain regions, particularly those dominated by flagellate populations (e.g. near the surface at U2), such estimates of the photoautotrophic carbon content are highly problematic. Given the caveats above, the adoption of the C:Chl ratios calculated by Holligan *et al.* (1984b) must be treated with caution. No information on C:Chl ratios for either the sub-tropical or diatom populations sampled during the 2000 cruise at PK was available from previous studies in the region. Within the diatom bloom sampled during the 2000 cruise, C:Chl values of 20 could perhaps be expected, similar to the estimated values for analogous spring blooms on the North East European continental shelf (Fasham *et al.* 1983).

6.5.2 Vertical partitioning of growth at U2: maintenance of the DCM

Vertical differences in C:Chl are likely to be of high significance when estimating the vertical profile of μ and hence the vertical partitioning of growth within highly stratified water columns. Holligan *et al.* (1984a) studied a site with similar hydrographic properties to the U2 site occupied during the 1999 cruise. Assuming the data from their site E5 (around 35 km Southwest of U2) to be representative of the vertical profile of phytoplankton C:Chl ratio within these seasonally stratified shelf waters during summer, the *in situ* productivity data from this site was used to calculate the vertical growth profile (*Fig. 6.6*).

The vertical decrease in C:Chl observed at E5 by Holligan *et al.* (1984a) was likely to have resulted from acclimation of the deeper phytoplankton populations to lower mean light levels. Indirect evidence that a similar process was operating at U2 during 1999 was provided by the

decrease with depth of the mean chlorophyll specific optical absorption cross sections $\overline{a^*}$ (*Fig. 6.6c*). Phytoplankton acclimate to lower irradiance by increasing the cellular chlorophyll content. This lowers the C:Chl ratio and decreases the chlorophyll specific absorption cross section due to self shading within the cell, the package effect (Falkowski *et al.* 1985; Dubinsky *et al.* 1986; Berner *et al.* 1989; Falkowski and Raven, 1997). The decrease in $\overline{a^*}$ observed at U2 in 1999 was therefore suggestive of high light acclimation within the surface and low light acclimation within the thermocline. This supports the observations of Holligan *et al.* (1984a) and lends confidence to the use of their reported C:Chl values for estimating the growth profile (*Fig. 6.6c*). Further indirect evidence for a decrease in C:Chl with depth at U2 may also be implied from the lower values of E_K within the thermocline as opposed to the surface (see *Fig. 5.7*). It has been suggested that variations in C:Chl may be inferred from variations in E_K, with a lower C:Chl relating to lower E_K (Anning *et al.* 2000). Hence, although the absolute values of C:Chl assumed for the U2 site may be inaccurate, there is some confidence in the relative decrease with depth.

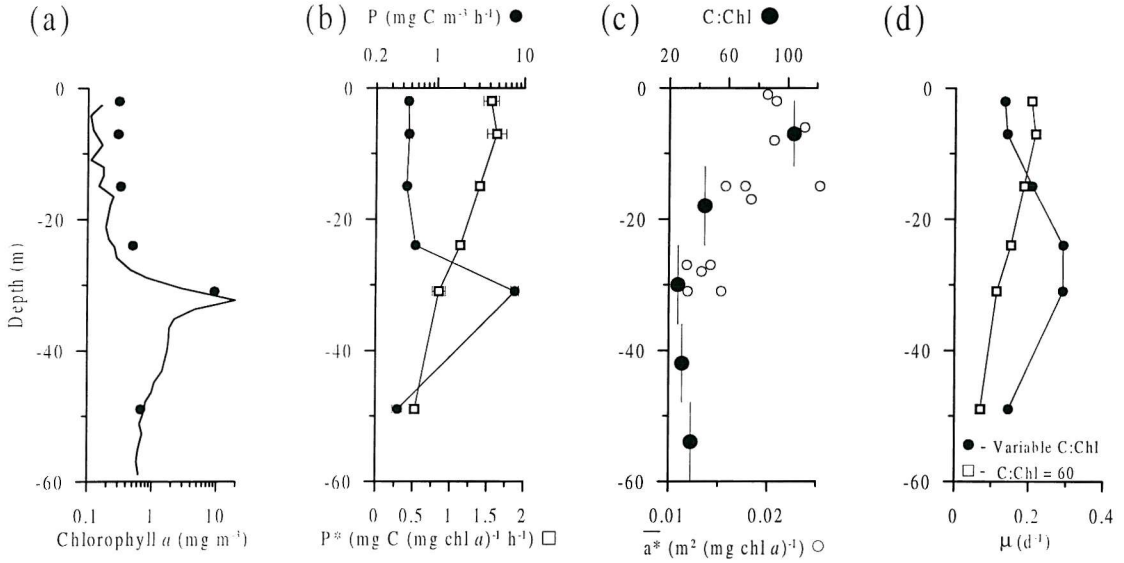

Fig. 6.6 Vertical profiles of production and estimated community growth at U2 on 8th – 9th August 1999. (a) Vertical chlorophyll from discrete samples (symbols) and calibrated FRRF F_M' measurement. Note logarithmic scale. (b) Profile of volume specific (closed symbols) and chlorophyll specific (open symbols) production. Data are ^{14}C simulated *in situ* values. Error bars for chlorophyll specific production are ± 1 s.d. for three replicates. Note: logarithmic scale for volume specific production, FRRF derived productivity values displayed similar patterns. (c) Spectral mean chlorophyll specific phytoplankton absorption cross section (open symbols) and C:Chl (filled symbols). C:Chl data are from Holligan *et al.* (1984a), their Table 5. (d) Vertical profile of specific growth rate assuming constant C:Chl of 60 (open symbols) and using the observations of Holligan *et al.* (1984a), i.e. decreasing C:Chl with depth (closed symbols).

The marked DCM at the U2 site was associated with the sharp thermocline and nitracline (*Fig. 6.6a, see also Fig. 3.5* & Sharples *et al.* 2001a). Volume specific production was maximal within the DCM, however chlorophyll specific production generally increased towards the surface (*Fig. 6.6b*). The estimated population growth rate assuming a vertically invariant C:Chl of 60 was thus also maximal in the near surface region (*Fig. 6.6d*). Conversely, when the likely decrease of C:Chl with depth (*Fig. 6.6c*) is accounted for, maximal growth rates were calculated for the region within and just above the thermocline and associated DCM (*Fig. 6.6d*).

The implications of a decrease in C:Chl with depth for the distribution and survival of the phytoplankton populations within the surface and thermocline at U2 were pronounced. Higher specific growth rates within the thermocline would tend to promote the development or maintenance of the high cell numbers observed within the DCM at this site. The vertical flux of nutrients into the thermocline at this site (Chapter 3 & Sharples *et al.* 2001a) and low surface nutrient concentrations also indicate that the DCM population would be responsible for the majority of community growth. Higher specific growth rates within the thermocline rather than for the near surface regions must therefore be considered the more realistic scenario.

6.5.3 Estimated site specific growth rates and controls

The specific growth rates (μ (d^{-1})) for all the sites studied during both the 1999 and 2000 cruises were pragmatically estimated using (Eq. 1.4) and assuming a fixed C:Chl. It is noted that loss terms due to respiration were not accounted for in these calculations (Geider, 1992). Specifically the mean growth rate for individual sites (μ_s) was calculated as:

$$\mu_s = \frac{\int P / \int B}{C:Chl} \qquad (6.2)$$

where $\int P$ and $\int B$ are the integrated daily water column production and chlorophyll concentration respectively (*Fig. 6.4a & d, Table 6.3*).

As the C:Chl ratio had to be assumed constant between sites, variations in the calculated specific growth rates were identical to the patterns of variability in $\int P/\int B$ (*Fig. 6.5*). The estimated site-specific gross growth rates, assuming C:Chl = 60, ranged from around 0.1 at U2 in 1999 to > 0.8 during the period when the diatom bloom dominated at PK in 2000. Thus

population growth rates at PK were close to maximal while growth rates at the highly stratified U2 & E sites were generally lower. The very low value of 0.1 d^{-1} calculated for the U2 site using Eq. 6.2 was lower than the mean value which may be inferred from *Fig 6.6d* (open symbols). This is likely to result from the influence of the high biomass within the thermocline on $\int P/\int B$ and again illustrates the problems associated with a lack of C:Chl data.

In order to evaluate the ultimate controlling factors on growth, the estimated μ_s values were compared to the integrated daily incident irradiance at the sea surface for all sites and to the estimated vertical nitrate fluxes, where available (*Fig. 6.7*). Integrated daily irradiance was higher for the 2000 cruise than during the 1999 cruise (*Fig. 6.7a*). Additionally, as previously mentioned, estimated vertical nitrate fluxes were greater in the regions dominated by internal tides. Thus the two factors likely to control population growth co-varied. Estimated growth rates were therefore increased with both irradiance and nutrient supply (*Fig. 6.7a & b*).

An increasing asymptotic relationship between F_v/F_m and the specific growth rate under conditions of nutrient limitation and saturating light was observed by Kolber *et al.* (1988), see also Falkowski and Kolber (1995). Parkhill *et al.* (2001) questioned the data of Kolber *et al.* (1988) and suggested that F_v/F_m is a sensitive indicator of nutrient starvation, but not necessarily nutrient limitation under conditions of balanced growth. However, balanced growth may be considered unlikely within many regions of the highly dynamic shelf sea ecosystems studied here, as physical variability was likely to alter irradiance and nutrients on daily-weekly timescales. Additionally, and in keeping with the majority of reported field studies, lower F_v/F_m was found in regions of low nutrients (Chapter 3).

The potential use of physiological indicators for distinguishing between nutrient and light limitation of growth was therefore investigated by comparing $\int P/\int B$ and μ_s with the surface values of F_v/F_m for individual sites. The measured photochemical efficiency (F_v/F_m) was found to be an increasing asymptotic function of $\int P/\int B$ and hence also the estimated growth rates (*Fig. 6.7c*), the relationship derived being similar to that reported by Kolber *et al.* (1988). Only two of the sites (E & U2) both with strong stratification and depleted surface nutrient concentrations, had markedly lower F_v/F_m (*Fig. 6.7c*). It is once again emphasised that the lack of accurate C:Chl estimates and likely variations of this ratio with depth, limits this analysis in terms of growth rates. However, the low near surface F_v/F_m values were clearly associated with those sites for which the lowest $\int P/\int B$ values were calculated.

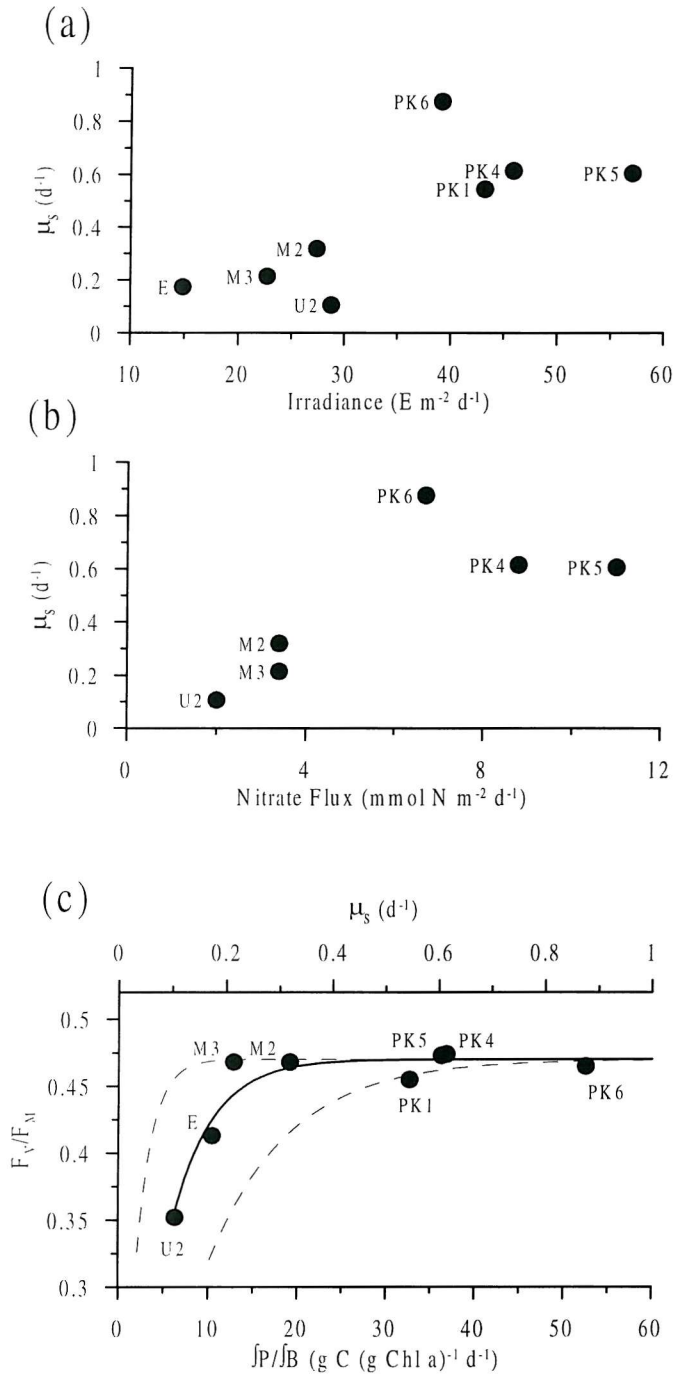

Fig. 6.7 Relationships between estimated gross site growth rate (μ_S) and environmental and physiological factors. (a) μ_S as a function of integrated daily irradiance (assuming C:Chl = 60) for all the sites where either FRRF or ^{14}C based estimates of *in situ* productivity were obtained. (b) μ_S as a function of the estimated vertical nitrate flux for stations where such calculations were possible. (c) Near surface F_v/F_m vs. $\int P/\int B$ for all sites where *in situ* productivity estimates were obtained. The calculated biomass specific productivity ($\int P/\int B$) was converted to an estimated site specific growth rate (μ_S) using a constant C:Chl ratio of 60, (see top axis). F_v/F_m is an increasing asymptotic function of μ_S, solid line: $F_V / F_M = 0.47(1 - e^{-13.5\mu_S})$, n = 8, $R^2 = 0.919$, $p < 0.001$. Dotted lines are the fits which would be derived if a constant C:Chl ratio of 20 or 120 were assumed, again with reference to the top axis.

6.6 Physically driven export

Ultimately the net growth at a site or within a region will depend on the balance between factors controlling the gross production (and growth) and the loss terms including respiration and grazing. Additionally, high turbulent mixing could cause physically driven export of phytoplankton from the upper euphotic layer. Direct evidence for such a mechanism was obtained during the occupation of site U2 during the 1999 cruise (Sharples *et al.* 2001a). Time series of the chlorophyll concentration and turbulent kinetic energy dissipation measured with the FLY profiler (Chapter 3) revealed a striking export of phytoplankton from the distinct DCM at around 06:00 on 9th August (*Fig. 6.8*).

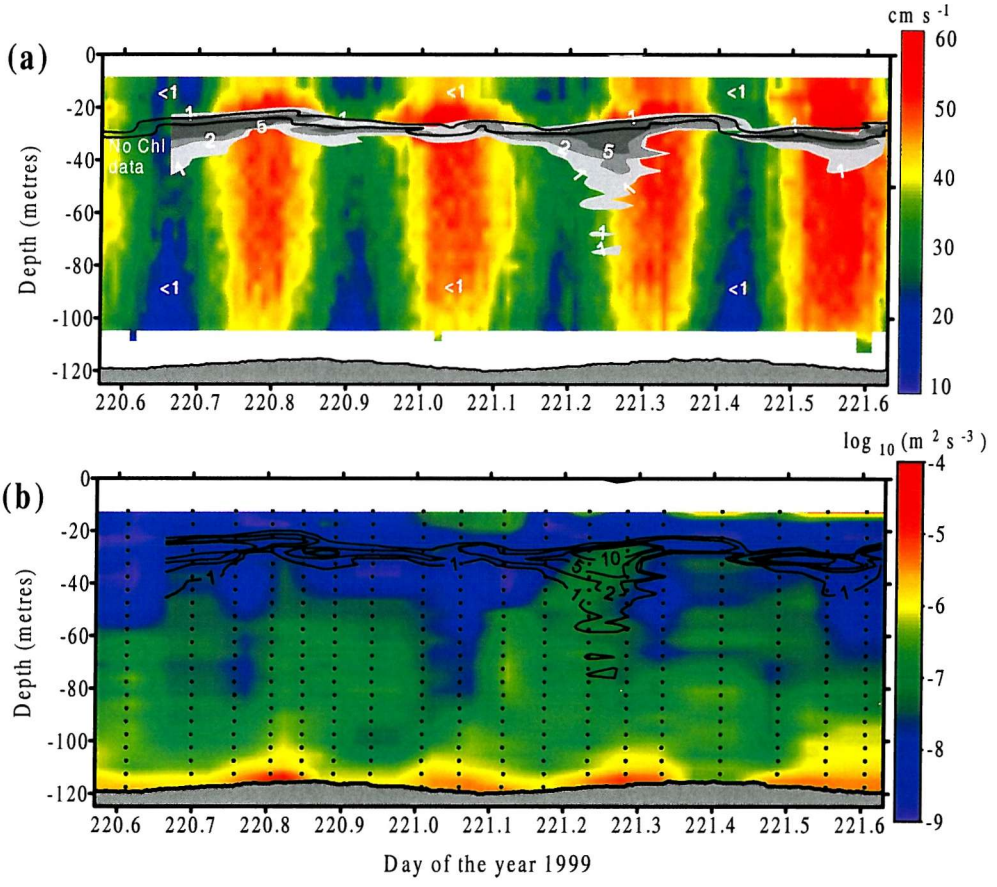

Fig. 6.8 Observations of physically driven export of phytoplankton at U2, 8th – 9th August 1999. (a) Time series of current speed from shipboard ADCP (cm s^{-1}, colours), Chlorophyll *a* concentration from calibrated CTD fluorometer (mg m^{-3}, grey shaded contours and white labels), and the depth of the 16 and 12 °C isotherms (black lines), indicating thermocline position. (b) Time series of turbulent kinetic energy dissipation rate ($\log_{10}$ (m^2 s^{-3}), colours) and chlorophyll *a* concentration contoured at 1, 2, 5 and 10 mg m^{-3} (lines). Vertical dotted lines indicate mean times for groups of FLY profiles. Grey speckled region at bottom indicates sea bed.

The export event coincided with the maximal turbulent dissipation rates measured within the thermocline (*Fig. 6.8b*) and resulted in the removal of phytoplankton from the DCM to the bottom mixed layer (*Fig. 6.8a*). Such tidally driven transport of phytoplankton cells from a region of active growth to a region where insufficient irradiance is available for photosynthesis constituted export production. Over some appropriate time-scale this export must balance the supply of newly available nutrients for growth. The potential daily export of chlorophyll from the thermocline at this site was estimated using the observed time series of turbulent diffusivities calculated from the FLY data and the vertical chlorophyll gradient (Sharples *et al.* 2001a). The calculation performed was thus similar to that used to calculate the vertical nitrate flux (§ 3.2.3). The estimated rate of chlorophyll entrainment was between 4 and 16 mg chl *a* m^{-2} d^{-1}. When combined with the estimated C:Chl ratio of around 30 for the thermocline population in this region (*Fig. 6.6c*) a physically driven export flux of 290 (± 180) mg C m^{-2} d^{-1} was thus calculated.

Similar calculations were also possible for the PK site during the 2000 cruise. Vertical chlorophyll gradients were estimated using the observed relationship between chlorophyll *a* and temperature (*Fig. 4.22*). The derived relationship for all samples collected prior to 2nd December 2000 was Chl *a* = 0.295 T – 4.474 (R^2 = 0.467, n = 48, p<0.001) and hence $\partial Chl/\partial T$ = 0.295 mg Chl *a* m^{-4}. For the 2nd December when the diatom bloom dominated at PK, the chlorophyll temperature relationship was well approximated by: Chl $a = 2.39 \times 10^{-13}$ $e^{1.73\,T}$ (R^2 = 0.907, n = 18, p<0.001) and thus $\partial Chl/\partial T = 4.12 \times 10^{-13}\ e^{1.73\,T}$. The vertical gradient of chlorophyll could then be approximated using similar arguments to the nitrate flux calculations at this site (see Eq. 4.6). Thus:

$$\frac{\partial Chl}{\partial z} = \frac{\partial Chl}{\partial T}\frac{\partial T}{\partial z} \qquad (6.3)$$

The time series of vertical chlorophyll distribution and vertically driven chlorophyll flux using the values of diffusivity estimated from the SCAMP profiles (Eq. 2.6), could therefore be calculated. The integrated flux was around 1 – 2 mg Chl *a* m^{-2} d^{-1} before 2nd December 2000 (PK2, PK4 & PK5) and 5 mg Chl *a* m^{-2} d^{-1} on 2nd December (PK6). Assuming a C:Chl ratio of 60 (see above), average physically driven carbon fluxes for the whole period were therefore estimated to be around 130 mg C m^{-2} d^{-1}, less than half of the fluxes calculated for the U2 site.

6.7 Discussion

In situ productivity

Generally good agreement using the FRRF and ^{14}C techniques for estimating *in situ* productivity was found for the four stations occupied during the 1999 cruise. For individual depths or equivalent light levels, this relationship principally resulted from the dependence of productivity on irradiance (*Fig. 6.2*). However some differences in the vertical distribution of P* and P were apparent, particularly at the M3 site. Under conditions of high vertical mixing the simulated *in situ* ^{14}C technique is likely to overestimate the degree of near surface photoinhibition within the water column. Phytoplankton cells *in situ* would not be exposed to super-saturating irradiances for as long as those constrained within a deck-board incubator. The vertical distribution of chlorophyll specific productivity at the fully mixed site M3 (*Fig. 6.1d*) produced productivity profiles that could be expected under conditions of no mixing (i.e. simulated *in situ* ^{14}C) or high mixing (i.e. truly *in situ* FRRF based measurements). The difference between the two vertical profiles was qualitatively similar to that predicted intuitively, the depth of the maximum productivity rate being lower in the water column using the ^{14}C method. The observed profiles also showed similarities with modelling studies (see Franks and Marra, 1994, their Fig 5). Different vertical patterns of productivity generated by the FRRF and ^{14}C techniques are therefore not surprising, especially under conditions of high mixing.

Comparable patterns of variability in the daily integrated productivity for the four sites during the 1999 cruise were obtained using the FRRF and ^{14}C techniques, despite some differences in the derived vertical profiles (*Table 6.1*). Such agreement suggests that although the ^{14}C technique may not predict the vertical distribution of productivity within the water column under conditions of high mixing, the predicted total amount of light utilised, and hence the total production, is similar to the light utilised *in situ*. For the M3 (highly mixed) site, this is perhaps not surprising as the distribution of chlorophyll throughout the water column was uniform.

Although absolute integrated values varied between techniques (*Table 6.1*), the magnitude of such discrepancies was within the range that could be explained by spectral effects (*Fig. 6.3 & Table 6.2*). Thus although the number of stations for which comparisons were possible was somewhat limited, the current study suggested that the FRRF and ^{14}C techniques produce comparable estimates of total integrated productivity within the same water column (*Table*

6.1). The study emphasised that the practicalities of applying the FRRF and ^{14}C methods to the same water column require careful consideration when comparing the techniques. Similar conclusions were drawn for comparisons between ^{14}C P* vs. E experiments and FRRF data (Chapter 5).

Biomass specific rates

For the 1999 study, the hypothesis that active growth results in the enhanced chlorophyll concentrations observed at shelf sea fronts was supported by higher productivity and particularly biomass (chlorophyll) specific productivity at the M2 site (*Figs. 6.4d & 6.5*). The higher total and specific productivity at the internal wave dominated sites also suggested that this system was more productive than the frontal system. However, as with much of the preceding and following discussion, it is emphasised that the frontal study in 1999 and the 1998 and 2000 internal wave studies were undertaken at different times of year and in different geographical locations. Specifically the 1999 cruise was performed in mid-summer at a latitude of around 49°N while the 1998 and 2000 cruises were performed in late spring at a latitude of around 35.5°S. Differences in the seasonal cycles of both physical forcing and phytoplankton growth between the regions may therefore have influenced the results obtained.

Nitrate fluxes

The vertical nitrate fluxes estimated during this study ranged from 2 mmol N m^{-2} d^{-1} at the highly stratified U2 site in 1999, through 3.5 – 10 mmol N m^{-2} d^{-1} for the open shelf internal wave sites during 1998, to 7 – 22 mmol N m^{-2} d^{-1} at the PK site in 2000. Such fluxes were comparable with other estimates in shelf seas. For example, Horne *et al.* (1996) estimated cross-thermocline fluxes of 3-11 mmol N m^{-2} d^{-1} for the frontal system around the Georges Bank region. Although these fluxes are generally higher than those estimated for the U2 site and the Ushant frontal system, the Georges Bank system is also strongly influenced by internal tides which are likely to enhance mixing (Brickman and Loder, 1993; Franks and Chen, 1996).

The estimated cross thermocline fluxes for the range of shelf sea situations investigated were generally more than an order of magnitude higher than open ocean estimates (Lewis *et al.* 1986; Planas *et al.* 1999). Thus the tidally dominated physical processes acting in shelf seas appear to be responsible for an enhanced supply of nutrients to surface and sub-surface

phytoplankton populations and hence an increase in summer growth and new production (Sharples *et al. 2001a & b*). Higher estimated vertical nitrate fluxes for the sites dominated by internal (baroclinic) tides, as opposed to the sites dominated by barotropic tides, can now be hypothesised to have resulted from the different nature of the physical forcing.

The thermocline structure was much more diffuse for the sites dominated by internal tides. Moreover, the 'staircase-like' structure of the stratification observed at both the PK and open ocean NE New Zealand sites (see e.g. Sharples *et al.* 2001b, their Figure 9) suggested the occurrence of active internal mixing. Comparing estimated and observed turbulent dissipation rates and diffusivities, mixing within the thermocline region was found to be at least an order of magnitude greater for the internal tide dominated sites (e.g. dissipation rates of $O(10^{-7}$ m^2 s^{-3}) for the sites off NE New Zealand as compared to $O(10^{-8} - 10^{-9}$ m^2 s^{-3}) for site U2 in the English channel). However, vertical nitrate gradients were around an order of magnitude higher at the U2 site (~4 mmol N m^{-4}) than for all the internal wave sites (~0.2 mmol N m^{-4}).

It is suggested that these characteristics of the thermocline region result from the difference between the mixing caused by barotropic and baroclinic tides over the shelf. Barotropic tides generate high dissipation rates due to the shear between the tidal currents and the sea bed, however the dissipation decreases up through the water column (*Figs. 3.3 & 6.8b*). The barotropic tide is therefore relatively inefficient at generating mixing within the thermocline. Hence, despite the high nutrient gradients found at the base of the thermocline, the tidally driven nitrate flux is relatively low. Conversely the baroclinic (internal) tide propagates within the water column density structure. Breaking and dissipation of the internal tide thus causes relatively efficient mixing within the thermocline. A more diffuse thermocline and higher vertical nitrate flux therefore results, despite the lower vertical nitrate gradients.

f-ratios and the balance of new and total production

Assuming the vertical nitrate supply was balanced by uptake, the combined productivity and nitrate flux estimates allowed the relative balance of new and total production to be investigated. Despite the large number of assumptions and hence inherent uncertainty in such calculations, reasonable values for the f-ratio were obtained (*Table 6.3*). The f-ratios calculated for the U2 and M sites were comparable with more direct observations previously performed in the region (Le Corre *et al.* 1993). Much of the production, particularly on the stratified side of the front, must therefore have been supported by regenerated nitrogen (Le Corre *et al.* 1993). The importance of new production may have been greater towards the transition region of the front (*Table 6.3*, see also Le Corre *et al.* 1993). The higher f-ratios estimated for the PK site during 2000 were consistent with a greater importance of new

production during spring and/or under conditions of increased vertical nitrate flux. If the high nitrate fluxes persist throughout the summer months, it can be hypothesised that dissipation of the internal tide in certain regions is responsible for higher f-ratios and hence increased new-production relative to shelf sea frontal systems.

Balances of new production and physical export

Physically driven export from the upper ocean is not normally considered as an important control on phytoplankton distribution and survival. Observations of turbulent dissipation rates and chlorophyll distributions at the U2 site indicated that entrainment of phytoplankton from the DCM was likely to have played a crucial role in the balance of new and export production (*Fig. 6.8,* Sharples *et al.* 2001a).

The estimated rate of physically driven carbon removal at U2 (290 mg C m^{-2} d^{-1}) was comparable to, and possibly exceeded, the estimated new production (160 mg C m^{-2} d^{-1}). Again it is recognised that such calculations were dependent on many assumptions. For example the two terms would exactly balance if, instead of the previously assumed phytoplankton C:N uptake and C:Chl ratios, values of 8 and 20 were used. Such variability is well within the range of observed values for the C:N and C:Chl ratios within phytoplankton populations. However it was hard to envisage any set of parameters which would suggest that the physical loss term was not important.

An approximate balance or slight excess of physically driven loss from the thermocline over the supply of new nitrate raises interesting questions for the maintenance of the DCM during summer. If the situation encountered over the single 24hr period in 1999 persisted, the DCM could not have supported any additional loss terms such as grazing pressure or sinking, without there being a decrease in the population. However the estimated fluxes into and out of the thermocline represented a single time point measurement between neap and spring tides. The flux of material both into and out of the thermocline is likely to be modulated over the spring-neap cycle (§ 3.4 & Sharples *et al.* 2001a). Additional mixing of nitrate into the thermocline driven by the spring-neap tidal cycle, may therefore be necessary for the long term maintenance of the DCM in highly stratified regions of shelf seas (Sharples *et al.* 2001a).

In contrast to the U2 site, for the internal tide dominated PK site, the estimated new production (960 mg C m^{-2} d^{-1}) greatly exceeded the estimated physical carbon removal (130 mg C m^{-2} d^{-1}).

From the limited number of locations studied, it therefore appears that the dissipation of tidal energy, and the form this dissipation takes, may be a significant factor controlling nutrient fluxes and new production during the spring and summer months within shelf seas. Additionally, through physical removal of phytoplankton from surface regions, variations in vertical mixing may also alter the balance of new and export production and hence the proportion of new production available to higher trophic levels. Studies of longer term balances between phytoplankton C:N uptake ratios and f-ratios with relation to variations in turbulent mixing both into and out of the thermocline are required to test such conjectures.

Growth rates

Estimated gross phytoplankton community growth rates were within expected ranges (0.1-1 d^{-1}), however some uncertainty in these values due to lack of good data on phytoplankton C:Chl ratios was inevitable. The importance of variability in C:Chl ratios, particularly vertical differences in highly stratified water columns, was illustrated using data from the U2 site. Realistic growth rates (~0.3 d^{-1}) within the thermocline were only obtained when an attempt was made to allow for decreasing C:Chl with depth as a result of shade acclimation of phytoplankton within the DCM (*Fig. 6.6*). Such observations reinforce the view that understanding of growth and productivity within shelf sea thermoclines may require knowledge of how phytoplankton balance the uptake of C, N and cellular stores of C, N & Chl in response to varying environmental forcing.

The estimated growth rates at all the sites, where such calculations were possible, were increasing functions of both the integrated daily irradiance and the estimated nitrate supply rates (*Fig. 6.7a & b*). Physiological indicators at the two sites (U2 & E) where very low surface nitrate concentrations (<0.1 mmol N m^{-3}) were observed, suggested nutrient stress of the phytoplankton populations in these regions (*Fig. 6.7c*). Taking into account the seasonal differences in the cruises and previous ideas concerning the productivity and growth of such systems, particularly tidal mixing fronts (Holligan, 1981), the following hypothesis is now formulated.

It is suggested that low production and growth rates at the more stratified mid-summer sites (U2 & E) were a consequence of nutrient limitation. For the remainder of the sites nutrient limitation was of relatively minor importance, with the availability of irradiance and efficiency of light utilisation therefore controlling production and growth.

Following this argument, higher growth at M2 than M3 would have resulted from the deep vertical mixing at M3 reducing the irradiance available to phytoplankton. While generally

higher growth and production at the PK site during 2000 was consistent with higher surface irradiance levels. Variations for individual days at PK appeared to be related to the arrival of the coastal diatom bloom at the sample site, suggesting higher maximal growth rates for the diatom population as opposed to the small cell dominated population within the sub-tropical water. The general increasing trend in maximal photosynthetic rates (P^*_{max}) observed at this site (*Fig. 6.6*) supports this view and emphasises the possible importance of the dominant functional group of phytoplankton in controlling growth within a region.

Summary and conclusions

Estimates of new and total productivity obtained during all cruises were combined and analysed in terms of the physical controls on phytoplankton growth. Good agreement was found between FRRF and ^{14}C techniques for estimating total water column productivity for the 1999 cruise, lending confidence to the use of the FRRF technique for estimating productivity during the 2000 cruise.

Observations from the 1999 cruise supported the hypothesis that phytoplankton production and growth rates are limited by inorganic nutrient supplies on the stratified side of tidal mixing fronts and by irradiance on the mixed side. Data collected from a number of sites where tidal dissipation was dominated by internal motions suggested that such systems support high rates of primary production with a significant contribution by new production.

The combined observations for all the cruises suggested that differences between physical regimes in diverse shelf sea regions are responsible for driving differences in phytoplankton production and growth. Physical processes may also effect the partitioning of production between new and regenerated forms and the export of carbon from the upper ocean. The summer time ecology of shelf seas is therefore strongly dependent on physical forcing as expressed by both the magnitude and form of tidal dissipation.

7. Summary and Conclusions

7.1 Evaluation of the FRRF technique

7.1.1 Scales of physiological variability

Phytoplankton physiology as measured using the FRRF technique was shown to vary at all the scales resolved. Horizontal spatial variability in σ_{PSII} and F_v/F_m was observed within both the European and New Zealand shelf seas (Chapters 3 & 4). Scales of variability ranged from the size of small eddy structures O(<10km), through to the scale of shelf sea fronts in the Western English channel (Chapter 3). Marked changes in σ_{PSII} were also observed between upwelled and sub-tropical water masses over spatial scales O(20 – 50km) on the North East New Zealand continental shelf (Chapter 4). Vertical spatial variability in both σ_{PSII} and F_v/F_m was observed at scales ranging upwards from a few meters within a highly stratified shelf sea thermocline (Chapter 3).

Temporal variability in σ_{PSII} (σ_{PSII}') and F_v/F_m ($\Delta F'/F_M'$) was observed due to both the diel cycle of incident solar radiation and physical forcing at scales from O(20 minutes – weeks). Changes in phytoplankton physiology in response to changes in irradiance were found to be rapid O(20min, Chapter 4) and characteristic diel cycles in physiology were observed at all the sites studied (Chapters 3 & 4). Tidally dominated physical variability also caused temporal changes in the physiology of certain phytoplankton populations. On timescales < 1day advective processes due to internal tides (Chapter 4) and high levels of turbulence within the water column (Chapter 3) affected the observed values of σ_{PSII}. At longer scales, changes in F_v/F_m and σ_{PSII} around a front appeared to result from the spring-neap tidal cycle (Chapter 3).

The FRRF technique provided information on phytoplankton physiology at scales impossible to measure using traditional bottle sampling techniques. Such changes in the photophysiology of PSII will in turn cause changes in the productivity and growth of the phytoplankton populations. Therefore the principal strength of the technique in the context of physical-biological interactions, is that hypotheses concerning the link between physical forcing and phytoplankton growth can be addressed using data free from the ambiguities associated with simple observations of biomass. It seems likely that such techniques will become crucial to an increased understanding of phytoplankton ecology.

7.1.2 Relationship of FRRF derived productivity to phytoplankton photosynthesis and carbon fixation

The FRRF technique measures physiological variability *in situ* at hitherto unobservable scales. However, the power of the technique is considerably enhanced if phytoplankton photosynthetic rates can also be derived from the physiological measurements (Kolber and Falkowski, 1993). The primary controls on productivity within any water column are the distribution of irradiance and biomass (chlorophyll). However changes in phytoplankton physiology, for example as a result of variations in nutrient supply or vertical mixing rates, will alter the efficiency with which the incoming solar radiation is converted to chemical energy via photosynthesis (Falkowski and Raven, 1997).

Carbon fixation rates estimated using ^{14}C incorporation experiments and a variety of models applied to *in situ* FRRF physiological data gave comparable results (Chapters 5 & 6). Both chlorophyll-specific and volume-specific productivity, as well as the depth integrated rates were similar between techniques. However, the dependence of these rates on the irradiance and biomass distributions was clearly emphasised when comparisons of ^{14}C and FRRF derived photosynthetic parameters were made (Chapter 5).

Although both spatial and temporal changes in the FRRF derived photophysiological characteristics of PSII were often accompanied by changes in photosynthetic parameters derived from carbon fixation, few robust relationships were observed. A previously unreported relationship between P^*_{max} and σ_{PSII} (σ_{PSII}') within natural phytoplankton communities was observed during both field studies for which the FRRF was deployed. A pattern of higher P^*_{max} and lower σ_{PSII} associated with regions of large cell (diatom) domination was consistent between both studies. It was unclear whether this relationship was determined by taxonomic variability, by the suggested physiological balance between light utilisation and electron turnover rates, or by some combination of both factors (Chapter 5). Further study of the relationships between FRRF derived physiological parameters and P^*_{max} is merited, particularly with reference to the derivation of photosynthetic rates from FRRF data.

To progress further it is essential to know why robust relationships between FRRF and ^{14}C derived physiology and productivity cannot be demonstrated. Are such problems a result of the complexities in performing these comparisons, or some lack in the current state of knowledge concerning the physiological balances between light utilisation and carbon

fixation? For example, the ^{14}C technique is known to be associated with many problems (e.g. Peterson, 1980; Carpenter and Lively, 1980; Fitzwater *et al.* 1987), however in the interests of pragmatism these are generally ignored. Continuously adjusting FRRF based measures of productivity in order that they conform to ^{14}C derived values may therefore be rather counter productive if errors in the ^{14}C technique are then incorporated into the FRRF estimates.

Additionally a variety of physiological processes can de-couple the rate of gross oxygen evolution (and hence FRRF derived ETR) from ^{14}C derived (~net) carbon fixation, including dark respiration, photorespiration, the Mehler reaction and variations in PQ (Suggett *et al.* 2001, see also § 5.4). The importance of these processes within the marine environment remains to be fully assessed. In particular, any possibility of variations due to changing environmental conditions and/or differences between taxonomic groups must be understood, before comparisons between the FRRF and ^{14}C techniques performed across ecological boundaries can be interpreted.

7.1.3 Extending the range of productivity estimates: what are the important parameters?

Ultimately the FRRF technique has the potential to measure changes in phytoplankton production over a large range of temporal and spatial scales. However, before this can be achieved, an understanding of the key physiological parameters controlling production, and how these are related to FRRF derived physiology, is required. Additionally, the usefulness of the FRRF technique for extending the areas over which measures of production can be obtained is limited if evaluating the production at any single site requires a complete diel cycle of changes in physiological parameters to be observed. It would be much more desirable if, for example, the data collected across a tidal mixing front using the SeaSoar undulator (Chapter 3) could be used to generate a transect of depth-integrated production across the system. Such estimates may require the combination of simple models with field data and certainly require evaluation of the importance of diel variability.

To illustrate these points, and as a tentative first step towards an increased utilisation of FRRF data, a further simplified model (MV) was developed based upon the various parameters required for the calculation of production. As previously mentioned the distribution of biomass (chlorophyll) and irradiance within a water column are certain to be significant in determining the integrated productivity. At a physiological level, the

maximal photosynthetic rate P^*_{max}, or the water column analogue P^*_{opt}, is the principal parameter driving changes in primary production (e.g. Behrenfeld and Falkowski, 1997; Sakshaug *et al.* 1997; Maraňón and Holligan, 1999). The results of the present study were consistent with this conclusion (Chapter 6).

The model therefore used the distribution of σ_{PSII} from the SeaSoar data and the observed empirical relationship between σ_{PSII} and P^*_{max} (Chapter 3) to estimate P^*_{max} across the frontal region. The chlorophyll distribution was estimated using the calibrated FRRF F_M measurement. The dark-acclimated (night-time) distributions of F_v/F_m and σ_{PSII} were used to calculate α^* (Eq. 5.4), with the effects of diel variations in all the photosynthetic parameters being ignored. Hence the integrated daily production for any site was modelled using the calculated values of α^*, P^*_{max} and chlorophyll, combined with the irradiance field. The MV model was thus a simplification of the MIV model (Chapter 5), the simpler model ignoring diel variability and assuming that a night-time profile of σ_{PSII} and F_v/F_m was representative of the mean physiological state of the phytoplankton community.

A limited sensitivity analysis was first performed using the *in situ* irradiance data from the four 24hr stations studied during the 1999 cruise (Chapter 3). Although the number of stations were limited, results indicated that the empirical model performed well, and that neglecting diel variability in physiology was of minor importance (*Table 7.1*). Higher production calculated using the MV model as opposed to the simulated *in situ* ^{14}C method at station M may have reflected enhanced photoinhibiton within the incubated samples (c.f. § 6.7). Spectral effects (c.f. § 6.3) were also not accounted for, and may have contributed to the differences between modelled and ^{14}C production.

For the frontal transects, the diel cycle of irradiance just beneath the sea surface (E(0)) was modelled at 30 minute intervals using a simple sinusoidal relationship with a midday maximum of $1300\mu Em^{-2}s^{-1}$. Light penetration through the water column was modelled using a chlorophyll dependent k_d, i.e. $k_d = 0.09 + 0.015$ chl *a* (Chapter 3). Sensitivity analysis, again performed for the four 24hr stations, indicated the influence of day to day variability in near surface irradiance caused by cloud. Potential problems estimating k_d from just the chlorophyll concentration were also evident, particularly for site E where coccoliths were present and site M3 where sediment may have been transported to the upper portion of the fully mixed water column by tidal mixing (*Table 7.1*).

	U2	E	M2	M3
$\int P_{14C}$ (g C m^{-2} d^{-1}) †	**0.80**	**0.50**	**1.30**	**0.90**
$\int P_{MIV}$ (g C m^{-2} d^{-1}, in situ irradiance)†	**1.10**	**0.50**	**1.40**	**1.40**
$\int P_{MV}$ (g C m^{-2} d^{-1}, in situ irradiance)	**0.70**	**0.51**	**1.90**	**1.40**
k_d (m^{-1}, observed)	0.094	0.190	0.149	0.142
k_d (m^{-1}, model)	0.097	0.117	0.131	0.117
'Cloud factor'	0.97	0.13	0.67	0.43
$\int P_{MV}$ (g C m^{-2} d^{-1}, clear sky)	**0.80**	**0.84**	**2.07**	**1.98**

Table 7.1 Results of FRRF productivity model MV for four 24hr stations studied during 1999 cruise. † indicates data from *Table 6.1.*

$\int P_{14C}$ is the daily integrated productivity using ^{14}C simulated *in situ* experiments.

$\int P_{MIV}$ is the MIV integrated productivity (Chapter 4).

$\int P_{MV}$ is the MV integrated productivity using *in situ* or modelled ('clear sky') irradiance, thus $\int P_{MV}$ (*in situ*) is equivalent to $\int P_{MIV}$ with no diel variability.

k_d observed and modelled are average over upper 20m of water column. The difference between the modelled ('clear sky') irradiance and the measured in situ irradiance was evaluated as the ratio of the integrated daily irradiance experienced at 20m, denoted 'cloud factor'.

Cross frontal transects of the integrated daily productivity using this model indicated small scale variations associated with physical variability which would be unresolvable using fixed stations (*Fig. 7.1*). Spring-neap adjustment of the distribution of production around the front was also revealed, further illustrating the potential to investigate patterns of productivity within highly dynamic systems (*Fig. 7.1*). The importance of the physiological state of the phytoplankton, at least in the context of the present model, in driving the pattern of productivity was investigated by regression of the integrated daily rate against various parameters. The sea-surface chlorophyll concentration accounted for <30% of the variance in productivity, whereas the near surface value of P^*_{max} (or equivalently σ_{PSII} for this model), accounted for 67%.

The possibility of using physiological parameters such as σ_{PSII} as proxies for P^*_{max} may also find utility in remote sensing applications (e.g. Behrenfeld and Falkowski, 1997; Chekalyuk *et al.* 2000). For example, the association of low σ_{PSII} and high P^*_{max} with the high chlorophyll coastal bloom off North East New Zealand provided additional information which could be utilised when estimating productivity from satellite derived sea-surface chlorophyll data such as *Fig. 4.21.*

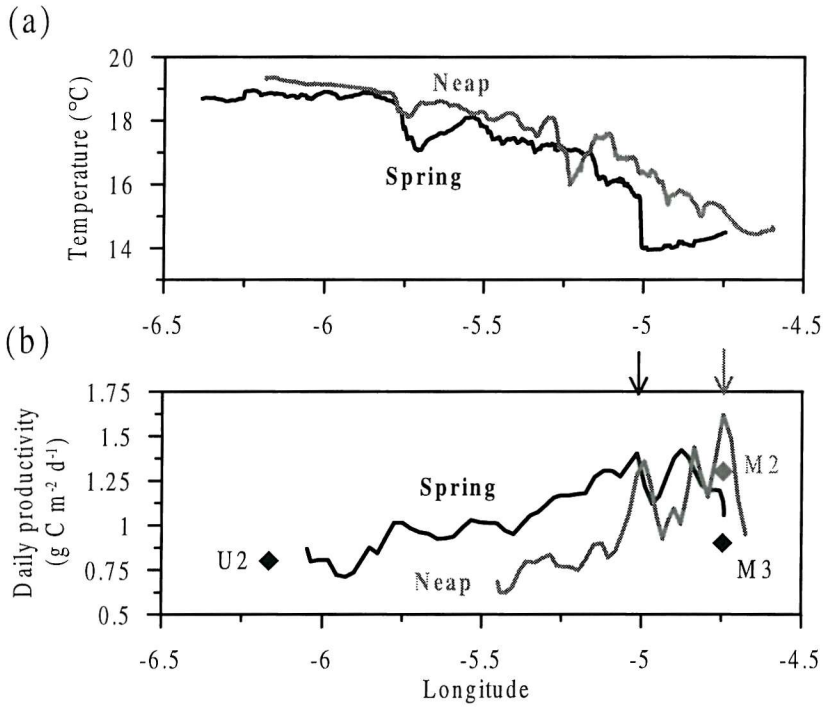

Fig. 7.1 Result of simple productivity model (MV) applied to cross-frontal FRRF data obtained using the SeaSoar undulator. (a) Sea surface temperature (°C) measured during two crossings of the front under spring (black line, 2nd August 1999) and neap (grey line, 8th – 9th August 1999) tidal conditions. (b) Integrated daily production (g C m^{-2} d^{-1}) calculated by applying the MV model to the FRRF data collected during the two frontal transects (lines), and estimated using simulated *in situ* ^{14}C experiments during the three 24hr stations occupied in the vicinity of the front, U2 (◆), M2(◆, neap) and M3 (◆, spring). SeaSoar data was averaged into vertical profiles with approximately 5km horizontal resolution. Variability in integrated production was apparent at these small scales. Arrows indicate the approximate frontal position defined as the point at which the 15°C isotherm outcropped at the surface.

In summary, it is becoming increasingly accepted that our ability to measure or model productivity over large spatial or temporal scales is currently limited by an inadequate understanding of the environmental controls on phytoplankton physiology, particularly P^*_{max} (Balch and Byrne, 1994; Behrenfeld and Falkowski, 1997; Sakshaug *et al.*1997; Maranón and Holligan, 1999; Seigel *et al.* 2001). Even if the (largely empirical) models used in the current study are invalid, the FRRF technique is likely to be a useful tool for addressing such problems due to the high resolution *in situ* physiological data obtained.

7.2 Physical controls on shelf sea productivity

7.2.1 Tidal mixing fronts

The suggestion that the high levels of surface chlorophyll observed in the vicinity of shelf sea fronts are a result of active growth (Pingree et al. 1975,1977; Holligan, 1981) was strongly supported by this study. The FRRF derived physiological data (Chapter 3), when combined with turbulent mixing and hydrographic data, indicated that phytoplankton growth was nutrient limited towards the stratified side of the front and light limited in the mixed regions. Estimates of production and growth rates across the front also indicated maximal values within the transition region of the front (Chapter 6, & *Fig. 7.1*).

Although direct observations of the loss terms (e.g. grazing), or the degree of passive accumulation within the frontal region, were not made (Lefevre, 1986; Franks, 1992a&b), these processes cannot be solely responsible for the distribution of biomass. In particular if changes in growth rates were not occurring, the following hypothesis would be expected to hold: *The variations in physical and environmental forcing across a shelf sea front do not result in differences of physiology or production within the associated phytoplankton communities.* Such a hypothesis is clearly falsified by the results of the current study.

7.2.2 Regions of high seasonal stratification

Two distinct ecological regimes exist within the water column in highly stratified regions of shelf seas, the thermocline and surface layer.

The 'oligotrophic' summer surface layer

The surface region is, to a large extent, isolated from the lower water column. None of the observed nutrient flux into the bottom of the thermocline appears to penetrate into the surface layer. The current study suggested that growth rates within these surface waters were low, contrasting with the suggestion that high growth rates exist within such low nutrient regions driven by the rapid turn-over of a regenerative system (Goldman *et al.* 1979). Physiological indicators (specifically a low F_v/F_m) also indicated nutrient limitation of growth within the surface layer. The influence of the possible external sources of nutrient on the ecology of the summer surface layer in highly stratified shelf seas remains an open question. For regions close to fronts, eddy activity may be important in transporting nutrients into the system (Pingree *et al.* 1979). Episodic storm events may also

be important (Sharples *et al.* 2001b). The degree to which dissolved organic matter, locked into the surface layer during the spring bloom, fuels production throughout the remainder of the year is also unknown (Anderson and Williams, 1998).

The shelf sea thermocline

A standard explanation for the enhanced biomass observed within the highly stratified seasonal thermocline in certain regions of shelf seas, is that growth above the thermocline is nutrient limited and growth below is light limited. Active growth within the thermocline is then supported by adequate irradiance from above and a flux of nutrients from below.

Physical and physiological data presented in the current study supported this hypothesis (Chapter 3). Physiological data (specifically a higher F_v/F_m) indicated that the phytoplankton population within the thermocline was relieved from nutrient stress as compared to the surface population. Physiological data also indicated that thermocline populations were adapted and/or acclimated to the low light levels experienced (Chapters 3 & 6). The availability of FRRF data were crucial in reaching these conclusions, as potential problems with ^{14}C incubation techniques were observed for thermocline populations (Chapter 3). New production within highly stratified shelf sea seasonal thermoclines was also shown to be fuelled by physically driven fluxes of nutrients (Chapter 3 and Sharples *et al.* 2001a).

Physically driven loss of phytoplankton from the thermocline region may be an important (and previously under-represented) mechanism governing the balance between nutrient supply rates, population growth and the accumulation of biomass within the shelf sea sub-surface chlorophyll maximum. Results from the current study indicated that over short time-scales O(day) vertical nutrient supply rates may be insufficient to maintain thermocline populations against physically driven export and additional loss terms such as grazing or sinking (Sharples *et al.* 2001a). However these conclusions are drawn from observations of a single site over one 24hr period.

Fluxes both into and out of the thermocline are likely to be modulated by the spring-neap cycle of tidal mixing and are also likely to vary from region to region, depending on the balance between surface buoyancy input and tidal mixing. This is illustrated by the spring-neap cycle of frontal position and inferred pulsed supply of nutrients for new production within the transition region of shelf sea fronts. The patches of high chlorophyll found within shelf sea thermoclines in this and other studies (e.g. Holligan 1981), tend to be close to frontal regions. This suggests that the mechanisms responsible for these dense

aggregations of phytoplankton are likely to be related to the mechanisms for enhanced production at fronts, again pointing to a tidal cause.

Many unanswered questions remain concerning the biological and physical aspects of the shelf sea thermocline region. The cause of the patchy nature of the chlorophyll concentration observed at the highly stratified site is unclear (Sharples *et al.* 2001a). Additionally the reason for the highly mono-specific nature of the phytoplankton communities which survive in these regions is not known. For example the adaptations which allowed the coccolithophore *Calyptrosphaera oblonga* to dominate within the base of the thermocline at U2 are unknown (Chapter 3 & Sharples *et al.* 2001a). The contribution of physical processes such as the spring-neap cycle and small internal waves also remains to be assessed. Thus in order to evaluate the processes occurring within the thermocline and associated chlorophyll maximum, more data, including longer time series at individual sites, are required.

7.2.3 Internal tide dominated regions

The internal tide was shown to dominate physical variability at a number of sites on the Northeast New Zealand continental shelf. At all the sites studied the dissipation of internal tidal energy was shown to generate a significant vertical flux of nutrients, increasing the potential for new production (Chapter 4 and Sharples *et al.* 2001b). Additionally the large amplitude displacements of the internal density structure were shown to have a marked influence on the light climate experienced by phytoplankton.

The influence such internal motions will have on the productivity and growth of phytoplankton is likely to be a function of the ability of the *in situ* phytoplankton population to acclimate to the changing irradiance and nutrient fields. For example it was shown that the *in situ* population could generally maintain acclimation to the instantaneous irradiance except under the highest vertical velocities. Additionally, the phytoplankton communities associated with the thermocline in areas dominated by strong internal tides tend to have a mixed species composition, this possibly representing a range of adaptations to a highly dynamic environment.

Marked spatial variability in the physical forcing further complicates quantification of the net influence of internal waves on phytoplankton growth. Internal wave propagation within shelf seas can be effected by changing bathymetry (Chapter 4 and Stevens *et al. In Prep.*).

Additionally the degree of internal wave dissipation is likely to vary depending on the distance from the generation point. Quantification of the influence of internal tidal processes on the productivity of shelf seas is thus a difficult problem and may need to be addressed using detailed physical-biological models.

7.2.4 Auxiliary energy and Ergoclines

The primary source of energy for photosynthesis and hence growth within the aquatic ecosystem is light. The dissipation of tidal energy at the nutricline physically transports nutrients towards the surface. This turbulent dissipation thus represents an additional source of 'auxiliary' energy acting to enhance productivity (Margalef, 1978; Legendre, 1981; Legendre and Demers, 1985). The auxiliary energy does not directly influence production, rather it relieves growth limitation by causing a transport to occur between two regions with differing limiting resources. Legendre and Demers (1985) and Legendre *et al.* (1986) pointed out that high production tends to occur at the regions where there is a strong gradient in auxiliary energy. They termed these regions ergoclines. Shelf sea thermoclines and tidal mixing fronts are two examples of ergoclines, where enhanced production may result from a supply of mechanical energy to the biological-physical system.

In the current study, auxiliary energy, in the form of turbulent dissipation, was directly measured at a number of sites (Chapters 3 & 4). It was suggested that the form of tidal dissipation is crucial in governing the balance of new and total production within shelf seas (Chapter 6). Baroclinic (internal) tides appeared to be more efficient at producing a vertical nutrient flux than barotropic tides. It is therefore hypothesised that regions dominated by baroclinic tidal mixing are likely to be more important in terms of new production (exhibit higher f-ratios), due to the greater levels of auxiliary energy acting on the nutrient gradient (Chapter 6).

The presence and/or behaviour of the *in situ* phytoplankton community may also be important in governing the nature of the ergocline. An example is the thermocline region, where biological uptake serves to enhance the nitracline (e.g. Sharples *et al.* 2001a). Such sharpening of the nitrate gradient may be further increased by the motility of the majority of species found in such regions (Holligan, 1981). Regardless of whether active migration plays a part, the net effect is an increase in the nitrate flux and a gradual deepening of the nitracline (Sharples *et al.* 2001a). The behaviour of the phytoplankton community may therefore be responsible for increasing the (new) production occurring at the ergocline. The

process of nitracline deepening brings the phytoplankton into contact with a region of higher auxiliary energy, specifically the bottom mixed layer. For the case in question this increases the chance of proportion of the population being permanently removed from the euphotic zone (see above and Sharples *et al.* 2001a). Thus the supply of mechanical energy can enhance production and drive active export at the ergocline.

Margalef, (1978) suggested that the varying forms of phytoplankton represent adaptations to different levels of turbulence. In keeping with such a view, variations in the physiological acclimation and/or adaptation of the *in situ* phytoplankton communities observed in the current study could be interpreted as responses to the degree of auxiliary energy. The concepts of auxiliary energy and ergoclines may therefore be useful in future investigations of the adaptations of specific taxa to certain environments.

7.3 Conclusions and further work

The FRRF technique was demonstrated to be capable of measuring phytoplankton physiology at scales relevant to those of physical forcing. Although more work is required to assess the assumptions and sensitivity of the models used in this study and elsewhere (Kolber and Falkowski, 1993; Suggett *et al.* 2001), the FRRF technique is also likely to extend the resolution of primary production measurements to these new scales. Such techniques therefore have the potential to increase significantly our understanding of the interaction between plankton ecology and physical forcing.

The novel application of *in situ* biological and physical sensors enabled detailed investigations of the dynamic properties of shelf sea ecosystems to be performed. Physical forcing, in the form of tidal energy, was shown to exert a strong control on phytoplankton physiology and hence production and growth within a variety of systems.

Ultimately the balances between physical forcing, new production, export and growth within shelf seas may be moderated by the physiological properties of the phytoplankton communities growing in these regions. Information on the physiology and behaviour of phytoplankton at a taxonomic level may therefore be needed. It is suggested that an adequate understanding of the biological-physical system is currently limited by a lack of knowledge concerning how phytoplankton balance light utilisation, carbon fixation, nitrogen assimilation and chlorophyll content, under such highly dynamic environmental conditions. The relative importance of the biological forcing (e.g. physiological

acclimation and species composition) and physical forcing (e.g. barotropic or baroclinic tides) in controlling the flux of energy and chemical constituents through the shelf sea ecosystem therefore remains a challenging field of study.

Further work

Interpretation of FRRF data

Current limitations in our ability to interpret field FRRF data principally result from inadequacies in the understanding of the relationships between photo-physiology and production. To a certain extent this problem may be rectified as more information collected in well defined ecological contexts emerges. However it is felt that further carefully controlled experimental work (e.g. Kolber *et al.* 1988; Parkhill *et al.* 2001), on both natural populations and cultures, is required to aid the interpretation of FRRF field data. Such work would promote the greater use of the instrument as a general oceanographic tool.

Studies of the response of carbon fixation physiology (^{14}C P* vs. E), photo-physiology (FRRF) and the cellular C, N and chlorophyll pools for laboratory cultures acclimating to different growth conditions would considerably enhance the ability to interpret the FRRF signal. In particular variations in response between different functional groups may indicate whether simple models of production based on FRRF data will be widely applicable across ecological domains.

For example a specific hypothesis to be tested is:

The relationships between σ_{PSII} and P^*_{max} observed within the current study were purely an artefact of the sampling strategy crossing between ecological provinces dominated by differing functional groups of phytoplankton.

A laboratory study of the acclimated state of various functional groups of phytoplankton under various degrees of nutrient or light limitation could address this hypothesis. An inverse relationship between P^*_{max} and σ_{PSII} for a single species under differing states of acclimation would go some way towards falsifying the hypothesis and therefore supporting a physiological explanation.

FRRF incubation experiments such as those performed during the 2000 cruise (Chapter 4), are likely to be useful for investigating the dynamic response of natural populations to changes in irradiance. Similar experiments designed to quantify responses to nutrient enrichment are also possible. Experiments using the apparatus utilised in the current study

to evaluate responses to iron enrichment have already been undertaken (E. Abraham and P. Boyd, *pers comm*).

Physical biological interactions in shelf seas

The combination of the FRRF technique with high quality physical data concerning turbulent dissipation and mixing was found to be a powerful tool for the study of highly dynamic ecosystems. Due to the limitations imposed by instrument failure during a number of the cruises in this study, particularly the CTD winch failure during the 1999 cruise, it was felt that the full potential of the sampling strategy has not yet been achieved. Further fieldwork, when combined with information concerning the balance of carbon and nitrogen uptake, has the potential to significantly increase our understanding of the shelf sea ecosystem. Continuation of the work, particularly focusing on the seasonal shelf sea thermocline, has recently been funded.

The deployment of the FRRF instrument on towed undulating vehicles was also found to be a useful tool. The ability to gain detailed physical and biological data in this way is likely to find utility in the investigation of dynamic ecosystems throughout the oceans. A field study of an energetic, open ocean, eddy dominated region has already been performed using some of the protocols developed as part of this work.

Species-specific physiology and adaptations

One final area of future work is likely to be the investigation of species dependent variability in photo-physiology within field populations. The FRRF instrument measures the physiological state of the bulk community. By investigating the physiological state of individual cells or size fractions, questions concerning the adaptations of different functional groups of phytoplankton to a specific environmental niche may be addressed. Work using flow cytometric techniques for assessing the fluorescence derived photo-physiology of individual cells is being performed by several groups (Olson *et al.* 1996; 2000, Gorbunov *et al.* 1999). Some limited work during the 1999 cruise suggested that a simpler method, whereby different size fractions are separated by gentle filtration then run through a benchtop FRRF, could produce similar data (see also Kolber *et al.* 1994; Boyd and Abraham, 2001). Further work using such techniques may prove useful in elucidating the contribution of individual taxa or functional groups to the productivity of marine ecosystems.

References

Agrawal, Y.C., Terray, E.A., Donelan, M.A., Hwang, P.A., Williams, A.J., Drennan, W.M., Kahma, K.K. and Kitaigorodskii, S.A., (1992) Enhanced dissipation of kinetic energy beneath surface waves. *Nature* **359** 219-220

Allen, J.F., (1992) Protein phosphorylation in regulation of photosynthesis. *Biochem. Biophys. Acta.* **1098** 275-335

Alpers, W., (1985) Theory of radar imaging of internal waves. *Nature* **314** 245-247

Anderson, G.C., (1969) Subsurface chlorophyll maximum in the northeast Pacific Ocean. *Limnol. Oceanogr.* **14** 386-391

Anderson, T.R. and Williams, P.J.L., (1998) Modelling the seasonal cycle of dissolved organic carbon at station E-1 in the English Channel *Estuar. Coast Shelf Sci.* **46** 93-109

Anning, T., MacIntyre, H.L., Pratt, S.M., Sammes, P.J., Gibb, S. and Geider, R.J., (2000) Photoacclimation in the marine diatom *Skeletonema costatum*. *Limnol. Oceanogr.* **45** 1807-1817

Babin, M., Morel, A. and Gagnon, R., (1994) An incubator designed for extensive and sensitive measurements of phytoplankton photosynthetic parameters. *Limnol. Oceanogr.* **39**694-702

Babin, M., Morel, A., Claustre, H., Bricaud, A., Kolber, Z. and P.G. Falkowski, (1996) Nitrogen and irrradiance-dependent variations in the maximum quantum yield of carbon fixation in eutrophic, mesotrophic and oligotrophic marine systems. *Deep-Sea Res. I* **43** 1241-1272

Baines, P.G., (1982) On internal tide generation models. *Deep Sea Res.* **29** 307-338

Balch, W.M. and Byrne, C.F., (1994) Factors affecting the estimate of primary production from space. *J. Geophys. Res.* **99** 7555-7570

Banse, K., (1992) Grazing, temporal changes of phytoplankton concentrations and the microbial loop in the open sea. *In* Falkowski, P.G. and Woodhead, A. (eds), Primary productivity and biogeochemical cycles in the Sea. Plenum Press, New York. 550pp

Barlow, R.G., Cummings, D.G. and Gibb, S.W., (1997) Improved resolution of mon- and divinyl chlorophylls *a* and *b* and zeaxanthin and lutein in phytoplankton extracts using reverse phase C-8 HPLC. *Mar. Ecol. Prog. Ser.* **161** 303-307

Batchelor, G.K., (1959) Small-scale variation of convected quantities like temperature in turbulent fluid. *Journal of Fluid Mechanics* **5** 113-133

Behrenfeld, M.J., Bale, A.J., Kolber, Z.S., Aiken, J., and Falkowski, P.G., (1996) Confirmation of iron limitation of phytoplankton photosynthesis in the equatorial Pacific Ocean. *Nature* **383** 508-511

Behrenfeld, M.J. and Falkowski, P.G., (1997) Photosynthetic rates derived from satellite-based chlorophyll concentration. *Limnol. Oceanogr.* **42** 1-20

Behrenfeld, M.J., Prasil, O., Kolber, Z.S., Babin, M. and Falkowski, P.G., (1998) Compensatory changes in Photosystem II electron turnover rates protect photosynthesis from photoinhibition. *Photosyn. Res.* **58** 259-268

Behrenfeld, M.J. and Kolber, Z.S., (1999) Widespread iron limitation of phytoplankton in the South Pacific Ocean. *Science* **283** 840-843

Bender M., Grande K., Johnson K., Marra J., Williams P.J.L., Sieburth J., Pilson M., Langdon C., Hitchcock G., Orchardo J., Hunt C., Donaghay P. and Heinemann K., (1987) A comparison of four methods for determining planktonic community production. *Limnol. Oceanogr.* **32** 1085-1098

Berges, J.A., Charlebois, D.O., Mauzerall, D.C. and Falkowski, P.G., (1996) Differential effects of nitrogen limitation on photosynthetic efficiency in photosystems I and II in microalgae. *Plant Physiol.* **110** 689-696

Berges, J.A. and Falkowski, P.G., (1998) Physiological stress and cell death in marine phytoplankton: Induction of proteases in response to nitrogen or light limitation. *Limnol. Oceanogr.* **43** 129-135

Berner, T., Dubinsky, Z., Wyman, K. and Falkowski, P.G., (1989) Photoadaptation and the "package" effect in *Dunaliella Tertiolecta* (Chlorophyceae). *J. Phycol.* **25** 70-78

Bisagni, J.J. and Sano, M.H., (1993) Satellite observations of sea-surface temperature variability on southern Georges Bank. *Cont. Shelf Res.* **13** 1045-1064

Bogucki, D. and Garrett, C., (1993) A simple-model for the shear induced decay of an internal solitary wave. *J. Phys. Oceanogr.* **23** 1767-1776

Bowers, D.G. and Simpson, J.H., (1987) Mean position of tidal fronts in European-Shelf seas. *Cont. Shelf Res.* **7** 35-44

Boyd, P.W., Aiken, J. and Kolber, Z., (1997) Comparison of radiocarbon and fluorescence based (pump and probe) measurements of phytoplankton photosynthetic characteristics in the Northeast Atlantic Ocean. *Mar. Ecol. Prog. Ser.* **149** 215:226

Boyd, P., LaRoche, J., Gall, M., Frew. R. and McKay, R.M.L., (1999) Role of iron, light and silicate in controlling algal biomass in subantarctic waters SE of New Zealand. *J. Geophys. Res.* **104** 13395-13408

Boyd, P.W., (2000) A mesoscale phytoplankton bloom in the polar Southern Ocean stimulated by iron fertilization. *Nature* **407** 695-702

Boyd, P.W. and Abraham, E.R., (2001) Iron-mediated changes in phytoplankton photosynthetic competence during SOIREE. *Deep Sea Res. II* **48** 2529-2550

Broecker, W. and Peng, T.H., (1982) Tracers in the sea. Eldiago Press, New York

Brickmann, D. and Loder, J.W., (1993) Energetics of the Internal Tide on Northern Georges Bank. *J. Phys. Oceanogr.* **23** 409-424

Bury, S.J., Boyd, P.W., Preston, T., Savidge, G., Owens, N.J.P., (2001) Size-fractionated primary production and nitrogen uptake during a North Atlantic phytoplankton bloom: implications for carbon export estimates. *Deep Sea Res.* **48** 689-720

Carpenter, E.J. and Lively, J.S., (1980) Review of estimate of algal growth using ^{14}C tracer techniques, p. 161-178. *In* Primary productivity in the sea. Brookhaven Symp. Biol 31. Plenum.

Chekalyuk, A.M., Hoge, F.E., Wright, C.W., Swift, R.N. and Yungel, J.K. (2000) Airborne test of laser pump-and-probe technique for assessment of phytoplankton photochemical characteristics. *Photosyn Res.* **66** 45-56

Claustre, H., (1994) The trophic status of various oceanic provinces as revealed by phytoplankton pigment signatures. *Limnol. Oceanogr.* **39** 1207-1211

Claustre, H., Kerherve, P., Marty, J.C. and Prieur, L. (1994) Phytoplankton photoadaptation related to some frontal physical processes. *J. Mar. Sys.* **5** 251-265

Cleveland, J.S., Bidigare, R. and Perry, M.J., (1989) Maximum quantum yield of photosynthesis in the northwestern Sargasso Sea. *J. Mar. Res.* **47** 869-886

Cloern, J.E., Grenz, C. and VidergarLucas, L. (1995) An empirical model of the phytoplankton chlorophyll:carbon ratio - The conversion factor between productivity and growth rate. *Limnol. Oceanogr.* **40** 1313-1321

Cooper, L.H.N., (1947) Internal waves and upwelling of oceanic water from mid-depths on to a continental shelf. *Nature* **159** 579

Copin-Montegut, C. and Copin-Montegut, G., (1983) Stoichiometry of carbon, nitrogen and phosphorus in marine particulate mater. *Deep Sea Res.* **30** 31-46

Cullen, J.J. and Eppley, R.W., (1981) Chlorophyll maximum layers of the southern California Bight and possible mechanisms of their formation and maintenance. *Oceanol. Acta.* **4** 23-32

Cullen, J.J., Stewart, E., Renger, E., Eppley, R.W. and Winant, C.D., (1983) Vertical motion of the thermocline and chlorophyll maximum layers in relation to currents on the Southern California Shelf. *J. Mar. Res.* **41** 239-262

Cullen, J.J. and Lewis, M.R., (1988) The kinetics of algal photoadaptation in the context of vertical mixing. *J. Plankton Res.* **10** 1039-1063

Cullen, J.J., Yang, X. and MacIntyre, H.L. (1992) Nutrient limitation of marine photosynthesis. *In* Falkowski, P.G. and Woodhead, A. (eds), Primary productivity and biogeochemical cycles in the Sea. Plenum Press, New York. 550pp

Daneri, G., Iriartem A., Garcia, V.M., Purdie, D.A. and Crawford, D.W., (1992) Growth irradiance as a factor controlling the dark respiration rates of marine phytoplankton. *J. Mar. Biol. Assoc. U.K.* **72** 723-726

Dasaro, E.A. and Dairiki, G.T., (1997) Turbulence intensity measurements in a wind-driven mixed layer. *J. Phys. Oceanogr.* **27** 2009-2022

DeBaar, H.J.W., (1994) Von Liebig Law of the minimum and plankton ecology. *Prog. Oceanogr.* **33** 347-386

Decker, M.B. and Hunt, G.L., (1996) Foraging by murres (*Uria* spp.) at tidal fronts surrounding the Pribilof Islands, Alaska, USA. *Mar. Ecol. Prog. Ser.* **139** 1-10

Denham, R.N., Bannister, R.W., Guthrie, K.M. and Crook, F.G., (1984) Surveys of the East Auckland and East Cape Currents. *Aust. J. Mar. Fres. Res.* **35** 491-504

Denman, K.L. and Gargett, A.E., (1983) Time and space scales of vertical mixing and advection of phytoplankton in the upper ocean. *Limnol. Oceanogr.* **28** 801-815

Dewey, R.K., Crawford, W.R., Gargett, A.E. and Oakey, N.S., (1987) A microstructure instrument for profiling oceanic turbulence in coastal bottom boundary layers. *J. Atmos. Oceanic. Technol.* **4** 288-297

Dickson, R.R., Gurbutt, P.A. and Narayana Pillai, V., (1980) Satellite evidence of enhanced upwelling along the European continental slope. *J. Phys. Oceanogr.* **10** 813-819

Dillon, T.M. and Caldwell, D.R., (1980) The Batchelor spectrum and dissipation in the upper ocean. *Journal of Geophysical Research* **85** 1910-1916

Dubinsky, Z., Falkowski, P.G. and Wyman, K., (1986) Light harvesting and utilisation by phytoplankton. *Plant Cell Physiol.* **27** 1335-1349

Dugdale, R.C. and Goering, J.J., (1967) Uptake of new and regenerated forms of nitrogen in primary productivity. *Limnol. Oceanogr.* **12** 196-206

Dusenberry, J.A., Olson, R.J. and Chisholm, S.W., (2001) Photoacclimation kinetics of single-cell fluorescence in laboratory and field populations of Prochlorococcus *Deep Sea Res. I* **48** 1443-1458

Effron, B. and Gong, G., (1983) A leisurely look at the bootstrap, the jack-knife and cross-validation. *Am. Stat.* **37** 36-46

Eppley, R.W., (1972) Temperature and phytoplankton growth in the sea. *J. Can. Fish. Res. Bd.* **70** 1063-1085

Eppley, R.W. and Peterson, B.J., (1979) Particulate organic matter flux and planktonic new production in the deep ocean. *Nature* **282** 677-680

Eppley, R.W., (1980) Estimating phytoplankton growth rates in the oligotrophic oceans, *in* Primary productivity in the sea, P.G. Falkowski, *Ed.* Plenum Press, New York, 531pp

Falkowski, P.G., (1980) Light-shade adaptation in marine phytoplankton, *in* Primary productivity in the sea, P.G. Falkowski, *Ed.* Plenum Press, New York, 531pp

Falkowski, P.G., (1983) Light-shade adaptation and vertical mixing of marine phytoplankton: A comparative field study. *J. Mar. Res.* **41** 215-237

Falkowski, P.G., (1984) Physiological responses of phytoplankton to natural light regimes. *J. Plankt. Res.* **6** 295-307

Falkowski, P.G., Dubinsky, Z. and Wyman, K., (1985) Growth-irradiance relationships in phytoplankton. *Limnol. Oceanogr.* **30** 311-321

Falkowski, P.G., Wyman, K., Ley, A.C. and Mauzerall, D.C., (1986) Relationship of steady-state photosynthesis to fluorescence in eukaryotic algae. *Biochim. Biophys. Acta.* **849** 183-192

Falkowski, P.G. and LaRoche, J., (1991) Acclimation to spectral irradiance in algae. *J. Phycol.* **27** 8-14

Falkowski, P.G., Ziemann, D., Kolber, Z. and Biefang, P.K., (1991) Nutrient pumping and phytoplankton response in a subtropical mesoscale eddy. *Nature* **352** 544-551

Falkowski, P.G., (1992) Molecular ecology of phytoplankton photosynthesis. Pp47-67. *In* Falkowski, P.G. and Woodhead, A. (eds), Primary productivity and biogeochemical cycles in the Sea. Plenum Press, New York. 550pp

Falkowski, P.G., Greene, R.M. and Geider, R.J., (1992) Physiological limitations on phytoplankton productivity in the ocean. *Oceanogr.* **5** 84-91

Falkowski, P.G., Greene, R. and Kolber, Z., (1994) Light utilization and photoinhibition of photosynthesis in marine phytoplankton. *In.* Photoinhibition of photosynthesis: from molecular mechanisms to the field. N.R. Baker and J.R. Bowyer *Eds. Bios Scientific Publishers Ltd. Oxford* pp407-432

Falkowski, P.G. and Kolber, Z.S., (1995)Variations in chlorophyll fluorescence yields in phytoplankton in the worlds oceans. *Austral. J. Plant Physiol.* **22** 341-355

Falkowski, P.G. and Raven, J.A., (1997) Aquatic photosynthesis *Blackwell Science* U.K. 375pp

Falkowski, P.G. (2000) Rationalizing elemental ratios in unicellular algae. *J. Phycol.* **36** 3-6

Fasham, M.J.R., Holligan, P.M. and Pugh, P.R., (1983) The spatial and temporal development of the spring phytoplankton bloom in the Celtic Sea, April, 1979. *Prog. Oceanog.* **12** 87-145

Fasham, M.J.R., Ducklow, H.W. and Mckelvie, S.M., (1990) A nitrogen-based model of plankton dynamics in the ocean mixed layer. *J. Mar. Res.* **48** 591-639

Finch, M.S., Hydes, D.J., Clayson, C.H., Weigl, B., Dakin, J. and Gwilliam, P. (1998) A low power ultra violet spectrophotometer for measurement of nitrate in seawater: introduction, calibration, and initial sea trials. *Anal. Chim. Acta.* **377** 167-177

Fitzwater, S.E., Knauer, G.A. and Martin, J.H., (1982) Metal contamination and its effects on primary production measurements. *Limnol. Oceanogr.* **27** 544-551

Flameling, I.A. and Kromkamp, J., (1998) Light dependence of quantum yields for PSII charge separation and oxygen evolution in eucaryotic algae. *Limnol. Oceanogr.* **43** 284-297

Fofonoff, N.P., (1969) Spectral characteristics of internal waves in the ocean. *Deep Sea Res. Oceanogr. Abstr.,* **16,** *suppl.* 59-71

Franks, P.J.S., (1992a) Phytoplankton blooms at fronts – patterns, scales, and physical forcing mechanisms. *Rev. Aquatic. Sci.* **6** 121-137

Franks, P.J.S., (1992b) Sink or swim: accumulation of biomass at fronts. *Mar. Ecol. Prog. Ser.* **82** 1-12

Franks, P.J.S. and Marra, J., (1994) A simple new formulation for phytoplankton photoresponse and an application in a wind-driven mixed-layer model. *Mar. Ecol. Prog. Ser.* **111** 143-153

Franks, P.J.S. and Chen, C.S., (1996) Plankton production in tidal fronts: A model of Georges Bank in summer. *J. Mar. Res.* **54** 631-651

Geider, R.J., (1987) Light and temperature dependence of the carbon to chlorophyll *a* ratio in microalgae and cyanobacteria: implications for physiology and growth of phytoplankton. *New Phytol.* **106** 1-34

Geider, R.J., (1992) Respiration: taxation without representation? *In* Falkowski, P.G. and Woodhead, A. (eds), Primary productivity and biogeochemical cycles in the Sea. Plenum Press, New York. 550pp

Geider R.J., Greene R.M., Kolber Z., Macintyre H.L. and Falkowski P.G., (1993). Fluorescence assessment of the maximum quantum efficiency of photosynthesis in the Western North-Atlantic. *Deep-Sea Res.* **40** 1205-1224

Geider, R.J., MacIntyre, H.L. and Kana, T.M. (1998) A dynamic regulatory model of phytoplanktonic acclimation to light, nutrients, and temperature *Limnol. Oceanogr.* **43** 679-694

Genty, B., Briantais, J-M., and Baker, N.R., (1989) The relationship between the quantum yield -of photosynthetic electron transport and quenching of chlorophyll fluorescence *Biochimica et Biophysica Acta.* **990** 87-92

Gerkema, T., (1996) A unified model for the generation and fission of internal tides in a rotating ocean. *J. Mar. Res.* **54** 421-450

Gibson, C.H. and Schwarz, W.H., (1963) The universal equilibrium spectra of turbulent velocity and scalar fields. *Journal of Fluid Mechanics* **16** 365-384

Gibert, M., Wilhelm, C. and Richter, M., (2000) Bio-optical modelling of oxygen evolution using *in vivo* fluorescence: Comparison of measured and calculated photosynthesis/irradiance (P-I) curves in four representative phytoplankton species. *J. Plant Physiol.* **157** 307-314

Goldman, J.C., McCarthy, J.J. and Peavey, D.G., (1979) Growth rate influence on the chemical composition of phytoplankton in oceanic waters. *Nature* **279** 210-215

Gorbunov, M.Y., Kolber, Z.S. and Falkowski, P.G., (1999) Measuring photosynthetic parameters in individual algal cells by Fast Repetition Rate fluorometry. *Photosyn. Res.* **62** 141-153

Gorbunov, M.Y., Kolber, Z.S., Lesser, M.P. and Falkowski, P.G., (2001) Photosynthesis and photoprotection in symbiotic corals. *Limnol. Oceanogr.* **46** 75-85

Gran, H.H. and Braarud, T., (1935) A quantitative study of the phytoplankton in the Bay of Fundy and the Gulf of Maine (including observations on hydrography, chemistry and turbidity). *J. Biol.Bd. Canada* **1** 279-433

Grande, K., Marra, D.J., Langdon, C., Heinemann, K. and Bender, M.L., (1989) Rates of respiration in the light measured using an ^{18}O isotope labelling technique. *J. Exp. Mar. Biol. Ecol.* **129** 95-120

Grasshoff, K.M., Erhardt, K.M., and Kremling, K., (1983) Methods of seawater analysis. Verlag-Chemie.

Graziano, L.M., Geider, R.J. and Olaizola, M., (1996) Nitrogen limitation of North Atlantic phytoplankton: analysis of physiological condition in nutrient enrichment experiments. *Aquat. Microb. Ecol.* **11** 53-64

Greene, R.M., Geider, R.J. and Falkowski, P.G., (1991) Effect of iron limitation on photosynthesis in a marine diatom. *Limnol. Oceanogr.* **36** 1772-1782

Greene, R.M., Kolber, Z.S., Swift, D.G., Tindale, N.W. and Falkowski, P.G., (1994) Physiological limitation of phytoplankton photosynthesis in the eastern equatorial Pacific determined from variability in the quantum yield of fluorescence. *Limnol. Oceanogr.* **39** 1061-1074

Guizien, K., Barthelemy, E. and Inall, M.E., (1999) Internal tide generation at a shelf break by an oblique barotropic tide: Observations and analytical modelling. *J. Geophys. Res.* **104** 15655-15668

Hansson, Ö. And Wydrzyski, T., (1990) Current perceptions of photosystem II. *Photosynth. Res.* **23** 131-162

Harrison, W.G., PLATT, T. and Lewis, M.R., (1987) F-ratio and its relationship to ambient nitrate concentration in coastal waters. *J. Plankt. Res.* **9** 235-248

Harrison, W.G., Harris, L.R. and Irwin, B.D., (1996) The kinetics of nitrogen utilization in the oceanic mixed layer: Nitrate and ammonium interactions at nanomolar concentrations. *Limnol. Oceanogr.* **41** 16-32

Hartig, P., Wolfstein, K., Lippemeier, S., Colijn, F., (1998) Photosynthetic activity of natural microphytobenthos populations measured by fluorescence (PAM) and C-14-tracer methods: a comparison. *Mar. Ecol. Prog. Ser.* **166** 53-62

Hawes, I., Gall, M. and Weatherhead, M., (1997) Photosynthetic parameters in water masses in the vicinity of the Chatham Rise, South Pacific Ocean, during late summer. *N. Z. J. Mar.Fresh. Res.* **31** 25-38

Heath, R.A., (1980) Eastwards oceanic flow past Northern New Zealand. *N. Z. J. Mar.Fresh. Res.* **14** 169-182

Helfrich, K.R., (1992) Internal solitary wave breaking and run-up on a uniform slope. *J. Fluid Mech.* **243** 133-154

Herzig, R. and Falkowski, P.G., (1989) Nitrogen limitation in *Isochrysis galbana* 1. Photosynthetic energy conversion and growth efficiencies. *J. Phycol.* **25** 462-471

Hofstraat, J.W., Duysens, L.N.M. and van Grondelle, R., (1994) Simple determination of photosynthetic efficiency and photoinhibition of *Dunaliella tertiolecta* by saturating pulse fluorescence measurements. *Mar. Ecol. Prog. Ser.* **103** 187-196

Holligan, P.M., Maddock, L. and Dodge, J.D., (1980) The distribution of dinoflagellates around the British-Isles in July 1977 – A Multivariate –Analysis *J. Mar. Biol. Assoc. UK.* **60** 851-867

Holligan, P.M., (1981) Biological implications of fronts on the northwest European continental shelf. *Phil. Trans. R. Soc. Lond. A* **302** 547-562

Holligan, P.M., Harris, R.P., Newell, R.C., Harbour, D.S., Head, R.N., Linley, E.A.S., Lucas, M.I., Tranter, P.R.G. and Weekley, C.M., (1984a) The vertical distribution and partitioning of organic carbon in mixed, frontal and stratified waters of the English Channel. *Mar. Ecol. Prog. Ser.* **14** 111-127

Holligan, P.M., Williams, P.J.LeB., Purdie, D. and Harris, R.P., (1984b) Photosynthesis, respiration and nitrogen supply of plankton populations in stratified, frontal and tidally mixed shelf waters. *Mar. Ecol. Prog. Ser.* **17** 201-213

Holligan, P.M., Pingree, R.D. and Mardell, G.T., (1985), Oceanic solitons, nutrient pulses and phytoplankton growth. *Nature* **314** 348-350

Holloway, P.E., (1984) On the semidiurnal internal tide at a shelf break region on the Australian north-west shelf. *J. Phys. Oceanogr.* **14** 1787-1799

Holloway, P.E., (1987) Internal hydraulic jumps and solitons at a shelf break region on the Australian North West shelf. *J. Geophy. Res.* **92** 5405-5416

Holloway, P.E., (1991) On the dissipation of internal tides, p449-468 *In* Tidal hydrodynamics, B.B. Paker (Ed.) Wiley

Holloway, P.E., (1994) Observations of internal tide propagation on the Australian north west shelf. *J. Phys. Oceanogr.* **24** 1706-1716

Holloway, P.E. (1996) A numerical model of internal tides with application to the Australian North West Shelf. *J. Phys. Oceanogr.* **26** 21-37

Holloway, P.E., Pelinovsky, E. and Talipova, T., (1999), A generalized Korteweg-de Vries model of internal tide transformation in the coastal zone. *J. Geophy. Res.* **104** 18333-18350

Horne, E.P.W., Loder, J.W., Harrison, W.G., Mohn, R., Lewis, M.R., Irwin, B. and Platt, T., (1989) Nitrate supply and demand at the Georges Bank tidal front. *Scientia Marina* **53** 145-158

Horne, E.P.W., Loder, J.W., Naimie, C.E. and Oakey, N.S., (1996) Turbulence dissipation rates and nitrate supply in the upper water column on Georges Bank. *Deep-Sea Res. Part II* **43** 1683-1712

Hseuh, Y. and O'Brien, J.J., (1971) Steady coastal upwelling induced by an along-slope current. *J. Phys. Oceanogr.* **1** 180-186

Huisman, J., van Oostveen, P. and Weissing, F.J., (1999) Critical depth and critical turbulence: Two different mechanisms for the development of phytoplankton blooms. *Limnol. Oceanogr.* **44** 1781-1787

Huthnance, J.M., (1989) Internal tides and waves near the continental shelf edge. *Geophys. Astrophys. Fluid.* **48** 81-106

Hydes, D.J., (1984) A manual of methods for the continuous flow determination of ammonia, nitrate-nitrite, phosphate and silicate in seawater. Institute of Oceanographic Sciences, Report, No.177, 37pp.

Inall, M.E., Rippeth, T.P. and Sherwin, T.J., (2000) Impact of non-linear waves on the dissipation of internal tidal energy at a shelf break. *J. Geophys. Res.* **105** 8687-8705

Jamart, B.M., Winter, D.F., Banse, K., Anderson, G.C. and Lam, R.K., (1977) A theoretical study of phytoplankton growth and nutrient distribution in the Pacific Ocean of the northwest U.S. coast. *Deep-Sea Res.* **24** 753-773

Jamart, B.M., Winter, D.F. and Banse, K., (1979) Sensitivity analysis of a mathematical model of phytoplankton growth and nutrient distribution in the Pacific Ocean of the northwest U.S. coast. *J. Plankt. Res.* **1** 267-290

Jeans, D.R.G. and Sherwin, T.J., (2001) The variability of strongly non-linear solitary internal waves observed during upwelling on the Portuguese shelf. *Cont. Shelf. Res.* **21** 1855-1878

Jeffrey, S.W., (1997) Application of pigment methods to oceanography. *In* Phytoplankton pigments in Oceanography. Jeffrey, S.W., Mantoura, R.F.C. and Wright, S.W., *Eds.* UNESCO Publishing 661pp

Jeffrey, S.W. and Vesk, M., (1997) Introduction to marine phytoplankton and their pigment signatures. *In* Phytoplankton pigments in Oceanography. Jeffrey, S.W., Mantoura, R.F.C. and Wright, S.W., *Eds.* UNESCO Publishing 661pp

Kahru, M., (1983) Phytoplankton patchyness generated by long internal waves – A model. *Mar Ecol. Prog. Ser.* **10** 111-117

Kamykowski, D. (1974) Possible interactions between phytoplankton and semi-diurnal internal tides. *J. Mar. Res.* **32** 68-89

Kana, T.M., (1992) Relationship between photosynthetic oxygen cycling and carbon assimilation in *Synechococcus* WH7803 (Cyanophyta). *J. Phycol.* **28** 304-308

Kirk, J.T.O., (1994) Light and photosynthesis in aquatic ecosystems. Cambridge University Press.

Kolber, Z., Zehr, J. and Falkowski, P.G., (1988) Effects of growth irradiance and nitrogen limitation on photosynthetic energy conversion in photosystem II. *Plant Physiol.* **88** 923-929

Kolber, Z., Wyman, K.D. and Falkowski, P.G., (1990) Natural variability in photosynthetic energy conversion efficiency; A field study in the Gulf of Maine. *Limnol. Oceanogr.* **35** 72-79

Kolber, Z. and Falkowski, P.G., (1993) Use of active fluorescence to estimate phytoplankton photosynthesis in situ. *Limnol. Oceanogr.* **38** 1646-1665

Kolber, Z.S., Barber, R.T., Coale, K.H., Fitzwater, S.E., Greene, R.M., Johnson, K.S., Lindley, S. and Falkowski, P.G., (1994) Iron limitation of phytoplankton photosynthesis in the Equatorial Pacific Ocean. *Nature* **371** 145-149

Kolber, Z. S., (1997) Fast Repetition Rate Fluorometry – A method for assessing ocean photosynthesis. *In* FAST^{tracka} FRRF Handbook, Chelsea Instruments, U.K.

Kolber, Z.S., Prášil, O. and Falkowski, P.G., (1998) Measurements of variable chlorophyll fluorescence using fast repetition rate techniques: defining methodology and experimental protocols. *Biochim. Biophys. Acta* **1367** 88-106

Kolber, Z.S., Van Dover, C.L., Niederman, R.A., Falkowski, P.G. (2000) Bacterial photosynthesis in surface waters of the open ocean. *Nature* **407** 177-179

Krause, G.H. and Weis, E., (1991) Chlorophyll fluorescence and photosynthesis: The basics. *Annu. Rev. Plant Physiol. Plant Mol. Biol.* **42** 313-349

Kyewalyanga, M.N., Platt, T. and Sathyendranath, S. (1997) Estimation of the photosynthetic action spectrum: Implication for primary production models. *Mar. Ecol. Prog. Ser.* **146** 207-223

Lamb, K.G., (1994) Numerical experiments of internal wave generation by strong tidal flow across a finite amplitude bank edge. *J. Geophys. Res.* **99** 843-864

Lande, R. and Yentsch, C.S., (1988) Internal waves, primary production and the compensation depth of marine-phytoplankton. *J. Plankt. Res.* **10** 565-571

Langdon, C. (1988) On the causes of interspecific differences in the growth-irradiance relationship for phytoplankton II. A general review. *J. Plankt. Res.* **10** 1291-1312

Largier, J.L., (1994) The internal tide over the shelf inshore of Cape Point Valley, South Africa. *J. Geophys. Res.* **99** 10027-10034

Laws, E.A., (1991). Photosynthetic quotients, new production and net community production in the open ocean. *Deep Sea Res.* **38** 143-167

Le Corre, P., L'Helguen, S. and Wafar, M., (1993) Nitrogen uptake by *Gyrodinium aureolum* in a tidal front. *Limnol. Oceanogr.* **38** 446-451

Le Fèvre, J., (1986) Aspects of the biology of frontal systems. *Adv. Mar. Biol.* **23** 163-299
Legendre, L. and Demers, S., (1986) Auxiliary energy, ergoclines and aquatic biological production. *Naturaliste Can. (Rev. ecol. syst.)* **112** 5-14

Legendre, L., Demers, S., LeFaivre, D., (1986) Biological production at marine ergoclines. *In* J.C.J. Nihoul (Ed.) *Marine Interfaces Ecohydrodynamics*. Elsevier, Amsterdam

Leichter, J.J., Wing, S.R., Miller, S.L., and Denny, M.W., (1996) Pulsed delivery of subthermocline water to Conch Reef (Florida Keys) by internal tidal bores. *Limnol. Oceanogr* **41** 1490-1501

Lewis, M.R. and Smith, C.J., (1983) A small-volume, short-incubation time method for the measurement of photosynthesis as a function of incident irradiance. *Marine Ecology Progress Series* **13** 99-102

Lewis, M.R., Cullen, J.J. and Platt, T., (1984a) Relationship between vertical mixing and photoadaptation of phytoplankton: similarity criteria. *Mar. Ecol. Prog. Ser* **15** 141-149

Lewis, M.R., Horne, E.P.W., Cullen, J.J., Oakey, N.S. and Platt, T., (1984b) Turbulent motions may control phytoplankton photosynthesis in the upper ocean. *Nature* **311** 49-50

Lewis, M.R., Harrison, W.G., Oakey, N.S., Hebert, D.L. and Platt, T., (1986) Vertical nitrate fluxes in the oligotrophic ocean. *Science* **234** 870-873

Ley, A.C., (1980) The distribution of absorbed light energy for algal photosynthesis. *In.* P.G. Falkowski, (Ed.) Primary Productivity in the sea. *Plenum Press New York*

Ley, A.C. and Mauzerall, D., (1982) Absolute absorption cross sections for photosystem II and the minimum quantum requirement for photosynthesis in *Chlorella vulgaris*. *Biochim. Biophys. Acta* **680** 95-106

Ley, A.C. and Mauzerall, D., (1986) The extent of energy transfer around photosystem II reaction centres in *Chlorella*. *Biochim. Biophys. Acta* **850** 234-248

Lien, R.C. and Gregg, M.C., (2001) Observations of turbulence in a tidal beam and across a coastal ridge. *J. Geophys. Res.* **106** 4575-4591

Loder, J.W. and Platt, T., (1985) Physical controls on phytoplankton production at tidal fronts. *In* Proceedings 19th European Marine Biology Symposium. P.E. Gibbs *(Ed.)* pp 3-21 *Cambridge University Press*

Loder, J.W., Drinkwater, K.F., Oakey, N.S. and Horne, E.P.W., (1993) Circulation, hydrographic structure and mixing at tidal fronts: The view from Georges Bank. *Phil. Trans. R. Soc. Lond. A* **343** 447-460

Loder, J.W., and Greenberg, D.A., (1986) Predicted positions of tidal fronts in the Gulf of Maine region. *Cont. Shelf Res.* **6** 397-401

Lueck, R.G. and Mudge, T.D., (1997) Topographically induced mixing around a shallow seamount. *Science* **276** 1831-1833

Mann, K.H. and Lazier, J.R.N., (1996) Dynamics of marine ecosystems (2nd edition), Blackwell Science, UK. 466pp

Marañón, E. and Holligan, P.M., (1999) Photosynthetic parameters of phytoplankton from 50 degrees N to 50 degrees S in the Atlantic Ocean. *Mar. Ecol. Prog. Ser.* **176** 191-203

Margalef, R., (1978) Life-forms of phytoplankton as survival alternatives in an unstable environment. *Oceanolg. Acta.* **1** 493-509

Masojídek, J., Grobbelaar, J.U., Pechar, L. and Koblížek, M., (2001) Photosystem II electron transport rates and oxygen production in natural waterblooms of freshwater cyanobacteria during a diel cycle. *J. Plankt. Res.* **23** 57-66

Mazé, R. and LeTareau, J.Y., (1990) Interaction between internal tides and energetic fluxes across the atmosphere-ocean interface over a continental-shelf break. *J. Mar. Res.* **48** 505-541

Millie, D.F., Paerl, H.W. and Hurley, J.P., (1993) Microalgal pigment assesments using high-performance liquid chromatography: A synopsis of organismal and ecological applications. *Can. J. Aquat. Sci.* **50** 2513-2527

Michallet, H. and Ivey, G.N., (1999) Experiments on mixing due to internal solitary waves breaking on uniform slopes. *J. Geophys. Res.* **104** 13467-13477

Millie, D.F., Paerl, H.W. and Hurley, J.P., (1993) Microalgal pigment assesments using high-performance liquid chromatography: A synopsis of organismal and ecological applications. *Can. J. Aquat. Sci.* **50** 2513-2527

Morin, P., Wafar, M.V.M. and Le Corre, P., (1993) Estimation of nitrate flux in a tidal front from satellite-derived temperature data. *J. Geophys. Res.* **98** 4689-4695

Moum, J.N., (1996) Efficiency of mixing in the main thermocline. *J. Geophys. Res.* **101** 12057-12069

Murphy, R.J., Pinkerton, M.H., Richardson, K.M., Bradford-Grieve, J.M. and Boyd, P.W., (2001) Phytoplankton distributions around New Zealand derived for SeaWiFS remotely-sensed ocean colour data. *N. Z. J. Mar.Fresh. Res.* **35** 343-362

New, A.L. and Pingree, R.D., (1990) Evidence for internal tidal mixing near the shelf break in the Bay of Biscay. *Deep Sea Res.* **37** 1783-1803

New, A.L. and Pingree, R.D., (2000) An intercomparison of internal solitary waves in the Bay of Biscay and resulting from Korteweg-de Vries-Type theory. *Prog. Oceanogr.* **45** 1-38

Oakey, N.S., (1982) Determination of the rate of dissipation of turbulent energy from simultaneous temperature and velocity shear microstructure measurements. *J. Phys. Oceanogr.* **12** 256-271

Obata, A., Ishizaka, J. and Endoh, M., (1996) Global verification of critical depth theory for phytoplankton bloom with climatological in situ temperature and satellite ocean colour data. *J. Geophys. Res.* **101** 20657-20667

Olaizola, M. and Yamamoto, H.Y., (1994) Short-term response of the diadinoxanthin cycle and fluorescence yield to high irradiance in *Chaetoceros Mulleri* (Bacillariophyceae). *J. Phycol.* **30** 606-612

Olaizola, M., LaRoche, J., Kolber, Z. and Falkowski, P.G., (1994) Non-photochemical quenching and the diadinoxanthin cycle in a marine diatom. *Photosynth. Res.* **41** 357-370

Olaizola, M., Geider, R.J., Harrison, W.G., Graziano, L.M., Ferrari. G.M. and Schlittenhardt, P.M., (1996) Synoptic study of variations in the fluorescence-based maximum quantum efficiency of photosynthesis across the North Atlantic Ocean. *Limnol. Oceanogr.* **41** 755-765

Olson, R.J., Chekalyuk, A.M., Sosik, H.M., (1996) Phytoplankton photosynthetic characteristics from fluorescence induction assays of individual cells. *Limnol. Oceanogr.* **41** 1253-1263

Olson, R.J., Sosik, H.M., Chekalyuk, A.M. and Shalapyononk, A., (2000) Effects of iron enrichment on phytoplankton in the Southern Ocean during late summer: active fluorescence and flow cytometric analyses. *Deep Sea Res. II* **47** 3181-3200

Osborn, T.R. and Cox, C.S., (1972) Oceanic finestructure. *Geophys. Fluid Dyn.* **3** 321-345

Osborn, T.R., (1974) Vertical profiling of velocity microstructure. *J. Phys. Oceanogr.***4** 109

Osborn, T.R., (1980) Estimates of the local rate of vertical diffusion from dissipation measurements. *J. Phys. Oceanogr.* **10** 83-89

Parkhill, J.P., Maillet, G., and Cullen, J.J., (2001) Fluorescence-based maximal quantum yield for PSII as a diagnostic of nutrient stress. *J. Phycol.* **37** 517-529.

Pederson, F.B., (1994) The oceanographic and biological tidal cycle succession in shallow sea fronts in the North Sea and English Channel. *Est. Coast Shelf Sci.* **38** 249-269

Peterson, B.J., (1980) Aquatic primary productivity and the $^{14}CO_2$ method: a history of the productivity problem. *Annu. Rev. Ecol. Syst.* **11** 359-385

Pineda, J., (1991) Predictable upwelling and the shoreward transport of planktonic larvae by internal tidal bores. *Science* **253** 548-551

Pineda, J., (1994) Internal tidal bores in the nearshore – Warm –water fronts, seaward gravity currents and the onshore transport of neustonic larvae. *J. Mar. Res.* **52** 427-458

Pineda, J., (1999) Circulation and larval distribution in internal tidal bore warm fronts. *Limnol. Oceanogr.* **44** 1400-1414

Pingree, R.D., Pugh, P.R., Holligan, P.M. and Forster, G.R., (1975) Summer phytoplankton blooms and red tides along tidal fronts in the approaches to the English Channel. *Nature* **258** 672-677

Pingree, R.D., Holligan, P.M. and Head, R.N., (1977) Survival of dinoflagellate blooms in the western English Channel. *Nature* **265** 266-269

Pingree, R.D., (1978) Cyclonic eddies and cross-frontal mixing *J. Mar. Biol. Assoc. U.K.* **58** 955-963

Pingree, R.D. and Griffiths, D.K., (1978) Tidal fronts on the shelf seas around the British Isles. *J. Geophys. Res.* **83** 4615-4622

Pingree, R.D., Holligan, P.M. and Mardell, G.T., (1978) The effects of vertical stability on phytoplankton distributions in the summer on the northwest European shelf. *Deep-Sea Res.* **25** 1011-1028

Pingree, R.D., Holligan, P.M. and Mardell, G.T., (1979) Phytoplankton growth and cyclonic eddies. *Nature* **278** 245-247

Pingree, R.D., (1979) Baroclinic eddies bordering the Celtic Sea in late summer *J. Mar. Biol. Assoc. U.K.* **59** 689-698

Pingree, R.D. and Mardell, G.T., (1981) Slope Turbulence, internal waves and phytoplankton growth at the Celtic Sea shelf-break. *Phil. Trans. R. Soc. Lond. A* **302** 663-682

Pingree, R.D., Mardell, G.T. and New, A.L., (1986) Propagation of internal tides from the upper slopes of the Bay of Biscay. *Nature* **321** 154-158

Planas, D., Agusti, S., Duarte, C.M., Granata, T.C. and Merino, M., (1999) Nitrate uptake and diffusive nitrate supply in the Central Atlantic. *Limnol. Oceanogr.* **44** 116-126

Platt, T., Gallegos, C.L. and Harrison, W.G., (1980) Photoinhibition of photosynthesis in natural assemblage of marine phytoplankton. *J. Mar. Res.* **38** 687-701

Post, A.F., Dubinsky, Z. and Falkowski, P.G., (1984) Kinetics of light intensity adaptation in a marine planktonic diatom. *Mar. Biol.* **83** 231-238

Prasil, O., Kolber, Z.S., Berry, J.A. and Falkowski, P.G., (1996) Cyclic electron flow around photosystem II *in vivo*. *Photosyn. Res.* **48** 395-410

Raven, J.A. and Johnston, A.M., (1991) Mechanisms of inorganic-carbon acquisition in marine phytoplankton and their implications for the use of other resources. *Limnol. Oceanogr.* **36** 1701-1714

Redfield, A.C., (1934) On the proportions of organic derivatives in sea water and their relation to the composition of plankton. *In* Daniel, R.J., James Johnston Memorial Volume. University Press of Liverpool.

Redfield, A.C., (1958) The biological control of chemical factors in the environment. *Am. Sci.* **46** 205-221

Riley, G.A., (1942) The relationship of vertical turbulence and spring diatom flowering. *J. Mar. Res.* **5** 67-87

Ruddick, B., Anis, A., Thompson, K, (2000) Maximum likelihood spectral fitting: The Batchelor spectrum. *J. Atmos. Ocean Tech.***17** 1541-1555

Sakshaug, E., Bricuad, A., Dandonneau, Y., Falkowski, P.G., Kiefer, D.A., Legendre, L., Morel, A., Parslow, J. and Takahashi, M., (1997) Parameters of photosynthesis: definitions, theory and interpretation of results. *J. Plankt. Res.* **19** 1637-1670

Sambrotto, R.N., Savidge, G., Robinson, C., Boyd, P., Takahashi, T., Karl, D.M., Langdon, C., Chipman, D., Marra, J. and Codispoti, L., (1993) Elevated consumption of carbon relative to nitrogen in the surface ocean. Nature **363** 248-250

Sambrotto, R.N. and Langdon, C., (1994) Water column dynamics of dissolved inorganic carbon (DIC), nitrogen and O_2 on Georges Bank during April 1990. *Cont. Shelf Res.* **14** 765-789

Sandstrom, H. and Elliot, J.A., (1984) Internal tide and solitons on the Scotian Shelf: A nutrient pump at work. *J. Geophys. Res.* **89** 6415-6426

Sandstrom, H. and Oakey, N.S., (1995) Dissipation in internal tides and solitary waves. *J. Phys. Oceanogr.* **25** 604-614

Savidge, G., (1976) A preliminary study of the distribution of chlorophyll-a in the vicinity of fronts in the Celtic and western Irish seas. *Estuar. Coast. Mar. Sci.* **4** 617-625

Siegel, D.A., Westberry, T.K., O'Brien, M.C., Nelson, N.B., Michaels, A.F., Morrison, J.R., Scott, A., Caporelli, E.A., Sorensen, J.C., Maritorena, S., Garver, S.A., Brody, E.A., Ubante, J., Hammer, M.A., (2001) Bio-optical modelling of primary production on regional scales: the Bermuda BioOptics project. *Deep Sea Res. II* **48** 1865-1896

Sharples, J. and Tett, P. (1994) Modelling the effect of physical variability on the midwater chlorophyll maximum. *J. Mar. Res.* **52** 219-238

Sharples, J., Greig, M.J. and Oliver, M.O., (1996) The potentially annual imact of the Pacific Ocean on the coastal zone of Northeast New Zealand. *In* Aung, T.H. (*Ed.*) Proceedings of the Ocean and Atmosphere Pacific international conference.

Sharples, J., (1997) Cross-shelf intrusion of subtropical water into the coastal zone of northeast New Zealand. *Cont. Shelf Res.* **17** 835-857

Sharples, J., Moore, C.M., Rippeth, T.P., Holligan, P.M., Hydes, D.J., Fisher, N.R. and Simpson, J.H. (2001a) Phytoplankton distribution and survival in the thermocline. *Limnol. Oceanogr.* **46** 486-496

Sharples, J., Moore, C.M. and Abraham, E.R., (2001b) Internal tide dissipation, mixing and vertical nitrate flux at the shelf edge of NE New Zealand. *J. Geophys. Res.* **106** 14069-14081

Shay, T.J. and Gregg, M.C., (1986) Convectively driven turbulent mixing in the upper ocean. *J.Phys. Oceanogr.* **16** 1777-1798

Shea, R.E. and Broenkow, W.W., (1982) The role of internal tides in the nutrient enrichment of Monterey Bay, California. *Estuar. Coast. Shelf Sci.* **15** 57-66

Sherwin, T.J., (1988) Analysis of an internal tide observed on the Malin Shelf, north of Ireland. *J. Phys. Oceanogr.* **18** 1035-1050

Simpson, J.H. and Hunter, J.H., (1974) Fronts in the Irish Sea. *Nature* **250** 404-406

Simpson, J.H., Edelsten, D.J., Edwards, A., Morris, N.C.G. and Tett, P.B., (1979) The Islay front: Physical structure and phytoplankton distribution. *Est. Coast Shelf Sci.* **9** 713-726

Simpson, J.H., (1981) The shelf-sea front: Implications of their existence and behaviour. *Philosophical Transactions of the Royal Society of London A* **302** 531-546

Simpson, J.H. and Bowers, D.G., (1981) Models of stratification and frontal movement in shelf seas. *Deep Sea Res. Part A* **28** 727-738

Simpson, J.H. and Sharples, J., (1994) Does the Earth's rotation influence the location of the shelf sea fronts? *J. Geophys. Res.* **99** 3315-3319

Simpson, J.H., Crawford, W.R., Rippeth, T.P., Campbell, A.R. and Cheok, J.V.S., (1996) The vertical structure of turbulent dissipation in shelf seas. *J. Phys. Oceanogr.* **26** 1579-1590

Simpson, J.H., Rippeth, T.P. and Campbell, A.R. (2000) The phase lag of turbulent dissipation in tidal flow, p. 57-67. *In* T.Yanagi (ed.), Interaction between estuaries, coastal seas and shelf seas. Terra Scientific.

Sims, D.W. and Quayle, V.A., (1998) Selective foraging behaviour of basking sharks on zooplankton in a small-scale front. *Nature* **393** 460-464

Smetacek, V. and Passow, U., (1990) Spring bloom initiation and the Sverdrup critical depth model. *Limnol. Oceanogr.* **35** 228-234

Sournia, A., Belin, C., Billard, C., Martial, C., Erard-le Denn, E., Fresnel, J., Lassus, P., Pastoureaud, A. and Soulard, R., (1992) The repetitive and expanding occurrence of a green bloom-forming dinoflagelate (Dinophyceae) on the coasts of France. *Crypotogamie Algol* **13** 1-13

Stanton, T.P. and Ostrovsky, L.A., (1998) Observations of highly nonlinear internal solitons over the continental shelf. *Geophys. Res. Lett.* **25** 2695-2698

Strass, V., (1990) On the calibration of large-scale fluorometric chlorophyll measurements from towed undulating vehicles. *Deep Sea. Res.* **37** 525-540

Strutton, P.G., Mitchell, J.G., Parslow, J.S. and Greene, R.M., (1997) Phytoplankton patchiness: quantifying the biological contribution using Fast Repetition Rate Fluorometry. *J. Plankt. Res.* **19** 1265-1274

Suggett, D., Kraay, G., Holligan, P., Davey, M., Aiken, J., Geider, R., (2001) Assessment of photosynthesis in a spring cyanobacterial bloom by use of a fast repetition rate fluorometer. *Limnol. Oceanogr.* **46** 802-810

Sukenik, A., Bennett, J., Mortain-Bertrand, A. and Falkowski, P.G., (1990) Adaptation of the photosynthetic apparatus to irradiance in *Dunaliella tertiolecta* A kinetic study. *Plant Physiol.* **92** 891-898

Sukenik, A., Bennett, J. and Falkowski, P.G., (1986) Light-saturated photosynthesis-limitation by electron transport or carbon fixation? *Biochim. Biophys. Acta.* **891** 205-215

Sverdrup, H.U., (1953) On conditions for the vernal blooming of phytoplankton. *J. Cons. Perm. Int. Exp. Mer.* **18** 287-295

Tassan, S. and Ferrari, G.M., (1995) An alternative approach to absorption measurements of aquatic particles retained on filters. *Limnol Oceanogr.* **40** 1358-1368

Tett, P., (1981). Modelling phytoplankton production at shelf-sea fronts. *Philos. T. Roy. Soc Lond. A* **302** 605-615

Timmermans, K.R., Davey, M.S., van der Wagt, B., Snoek, J., Geider, R.J., Veldhuis, M.J.W., Gerringa, L.J.A. and de Baar, H.J.W., (2001) Co-limitation by iron and light of *Chaetoceros brevis*, *C. dichaeta* and *C. calcitrans* (Bacillariophyceae). *Mar. Ecol. Prog. Ser.* **217** 287-297

Townsend, D.W., Keller, M.D., Sieracki, M.E., Ackleson, S.G., (1992) Spring phytoplankton blooms in the absence of vertical water column stratification. *Nature* **360** 59-62

van Kooten, O. and Snel, J.F.N., (1990) The use of chlorophyll fluorescence nomenclature in plant stress physiology. *Photosyn. Res.* **25** 147-150

Varela, R.A., Cruzado, A., Tintoré, J. and Iadona, E.G., (1992) Modelling the deep chlorophyll maximum: a coupled physical-biological approach. *J. Mar. Res.* **50** 441-463

Vassiliev, I.R., Prasil, O., Wyman, K., Kolber, Z., Hanson, A.K., Prentice, J. and Falkowski, P.G., (1994) Inhibition of PSII photochemistry by PAR and UV radiation in natural phytoplankton communities. *Photosyn. Res.* **42** 51:64

Vesecky, W. and Stewart, R.H., (1982) The observation of ocean surface radar phenomena using imagery from the Seasat synthetic aperture radar; An assessment. *J. Geophys. Res.* **87** 3397-3430

Videau, C., (1987) Primary production and physiological state of phytoplankton at the Ushant tidal front (west coast of Brittany, France). *Mar. Ecol. Prog. Ser.* **35** 141-151

Welschmeyer, N.A., (1994) Fluorometric analysis of chlorophyll a in the presence of chlorophyll b and phaeopigments. *Limnol. Oceanogr.* **39** 1985-1992

Williams, P.J.L. and Robertson, J.E. (1991) Overall Planktonic oxygen and carbon-dioxide metabolisms – The problem of reconciling observations and calculations of photosynthetic quotients *J. Plankt. Res.* **13**: S153-S169 Suppl.

Williams, P.J.L., Robinson, C., Sondergaard, M., Jespersen, A.M., Bentley, T.L., Lefevre, D., Richardson, K. and Riemann, B. (1996) Algal C-14 and total carbon metabolisms .2. Experimental observations with the diatom *Skeletonema costatum*. *J. Plankt. Res.* **18** 1961 - 1974

Xing, J.X. and Davies, A.M., (1998) A three-dimensional model of internal tides on the Malin-Hebrides shelf and shelf edge. *J. Geophys. Res.* **103** 27821-27847

Appendix 1

Scaling arguments and mixing in stratified fluids

In order to estimate vertical transportation by turbulent mixing in stratified fluids, it is usually necessary to make a large number of simplifying assumptions. Estimates of vertical velocities and displacements can often only be made in terms of dimensional arguments. Length scales of mixing can be derived in terms of the rate of dissipation of turbulent kinetic energy (TKE) (ε) the viscosity (υ), the molecular diffusivity (D) and the degree of stratification within the water column represented by the buoyancy frequency (N^2). The three important length scales which result are: The Batchelor length scale ($L_B=(D^2\upsilon/\varepsilon)^{1/4}$) characterizing the scale at which molecular diffusivity of heat balances turbulent heat transport; The Kolmogorov length scale ($L_K=(\upsilon^3/\varepsilon)^{1/4}$) characterizing the scale of eddies at which dissipation occurs and the Osmidov length scale ($L_O=(\varepsilon/N^3)^{1/2}$) which characterizes the size of the largest eddies with sufficient KE to overturn (e.g. Gargett, 1997). In addition the turbulent velocity q can be related to ε and a vertical turbulent length scale *l* using:

$$\varepsilon \approx \frac{q^3}{l} \qquad \text{(A1.1)}$$

(Tennekes and Lumley, 1972).

Vertical mixing is often parameterized using the vertical eddy diffusivity (K_z) (Tennekes and Lumley, 1972). If we assume a local balance between dissipation and the rate of supply of TKE, as well as an isotropic turbulence field, K_z can be related to ε in a stratified water column using:

$$K_z = 0.2\frac{\varepsilon}{N^2} \qquad \text{(A1.2)}$$

(Osborn, 1980).

It is clear that if we have characteristic length and velocity scales then it is a straightforward assumption to derive a characteristic time-scale T_t. The time-scales for transport in large turbulent eddies and the time-scale for diffusive transport over distance l are therefore:

$$T_t = \left(\frac{l^2}{\varepsilon} \right)^{1/3} \tag{A1.3}$$

and

$$T_t = \frac{l^2}{2K_z} \tag{A1.4}$$

respectively (Denman and Gargett, 1983). These last two equations allow estimates to be made of the time taken for turbulent transport within mixed layers etc.

Appendix 2

Checks on FRRF data quality and analysis

A series of checks were carried out on both the consistency between different FRRF instruments and the sensitivity of parameter retrieval to corrections for scattering and instrument response, (see Chelsea Instruments FAST^{tracka} manual). In addition the sensitivity of parameter retrieval to the software used for curve fitting and the precise form of the model fitted was also investigated.

Inter instrument comparisons:- A series of discrete samples were run on the two different instruments utilised during the Nov-Dec 2000 cruise. Samples were collected from the CTD rosette and dark adapted for a period of 15-20 minutes before being analysed in the dark chamber of both FRRF's. Data points correspond to the mean values of 9 repeated measurements. Results indicated good agreement between instruments with values of both F_v/F_m and σ_{PSII} highly correlated with a regression slope not significantly different to unity (*Fig A2.1*).

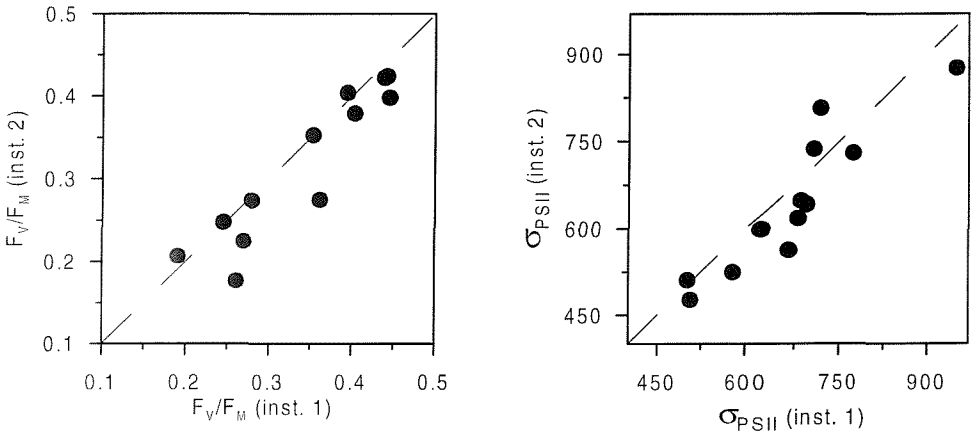

Fig A2.1 Comparisons of F_v/F_m and σ_{PSII} from two instruments deployed during cruise on NorthEast New Zealand continental shelf, Nov-Dec 2000. Points are averages of 16 repeat measurements of a dark acclimated sample. Left: F_v/F_m, $R^2 = 0.859$, n=12, $p<0.001$, $Y = 1.03X - 0.036$. Right: σ_{PSII}, $R^2 = 0.828$, n=12, $p<0.001$, $Y = 1.02X - 45.1709$. All slopes were calculated using a model II fit.

Software comparisons:- Raw data were fitted to the model of Kolber *et al.* (1998) using two software routines, a version of the manufacturers custom software (FRS 1.4-1.6) and code designed in MATLAB™, this code being a development of the V4 software produced and made available to the FRRF community by S. Laney. The V4 code can be downloaded at http://picasso.oce.orst.edu/ORSOO/FRRF/ or http://hawkeye.dmc.maine.edu/reduce/reduce.html.

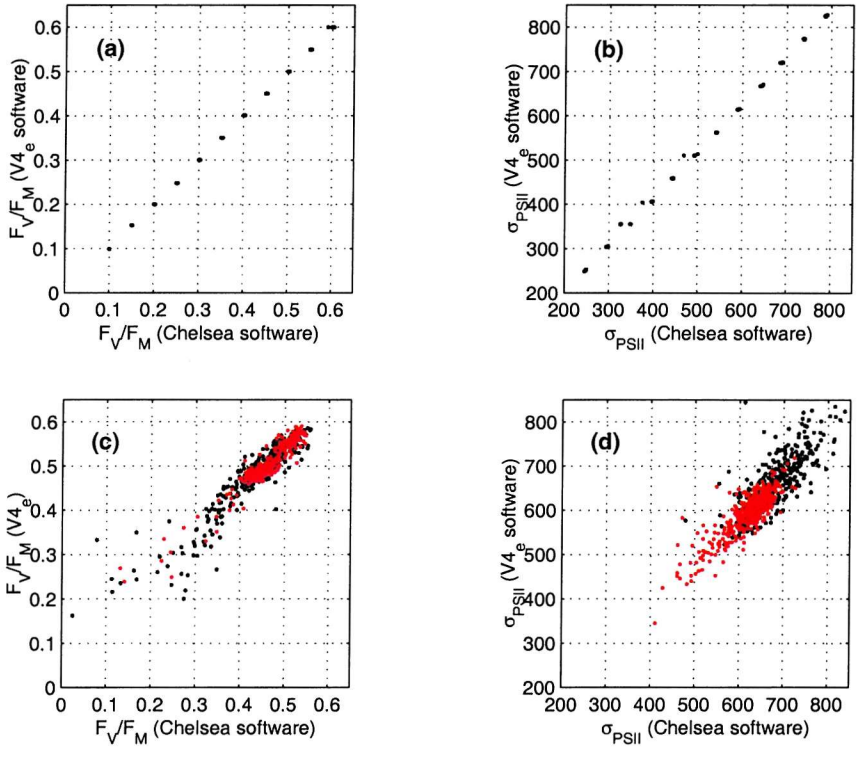

Fig A2.2 Comparison of artificial (top) and field (bottom) data sets analysed using the CI custom software and the MATLAB™ based routines. (a) F_v/F_m compared on artificial data set, $R^2 = 0.9999$, n = 144; (b) σ_{PSII} compared on artificial data set, $R^2 = 0.9989$, n = 144; (c) F_v/F_m compared for two 24hr periods of vertical CTD casts during August 1999 cruise, black, U2 (see chapter 3), $R^2 = 0.8559$, n = 377, red, M2, $R^2 = 0.8896$, n = 398; (d) σ_{PSII} compared for same two 24hr periods, red, $R^2 = 0.5709$, n = 377, black, $R^2 = 0.7355$, n=398.

As of time of writing, a new version of this code is under development, to be called V5 (S. Laney, pers. comm.), the edited version of V4 (V4e) utilised in the majority of this thesis incorporates a number of slight changes some of which are likely to be incorporated in V5. V4e also utilises a different non-linear least squares fitting routine to that utilised in V4. In order to verify that there was no bias introduced by the use of either fitting routine, a

number of artificial data sets were generated using the model and analysed using both software types. In addition a number of field data sets were analysed using both sets of code. Results were again very encouraging with no major differences between analysis techniques for either artificial or field data (*Fig A2.2*).

Model and noise dependency:- Raw FRRF saturation data can be fitted to a simplified model which assumes no energy transfer between PSII reaction centres (Eq. 1.5). Alternatively if the PSII reaction centres share excitation energy a more complicated relationship can be developed (Kolber *et al.* 1998):

$$f(t) = F_0 + (F_M - F_0)\left(C(t)\frac{1-p}{1-C(t)p}\right) \qquad \text{(A2.1)}$$

where $f(t)$ is the fluorescence at time t, p is the proportion of energy transfer between reaction centres and $C(t)$ is the fraction of closed reaction centres at time t, given by:-

$$C(t) = \int_0^t \sigma_{PSII} i(v) \frac{1-C(v)}{1-C(v)p} dv \qquad \text{(A2.2)}$$

where $i(t)$ is the excitation energy at time t (Kolber *et al.* 1998).

The degree of PSII reaction centre connectivity essential alters the degree to which the initial slope deviates from a standard exponential form (Eq. 1.5). Fitting an additional parameter (p) to the raw FRRF data could introduce added problems, particularly with noisy data sets as the degrees of freedom in the fit increases. The FRS software utilises the more complicated model (Eqs. A2.1 & A2.2), whereas the V4 and V4e software can be set-up to use either the simpler or more complex models. In order to asses the influence of using the simpler model to retrieve the standard two parameters (F_v/F_m and σ_{PSII}), from data with varying degrees of connectivity, a large artificial data was produced using the more complex model, then analysed using the simpler model. The data set was produced using a range of values for p, F_v/F_m, and σ_{PSII}. Additional random gaussian noise at a range of levels was also added to the individual fluorescence transients. Errors in the recovered values were a complex function of the noise, connectivity and variable fluorescence (as signified by low F_v/F_m), (*Figs A2.3 & A2.4*).

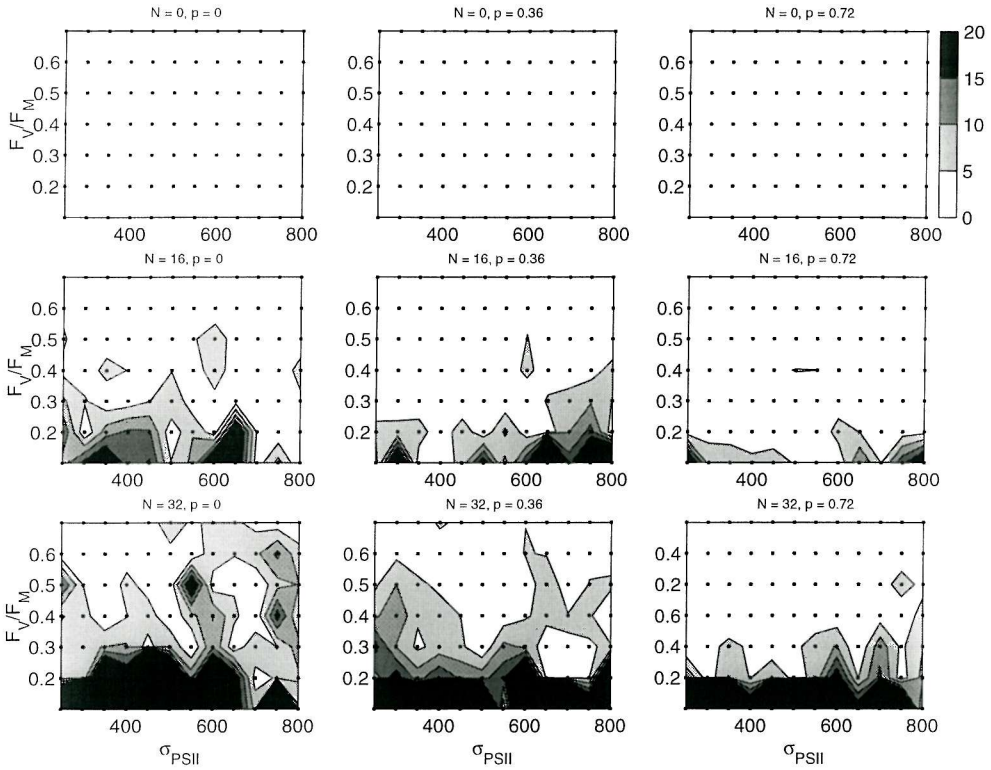

Fig A 2.3 Contours of percentage error between true and recovered values of F_v/F_m for a large artificial data set generated using the complex model and analysed using the simpler exponential relationship. The contours are plotted on axes corresponding to the true values of σ_{PSII} and F_v/F_m used to generate the data set. Each individual plot corresponds to the percentage noise (N) and degree of connectivity (p) indicated. Individual data points are marked on plots and correspond to the mean value of the parameters recovered from ten repeat fluorescence saturation curves generated at the noise level indicated. Thus 840 fluorescence saturation curves were generated and analysed for each individual plot, the entire data set consisting of 7560 curves.

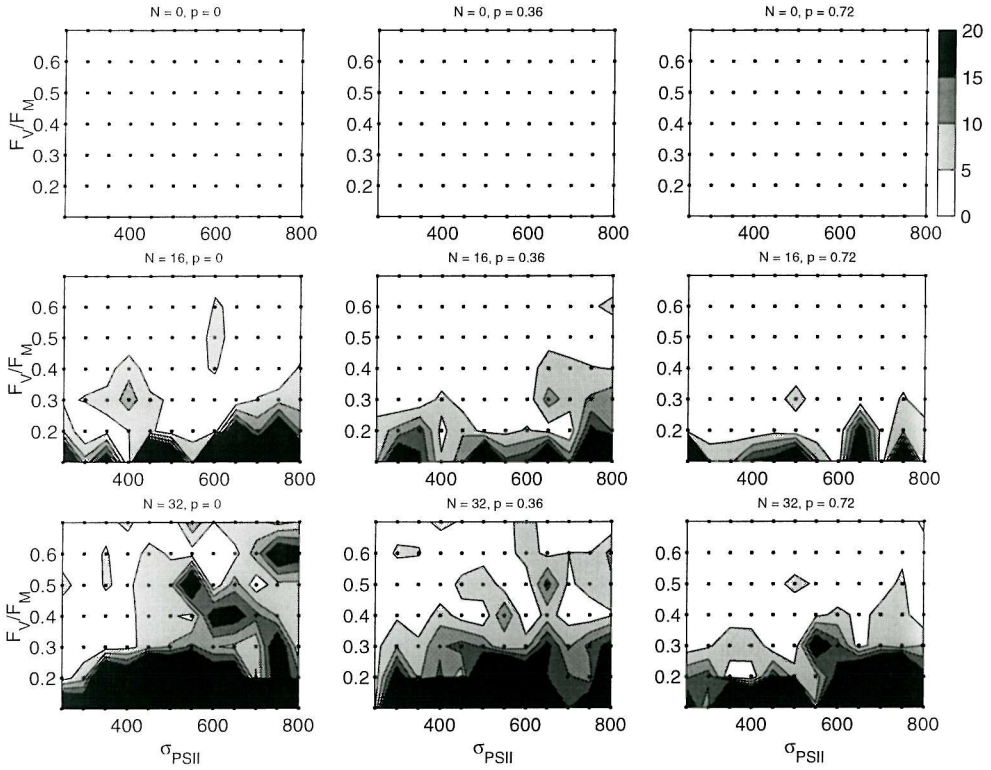

Fig A 2.4 As A2.3 for percentage error in σ_{PSII}.

In general the errors introduced were less than 10% except at low values of F_v/F_m and low signal to noise ratios. The degree of connectivity had a relatively minor effect on recovered values. These errors were generally of the same order as estimated uncertainties in the individual fits from both field and artificial data sets, which were typically less than 10% except at low absolute values of variable fluorescence (i.e. low chlorophyll and/or high light regions with high non-photochemical quenching).

Scatter and IRF calibrations:- Finally, scattering and variations in the instrument electronic response during a saturation protocol have the potential to introduces errors in retrieved parameters (see manufacturers instrument manual). Blanks for scatter calibration were run using Milli-Q water, while the instrument response function (IRF) was evaluated using a chlorophyll extract (*Fig A2.5*).

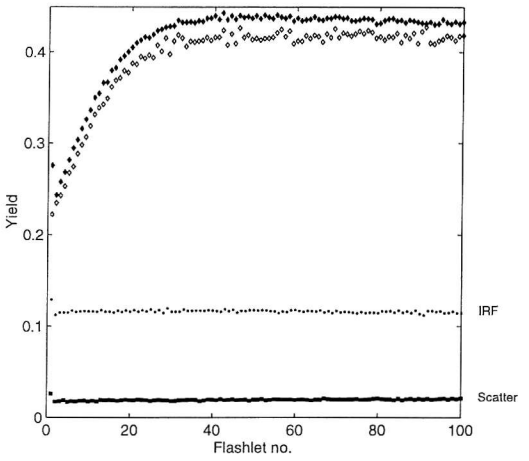

Fig A2.5 Measured scatter blank (squares) and IRF (circles) as well as a measured sample (filled diamonds) and corrected sample (open diamonds).
Correction applied is:
$f^{cor}(n) = f(n)./IRF(n) - S(n)$,
where n is the flashlet number and f, IRF and S are the measured signals for the sample, chlorophyll standard and Milli_Q water respectively

Unfortunately the possible importance of such corrections was not fully appreciated until towards the end of the study, hence IRF's were not available for many of the data sets. However analysis of a subset of the field data both before and after blank correction indicated that σ_{PSII} was very insensitive to this procedure (*Fig A2.6a*). Variations were apparent in the values of F_v/F_m obtained, although differences were again minor and tended to be associated with lower chlorophyll regions (*Fig A2.6b*).

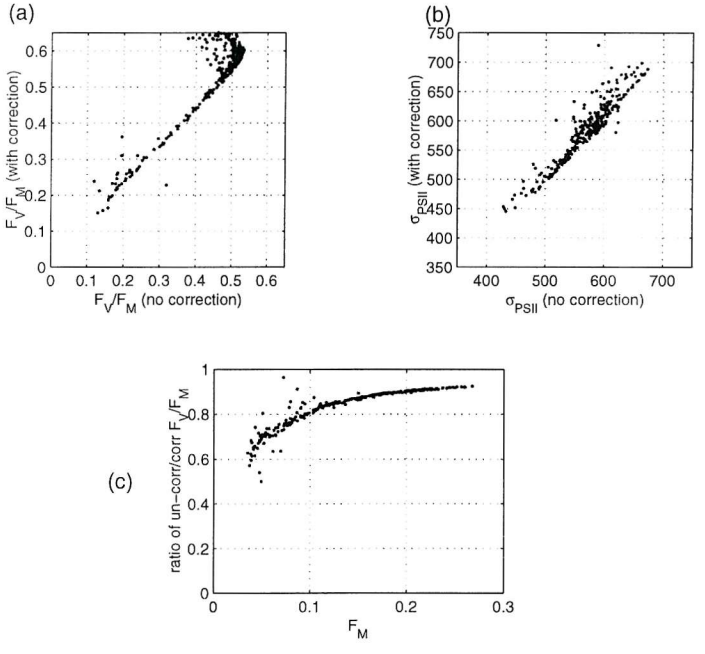

Fig A2.6. Comparison of field data set analysed with and without correction for scattering and instrument response. The two values of F_v/F_m (a) and σ_{PSII} (b) are highly correlated (F_v/F_m, R^2 = 0.8186; σ_{PSII}, R^2 = 0.8789, n = 334).
(c). Some variation in values of F_v/F_m recovered is apparent and is related to chlorophyll concentration as indicated by maximal fluorescence.

Appendix 3

Persons responsible for data collection

Cruise	**Nov-Dec 1998**	**Nov-Dec 2000**	**August 1999**
CTD package	E. Abraham (K. Downing, J. Sharples)	E. Abraham (M. Moore, C. Stevens)	D. Teare, J. Short
FRRF Deployment	n/a	M. Moore, E. Abraham, P.Boyd	M. Moore, E. Abraham, D. Suggett
Microstructure	M. Moore, J.Sharples	C. Stevens (M. Moore)	N. Fisher, T. Rippeth, J. Simpson, R. Wilton (M. Moore, J. Sharples)
Moorings			N/a
Nutrients: sampling	S. Bury, (P. Boyd, M. Moore)	M. Gall, (P. Boyd, M. Moore)	D. Hydes
Nutrients: analysis	S. Pickmere, F. Richards	S. Pickmere, F. Richards	D. Hydes
Chl: sampling	S. Bury, (P. Boyd, M. Moore)	M. Gall, (P. Boyd, M. Moore)	P. Holligan, (D. Suggett)
Chl: analysis	L. Hawke	L. Hawke	P. Holligan
HPLC: sampling	n/a	n/a	P. Holligan, (D. Suggett)
HPLC: analysis			C. Lucas
Absorption: sampling	n/a	n/a	P. Holligan, (D. Suggett)
Absorption: analysis		n/a	C. Lucas
^{14}C –expts	n/a	M. Gall	M. Lucas

Table of persons primarily responsible for collection of data during the 3 cruises. Names in parenthesis indicate some involvement in data acquisition. Mat Pinkerton was responsible for the analysis of SeaWiFS data during the 2000 cruise.

Appendix 4

Chlorophyll against Fm or F

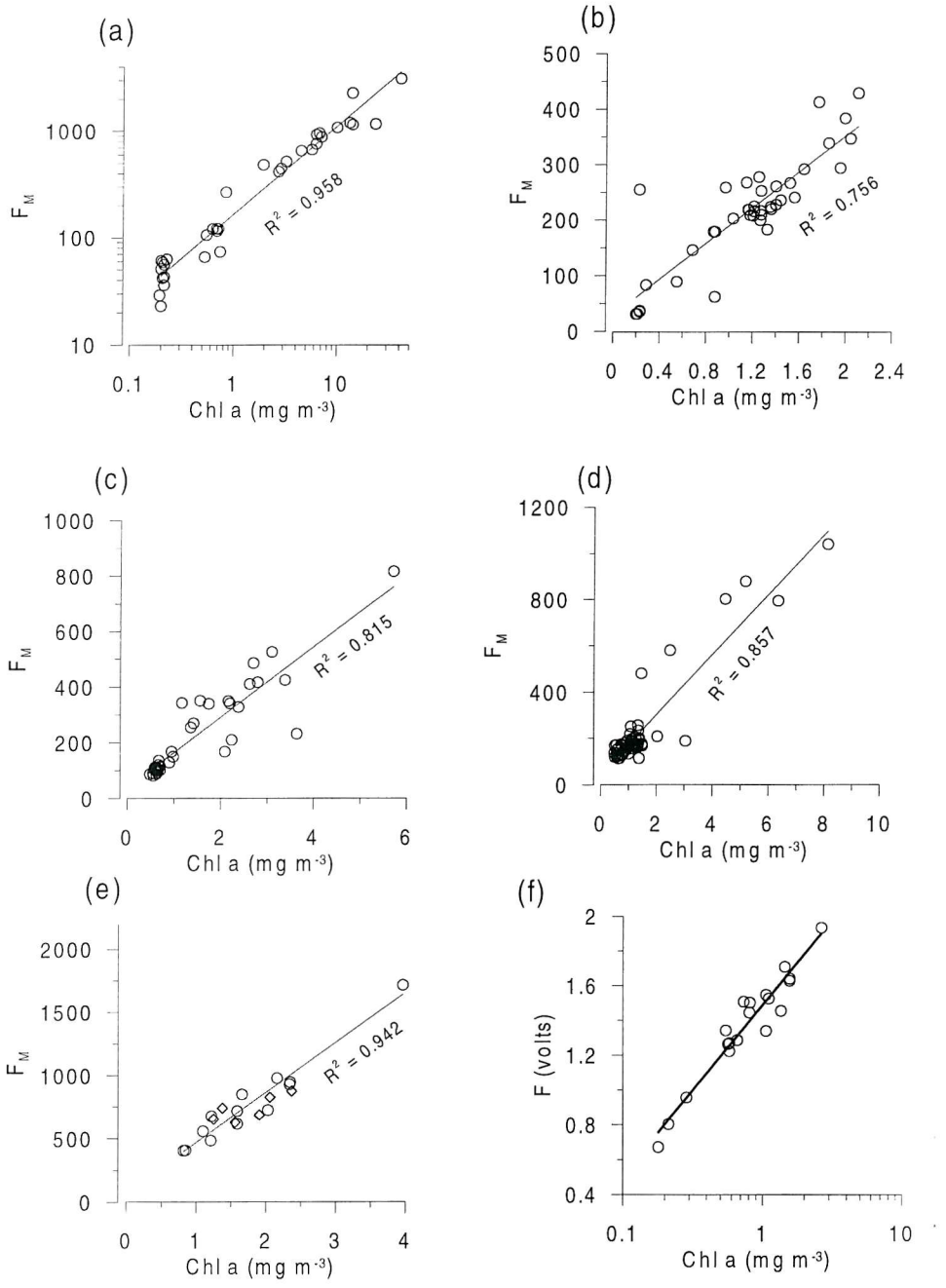

F_M vs. Chlorophyll a concentration for all four 25hr stations occupied during CH 145 and Seasoar runs.
(a) U2, (b) E, (c) M2, (d) M3, all FRRF
(e) Seasoar FRRF, (2nd ◇ and 8th ○ August)
(f) Seasoar standard fluorometer (note Aquatracka fluorometer utilises a logarithmic amplifyer)

Appendix 5

Relationships between nutrients during CH145

(a)

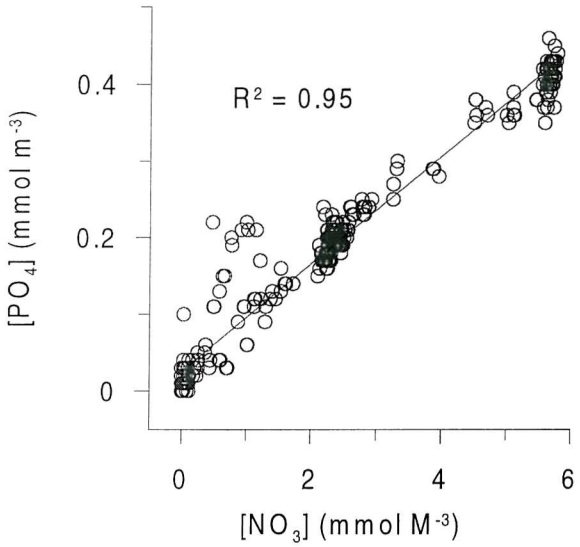

(b)

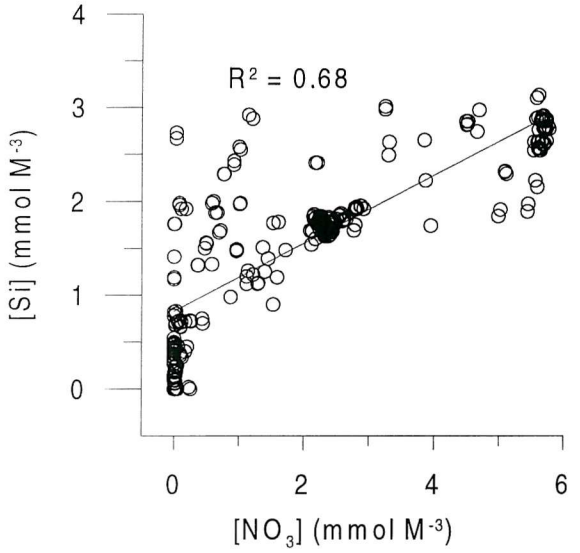

Plots of Nitrate vs. (a) Phosphate and (b) Silicate, for bottle samples collected in the Western English Channel 1st - 14th August 1999, aboard *RV Challenger*. (CH 145)

Appendix 6

Detailed temperature and velocity structure during 2000 internal wave experiment for period 26th November – 3rd December

Temperature contours and velocity vectors normalised to bore propagation direction, for both principal moorings (IW1/00 and IW2/00) from the period when site was occupied by ship.

Time for each day runs from midnight, axis is labelled in minutes. Large arrow to top left of each plot indicates a horizontally off-shore current of 50 cm s^{-1}. See also Fig. 4.13.

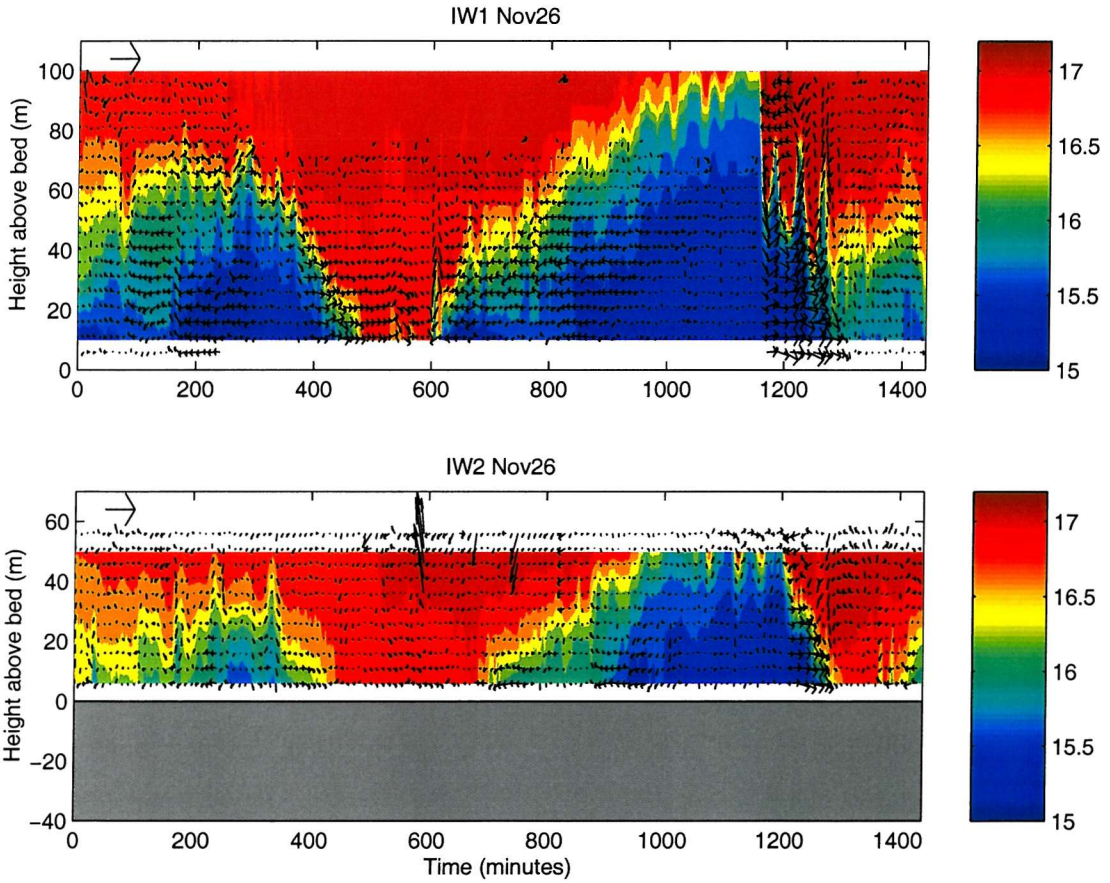

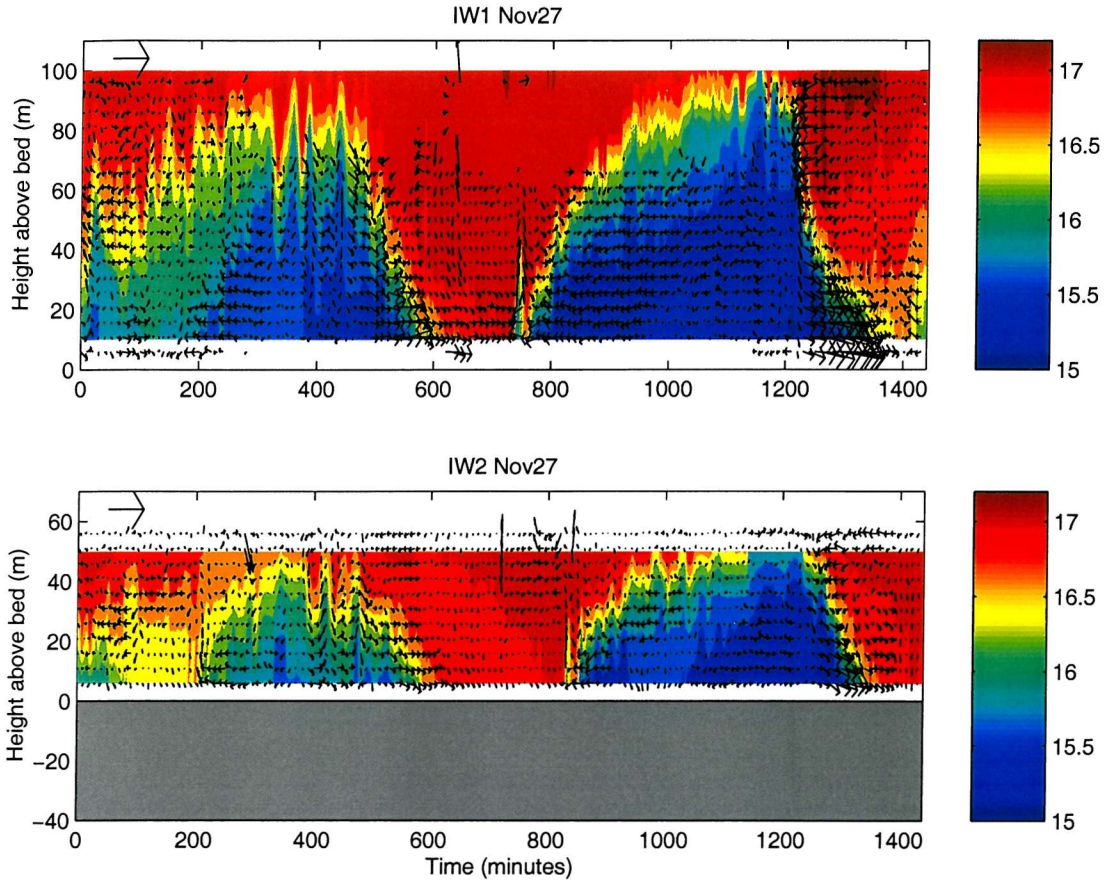
IW1 Nov27
Height above bed (m)
100
80
60
40
20
0
0
200
400
600
800
1000
1200
1400
17
16.5
16
15.5
15
IW2 Nov27
Height above bed (m)
60
40
20
0
−20
−40
0
200
400
600
800
1000
1200
1400
Time (minutes)
17
16.5
16
15.5
15

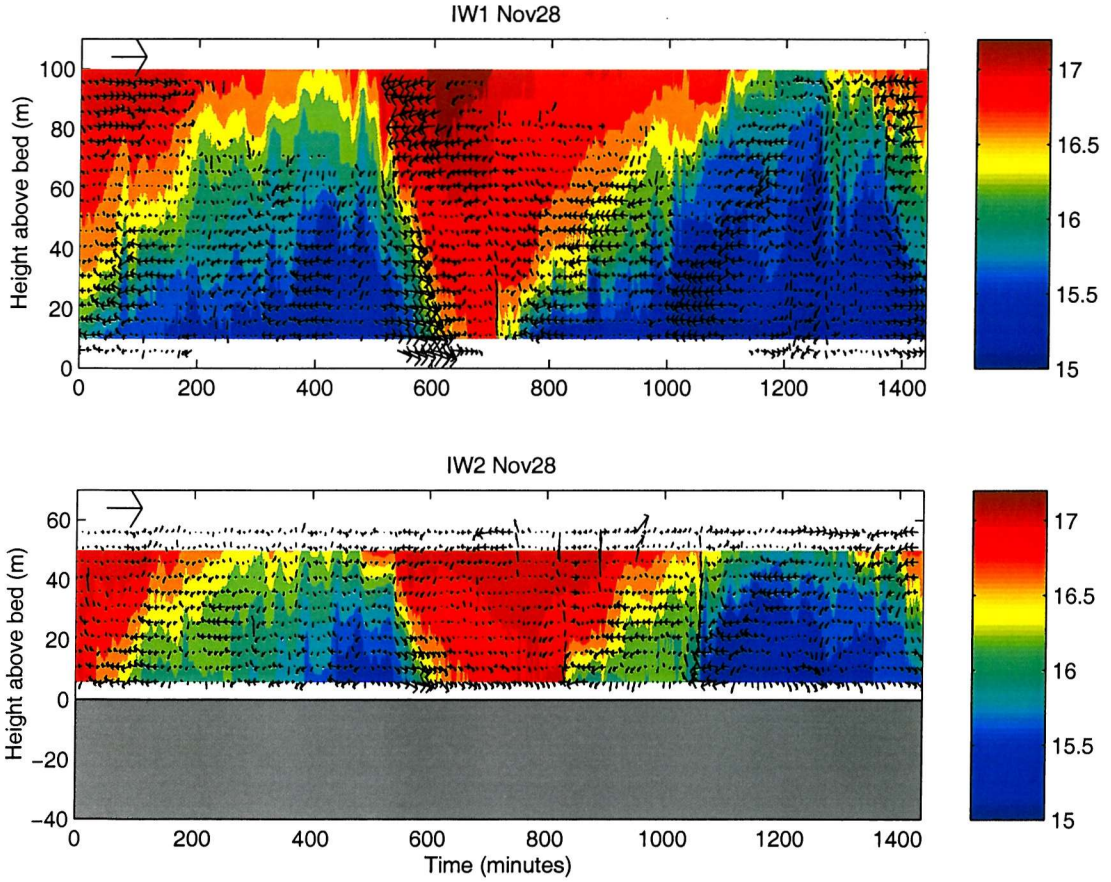
IW1 Nov28
Height above bed (m)
100
80
60
40
20
0
0
200
400
600
800
1000
1200
1400
17
16.5
16
15.5
15
IW2 Nov28
Height above bed (m)
60
40
20
0
−20
−40
0
200
400
600
800
1000
1200
1400
Time (minutes)
17
16.5
16
15.5
15

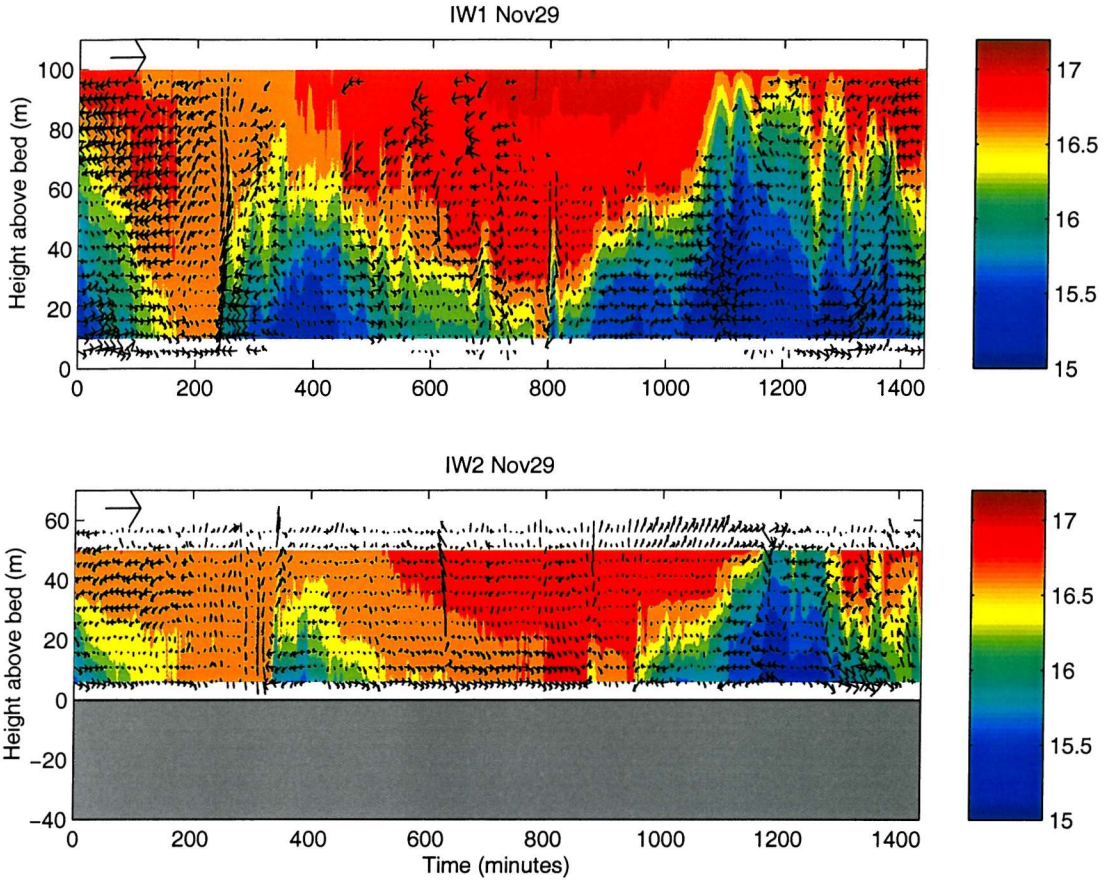
IW1 Nov29
Height above bed (m)
100
80
60
40
20
0
0
200
400
600
800
1000
1200
1400
17
16.5
16
15.5
15
IW2 Nov29
Height above bed (m)
60
40
20
0
−20
−40
0
200
400
600
800
1000
1200
1400
Time (minutes)
17
16.5
16
15.5
15

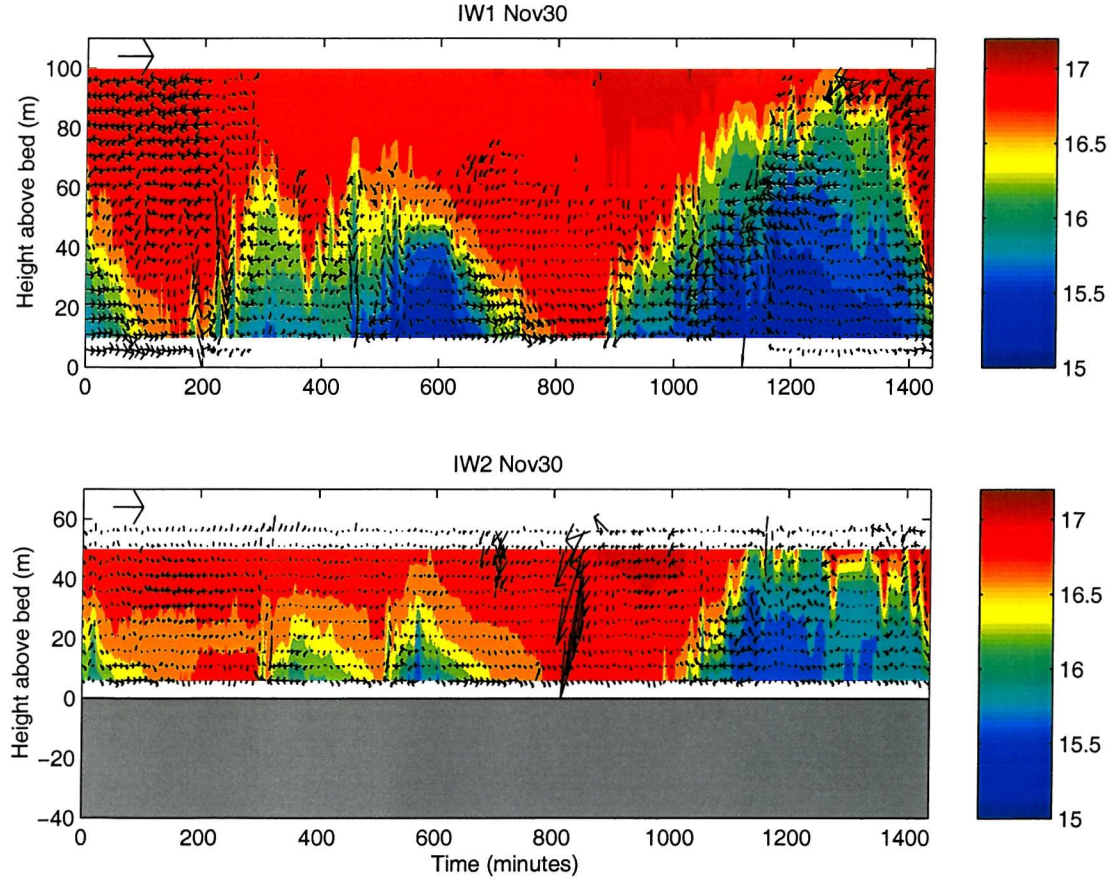
IW1 Nov30
Height above bed (m)
100
80
60
40
20
0
0
200
400
600
800
1000
1200
1400
17
16.5
16
15.5
15
IW2 Nov30
Height above bed (m)
60
40
20
0
−20
−40
0
200
400
600
800
1000
1200
1400
Time (minutes)
17
16.5
16
15.5
15

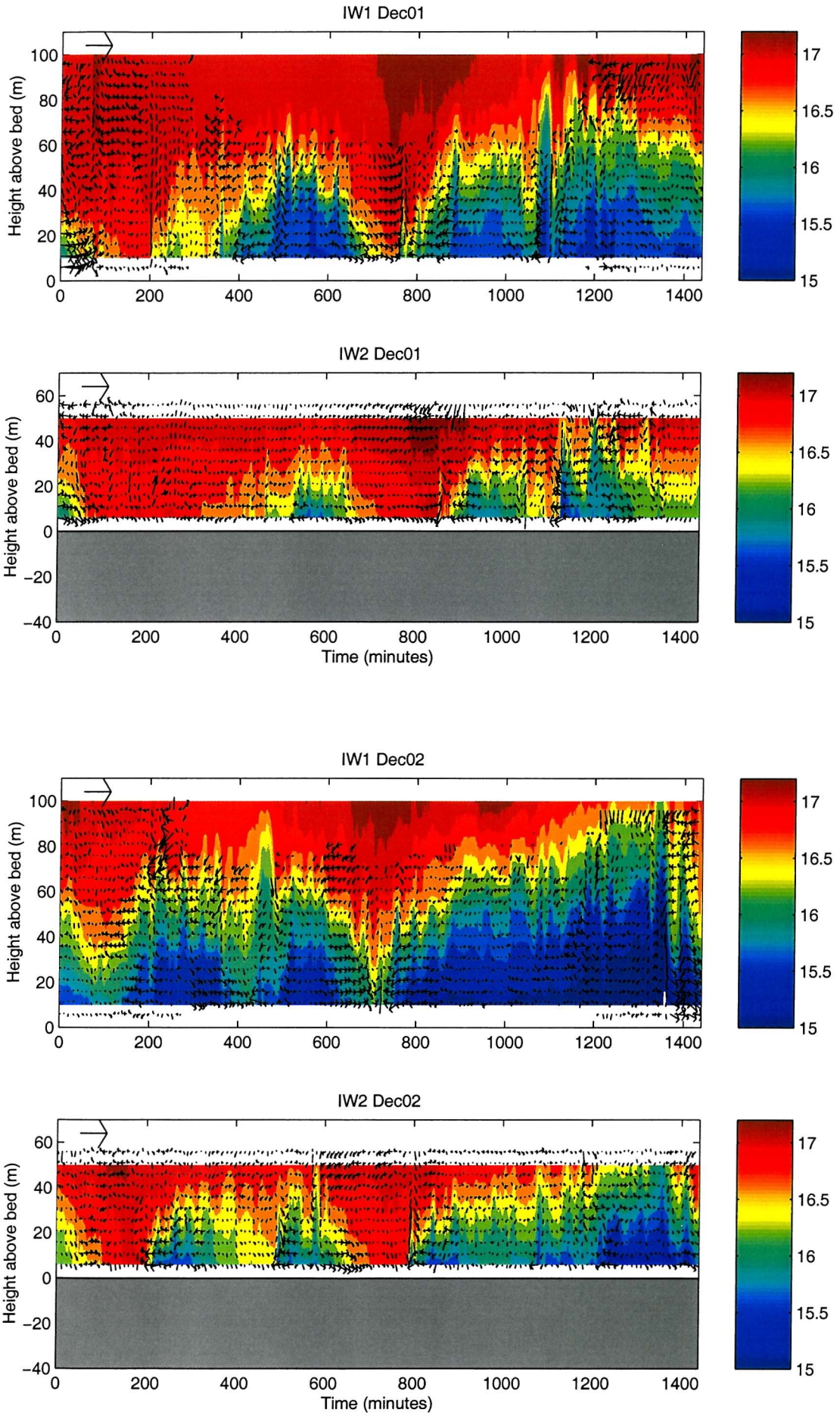
IW1 Dec01
Height above bed (m)
100
80
60
40
20
0
0
200
400
600
800
1000
1200
1400
17
16.5
16
15.5
15
IW2 Dec01
Height above bed (m)
60
40
20
0
−20
−40
0
200
400
600
800
1000
1200
1400
Time (minutes)
17
16.5
16
15.5
15
IW1 Dec02
Height above bed (m)
100
80
60
40
20
0
0
200
400
600
800
1000
1200
1400
17
16.5
16
15.5
15
IW2 Dec02
Height above bed (m)
60
40
20
0
−20
−40
0
200
400
600
800
1000
1200
1400
Time (minutes)
17
16.5
16
15.5
15

Vertical particle trajectories tracked using the ADCP vertical velocity vs. isotherm displacements. Colours are temperature contours as measured by thermistors on moorings. Black lines are particles with trajectory tracked using the measured vertical velocities from ADCP. Particles are injected into the time series of vertical velocities every hour at a 5 meter interval, then tracked until they leave the domain. Patterns were broadly similar for all days. During the majority of the time, isotherm displacements as indicated by temperature contours, are closely tracked by vertical movements. However during the period when denser water runs up the slope (e.g. 1000 – 1800 hrs on 26th November), isotherms cross particle paths due to the dominance of lateral gradients in temperature combined with significant on-shore flow at these times.

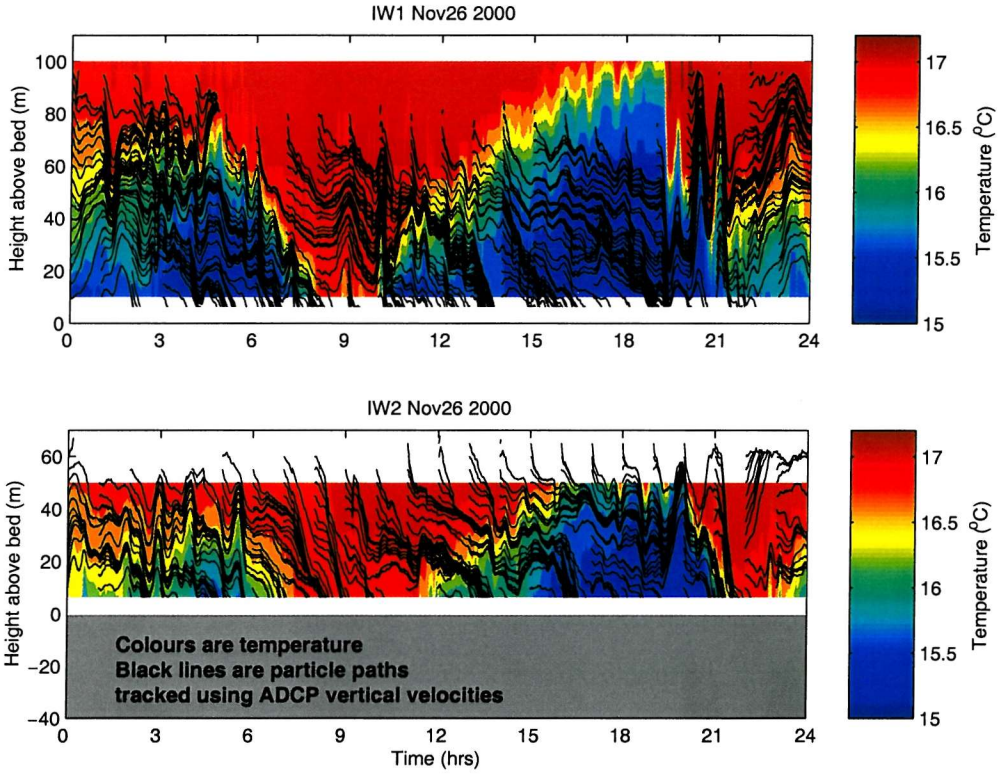

Appendix 7

Chlorophyll calibrations of fluorometer and transmissometer measurements during the 2000 Poor Knights islands cruise.

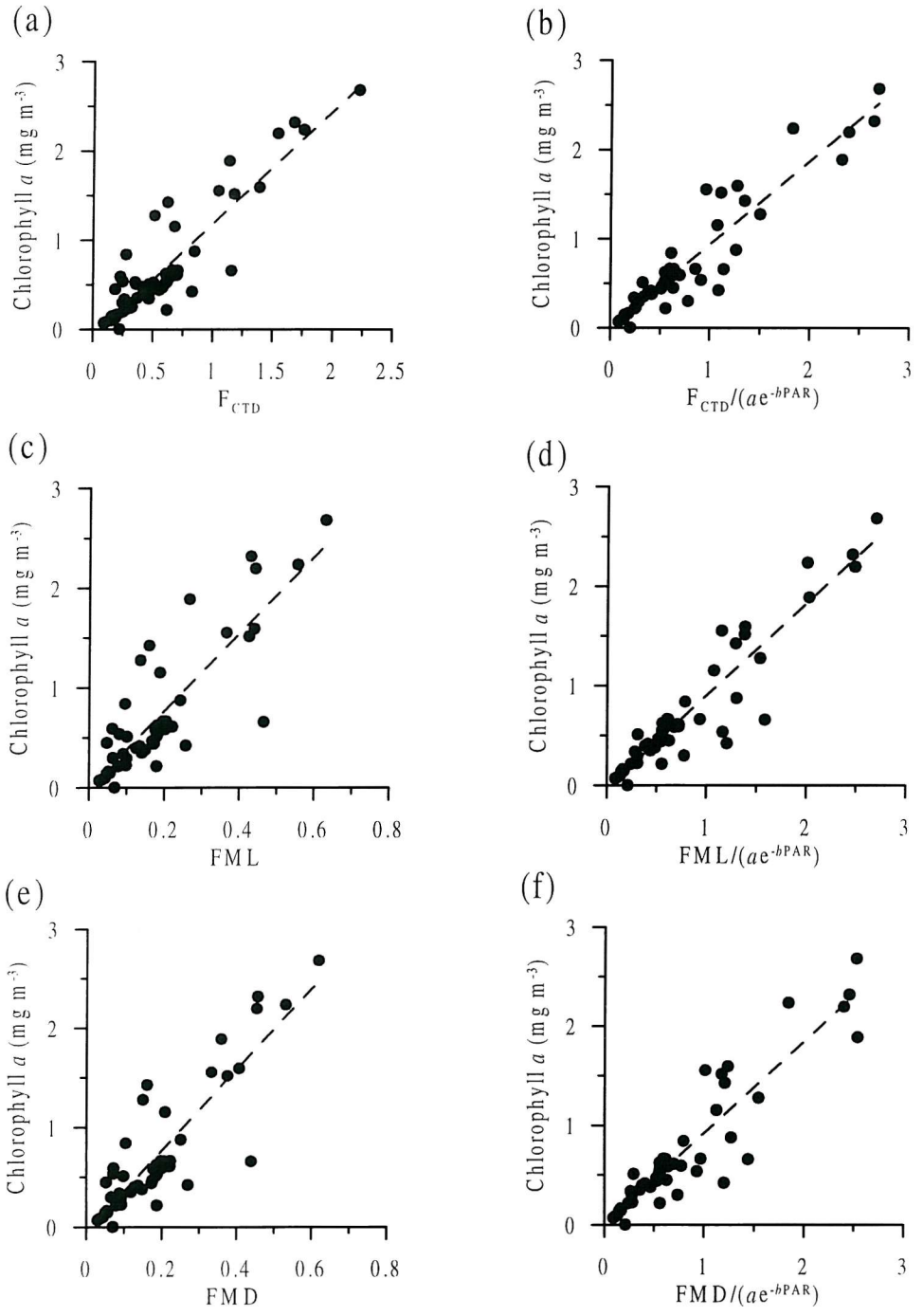

Fig. A5.1 Fluorescence vs. chlorophyll for all data collected during 2000 internal waves cruise. (a) Wetlabs (CTD) fluorometer vs. chlorophyll, (b) empirical relationship using Wetlabs (CTD) fluorometer and irradiance vs. chlorophyll. (c) FRRF F_M measured in light chamber vs. chlorophyll, (d) empirical relationship using FRRF F_M measured in light chamber and irradiance vs. chlorophyll. (e) FRRF F_M measured in dark chamber vs. chlorophyll, (f) empirical relationship using FRRF F_M measured in dark chamber and irradiance vs. chlorophyll.

Calculated model II regressions for all fits (*Fig. A5.1*) were:

(a) Chl = 1.4094 F_{CTD} – 0.151 , R^2 = 0.841, n = 56, p < 0.001

(b) Chl = $F_{CTD}/(1.113e^{-0.0059\ PAR})$, R^2 = 0.877, n=56, p < 0.001

(c) Chl = 4.685 F_M – 0.166 , R^2 = 0.759, n = 51, p < 0.001

(d) Chl = $F_M/(0.3248e^{-0.0065\ PAR})$, R^2 = 0.870, n=51, p < 0.001

(e) Chl = 4.574 F_M – 0.137 , R^2 = 0.716, n=51, p < 0.001

(f) Chl = $F_M/(0.3353e^{-0.0062\ PAR})$, R^2 = 0.849, n=51, p < 0.001

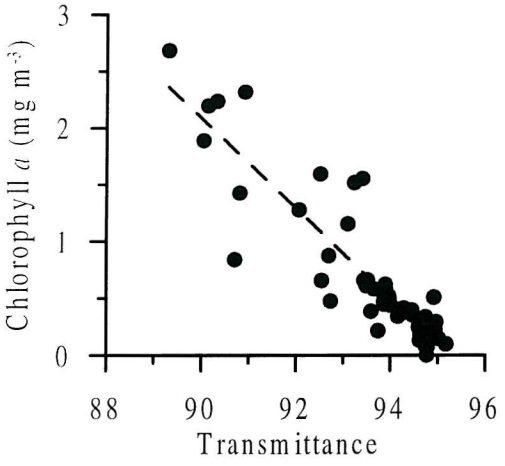

Fig. A5.2 Transmittance vs. chlorophyll for all data collected during 2000 internal waves cruise.

Calculated model II regression was:

Chl = 41.941 – 0.4411 Transmittance, R^2 = 0.808, n = 56, p < 0.001

Appendix 8

A model of phytoplankton photoacclimation within a photosynthetron

A simple model was formulated in order to investigate the possible influence of phytoplankton photoacclimation during the course of a P* vs. E experiment. The aim was to investigate the values of photosynthetic parameters obtained (specifically α^*), with reference to attempted comparisons between ^{14}C and FRRF derived productivity and physiological indices. The model was designed to simulate the collection and incubation of a sample from a variety of irradiances *in situ* within a water column. The acclimation of this sample to the irradiances experienced within a photosynthetron during a P* vs. E experiment was then modelled using parameterisations derived from field data collected during the 1999 and 2000 cruises.

It was assumed that the fully acclimated state of the phytoplankton sample could be modelled using a simple expression (Eq. A8.1). Such a model was not meant to represent any one physiological mechanism, but rather the combined effect of a number of processes (e.g. photochemical and non-photochemical quenching etc.). The expressions chosen to describe both $\Delta F'/F_M'$ and σ_{PSII}' at irradiance E were:

$$\Delta F'/F_M' = 0.5 - 0.0004\,E \qquad \text{(A8.1ai)}$$

$$\Delta F'/F_M' = 0.5 - 0.00127\,E + 1.45\times10^{-6}\,E^2 - 5.54\times10^{-10}\,E^3 \qquad \text{(A8.1aii)}$$

$$\sigma_{PSII}' = 700 - 0.4\,E \qquad \text{(A8.1b)}$$

With two options being chosen for $\Delta F'/F_M'$, a simple linear (Eq. A8.1ai) and more complex cubic (Eq. A8.1aii) relationship. These empirical models were capable of reproducing realistic relationships between $\Delta F'/F_M'$, σ_{PSII}' and irradiance (*Fig. A8.1*).

In order to model the collection of samples from within the water column in a number of different physiological states, the sample was initially chosen to be fully acclimated to three levels of *in situ* irradiance (0, 100 and 500 μ E $m^{-2}s^{-1}$). Acclimation away from this state to the fully acclimated state for individual light levels within the photosynthetron (i.e. corresponding to sub-samples), was then modelled using a simple first order rate expression (Falkowski, 1983; Lewis *et al.* 1984a; Cullen and Lewis, 1988). The rate

constant (γ) was chosen = 2 hr^{-1} i.e. acclimation half times $\tau_{a1/2} \approx 20$ minutes in agreement with observations during the 2000 cruise (*Fig. 4.26,* § 4.3.4) and similar to previous results (Kolber and Falkowski, 1993).

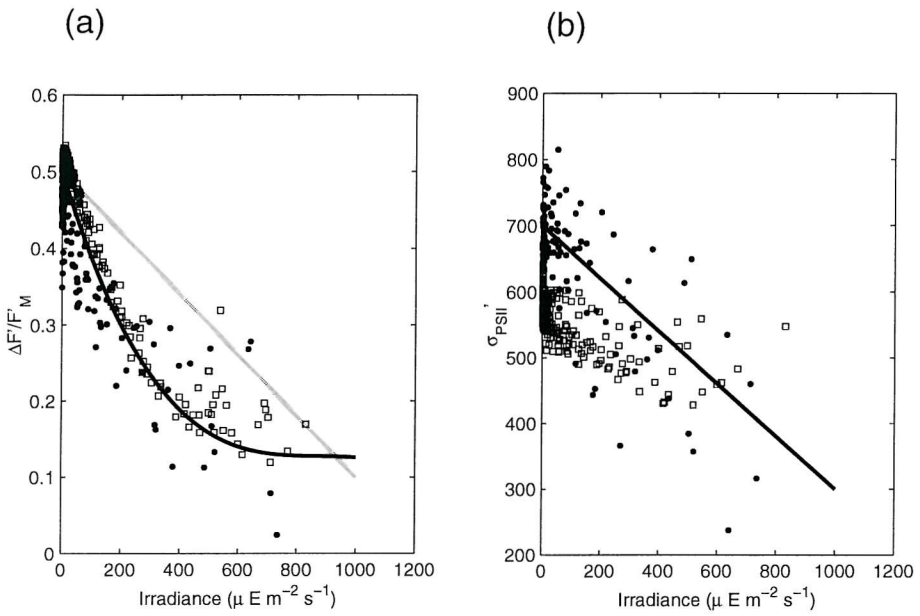

Fig A8.1 Relationships between $\Delta F'/F_M'$, σ_{PSII}' and irradiance from 1999 and 2000 cruises and empirical models used. (a) $\Delta F'/F_M'$ vs. irradiance for site U2 during the 1999 cruise (closed circles) and site PK on 30th November during the 2000 cruise (open squares). Solid lines are models, (grey - Eq. A8.1ai) and (black - Eq. A8.1aii). (b) σ_{PSII}' vs. irradiance for site U2 during the 1999 cruise (closed circles) and site PK on 30th November during the 2000 cruise (open squares). Solid line is modelled expression (Eq. A8.1b).

Time series of $\Delta F'/F_M'$ and σ_{PSII}' for each light level within the photosynthetron were thus generated (*Figs. A8.2 & Figs. A8.3*). As expected, individual 'sub-samples' followed first order kinetics from the acclimated state at the *in situ* irradiance to the acclimated state for the irradiance within the photosynthetron (*Figs. A8.2 & Figs. A8.3*).

The instantaneous productivity rate (P*) was then calculated from the time series of $\Delta F'/F_M'$, σ_{PSII}' and irradiance using (Eq. 1.11a). i.e. FRRF productivity model MI (§ 5.2.5). An example of P* at all times and irradiances shows that photoinhibition at high irradiances becomes progressively more important as incubation times increase (*Fig. A8.4a & b*). Instantaneous P* vs. E relationships indicate that P^*_{max} decreases with incubation

time (*Fig. A8.4d*). In order to simulate the P* vs. E curve that would be measured using ^{14}C uptake over the incubation time (T_{inc}), the values of instantaneous P* from time zero to T_{inc} have to be integrated ($\int_0^{T_{inc}} P^* \, dt$). Simulated P* vs. E curves generated using this method (*Fig. A8.4c*) were then fitted to the model of Platt *et al.* (1980) in order to derive α^* and P^*_{max}. The derived curves were similar to the observations of Suggett *et al.* (2001) (their Figure 2b), with higher photoinhibition and α^* as incubation times increase.

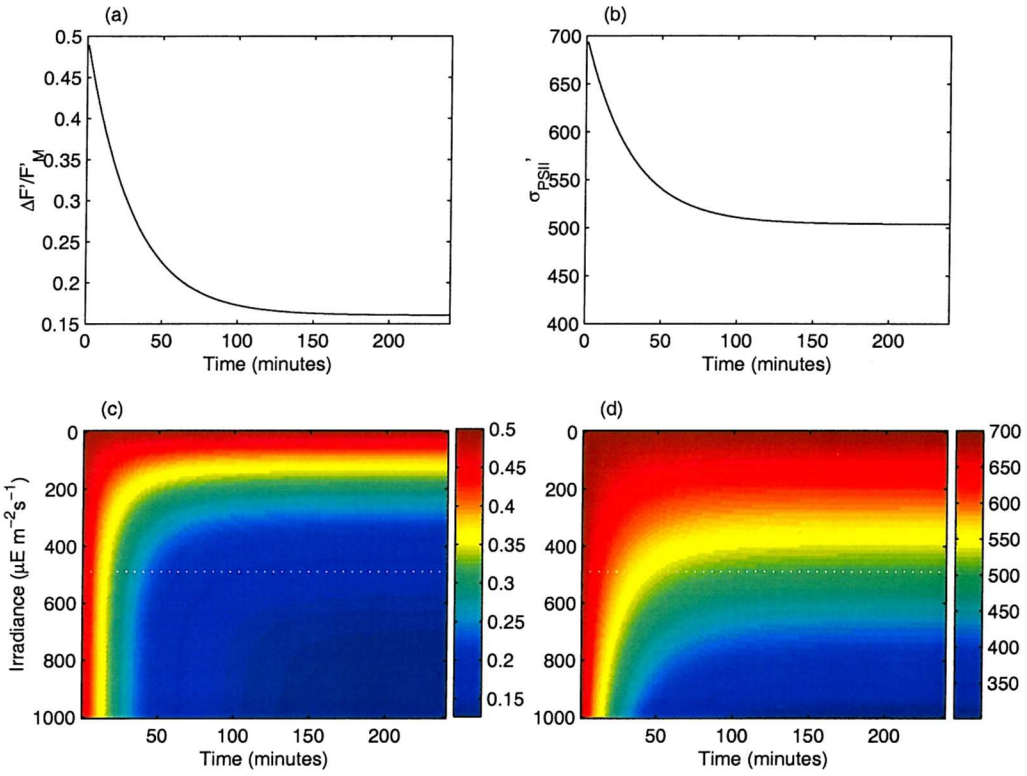

Fig A8.2 Acclimation of a sample (series of sub-samples) from the *in situ* state towards the fully acclimated state within the modelled photosynthetron. Simulated sample was collected at an *in situ* irradiance of 0, thus initial values of $\Delta F'/F_M'$ and σ_{PSII}' were 0.5 and 700 respectively (Eq. A8.1). Values are generated using the (Eq. A8.1aii) form for $\Delta F'/F_M'$.

(a) Time series of $\Delta F'/F_M'$ for a 'sub-sample' held at an irradiance of 490 μ E m^{-2} s^{-1}.

(b) Time series of σ_{PSII}' for a 'sub-sample' held at an irradiance of 490 μ E m^{-2} s^{-1}.

(c) Contours of $\Delta F'/F_M'$ for all times (0-120 minutes) and irradiances. Dotted white line indicates irradiance of 490, i.e. data in (a).

(d) Contours of σ_{PSII}' for all times (0-120 minutes) and irradiances. Dotted white line indicates irradiance of 490, i.e. data in (b).

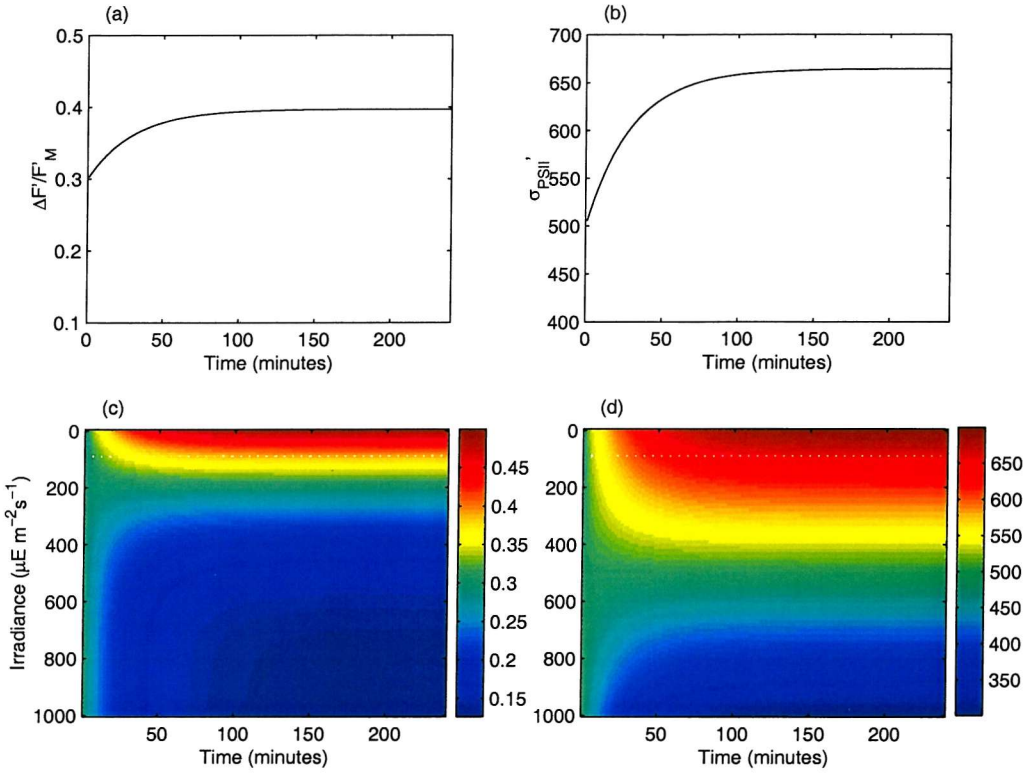

Fig A8.3 As Fig. A8.2 Acclimation of a sample (series of sub-samples) from the *in situ* state towards the fully acclimated state within the modelled photosynthetron. Simulated sample was collected at an *in situ* irradiance of 500, thus initial values of $\Delta F'/F_M'$ and σ_{PSII}' were 0.3 and 500 respectively (Eq. A8.1).

Values are generated using the (Eq. A8.1aii) form for $\Delta F'/F_M'$.

(a) Time series of $\Delta F'/F_M'$ for a 'sub-sample' held at an irradiance of 90 μ E m^{-2} s^{-1}.

(b) Time series of σ_{PSII}' for a 'sub-sample' held at an irradiance of 90 μ E m^{-2} s^{-1}.

(c) Contours of $\Delta F'/F_M'$ for all times (0-120 minutes) and irradiances. Dotted white line indicates irradiance of 90, i.e. data in (a).

(d) Contours of σ_{PSII}' for all times (0-120 minutes) and irradiances. Dotted white line indicates irradiance of 90, i.e. data in (b).

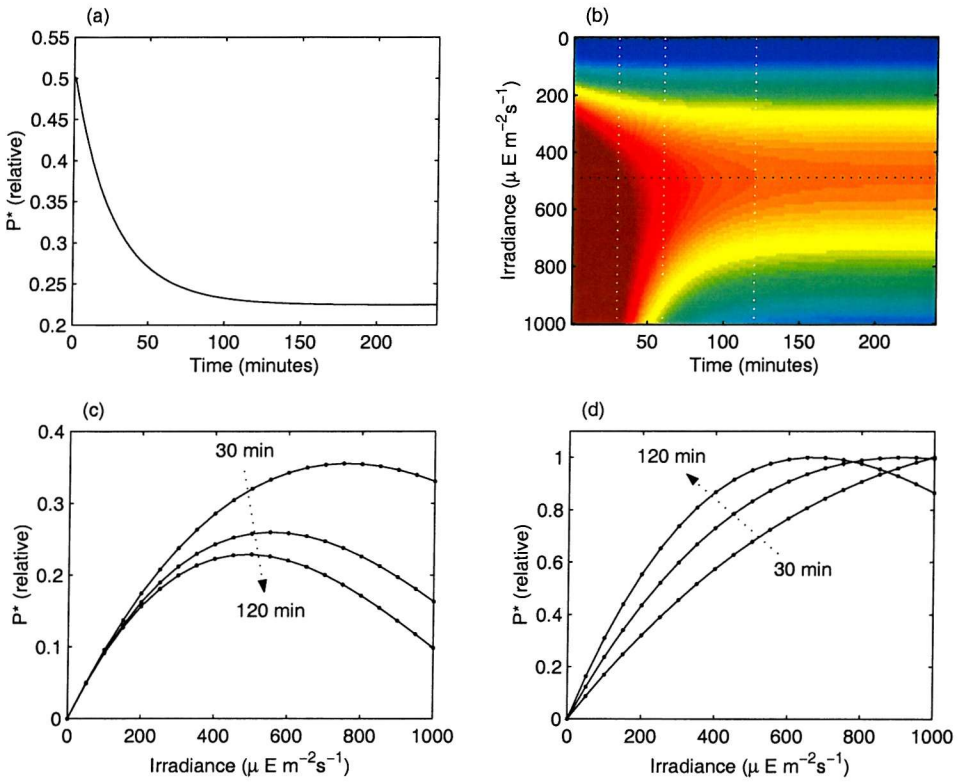

Fig A8.4 Modelled instantaneous P* and derived P* vs. E curves for a sample adapting from an initial irradiance of 0 to the irradiance within a photosynthetron.

Values are generated using the (Eq. A8.1ai) form for $\Delta F'/F_M'$.

(a) Time series of instantaneous P* for a 'sub-sample' held at an irradiance of 490 μ E m^{-2} s^{-1}.

(b) Contours of instantaneous P* for all times (0-240 minutes) and irradiances. Dotted black line indicates irradiance of 490, i.e. data in (a).Dotted white lines indicate incubation times of 30, 60 and 120 minutes i.e. data in (c) and upper integration limits (T_{int}) for (d).

(c) Instantaneous P* vs. E at 30, 60 and 120 minutes.

(d) Modelled P* vs. E curves as measured by an uptake measurement run over T_{int} = 30, 60 and 120 minutes, i.e. instantaneous P* integrated from 0 – T_{int}.

P* in (a - c) was normalised to the maximum modelled instantaneous P*. P* vs. E curves in (d) were normalised to the value of P^*_{max} before plotting each curve, in order to emphasise the changes in α* and photoinhibition (Platt *et al.* 1980).